CONTACT

+33 6 43 35 62 54

Jeanne.kergomard@orange.fr

12 rue Sophie Michel
35700 Rennes

www.linkedin.com/in/jeanne-kergomard-8215a0151

https://www.researchgate.net/profile/Jeanne-Kergomard

COMPÉTENCES

Biochimie alimentaire
Biophysique des interfaces fluides
Physiologie digestive humaine
Formulation d'émulsions
Physico-chimie des lipides
Microfluidique
Suivi oxydatif (PV, TBARS)
Chimie analytique (GC, HPLC, RMN..)
Analyse d'image (Fiji, Gwyddion)
Chimie organique

Gestion de projet
Encadrement
Vulgarisation scientifique
Veille bibliographique
Rédaction d'articles

LANGUES

Français: Langue maternelle
Anglais: Professionnel (TOEIC: 940)
Russe: Intermédiaire
Espagnol: Débutante

QUALITÉS

Curieuse
Sociable
Autonome
Créative
Organisée
Eloquente
Rigoureuse
Passionnée

Jeanne KERGOMARD, 26 ans

PhD Physique: biologie et environnement
Ingénieure chimiste
Postdoctorante à l'INRAE de Nantes

EXPERIENCES PROFESSIONNELLES

Depuis janvier 2023 – Institut National de Recherche pour l'Agriculture, l'Alimentation et l'Environnement (**INRAE**) de Nantes UMR BIA 1268 – équipe ISD – sous la direction de C. Berton-Carabin – Projet **VESTA**
« Développement de particules de Pickering biosourcées pour la stabilisation physique et oxydative d'émulsions alimentaires »

Octobre 2019 à Décembre 2022 – Institut de Physique de Rennes (**IPR**) UMR 6251 - Institut National de Recherche pour l'Agriculture, l'Alimentation et l'Environnement (**INRAE**) de Montpellier UMR IATE 1208- sous la direction de V. Vié (IPR), C. Bourlieu (INRAE)
« Activité enzymatique sur lipides végétaux : couplage de mesures interfaciales à l'échelle moléculaire (nm) et de mesures cinétiques de dégradation à l'échelle de l'objet (µm). »

Mars à Septembre 2019 - IPR UMR 6251 et INRAE de Montpellier UMR 1208 – en collaboration avec le groupe **Nestlé** (NRC Lausanne)
Stage de fin d'étude, supervisé par V. Vié (IPR), C. Bourlieu (INRAE), T. J. Wooster (NRC) and O. Schafer (NRC)
« Comportement interfacial et stabilité à l'oxydation de corps gras végétaux »

Mai à Juillet 2018 - Université Suédoise des Sciences Agricoles (SLU) – Malmö - Plant Breeding Dpt
Stage de recherche supervisé par W. Newson (SLU)
« Formulation de biopolymères à base de protéines de gluten de blé »

Juin à août 2017 - **CARGILL** Crevin (35) – Stage ouvrier
« Analyses de fourrage par technologie Infra-rouge »

FORMATION - ÉDUCATION

2019 à 2022 – **Université de Rennes 1**
Doctorat (spécialité Physique: Environnement et Biologie) supervisé par V. Vié (IPR)et C. Bourlieu (INRAE/CIRAD)

2014 à 2019 – **Ecole Nationale Supérieure de Chimie de Rennes**
Diplôme d'Ingénieur chimiste généraliste (Octobre 2019)
Spécialités *Chimie et Biotechnologies Agri/Agro/Santé- Formulation*
Majeure *Chimie et Technologie pour le Vivant (CTV)*

IMPLICATION SCIENTIFIQUE ET SOCIALE

Les Restos du cœur 2022-2023 – Bénévole Resto' Bus
IPR 2020-2022 – Représentante des doctorants au Conseil d'Unité
ACiD 2019-2021 – Association de doctorants - Responsable communication
JMC 2021 – Membre du comité d'organisation
Pint of Science 2019-2020 – Manager d'évènements à l'échelle locale
IMBL Montpellier 2019 – Membre du comité d'organisation

PRIX ET DISTINCTIONS

2023 – Prix de thèse – Fondation Rennes 1 – section matériaux
2023 – Prix du poster – Journées Chevreul, Paris, 200€
2022 - European Travel grant winner – AOCS Atlanta– 750€

PRODUCTION SCIENTIFIQUE

Articles scientifiques (4)

2022 – J. Kergomard et al., Interfacial adsorption and activity of pancreatic lipase-related protein 2 onto heterogeneous plant lipid model membrane, Biochimie, doi.org/10.1016/j.biochi.2023.04.001.

2022 – J. Kergomard et al., Modulation of gastric lipase adsorption onto mixed galactolipid-phospholipid films by addition of phytosterol, Colloids and Surfaces B: Biointerfaces, 10.1016/j.colsurfb.2022.112933

2022 – J. Kergomard et al., Interfacial Interfacial organization and phase behavior of mixed galactolipid-DPPC-phytosterol assemblies at the air-water interface and in hydrated mesophases, Colloids and Surfaces B: Biointerfaces, 10.1016/j.colsurfb.2022.112646

2021 – J. Kergomard et al., Stability to oxidation and interfacial behavior at the air/water interface of minimally-processed versus processed walnut OB , Food Chemistry, 2021, 10.1016/j.foodchem.2021.129880

Article de revue (1)

2021 – J. Kergomard et al., Digestibility and oxidative stability of plant lipid assemblies: An underexplored source of potentially bioactive surfactants?, Critical Reviews in Food Science and Nutrition, 2021, 10.1080/10408398.2021.2005532

Chapitre d'ouvrage (1)

2021 – C. Bourlieu, N. Barouh, J. Kergomard et al., Polar Lipids, Handbook of Dairy Foods Analysis, CRC Press, 2020, 978-0367343132. DOI: 10.1201/9780429342967

Communication orale dans des congrès (4)

2022 – J. Kergomard et al., Interfacial adsorption of gastrointestinal lipases onto heterogenous biomimetic vegetal membranes. AOCS Annual Meeting & Expo, Mai 2022, Atlanta, USA

2021 – J. Kergomard et al., Modulation of gastric lipase adsorption onto mixed galactolipid-DPPC films by the addition of phytosterols. Euro Fed Lipid, Octobre 2021, Leipzig – Online

2021 – J. Kergomard et al., Modulation of gastric lipase adsorption onto mixed galactolipid-DPPC films by the addition of phytosterols. Gerli, Septembre 2021, Bordeaux, France

2020 – J. Kergomard et al., Oxidative and interfacial behavior of oil bodies from walnut. Journées CHEVREUL 2020, Société Française pour l'étude des Lipides (SFEL), Dec 2020, Paris, France.

Posters dans des congrès (4)

2022 – J. Kergomard et al., What are the mechanisms of gastrointestinal lipases adsorption onto heterogenous biomimetic vegetal membranes? 7th International Conference on Food Digestion ICFD 2022, May 2022, Cork, Ireland.

2021 – J. Kergomard et al., Effects of processing and concentration on the oxidative stability and interfacial behavior of tree nuts oil bodies (OB). Euro Fed Lipid 2021, Oct 2021, Leipzig - Online, Germany

2021 – J. Kergomard et al., Stability to oxidation and interfacial behavior at the air-water interface of minimally-processed versus processed walnut oil-bodies. Lipid droplets & Oleosomes - 2nd International Conference, Dec 2021, Strasbourg, France

2020 – J. Kergomard et al., Oxidative and interfacial behavior of native oil bodies from walnut. Euro Fed Lipid Seville 2019, Oct 2019, Séville, Spain.

Food Chemistry 360 (2021) 129880

Contents lists available at ScienceDirect

Food Chemistry

journal homepage: www.elsevier.com/locate/foodchem

Stability to oxidation and interfacial behavior at the air/water interface of minimally-processed versus processed walnut oil-bodies

Jeanne Kergomard [a,b,c], Gilles Paboeuf [a,d], Nathalie Barouh [c], Pierre Villeneuve [c], Olivier Schafer [e], Tim J. Wooster [e], Claire Bourlieu [b], Véronique Vié [a,d,*,1]

[a] IPR Institute of Physics, UMR UR1 CNRS 5261, Rennes 1 University, France
[b] IATE, Univ Montpellier, INRAE, Institut Agro, Montpellier, France
[c] QUALISUD, Univ Montpellier, CIRAD, Institut Agro, IRD, Univ Réunion, Montpellier, France
[d] Univ Rennes 1, CNRS, ScanMAT – UMS 2001 F-35042 Rennes, France
[e] Institute of Materials Science, Nestlé Research, Lausanne, Switzerland

ARTICLE INFO

Keywords:
Walnut beverage emulsion
Oil bodies
Oxidative stability
Ellipsometry
Minimalist processes

ABSTRACT

Oil bodies (OB), the form of triacylglycerol storage in seeds, are interesting natural assemblies for nutritional applications. In walnuts, OB contain an important amount of polyunsaturated fatty acids that could be interesting food ingredients but may be prone to oxidation. The oxidative and interfacial behavior of walnut OB, either minimally-processed or after processing, were compared with processed complex walnut juice. The good oxidative stability of minimally-processed OB over 10 days (PV $\leq$ 8.4 meq O_2/kg, TBARS = 1.4 mmol eq MDA/kg) and of processed walnut complex matrixes over 20 days (PV $\leq$ 4.8 meq O_2/kg, TBARS = 1.4 mmol eq MDA/kg) was evidenced. In comparison, processing of OB promoted their oxidation. The interfacial studies led to the proposition of a new model of adsorption for minimally-processed OB that will be useful to design functional emulsion or foam in which OB act as emulsifiers.

1. Introduction

Oleosomes or oil bodies (OB) are very specific lipoproteic entities that enable plants to store the energy they need for germination and growth (Khor, Shen, & Kraemer, 2013; Walther & Farese, 2012). OB vary in size from nanoscopic (500 nm) to a few micrometers (2.5 μm) (Frandsen, Mundy, & Tzen, 2001). The structure of an OB is based on a triacylglycerol (TAG) core droplet (94–98% wt.) surrounded by a monolayer of phospholipids (PL) (0.6–2% wt.) with embedded proteins (0.6–3% wt.) (Huang, 1994; Napier, Beaudoin, Tatham, Alexander, & Shewry, 2001). Such lipoproteic monolayer protects the OB from chemical or mechanical stresses (Nikiforidis, Matsakidou, & Kiosseoglou, 2014). Three types of proteins are present in the lipid monolayer, oleosins, caleosins and stereosins; oleosins being the most abundant (1–4% wt.) (Napier et al., 2001). Thanks to the presence of oleosins, OB are remarkably stable against aggregation and coalescence (Barre, Simplicien, Cassan, Benoist, & Rougé, 2018; Napier et al., 2001; Nikiforidis et al., 2014). This stability is attributed to the steric hindrance

Abbreviations: AFM, atomic force microscopy; ALA, α-linolenic acid; BAM, brewster angle microscopy; BuOH, butanol; CLSM, confocal laser scanning microscopy; DELTA, ellipsometric angle; DAG, diacylglycerol; EggPC, phosphatidylcholine from egg yolk; EggPC-WOIL, model solution containing EggPC (2% wt) and WOIL (95% wt) diluted at 4% wt; EtOH, ethanol; FA, fatty acid; FAME, fatty acid methyl ester; FFA, free fatty acid; He-Ne, helium-neon; HHP, high-pressure homogenization; HHPT, high-pressure homogenization following by a heat treatment; HNO_3, Nitric acid; HPLC, high performance liquid chromatography; LA, linoleic acid; MAG, monoacylglycerol; MDA, malondialdehyde; MeOH, methanol; MP, minimally processed; NaCl, sodium chloride; OB, oil body; Oleo-TAG, model solution containing oleosins (3% wt) and TAG (95% wt) diluted at 4% wt; Oleo-WOIL, model solution containing oleosins (3% wt) and WOIL (95% wt) diluted at 4% wt; PI, surface pressure; pH, potential hydrogen; PC, phosphatidylcholine; PE, phosphatidylethanolamine; PI, phosphatidylinositol; pI, isoelectric point; PL, phospholipid; PS, phosphatidylserine; PUFA, polyunsaturated fatty acids; PV, peroxide value; QNM, quantitative nanomechanic; Rd-DOPE, 1,2-dipalmitoyl-*sn-glycero*-3-phosphoethanolamin-N-(lissamin rhodamin B sulfonyl); TAG, triacylglycerol; TBA, thiobarbituric acid; TBARS, thiobarbituric acid reactive substances; TCA, trichloroacetic acid; TLC, thin-layer chromatography; Tris-HCl, tris(hydroxymethyl)aminomethane hydrochloride; UP, ultrapure (water); WOIL, commercial walnut oil.

* Corresponding author at: Institut de Physique de Rennes, Campus de Beaulieu, UMR UR1 CNRS 5261, Université de Rennes 1, 35042 Rennes cedex, France.
E-mail address: veronique.vie@univ-rennes1.fr (V. Vié).
[1] Institut de Physique de Rennes, campus de Beaulieu, 35042 Rennes cedex France.

https://doi.org/10.1016/j.foodchem.2021.129880
Received 20 November 2020; Received in revised form 12 April 2021; Accepted 13 April 2021
Available online 1 May 2021

and to the negatively charged surface of the monolayer at physiological pH, leading to electrostatic repulsion between OB and reducing aggregation (Shimada, Hayashi, & Hara-Nishimura, 2018). The natural stability of these assemblies explains the considerable attention recently paid to OB (Nikiforidis, 2019). In addition, they can be considered as minimally processed entities that deliver TAG, liposoluble vitamins, and proteins for human nutrition. While a multitude of products is derived from nuts and seeds, few exist where the OB remains in its native or minimally-processed form.

Walnuts are among the most widely consumed commercially grown tree nuts in the world (Hayes, Angove, Tucci, & Dennis, 2016). Their consumption is associated with many health benefits, including reducing the risk of cardiovascular disease, and neurological disorders (Simopoulos, 2002). These benefits are attributed to their fatty acid (FA) profile, which is rich in polyunsaturated fatty acids (PUFA) (Hayes et al., 2016). Walnut lipids contain 90% unsaturated FA, of which 12–16% is α-linolenic acid (ALA, C18:3, ω3) that very likely explain the cardioprotective effects of a diet rich in walnuts (Maguire, O'Sullivan, Galvin, O'Connor, & O'Brien, 2004). Walnut lipids are also considered to be a good source of vitamins and dietary fibers (Miraliakbari & Shahidi, 2008). To date, most research on walnut lipids has focused on their chemical composition (Venkatachalam & Sathe, 2006). In addition to TAG, tree nut lipids contain phytosterols, PL, and tocopherols, which are known to confer good oxidative stability to oil in water emulsion (Samdani, McClements, & Decker, 2018).

Several studies have been dedicated to OB colloidal stability, with special emphasis on soybean source (Kapchie, Yao, Hauck, Wang, & Murphy, 2013; Zhao, Chen, Yan, Kong, & Hua, 2016). The chemical stability during the storage of emulsions prepared with OB from oilseeds has been investigated, including issues of endogenous hydrolytic activity (De Chirico et al., 2020) and oxidative sensitivity (Chen, McClements, Gray, & Decker, 2012). Nevertheless, the use of oilseed OB with high PUFA content is limited because of their susceptibility to oxidation (Nuchi, Hernandez, McClements, & Decker, 2002). Lipid oxidation is an undesirable reaction in food applications and the dispersion of lipids in emulsions further increases this phenomenon by increasing contact with oxygen and pro-oxidant species. This explains why lipid oxidation is a major cause of degradation during the manufacture and storage of food products (Villière, 2005), and also explains why the use of OB in beverages requires a good understanding of their physical and chemical stability to obtain a product that meets consumer expectations.

Despite the high number of publications on vegetal juices and OB chemical characterization (Tzen, Cao, Laurent, Ratnayake, & Huang, 1993), questions remain open regarding the interfacial behavior of OB. Some insights have been gained into the physical stability of natural OB (White et al., 2008) and their organization at the interface (Bettini, Santino, Giancane, & Valli, 2014; Waschatko, Schiedt, Vilgis, & Junghans, 2012). However, the mechanism of interfacial organization of native OB has not yet been fully elucidated, especially when the objects have been degraded by oxidation, even though such characterization could help understand plant-based beverage reactivity.

The aim of this study was thus to investigate the oxidative behavior of walnut OB using accelerated oxidative storage conditions, to determine the chemical stability of those lipoprotein assemblies when they are in a complex matrix (walnut beverage) or in isolated form at different levels of processing (minimum level, homogenized only, homogenized plus heat-treated). Biophysical tools were used to understand the organization of OB at the interface, and the behavior of their three different constituents, TAG, PL, and proteins (oleosins). Such investigations are required to better understand the reactivity of OB and are of interest for a large panel of food technological applications.

2. Materials and methods

All chemicals were purchased from Sigma Aldrich Ltd. (St. Louis, MO), except for ultrapure (UP) water, hexane, and acetic acid purchased from Honeywell Research Chemicals (Charlotte, NC, USA). If not stated otherwise, all biochemical characterizations were conducted at least in triplicate and biophysical characterizations at least in duplicate.

2.1. Preparation of the complex matrixes and isolation and purification of OB

Walnut kernels (*Juglans regia* L., *Chandler variety, origin Chile*) were supplied by Sun-Snack AG (St Margrethen, Switzerland). Walnut kernels were soaked in 2% wt. NaCl solution (ratio nuts/solution, 1:20 w/v) and stirred for 16 h at 200 rpm (Legallais IKA, KS4000 i control) to remove tannins, astringency and soluble impurities in the skin (Ghaderi-Ghahfarrokhi, Sadeghi-Mahoonak, Alami, & Mousavi Khanegah, 2017). Sodium azide (0.02% wt.) was added to the final preparation to insure preservation.

2.1.1. Complex matrix preparations: Walnut beverages with or without added sodium caseinates (3% wt.)

The procedure for complex matrix preparation was provided by the Institute of Materials Science (Nestlé Research). After soaking and rinsing twice with UP water, 38 g aliquots of walnut kernels were dried, redispersed in 500 mL of UP water and boiled at 90 °C in the food processor (Vorwerk Thermomix TM31) for 10 min while blending at low-speed. For one modality of walnut complex matrix including additional emulsifiers, these emulsifiers, i.e. sodium caseinates (3% wt.) were added at this stage. Another modality was produced without sodium caseinates (called hereafter walnut complex matrix). Then, the mixture was blended at maximum power (stage 10). The coarse nut emulsions were pre-homogenized using a high shear laboratory mixer (Silverson, L5M-A) at a shearing speed of 8 000 rpm for 1 min with a square head. The emulsion was sieved through a 300 μm stainless steel sieve to get rid of large solid particles that could hinder high pressure homogenization. To obtain a fine emulsion with a relatively small particle size, the emulsion was passed through a two-stage laboratory homogenizer (Niro Soavi, Panda 2 K) with heads set at 3.0×10^7 Pa and 8.0×10^6 Pa.

2.1.2. Isolation and purification of OB

OB were isolated from walnut kernels and purified using the method of Kapchie, Hauck, Wang, and Murphy (2011). After soaking and rinsing twice with UP water, the walnut kernels were manually ground with a pestle and mortar. Aliquots (50 g) of walnut kernels were mixed with UP water at ratio of 1:6 (g/mL) and stirred at 10 000 rpm for 5 min in a lab disperser (Ultra-turrax, IKA, T18 digital). The mixture was sieved in 315 μm stainless-steel sieve. The first wash consisted of centrifuging the filtered solution at 4000 *g* at 4 °C for 30 min (Beckman Coulter, Avanti J-E). The layer of cream at the top of the tube was collected and washed three times in buffer solution (0.1 M Tris-HCl, 4 M sucrose, 0.5 M NaCl, pH 8.6, ratio 1:6 g/mL) by centrifugation at 4000 *g* at 4 °C for 30 min. The upper phase was collected each time. All the upper phases were pooled, then washed twice in UP water (ratio 1:6 g/mL) by centrifugation at 4 000 *g* at 4 °C for 30 min. The resulting cream layer of isolated OB was dispersed (4% w/v) in a 0.1 M Tris-HCl solution at pH 7. A diagram for the procedure of OB isolation and purification is available in Fig. S1 (Supplementary Material).

2.2. Processing of dispersed isolated OB

High-pressure homogenization (HHP) treatments were carried out in a two-stage high-pressure homogenizer (Niro Soavi, Panda 2 K) by applying 3.0×10^7 Pa and 8.0×10^6 Pa, for first and second head respectively. One fraction of isolated HHP OB was subjected to an additional heat treatment (modality called hereafter HHPT) at 90 °C for 10 min. The minimally processed (MP) sample underwent no processing. In total, three modalities were obtained based on the dispersed OB cream layer solution, named respectively, MP, HHP and HHPT,

according to the operation units applied.

2.3. Oxidation test challenge to monitor the chemical stability of OB in isolated forms or in complex matrixes

2.3.1. Storage test set-up

The OB emulsions were divided into 8 mL triplicates in amber centrifuge tubes and stored in an incubator (Legallais IKA KS4000 i control) at 40 °C for 20 days under constant agitation at 110 rpm (Genot & Michalski, 2010). Aliquots were taken at days 0, 1, 3, 6, 9, 12, 15 and 20 for analysis of levels of oxidation in the samples (PV and TBARS assays).

2.3.2. Monitoring of lipid oxidation using PV and TBARS assays

Peroxide values (PV) were first determined, using the method of Mihaljević, Katušin-Ražem, and Ražem (1996) and Shantha and Decker (1994). This PV index is indicative of the number of active oxygen atoms in the organic chains, leading to the formation of unstable primary oxidation products such as hydroperoxide. 250 μL aliquot of the sample was added to 500 μL of a mixture of methanol and butanol MeOH/BuOH (3:1 v/v) and vortexed for 10 s, and 30 μL of the diluted sample were placed on a clear microplate (ANSI/SLAS (SBS) format) with 230 μL of MeOH/BuOH (3:1 v/v), 2.5 μL of iron chloride solution and 2.5 μL of ammonium thiocyanate. After 10 min of reaction, absorbance was measured at 532 nm using a microplate reader (Nanoquant Infinite 200 Pro, TECAN, Gröedig, Austria). Contribution of protein to PV was eliminated by comparison with the iodometric normalized method of determination of peroxide index (*Norme Française* NF T60-220, 1968). The results are expressed in meq O_2/kg of oil.

The thiobarbituric acid reactive substances (TBARS) assay, adapted from Ghani, Barril, Bedgood, and Prenzler (2017) and Ohkawa, Ohishi, and Yagi (1979), was performed. The TBARS assay measures the equivalent concentration of reactive malondialdehyde (MDA), a secondary oxidation product produced by the degradation of unstable peroxide lipids. 50 μL aliquot of the sample was added to 50 μL of UP water, 200 μL of a solution containing 15% (w/w) of trichloroacetic acid (TCA), 0.375% (w/v) of thiobarbituric acid (TBA) and 0.25 mol/L of hydrochloric acid. The tubes were placed in warm water (90 °C) for 15 min, then in ice for 5 min and centrifuged for 10 min at 7 700 g (centrifuge 5427, Eppendorf). Aliquots (200 μL) of the sample were placed on a clear microplate (ANSI/SLAS (SBS)) and absorbance was measured at 532 nm using a microplate reader (Nanoquant Infinite 200 Pro, TECAN, Gröedig, Austria). The results are expressed in mmol equivalent MDA/kg of oil.

2.4. Chemical characterization of walnut kernels

Walnut kernels (2 g) were ground and incorporated into 5 mL of UP water and 40 mL of Folch solution (chloroform/methanol 2:1 v/v) (Folch, 1957). The mixture was passed through a lab disperser (Ultra-turrax, IKA, T18 digital) for 1 min at between 9 500 and 13 500 rpm. In a 500 mL separating funnel, the solution was washed once with 22.5 mL of NaCl solution at 0.73%, then twice with 50 mL of a solution containing 40 mL of Folch and 10 mL of NaCl solution at 0.58%. The lower phase was collected between each wash and solvents were evaporated under reduced pressure.

2.4.1. Lipid class composition of walnut Folch extracts by thin-layer chromatography (TLC)

Neutral lipids were separated by one-dimensional migration using hexane/diethylether/acetic acid (65:35:1 v/v/v) in an automatic TLC sampler (Camag, Muttenz, Switzerland) controlled by a Wincats software system (2008) (Bourlieu, Rousseau, Briard-Bion, Madec, & Bouhallab, 2012). After migration, the silica plates were dried at 70 °C for 2 min and then revealed with a 15.9% solution of copper sulfate in an orthophosphoric acid/water (92:8 v/v) solution. For each sample, 0.5 mg/mL of lipid solution was used to automatically apply 4 and 8 μL on the thin layer. After revelation, the silica plates were subjected to laser UV detection (Camag TLC scanner 3, Muttenz, Switzerland). The wavelength of maximum absorption was 500 nm, the spots were quantified and spot intensities integrated with Wincats software (2008). Calibration curves were performed with standards of TAG, diacylglycerol (DAG), monoacylglycerol (MAG) and FFA (palmitic, oleic and linoleic acids).

2.4.2. Fatty acid composition of walnut Folch extracts by gas chromatography (GC)

Fatty acid methyl esters (FAME) were prepared from the walnut Folch extracts (Piombo et al., 2006). Aliquots (5 μL) of methylated Folch extract were analyzed by GC (Focus GC, Thermo Electron Corporation, Massachusetts, USA) equipped with a split injector (ratio of 1/20), a CP-Cil 88 Varian capillary column (50 m × 0.25 mm with a 0.2 μm thick film; Chrompack, Middelburg, The Netherlands) and 1 mL/min of helium as carrier gas. FAME were analyzed using a flame ionization detector and ChromCard Data System (version 2005; Thermo Electron Corporation, Massachusetts, USA).

The column temperature started at 150 °C, increased from 150 °C to 225 °C at a rate of 5 °C/min and maintained at 225 °C for 10 min. These chromatographic conditions allowed the correct and rapid separation of all FAME from C10:0 to C24:1. FAME were identified using a mixture of methyl esters as external standard (Mixture ME 100, Larodan, Sweden). The injector and detector temperatures were 250 °C and 270 °C respectively. FA contents are expressed in g per 100 g of fresh product.

2.4.3. Tocopherol content of walnut Folch extracts by high performance liquid chromatography (HPLC)

HPLC analysis on Folch extracts was performed using the 1290 Agilent System (Massy, France) equipped with a C18 column (250 mm × 4.6 mm i.d., 5 μm, HALO(R)-5 column, AMT, Wilmington, Delaware, USA) and a fluorescence detector, to detect and quantify four distinct tocopherols (α, β, δ and γ) (Moustiés et al., 2019). The mobile phase consisted of ethanol/methanol (40:60 v/v) in isocratic conditions. The temperature of the column was maintained at 25 °C and the flow rate was 0.8 mL/min. Fluorescence detection was set at 296 nm for excitation and 330 nm for emission. The injection volume was 20 μL and the calibration curves were performed with standard solutions from 0.1 to 1.5 mg/L. Each sample was analyzed with three repetitions.

2.5. Structural characterization of dispersed isolated OB as their native form or after different physico-chemical treatments during the oxidation challenge

2.5.1. Droplet size of isolated OB in MP, HHP, and HHPT matrixes

The size distributions of OB were measured by laser light scattering using a Mastersizer 3000 (Malvern Instruments, Malvern, UK), with two laser sources. The refractive indexes used were 1.333 for water and 1.460 for dispersed OB respectively. The samples were diluted directly in the measurement cell of the apparatus in order to reach 7% obscuration. Several parameters were calculated from the size distribution: the mode diameter, which corresponds to the population of the most frequent OB in the volume distribution, the surface-weighted average diameter of the OB d_{32} (μm), defined as $\Sigma n_i d_i^3 / \Sigma n_i d_i^2$, and the specific surface area calculated according to the equation $S = 6.\phi / d_{32}$ (where ϕ is the volume fraction of lipid in the emulsion).

2.5.2. Study of MP, HHP and HHPT matrix microstructure using Confocal laser scanning microscopy (CLSM)

The matrix microstructure was observed using a CLSM system (Leica SP8, Heidelberg, Germany) on an inverted microscope operated with an argon laser (excitation at 488 nm) and two He-Ne lasers (excitation at 543 and 633 nm) that enabled multi-imaging of a sample by selecting the correct excitation wavelength and filters to collect the light emitted

from a given stain. A 64x oil-immersion objective was used for all images. Three fluorescent dyes were used, as already detailed by Bourlieu et al. (2015) to locate i) proteins - Fast Green FCF (6:100 v/v, $\lambda_{ex} = 633$ nm - λ_{em} = 655–755 nm, Invitrogen), ii) non-polar lipids - Lipidtox (0.2:100, v/v, $\lambda_{ex} = 488$ nm - $\lambda_{em} = 590$ nm, Invitrogen) and iii) polar lipids - Rd-DOPE (1:100, v/v, 16:0 Liss Rhod PE *1,2*-dipalmitoyl-*sn-glycero-3*-phosphoethanolamin-N-(lissamin rhodamin B sulfonyl), $\lambda_{ex} = 543$ nm – $\lambda_{em} = 590$ nm, Avanti Polar Lipids). The three dyes were added in a 200 μL aliquots at least 10 min before observation. 10 μL samples were then placed on a glass slide just before observations. The software used for CSLM images was EZ-C1 version 3.40 (Nikon).

2.5.3. ζ-potential measurements of isolated OB in MP, HHP and HHPT matrixes

The apparent ζ -potential of OB in several emulsions diluted at 1:200 v/v in UP water was determined by measuring electrophoretic mobility (u) at 25 °C using laser Doppler electrophoresis (Nano Z PSS Z300, Nicomp). Measurements were made at 3 mV for 7 min. Henry's law relates U to the particle ζ–potential.

2.6. Interfacial behavior of isolated MP OB at the air/water interface

2.6.1. Preparation of model solutions

To obtain an overview of the different interfacial behaviors of MP OB compounds (TAG, proteins, and PL) several model solutions were prepared based on the proportions of OB constituents in their native form. A solution containing oleosins and TAG (named oleo-TAG) extracted from walnut OB was prepared by introducing 3% wt. oleosins and 95% wt. TAG, diluted to 4% wt. in a solution of 1 M Tris-HCl pH 7. To promote solubilization of the oleosins, TAG were first emulsified in the Tris-HCl solution and then sonicated for 30 s at 1.5 W before the oleosins were incorporated. A second sample containing 3% wt. oleosins and 95% wt. commercial walnut oil (La Tourangelle, France) was also prepared using the same procedure. Another model solution containing L-α-phosphatidylcholine powder from eggPC and commercial walnut oil (named EggPC-WOIL) was prepared by adding 2% wt. of EggPC and 95% wt. of previously emulsified commercial walnut oil, diluted to 4% wt. in a 0.1 M Tris HCl solution at pH 7. Another solution containing 4% wt. of commercial walnut oil diluted in a 0.1 M Tris-HCl solution at pH 7 was also prepared. The model solutions were named respectively oleo-TAG, oleo-WOIL, EggPC-WOIL and WOIL, according to their composition.

2.6.2. Ellipsometry and surface pressure measurements

Experiments were performed using a circular Teflon trough (volume 8 mL, surface area 27 cm^2). After 5 min of acquisition in UP water to define the zero, the water was replaced by the 4% wt. OB or model sample diluted at a rate of 22.5 mg/L in UP water (1/1600) in the Langmuir trough. The surface pressure (PI, mN/m) and the ellipsometric angle (DELTA, °) were recorded simultaneously at 21.5 °C. The surface pressure was measured according to the Wilhelmy-plate method using a filter paper connected to a microelectronic feedback system to measure the surface pressure (Nima Technology, UK). Values of PI were recorded every 15 s with a precision of ±0.2 mN/m. Ellipsometric measurements were carried out with a home-made automated ellipsometer in a "null ellipsometer" configuration (Berge & Renault, 1993; Bourlieu et al., 2020). The laser beam probed a surface of 1 mm^2 and a depth in the order of 1 μm and provided insight into the number of molecules at the interface. Values of DELTA were recorded every 15 s with a precision of ± 0.5°.

2.6.3. Study of interfacial film structures by atomic force microscopy (AFM)

For AFM imaging, interfacial films were transferred onto a freshly-cleaved mica plate using the Langmuir-Blodgett method. The transfer took place at the end of the kinetic adsorption in the Langmuir through, after the surface pressure of the sample reached a plateau. Barriers were set at a low speed of 10 cm^2/min and the surface pressure was held constant during the transfer. The mica plate was further observed with an AFM (Multimode Nanoscope 5, Bruker, France) in QNM mode in air (20 °C) with standard silicon cantilevers (0.3 N/m), and at a scan rate of 1 Hz. The force was minimized during all scans. To check the integrity of the samples after the different scans and zooms, the same zone was imaged at the end of the analysis. The scanner size was 100 × 100 μm^2. The processed images were analyzed by the open-source platform Gwyddion.

2.7. Statistical analysis

All results are presented as mean ± SD. Statistical significance between the OB dispersions was tested by one-way ANOVA. Statistical significance between the two complex matrixes was tested by *t*-test. Both tests were conducted using R software (R.2.13.0, http://cran.r-project.org). Statistical Differences between groups were declared significant at $p < 0.05$.

3. Results

3.1. Chemical composition of walnut Folch extract

As expected, lipid class analyses confirmed the presence of TAG, DAG, phytosterols, MAG, PL, and FFA in the walnut kernels. The results identified high concentrations of unsaturated fatty acids (~93% w/w of oil), especially of linoleic acid (LA, C18:2, ω6) (average = 69.8 ± 7.4% w/w of oil), in a range similar to those found by other authors (Christopoulos & Tsantili, 2015; Maguire et al., 2004). Palmitic acid (C16:0, average = 6.8 ± 0.7% w/w of oil) was the main saturated fatty acid. In terms of liposoluble vitamins, only vitamin E isomers were detected (average = 41.0 ± 20.7 mg/100 g of oil), with a large majority of γ -tocopherols (average = 36.9 ± 15.6 mg/100 g of oil). The total concentrations of fatty acids and the tocopherol contents of OB extracted from walnut are shown Fig. S1 (supplementary material).

3.2. Characterization of OB minimally-processed structure and impact on oxidative behavior

CLSM was performed to visualize the microstructure of isolated walnut OB. Selective fluorescent probes were used to locate TAG, PL and proteins. As expected, the structure of OB was in agreement with the model proposed by Huang (1994). Fig. 1.A.a. shows OB as a green spherical droplet of TAG surrounded by a red layer of PL embedded in blue proteins. In agreement with the results reported by Gallier, Tate, and Singh (2013), OB ranged in size from 0.5 to 10 μm (Fig. 1.A.b.). The ζ-potential of the isolated solution was also measured to judge the general physical stability of the emulsion. A moderate absolute value of the ζ-potential was evidenced (-34.0 ± 0.6 mV), providing sufficient negative charge to prevent aggregation or flocculation phenomena.

The oxidative behavior of the minimally processed (MP) isolated OB solution was monitored by measuring the formation of primary (PV) and secondary (TBARS) lipid oxidation products during storage. This test was conducted at neutral pH for a period of 20 days of storage at 40 °C. The results are shown in Fig. 2.A (MP OB). PV and TBARS did not change much during the first 10 days of storage, pointing a good stability to oxidation phenomenon. After 10 days, the PV concentration began to increase slightly, followed by TBARS after 12 days, due to the transformation of unstable primary products into secondary products. Nevertheless, the change was limited, indicating good stability of OB in their minimally-processed state.

3.3. Impact of processing on the structure and oxidative behavior of isolated OB

The effects of high-pressure homogenization and heat treatment on

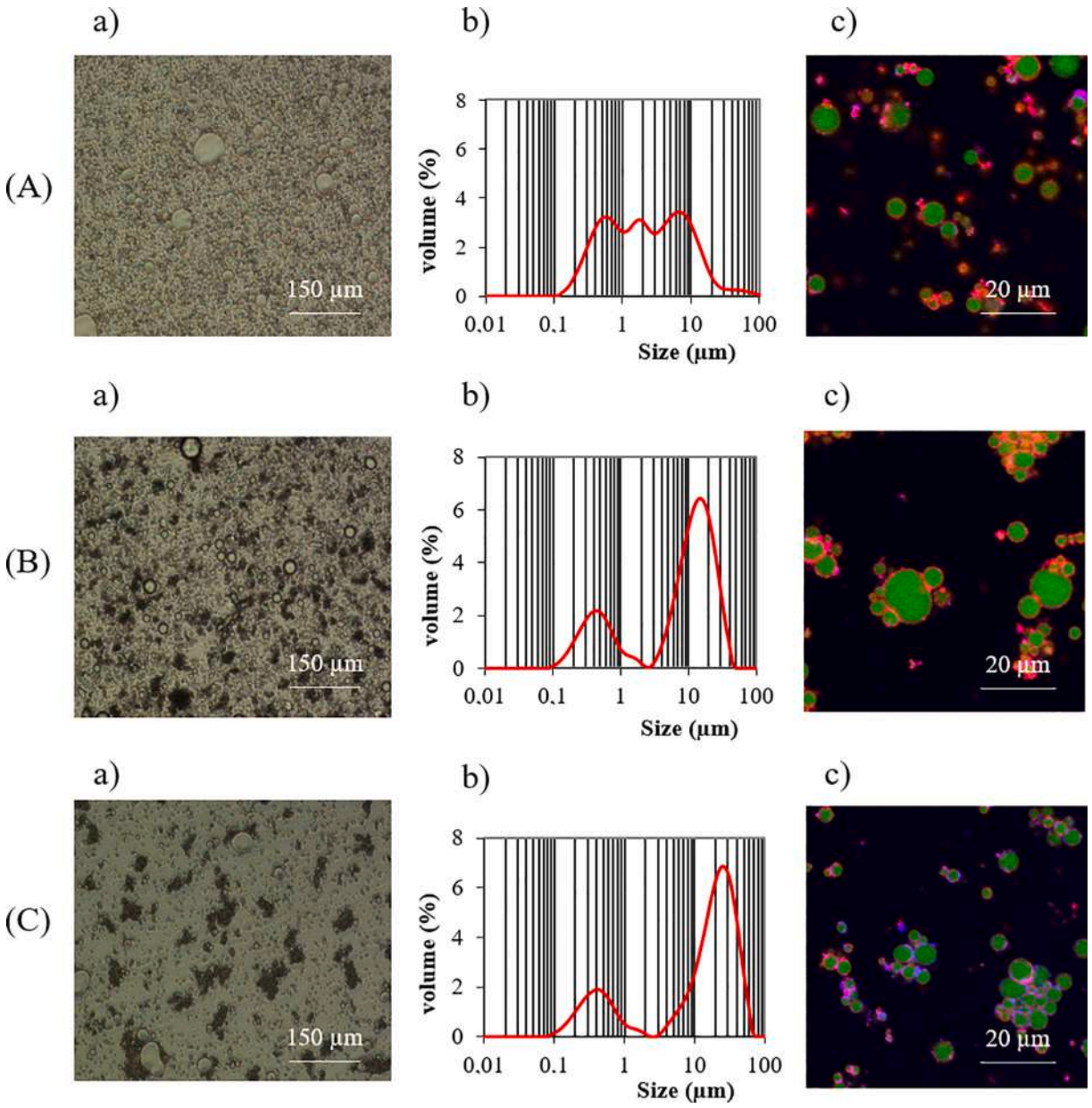

Fig. 1. a) Optical microscopy, b) particle size distribution and c) confocal laser scanning microscopy (red dye: PL, blue dye: proteins, green dye: TAG) of isolated OB emulsions having undergone different treatment(s). (A) MP OB b) trimodal, modes: 7.64 µm, 0.675 µm, 2.13 µm; (B) HHP OB b) bimodal, modes: 16.4 µm, 0.523 µm; and (C) HHPT OB b) bimodal, modes: 31.1 µm, 0.523 µm. (For interpretation of the references to colour in this figure legend, the reader is referred to the web version of this article.)

the structure and oxidative stability of isolated OB were studied (Fig. 2.A - HHP OB, HHPT OB). PV and TBARS of HHP and HHPT OB dispersions increased significantly from the 5th day of the test on, revealing lower chemical stability than for MP OB. The oxidation phenomenon was even faster when the OB had undergone an additional heat treatment (HHPT) downstream. In addition, a sensory test (sniffing, n = 2) revealed the development of negative off-flavors in the products from the 6th day of accelerated storage in the HHPT samples, compared to from the 9th and 15th day for HHP and MP OB respectively. In terms of structure modification, the CLSM images revealed a reorganization of the membrane of the processed OB, and different impacts depending on the process applied (Fig. 1). In the HHP OB sample, fragments of the red and blue layer were missing, indicating membrane damage. In the HHPT OB sample, the membrane was more deteriorated and a blue layer of protein formed, around which objects aggregated. These observations are consistent with the changes in the granulometric profile, in which the largest objects doubled in size (16.4 to 31.1 µm) in isolated HHP OB compared with HHPT OB (Fig. 2). The phenomenon of increasing particle size after homogenization and even more after heat treatment has already been reported in research on walnut OB by Chen, Lu, Yu, Kong, and Hua (2014). It had also been reported in OB from other sources, such as peanuts, on which Zaaboul, Raza, Cao, and Yuanfa (2019) observed severe aggregation and coalescence between OB after HHP followed by sterilization at 95 °C for 15 min.

3.4. Oxidative behavior of OB in complex matrixes (HHPT walnut beverages with or without added sodium caseinates)

Two complex HHPT walnut matrixes with or without 3% wt. of sodium caseinates, representative of commercial walnut-based beverages, were prepared to evaluate the impact of additional ingredients in the complex matrix (fibers, walnut proteins, added emulsifiers…) on the

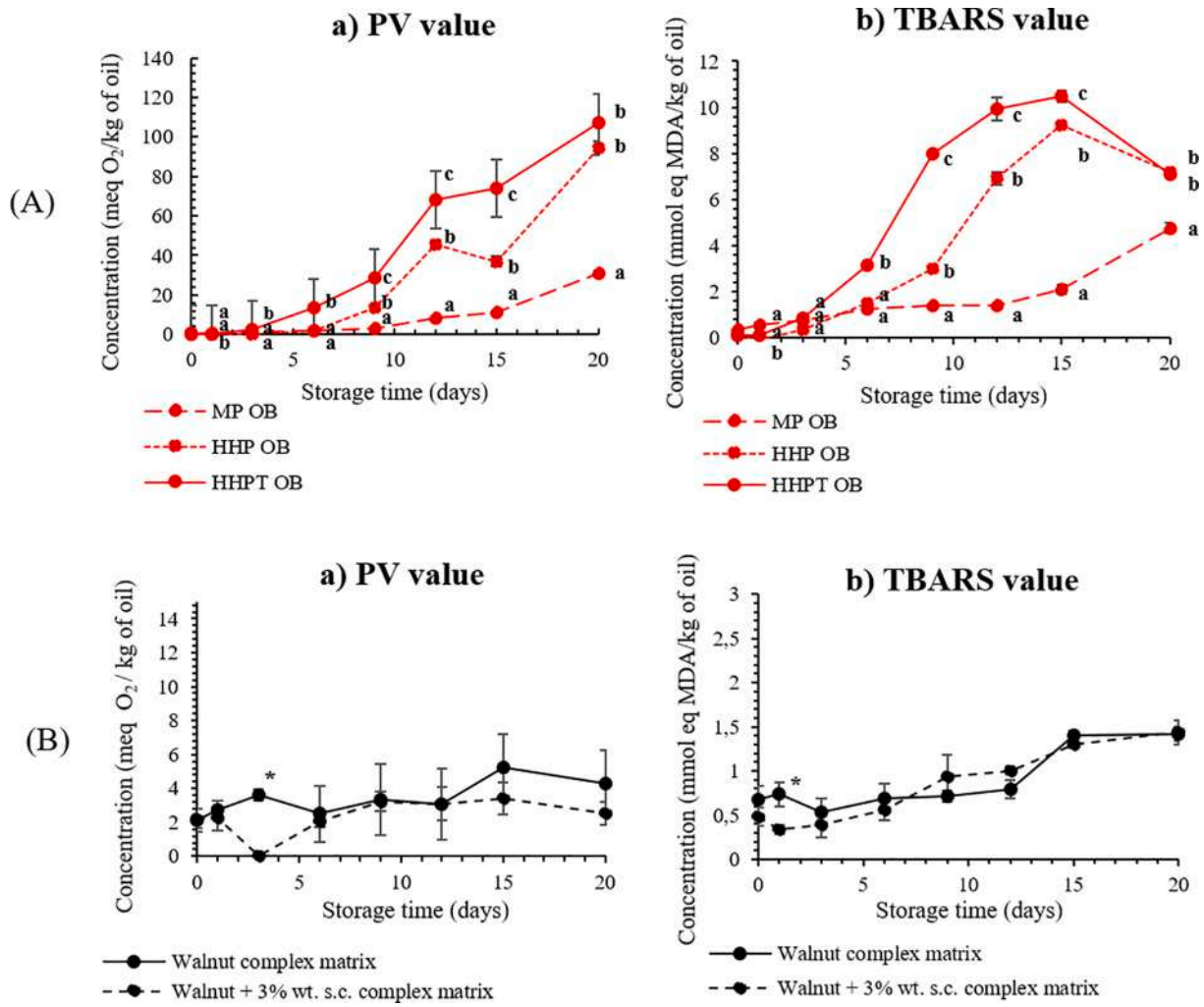

Fig. 2. a) PV and b) TBARS values during 20 days at 40 °C and 110 rpm of (A) processed isolated walnut OB (MP, HHP, HHPT); and (B) walnut complex matrixes with and without 3% wt. of sodium caseinates. Data shown are average of three replicates.

oxidative stability of the system. Good chemical stability of complex matrixes was observed in the short term (10 days) Fig. 2.B. Both complex matrixes, i.e., with and without sodium caseinates remained quite stable to oxidation even after 20 days, with low oxidation values. More precisely, after 20 days of storage at 40 °C, the complex matrix with no sodium caseinates reached a PV value of 4.8 meq O_2/kg of oil compared to 2.5 meq O_2/kg of oil in the complex matrix containing sodium caseinates. The TBARS values for the complex matrixes, with and without sodium caseinate(s), were both at 1.4 mmol eq MDA/kg of oil.

Finally, MP OB and HHPT complex matrixes were quite stable to oxidation. Processing isolated OB with HHP or HHPT treatments decrease their stability to oxidation. In comparison, processing walnut complex matrixes (global walnut juice) with or without additional emulsifiers (sodium caseinate) did not induce such oxidative instability.

3.5. Behavior of minimally-processed (MP) fresh versus oxidized OB at the air/water interface

Since MP OB seem quite stable to oxidation and can be considered as interesting ingredients for human nutrition, we investigated further their behavior at the air/water interface to gather original data about their behavior when dispersed in an emulsion or foam. Comparison of fresh versus oxidized OB could be helpful to food engineers to detect MP OB degradation in a food system. The interfacial behaviors of fresh and oxidized MP OB solutions (PV = 30.8 ± 1.2 meq O_2/kg of oil) were characterized using biophysical tools (tensiometry, ellipsometry, atomic force microscopy). Fig. 3 summarizes the adsorption kinetics and the AFM images obtained for the two samples at 22.5 mg/L of MP OB. The surface pressure of the fresh MP OB increased from 0 mN/m to approximately 13 mN/m (Fig. 3.A.a.) in less than one minute. After this initial step, the surface pressure continued to increase more progressively for a period of 4.5 h until it reached a plateau at 19.8 ± 0.7 mN/m. The ellipsometric angle followed a similar pattern until it reached a final value of 9 ± 0.5°, illustrating the rise of matter at the interface due to the amphiphilic nature of OB. In contrast, in the oxidized MP OB solution diluted at 22.5 mg/L, the final surface pressure and ellipsometric angle were respectively 15 ± 0.8 mN/m and 5.1 ± 0.5°, lower than those in the fresh MP OB solution. This points to a different organization of the particles at the interface as well as the formation of a thinner monolayer in the case of oxidized OB.

After 4.5 h of stabilization of tensiometry and ellipsometry signals, a Langmuir-Blodgett transfer of the interfacial film was performed and imaged using AFM. The resulting images Fig. 3.b. provide information on the interfacial reorganization of OB objects in fresh and oxidized MP OB samples. A background with height variation of 0.6 nm was observed in the image of the fresh MP OB (Fig. 3.A.b.), with the presence of evenly spread generally large protuberances of different lateral sizes and 4 nm in height. Bright "peaks" of 6–8 nm were observed at the center of some protuberances. Smaller bright domains, around 1.5–2 nm in height, were also visible. These smaller domains were not spherical but mainly

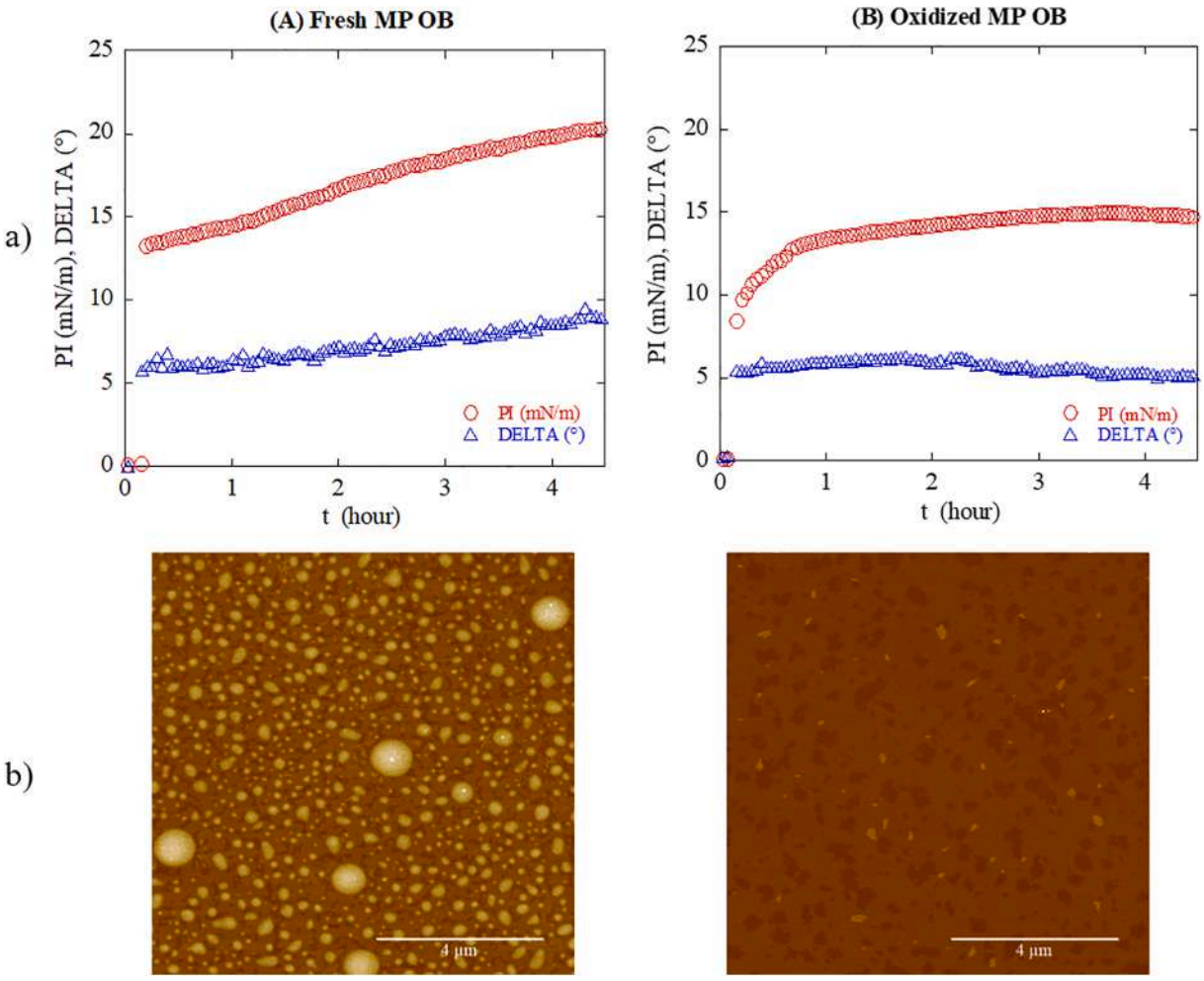

Fig. 3. a) Evolution of surface pressure (red circles; PI, mN/m) and ellipsometric angle (blue triangle; DELTA, °) during the 4.5 h experiments of adsorption on air–water interface and b) monolayer AFM images (10 × 10 µm^2) and size profiles after 4.5 h experiments of isolated solution of (A) Fresh MP OB (PI_f = 20.3 mN/m; $DELTA_f$ = 9.2°) and (B) Oxidized MP OB (PI_f = 14.7 mN/m; $DELTA_f$ = 5.1°) diluted in UP water at 22.5 mg/L. (For interpretation of the references to colour in this figure legend, the reader is referred to the web version of this article.)

had edges. The AFM image of oxidized MP OB emulsion (Fig. 3.B.b) shows a different interfacial organization, with the same background as that of the fresh MP OB solution, but with no protuberance.

To better understand the interfacial structure of MP OB observed in AFM images, a RhoPE dye was incorporated in the MP OB sample to locate the PL in the interfacial film using fluorescence microscopy. The images of the fluorescent sample observed with CLSM (Fig. 4.a) showed that the layer was heterogenous, with continuous fluorescence (RhoPE) in the background, indicating the presence of PL (in red). The AFM images were then recorded on the most homogeneous parts (Fig. 4.b). The AFM images of MP OB with and without the RhoPE were similar, indicating that the fluorescent probes do not affect the interfacial organization of the sample. In addition, as described in the followed section, model solutions were prepared to identify precisely the other components in the interfacial films.

3.6. Behaviors of model solutions at the air/water interface

When OB rise to the air/water interface, they are likely to open and the competing interactions of their three different components will then

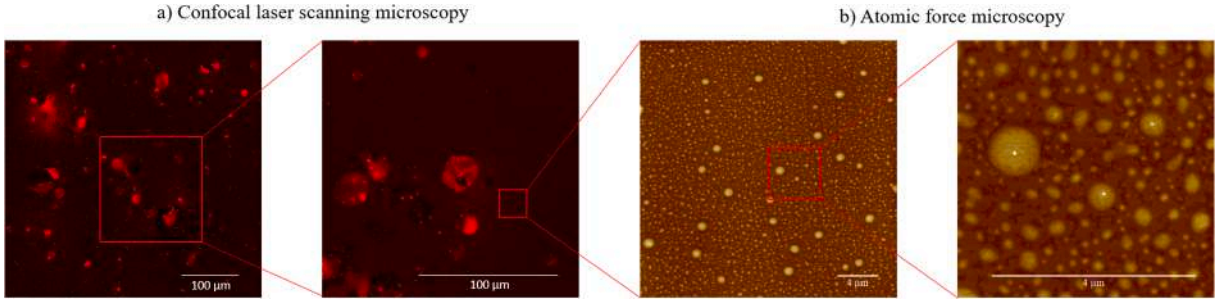

Fig. 4. a) Confocal Laser Scanning Microscopy (448 × 448 µm^2 and 184 × 184 µm^2) and b) Atomic force microscopy images (25 × 25 µm^2 and 5 × 5 µm^2) of monolayer of MP OB isolated solution diluted at 22.5 mg/L in UP water dyed with Rhodamine PE.

determine the physical configuration of the interface: TAG, PL, oleosins but also, probably, some still intact OB. To elucidate the mechanism of organization at the air/water interface, model samples were prepared. These models were initially formulated at 4% wt. of lipid in Tris-HCl solution at pH 7, before being diluted at 22.5 mg/L in UP water. We first compared two model solutions. The first one was formulated with oleosins and TAG, prepared using the same ratio as that found in natural OB (3% wt. oleosins, 95% wt. TAG or commercial walnut oil). The second model solution was only composed by commercial walnut oil (95% wt). In the AFM images of oleo-TAG (Fig. 5.A) and oleo-WOIL (Fig. 5.B), bright "peaks" 4 to 8 nm in height and irregularly shaped domains 1.5–2 nm in height were visible, similar to those present in the AFM image of the MP OB sample. However, the "peaks" did not appear in the WOIL sample (Fig. 5.C), in which irregular protuberances between 2 and 6 nm in height were observed, in addition to domains 1 nm in height, which we assumed to be gel-phase TAG. To complete these observations, the EggPC-WOIL sample containing 2% wt. of EggPC and 95% wt. of commercial walnut oil, was then compared to the WOIL sample. The ellipsometric angle of the EggPC-WOIL sample reached a higher value of 6.3° after 4.5 h, compared to 5.2° for the WOIL sample, reflecting the greater thickness of the interfacial film. The AFM image of the EggPC-WOIL sample (Fig. 5.D) showed a denser background material, with homogeneous protuberances 6 nm in height, compared to the AFM images of the WOIL sample (Fig. 5.C).

4. Discussion

4.1. The good chemical stability of walnut OB is evidenced in both processed complex matrixes and in minimally-processed isolated form

Despite the limited physical stability of walnut beverages (Y. Chen et al., 2014), the results of storage test under accelerated oxidation conditions highlighted the good chemical stability of these plant-based beverages, thus increasing their interest for food applications. The remarkable stability to oxidation of the processed complex matrixes can be explained by the presence of endogenous proteins that form a second protective layer around OB. Additionally, large quantities of AO compounds such as γ-tocopherols, but also various phenolic compounds (polyphenols, phenolic acids such as gallic, ellagic, and flavonoids) as described by Zhang, Liao, Moore, Wu, and Wang (2009), help delay the oxidation phenomenon.

In the complex matrix with added sodium caseinates, we could have expected an enhancement of stability linked to the addition of this emulsifier. Indeed, Haahr and Jacobsen (2008), who evaluated the effect of several types of emulsifiers - including sodium caseinates - on the oxidative stability of 10% wt. oil in water emulsions containing ω3 rich fish oil, demonstrated an antioxidant (AO) effect of sodium caseinates. In their study, the emulsion stabilized by sodium caseinates was shown to oxidize more slowly than the emulsion stabilized with Tween 80, despite the much more negative ζ -potential of sodium caseinates at pH 7. The difference in oxidative stability was associated with the ability of sodium caseinates to chelate iron (Sugiarto et al., 2010) and to form a 10-nm-thick layer at the surface of dispersed oil droplet, thus protecting unsaturated FA from oxidation (Hu et al., 2003). In our study, sodium caseinates did not appear to provide significant additional oxidative stability to the walnut complex matrix, suggesting that the system is already relatively stable with respect to oxidation.

Similarly, to processed walnut complex matrixes, MP OB exhibited good chemical stability over the first 10 days of storage, thanks to their native structure and fat-soluble AO content. The limited difference in the concentration of oxidation products indicates that isolating OB did not affect their protection capacity against oxidation, underlining the interest of using these minimally-processed compounds in food applications. Similar results were obtained on soybean OB by Kapchie et al. (2013), who found low oxidation of isolated OB suspensions without the presence of prooxidant metal species at physiological pH and after 12 days of storage at 60 °C, while the PV was 14 meq O_2/kg and TBARS was 0.4 mmol eq MDA/kg. Ding, Xu, Qi, Jiang, and Sui (2018) also studied the chemical stability of isolated OB dispersions for 14 days in the dark at room temperature. Their results confirmed the good stability to

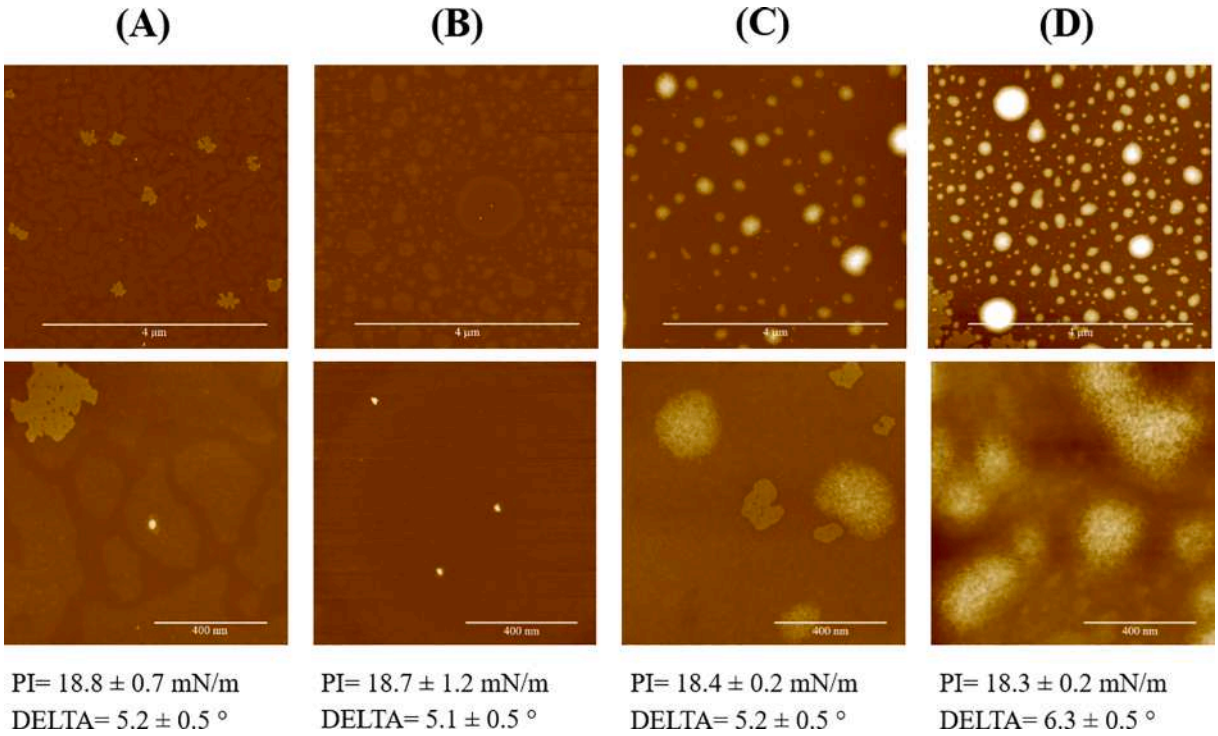

Fig. 5. AFM images (5 × 5 µm^2 and 1 × 1 µm^2) of Langmuir-Blodgett films of 22.5 mg/L of a) oleo-TAG; b) Oleo-WOIL; c) WOIL; and d) EggPC-WOIL after 4.5 h of acquisition. Final values of surface pressure (PI, mN/m) and ellipsometric angle (DELTA, °) were recorded at 4.5 h of acquisition when the films were transferred on mica plate.

oxidation of the emulsions, with low PV and TBARS of 7 meq O_2/kg and 0.003 mmol eq MDA/kg respectively after 14 days.

4.2. Processed OB (HHP and HHPT) were less stable to oxidation than MP OB

The processing operations, i.e. homogenization and heat-treatment, resulted in the reorganization of the OB membrane, increasing exchanges with reactive species. This change in the membrane led to a significant increase in oxidation compared to MP OB, despite the similar chemical composition of the systems. These results confirm the importance of the native assembly in the chemical stability of OB, underlining the need to rethink food processing to insure better preservation of natural assemblies and their properties when these assemblies are used in quite purified forms.

Overall, the oxidation of these MP OB reduced the internal cohesion of the OB and consequently also that of its components, leading to a different interfacial organization.

4.3. The adsorption mechanism of isolated MP OB was determined at the air/water interface and differ from the one proposed for soybean OB

The combination of simultaneous ellipsometry, tensiometry and AFM results of MP OB and model solutions made it possible to examine the behavior of minimally-processed walnut OB at the air/water interface. Overall, biophysical results indicate that isolated fresh MP OB retained their native microstructure when adsorbed to the air/water interface. The model solutions containing oleosins (3% wt.) led us attribute the 6–12 nm height "peaks" on the fresh OB AFM images to the presence of oleosins. Indeed, a height of 12 nm was determined for soybean oleosins by Zielbauer et al. (2018) using small angle neutron scattering, which correspond to the height of the "peaks" obtained in AFM size profiles. Big bright protuberances 4 nm in height visible on the AFM images of MP OB were identified as oleosins, PL and TAG assemblies, that remained very cohesive due to hydrophobic interactions.

In contrast, the structural modification of the membrane caused by oxidation reduce cohesion between the different components, as revealed by the results of the biophysical analysis. The final ellipsometric angle and surface pressure were indeed lower than in the fresh MP OB sample. The AFM images reinforced these results, showing a different interfacial organization when the objects were oxidized, in particular the absence of TAG, PL and oleosins assemblies. Smaller domains (1 nm in height) were probably lipid domains in crystalline phase, composed of palmitic and stearic saturated FA. This observation tends to confirm the thermotropic crystalline mesophase of OB membrane proposed by Nikiforidis (2019) and suggests that oxidation led to the

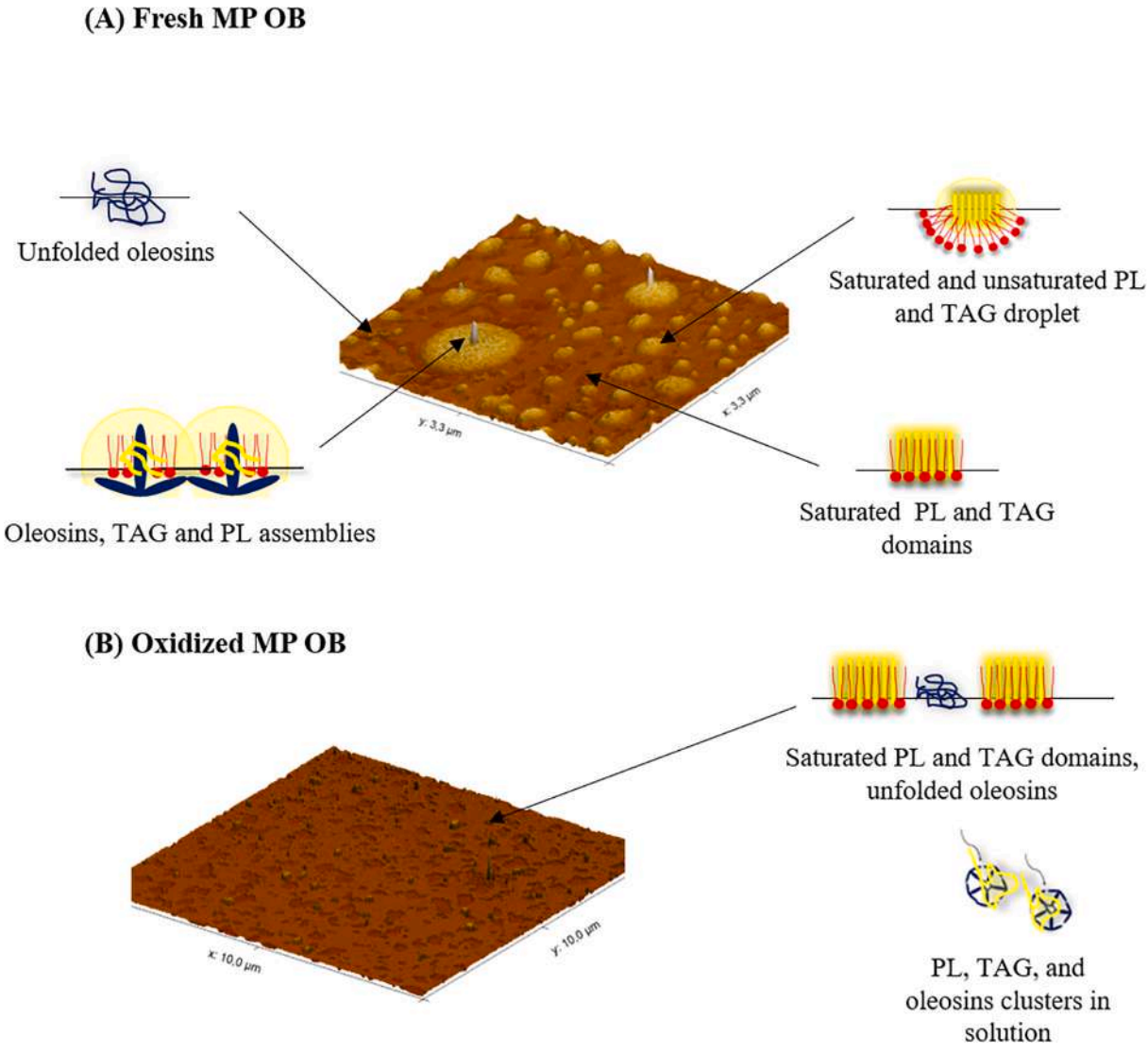

Fig. 6. Proposed mechanisms of OB organization at the air–water interface for (A) Fresh MP OB; and (B) Oxidized MP OB.

solubilization of oxidized unsaturated TAG and PL. Such solubilized oxidized entities may then participate in the diffusion of oxidation between assemblies.

Waschatko et al. (2012) proposed different models for the structural organization of soybean OB interface. Fig. 6.A presents a model for the organization of walnut OB at interfaces based on the models of Waschatko et al., emphasizing the new understanding enabled by the results we obtained in the present study. When the isolated fresh OB solution is deposited in the Langmuir trough, OB rise to the interface before opening. When the lateral surface pressure is sufficient to maintain cohesion of the components, they remain assembled and form protuberances, visible at the interface, with the central hydrophobic domain of oleosin oriented toward the surface. In addition, mixtures of unsaturated and saturated fats can form fat droplets, as confirmed by the presence of irregularly shaped globules in the AFM images of isolated fresh MP OB. Low height domains of saturated TAG and PL complete the interface background. When the membrane structure is altered by protein cleavage (Waschatko et al., 2012) or by oxidation, the lateral pressure is no longer sufficient to maintain the assemblies of oleosins, TAG and PL, as illustrated in the model proposed in Fig. 6.B. The rigid native "T" conformation of oleosins is no longer preserved, and some oleosins are presumed to unfold at the interface or are solubilized as protein-lipid clusters. Like in the fresh sample, saturated PL and TAG domains also form at the interface, but oxidation is responsible for the solubilization of unsaturated lipids, leading to the disappearance of fat globule in the AFM images of the oxidized sample.

This better understanding of the interfacial behavior of MP OB from different botanical sources will ease the development of innovative emulsions or foams in which MP OB can be used as functional ingredients. They will be specifically useful to design heterogeneous systems in which OB will be used as emulsifiers.

5. Conclusions

Oxidation tests and biophysical tools were used to study the oxidative and interfacial behavior of walnut OB in different matrixes. Strong chemical stability of the complex walnut matrixes was evidenced under accelerated oxidation conditions, thanks to the presence of many endogenous proteins and antioxidant compounds. Isolation of OB from the complex matrix did not alter their protection against oxidation, thanks to their native assembly as well their fat-soluble antioxidant content. Nevertheless, processing of OB accelerated their chemical oxidation.

The organizational mechanism at the air/water interface of walnut MP OB is demonstrated. When MP OB adsorb at an air/water interface, the good cohesive ability of their native assembly allows them to keep intact their microstructure. Oxidation was shown to alter this internal cohesion of OB by structural modification of the membrane.

Taken together, our results show that when OB are incorporated in the structure of new food products, their chemical and physical stability during the design process should be taken into consideration. Indeed, alteration of the physical structure of OB during processing may affect their chemical stability during storage and hence the quality of the final product expected by the consumer. This finding underlines the need to rethink food processing to preserve natural assemblies and their beneficial properties.

Declaration of Competing Interest

The authors declare that they have no known competing financial interests or personal relationships that could have appeared to influence the work reported in this paper.

Acknowledgments

The authors acknowledge Carine Alcon and the imaging facility MRI ('*Montpellier Ressources Imagerie*', Montpellier, France), member of the national infrastructure France-BioImaging infrastructure supported by the French National Research Agency (ANR-10-INBS-04, «Investments for the future»). We also would like to thank the MRic platform ('Microscopy Rennes Imaging Center', Rennes, France) for technical assistance with the confocal laser scanning microscope. Finally, the 2CBioMIF platform (ScanMAT-UMS 2001, Rennes, France) is acknowledged for allowing the biophysical characterization of the samples presented in this article.

C. Bourlieu, V. Vié and J. Kergomard were responsible for the design and the content of the manuscript. All the authors participated in the experimental design, the collection, the interpretation of data. J. Kergomard wrote the manuscript and all the authors were involved in reviewing and correcting the manuscript. All the authors approved submission of the final article.

Appendix A. Supplementary data

Supplementary data to this article can be found online at https://doi.org/10.1016/j.foodchem.2021.129880.

References

Barre, A., Simplicien, M., Cassan, G., Benoist, H., & Rougé, P. (2018). Oil bodies (oleosomes): Occurrence, structure, allergenicity. *Revue Française d'Allergologie, 58* (8), 574–580. https://doi.org/10.1016/j.reval.2018.10.005.

Berge, B., & Renault, A. (1993). Ellipsometry Study of 2D Crystallization of 1-Alcohol Monolayers at the Water Surface. *Europhysics Letters (EPL), 21*(7), 773–777. https://doi.org/10.1209/0295-5075/21/7/010.

Bettini, S., Santino, A., Giancane, G., & Valli, L. (2014). Reconstituted oil bodies characterization at the air/water and at the air/oil/water interfaces. *Colloids and Surfaces B: Biointerfaces, 122*, 12–18. https://doi.org/10.1016/j.colsurfb.2014.06.044.

Bourlieu, C., Mahdoueni, W., Paboeuf, G., Gicquel, E., Ménard, O., Pezennec, S., … Vié, V. (2020). Physico-chemical behaviors of human and bovine milk membrane extracts and their influence on gastric lipase adsorption. *Biochimie, 169*, 95–105. https://doi.org/10.1016/j.biochi.2019.12.003.

Bourlieu, C., Ménard, O., De La Chevasnerie, A., Sams, L., Rousseau, F., Madec, M.-N., … Dupont, D. (2015). The structure of infant formulas impacts their lipolysis, proteolysis and disintegration during in vitro gastric digestion. *Food Chemistry, 182*, 224–235. https://doi.org/10.1016/j.foodchem.2015.03.001.

Bourlieu, C., Rousseau, F., Briard-Bion, V., Madec, M.-N., & Bouhallab, S. (2012). Hydrolysis of native milk fat globules by microbial lipases: Mechanisms and modulation of interfacial quality. *Food Research International, 49*(1), 533–544. https://doi.org/10.1016/j.foodres.2012.07.036.

Chen, Y., Lu, Y., Yu, A., Kong, X., & Hua, Y. (2014). Stable mixed beverage is produced from walnut milk and raw soymilk by homogenization with subsequent heating. *Food Science and Technology Research, 20*(3), 583–591. https://doi.org/10.3136/fstr.20.583.

Chen, B., McClements, D. J., Gray, D. A., & Decker, E. A. (2012). Physical and oxidative stability of pre-emulsified oil bodies extracted from soybeans. *Food Chemistry, 132* (3), 1514–1520. https://doi.org/10.1016/j.foodchem.2011.11.144.

Christopoulos, M. V., & Tsantili, E. (2015). Oil composition in stored walnut cultivars—Quality and nutritional value. *European Journal of Lipid Science and Technology, 117*(3), 338–348. https://doi.org/10.1002/ejlt.201400082.

De Chirico, S., di Bari, V., Romero Guzmán, M. J., Nikiforidis, C. V., Foster, T., & Gray, D. (2020). Assessment of rapeseed oil body (oleosome) lipolytic activity as an effective predictor of emulsion purity and stability. *Food Chemistry, 316*, 126355. https://doi.org/10.1016/j.foodchem.2020.126355.

Ding, J., Xu, Z., Qi, B., Jiang, L., & Sui, X. (2018). Physicochemical and oxidative stability of a soybean oleosome-based emulsion and its in vitro digestive fate as affected by (−)-epigallocatechin-3-gallate. *Food & Function, 9*(12), 6146–6154. https://doi.org/10.1039/C8FO01215F.

Folch, J. (1957). A simple method for the isolation and purification of total lipids from animal tissues. *Journal of Biological Chemistry, 226*, 497–509.

Frandsen, G. I., Mundy, J., & Tzen, J. T. C. (2001). Oil bodies and their associated proteins, oleosin and caleosin. *Physiologia Plantarum, 112*(3), 301–307. https://doi.org/10.1034/j.1399-3054.2001.1120301.x.

Gallier, S., Tate, H., & Singh, H. (2013). In Vitro gastric and intestinal digestion of a walnut oil body dispersion. *Journal of Agricultural and Food Chemistry, 61*(2), 410–417. https://doi.org/10.1021/jf303456a.

Genot, C., & Michalski, M.-C. (2010). Impact métabolique des structures et de l'oxydation des lipides dans les aliments. Innovations Agronomiques (10), 43-67. (2010). http://agris.fao.org/agris-search/search.do?recordID=LV2016008646.

Ghaderi-Ghahfarrokhi, M., Sadeghi-Mahoonak, A. R., Alami, M., & Mousavi Khanegah, A. (2017). Effect of processing treatments on polyphenol removal from kernel of two Iranian acorns varieties. *International Food Research Journal, 24*(1), 86–93.

Ghani, M. A., Barril, C., Bedgood, D. R., & Prenzler, P. D. (2017). Measurement of antioxidant activity with the thiobarbituric acid reactive substances assay. *Food Chemistry, 230*, 195–207. https://doi.org/10.1016/j.foodchem.2017.02.127.

Haahr, A.-M., & Jacobsen, C. (2008). Emulsifier type, metal chelation and pH affect oxidative stability of n-3-enriched emulsions. *European Journal of Lipid Science and Technology, 110*(10), 949–961. https://doi.org/10.1002/ejlt.v110:1010.1002/ejlt.200800035.

Hayes, D., Angove, M. J., Tucci, J., & Dennis, C. (2016). Walnuts (Juglans regia) chemical composition and research in human health. *Critical Reviews in Food Science and Nutrition, 56*(8), 1231–1241. https://doi.org/10.1080/10408398.2012.760516.

Huang, A. H. C. (1994). Structure of plant seed oil bodies. *Current Opinion in Structural Biology, 4*(4), 493–498. https://doi.org/10.1016/S0959-440X(94)90210-0.

Kapchie, V. N., Hauck, C. C., Wang, H., & Murphy, P. A. (2011). Process improvement for semipurified oleosomes on a pilot-plant scale. *Journal of Food Science, 76*(6), C853–C860. https://doi.org/10.1111/j.1750-3841.2011.02278.x.

Kapchie, V. N., Yao, L., Hauck, C. C., Wang, T., & Murphy, P. A. (2013). Oxidative stability of soybean oil in oleosomes as affected by pH and iron. *Food Chemistry, 141*(3), 2286–2293. https://doi.org/10.1016/j.foodchem.2013.05.018.

Khor, V. K., Shen, W.-J., & Kraemer, F. B. (2013). Lipid Droplet Metabolism. *Current opinion in clinical nutrition and metabolic care, 16*(6), 632–637. https://doi.org/10.1097/MCO.0b013e3283651106.

Maguire, L. S., O'Sullivan, S. M., Galvin, K., O'Connor, T. P., & O'Brien, N. M. (2004). Fatty acid profile, tocopherol, squalene and phytosterol content of walnuts, almonds, peanuts, hazelnuts and the macadamia nut. *International Journal of Food Sciences and Nutrition, 55*(3), 171–178. https://doi.org/10.1080/09637480410001725175.

Mihaljević, B., Katušin-Ražem, B., & Ražem, D. (1996). The reevaluation of the ferric thiocyanate assay for lipid hydroperoxides with special considerations of the mechanistic aspects of the response. *Free Radical Biology and Medicine, 21*(1), 53–63. https://doi.org/10.1016/0891-5849(95)02224-4.

Miraliakbari, H., & Shahidi, F. (2008). Lipid class compositions, tocopherols and sterols of tree nut oils extracted with different solvents. *Journal of Food Lipids, 15*(1), 81–96. https://doi.org/10.1111/j.1745-4522.2007.00104.x.

Moustiés, C., Bourlieu, C., Barea, B., Servent, A., Alter, P., Lebrun, M., … Avallone, S. (2019). Lipid composition and state of oxidation of fortified infant flours in low-income countries are not optimal and strongly affected by the time of storage. *European Journal of Lipid Science and Technology, 121*(11), 1900173. https://doi.org/10.1002/ejlt.v121.1110.1002/ejlt.201900173.

Napier, J. A., Beaudoin, F., Tatham, A. S., Alexander, L. G., & Shewry, P. R. (2001). The seed oleosins : Structure, properties and biological role. In Advances in Botanical Research (Vol. 35, p. 111-138). Academic Press. DOI:10.1016/S0065-2296(01)35005-X.

Nikiforidis, C. V. (2019). Structure and functions of oleosomes (oil bodies). *Advances in Colloid and Interface Science, 274*, 102039. https://doi.org/10.1016/j.cis.2019.102039.

Nikiforidis, C. V., Matsakidou, A., & Kiosseoglou, V. (2014). Composition, properties and potential food applications of natural emulsions and cream materials based on oil bodies. *RSC Advances, 4*(48), 25067–25078. https://doi.org/10.1039/C4RA00903G.

Nuchi, C. D., Hernandez, P., McClements, D. J., & Decker, E. A. (2002). Ability of lipid hydroperoxides to partition into surfactant micelles and alter lipid oxidation rates in emulsions. *Journal of Agricultural and Food Chemistry, 50*(19), 5445–5449. https://doi.org/10.1021/jf020095j.

Ohkawa, H., Ohishi, N., & Yagi, K. (1979). Assay for lipid peroxides in animal tissues by thiobarbituric acid reaction. *Analytical Biochemistry, 95*(2), 351–358. https://doi.org/10.1016/0003-2697(79)90738-3.

Piombo, G., Barouh, N., Barea, B., Boulanger, R., Brat, P., Pina, M., & Villeneuve, P. (2006). Characterization of the seed oils from kiwi (Actinidia chinensis), passion fruit (Passiflora edulis) and guava (Psidium guajava). *Oléagineux, Corps Gras, Lipides, 13*(2–3), 195–199. https://doi.org/10.1051/ocl.2006.0026.

Samdani, G. K., McClements, D. J., & Decker, E. A. (2018). Impact of phospholipids and tocopherols on the oxidative stability of soybean oil-in-water emulsions. *Journal of Agricultural and Food Chemistry, 66*(15), 3939–3948. https://doi.org/10.1021/acs.jafc.8b00677.

Shantha, N. C., & Decker, E. A. (1994). Rapid, sensitive, iron-based spectrophotometric methods for determination of peroxide values of food lipids. *Journal of AOAC International, 77*(2), 421–424. https://doi.org/10.1093/jaoac/77.2.421.

Shimada, T. L., Hayashi, M., & Hara-Nishimura, I. (2018). Membrane dynamics and multiple functions of oil bodies in seeds and leaves. *Plant Physiology, 176*(1), 199–207. https://doi.org/10.1104/pp.17.01522.

Simopoulos, A. P. (2002). The importance of the ratio of omega-6/omega-3 essential fatty acids. *Biomedicine & Pharmacotherapy = Biomedecine & Pharmacotherapie, 56*(8), 365–379. https://doi.org/10.1016/s0753-3322(02)00253-6.

Tzen, J., Cao, Y., Laurent, P., Ratnayake, C., & Huang, A. (1993). Lipids, proteins, and structure of seed oil bodies from diverse species. *Plant Physiology, 101*(1), 267–276. https://doi.org/10.1104/pp.101.1.267.

Venkatachalam, M., & Sathe, S. K. (2006). Chemical composition of selected edible nut seeds. *Journal of Agricultural and Food Chemistry, 54*(13), 4705–4714. https://doi.org/10.1021/jf0606959.

Villière, A. (2005). Approche physico-chimique et sensorielle de l'oxydation des lipides dans des émulsions stabilisées par des protéines [These de doctorat, Nantes]. https://www.theses.fr/2005NANT2042.

Walther, T. C., & Farese, R. V. (2012). Lipid droplets and cellular lipid metabolism. *Annual Review of Biochemistry, 81*(1), 687–714. https://doi.org/10.1146/annurev-biochem-061009-102430.

Waschatko, G., Schiedt, B., Vilgis, T. A., & Junghans, A. (2012). Soybean oleosomes behavior at the air-water interface. *The Journal of Physical Chemistry B, 116*(35), 10832–10841. https://doi.org/10.1021/jp211871v.

White, D. A., Fisk, I. D., Mitchell, J. R., Wolf, B., Hill, S. E., & Gray, D. A. (2008). Sunflower-seed oil body emulsions: Rheology and stability assessment of a natural emulsion. *Food Hydrocolloids, 22*(7), 1224–1232. https://doi.org/10.1016/j.foodhyd.2007.07.004.

Zaaboul, F., Raza, H., Cao, C., & Yuanfa, L. (2019). The impact of roasting, high pressure homogenization and sterilization on peanut milk and its oil bodies. *Food Chemistry, 280*, 270–277. https://doi.org/10.1016/j.foodchem.2018.12.047.

Zhang, Z., Liao, L., Moore, J., Wu, T., & Wang, Z. (2009). Antioxidant phenolic compounds from walnut kernels (Juglans regia L.). *Food Chemistry, 113*(1), 160–165. https://doi.org/10.1016/j.foodchem.2008.07.061.

Zhao, L., Chen, Y., Yan, Z., Kong, X., & Hua, Y. (2016). Physicochemical and rheological properties and oxidative stability of oil bodies recovered from soybean aqueous extract at different pHs. *Food Hydrocolloids, 61*, 685–694. https://doi.org/10.1016/j.foodhyd.2016.06.032.

Zielbauer, B. I., Jackson, A. J., Maurer, S., Waschatko, G., Ghebremedhin, M., Rogers, S. E., … Vilgis, T. A. (2018). Soybean oleosomes studied by small angle neutron scattering (SANS). *Journal of Colloid and Interface Science, 529*, 197–204. https://doi.org/10.1016/j.jcis.2018.05.080.

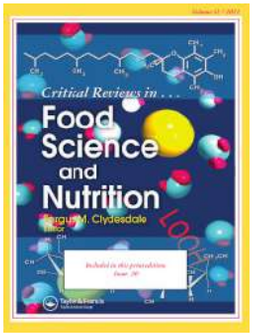

Critical Reviews in Food Science and Nutrition

ISSN: (Print) (Online) Journal homepage: https://www.tandfonline.com/loi/bfsn20

Digestibility and oxidative stability of plant lipid assemblies: An underexplored source of potentially bioactive surfactants?

Jeanne Kergomard, Frédéric Carrière, Nathalie Barouh, Pierre Villeneuve, Véronique Vié & Claire Bourlieu

To cite this article: Jeanne Kergomard, Frédéric Carrière, Nathalie Barouh, Pierre Villeneuve, Véronique Vié & Claire Bourlieu (2021): Digestibility and oxidative stability of plant lipid assemblies: An underexplored source of potentially bioactive surfactants?, Critical Reviews in Food Science and Nutrition, DOI: 10.1080/10408398.2021.2005532

To link to this article: https://doi.org/10.1080/10408398.2021.2005532

Published online: 29 Nov 2021.

CRITICAL REVIEWS IN FOOD SCIENCE AND NUTRITION
https://doi.org/10.1080/10408398.2021.2005532

Taylor & Francis
Taylor & Francis Group

REVIEW

Digestibility and oxidative stability of plant lipid assemblies: An underexplored source of potentially bioactive surfactants?

Jeanne Kergomard[a,b], Frédéric Carrière[c], Nathalie Barouh[a*], Pierre Villeneuve[a#], Véronique Vié[b] and Claire Bourlieu[a*]

[a]INRAE/UM/Institut Agro, UMR 1208 IATE, Montpellier France; [b]IPR Institute of Physics, UMR UR1 CNRS 6251, Rennes 1 University, Rennes, France; [c]Aix Marseille Université, CNRS, UMR7281 Bioénergétique et Ingénierie des Protéines, Marseille, France

ABSTRACT

Most lipids in our diet come under the form of triacylglycerols that are often redispersed and stabilized by surfactants in processed foods. In plant however, lipid assemblies constitute interesting sources of natural bioactive and functional ingredients. In most photosynthetic sources, polar lipids rich in ω3 fatty acids are concentrated. The objective of this review is to summarize all the knowledge about the physico-chemical composition, digestive behavior and oxidative stability of plant polar lipid assemblies to emphasize their potential as functional ingredients in human diet and their potentialities to substitute artificial surfactants/antioxidants. The specific composition of plant membrane assemblies is detailed, including plasma membranes, oil bodies, and chloroplast; emphasizing its concentration in phospholipids, galactolipids, peculiar proteins, and phenolic compounds. These molecular species are hydrolyzed by specific digestive enzymes in the human gastrointestinal tract and reduced the hydrolysis of triacylglycerols and their subsequent absorption. Galactolipids specifically can activate ileal break and intrinsically present an antioxidant (AO) activity and metal chelating activity. In addition, their natural association with phenolic compounds and their physical state (Lα state of digalactosyldiacylglycerols) in membrane assemblies can enhance their stability to oxidation. All these elements make plant membrane molecules and assemblies very promising components with a wide range of potential applications to vectorize ω3 polyunsaturated fatty acids, and equilibrate human diet.

KEYWORDS

Plant membrane; polar lipids; digestive lipolysis; antioxidants; surfactants

1. Introduction

Lipids are very important nutrients for human health but also for living's growth, playing several key roles in the homeostatic regulation of metabolism in both plants and animals, in particular through three main functions: (i) Lipids can be used for energy storage in their neutral form (triacylglycerols, TAG); (ii) lipids also play a crucial role in membrane structure. Indeed, polar lipids possess amphipathic structure and self-association properties, which allow them to define the cells and to segregate cellular compounds into organelles; (iii) finally, many lipids are signaling molecules or at the basis of primary and secondary messengers such as eicosanoids or resolvins, which play a key role in signal transduction and molecular recognition processes.

The digestion of lipids from the diet must provide two essential polyunsaturated fatty acids (PUFA): linoleic (LA, C18:2, ω6) and α-linolenic acid (ALA, C18:3, ω3). These two essential fatty acids (FA) are at the basis of an elongation and desaturation pathway, resulting in highly bioactive long chain (LC) PUFA such as arachidonic acid (ARA, C20:4, ω6), eicosapentaenoic acid (EPA, C20:5, ω3) and docosahexaenoic acid (DHA, C22:6, ω3). Nevertheless, the synthesis pathway of EPA and DHA from ALA exhibit a low conversion efficiency. Thus it is also recommended to consume foods rich in its two essential FA. These LC-PUFA play indeed a crucial role in the homeostatic regulation of the body by producing signaling oxygenated lipids called eicosanoids and pro-resolving lipid mediators (such as resolvins, protectins and maresins) (Saini and Keum 2018). ω3 and ω6 FA exhibit opposite metabolic effects and compete for the synthesis of lipid mediators through their biosynthetic enzymes. Thus, a balanced consumption of ω3 and ω6, with an optimal ω6/ω3 ratio of 4 and an adequate intake of each type of FA is recommended (Anomynous 2011).

Nevertheless, over the last three decades, the ω6/ω3 ratio has considerably increased in Western diets, going from 1:1 up to 20:1 in very rich diets, due to a significant increase in the intake of ω6 and a concomitant decrease in the intake of ω3 (El Hadi et al. 2019). Meanwhile, an increase in overweight and obesity incidence has been observed. This increase is certainly multifactorial, but very likely linked to metabolic imbalances, including changes in the FA composition of diets. It is therefore essential to

CONTACT Claire Bourlieu claire.bourlieu-lacanal@inrae.fr
*Present address: CIRAD, UMR QUALISUD, F34398 Montpellier-France.
#Present address: Qualisud, Univ Montpellier, Avignon Université, CIRAD, Institut Agro, Université de La Réunion, Montpellier, France.

maintain our efforts and set up nutritional strategies to decrease the ω6/ω3 ratio in our diets and recover normal homeostasis, in particular by increasing our intake of LC-PUFA ω3, such as EPA and DHA, while limiting the intake of total lipids (Enos et al. 2014). Such strategy can be achieved by favoring fish rather than meat in the diet, but also by increasing our ω3 rich vegetable oils intake. More recently, it has also been proposed to enrich our diet with green vegetal-derived lipids, as an alternative source of essential PUFA (Lane et al. 2014).

Indeed, some plant membrane assemblies or polar lipids blends are able to improve the assimilation of specific ω3 PUFA, that are better absorbed under the form of phospholipids (PL) than TAG (Robert, Couëdelo, Vaysse, et al. 2020). However, this better absorption has been proved for long chain ω3 PUFA but disproved for ALA (Robert et al. 2021). In addition to PL, plant and algae membranes also include galactolipids (GL), associated to micronutrients, whose consumption leads to the production of essential ω3 (Sahaka et al. 2020). The great abundance of plants and algae on earth explains that these GL represent the major class of acylglycerol lipids in nature, and thus the principal source of FA (80% versus 20% in PL and vegetal TAG), including essential PUFA (Gounaris and Barber 1983). Furthermore, green vegetal and seeds such as walnuts or flax contain significant quantities of ALA (60–70% wt. of total fatty acids) (Saini and Keum 2018) and are rich in phenolic compounds and other phytochemical derivatives.

As a consequence, the consumption of PUFA-rich vegetal drinks has grown steadily in recent years. This trend is boosted by new nutritional recommendations and an awareness of the beneficial environmental and health effect of plant derived fats and proteins. Vegetal drinks are generally under the form of emulsions, containing proteins, fibers but also oil bodies, which are lipoprotein assemblies composed of a TAG core encapsulated in a phospholipid-protein monolayer. The interest of these vegetal beverages is that they naturally contain surfactant molecules that can stabilize these emulsions while presenting a good PUFA and global nutritional profile. If seed-based beverages have been developed, they are not very diversified in terms of botanical sources and the leafy parts of plants remain, to date, under-exploited in the field of human nutrition. In addition to their fibers and bioactive pigments contents, these leafy parts do contain lipids although it is most of the time ignored – many leafy juices are for instance wrongly labeled "lipid-free." The digestibility of these specific plant lipids is also poorly known, in particular concerning GL, despite their human consumption can reach 200 mg by day (De Caro et al. 2008) and could be boosted up by using plant assemblies as functional ingredients.

However, in order to use properly plant polar lipids and lipoproteic assemblies, it is crucial to understand their digestive behavior and their oxidation stability. It is thus the objective of the present review to summarize most of the recent data about plant lipid assemblies (membrane and OB), their physico-chemical composition and digestive behavior. These elements will be detailed in three complementary paragraphs to unveil the potentials of these lipids as vectors of omega 3 PUFA and to modulate the digestion in given nutritional targets.

2. Plant membrane assemblies' description

2.1. Plasma membranes of plant cells

The plasma membrane is the most complex plant cell membrane, containing lipids and proteins in proportions that vary according to the type of cell and plant species. The plasma membrane defines an interface between cells and their environment. Although many cellular functions are performed by protein compounds (e.g., signal recognition or transduction), lipids also play a crucial role in the membrane or in the signal transduction. Three main classes of lipids are present in the plasma membrane of plant cells, namely PL (28–50% wt.), sphingolipids (6–30% wt.), and sterols (23–52% wt.). The proportions and acyl chain lengths of these lipids influence the physical state and the properties of the formed lipid bilayer (Furt, Simon-Plas, and Mongrand 2011). Compared to other cell membranes in the animal kingdom, plant plasma membranes are predominantly rich in phytosterols, with a sterol/PL ratio ranging from 0.6 to 1.5 wt.

The structural PL composing the plant plasma membrane are mainly phosphatidylcholine (PC) and phosphatidylethanolamine (PE) (68–80% wt.), as well as phosphatidylglycerol (PG), phosphatidylinositol (PI), phosphatidylserine (PS) and phosphatidic acid (PA); regarding FA composition, the membrane is mainly composed of palmitic acid (C16:0, 18–70% wt.) and LA (C18:2, ω6, 20–60% wt.), as well as ALA (C18:3, ω3, 7–26% wt.) (Furt, Simon-Plas, and Mongrand 2011). A greater diversity of sphingolipids and sterols is observed in plants than in animals. These two compounds are essential structural compounds of membranes since they regulate the lipid packing and the phase transitions of the membrane bilayers (Piironen et al. 2000).

2.2. Chloroplast membranes

Chloroplasts are flattened disc-shaped organelles of 2 to 10 µm in diameter, present in the cell's cytoplasm of photosynthetic plants (Figure 1). They contain grana, which are characteristic cylindrical stacks composed of 400 nm diameter membrane disks, comprising between 5 and 20 layers of thylakoid membranes (Pribil, Labs, and Leister 2014). The inner chloroplast envelope and the thylakoid membrane exhibit a similar lipid composition, in contrast to the outer chloroplast envelope, which exhibits a typical "eukaryotic cells" composition. Thylakoids are the photosynthetic membrane of chloroplasts and exhibit a fluid architecture, based on more than 100 different globular proteins (60–70% wt.) dispersed in a lipid matrix. This lipid matrix self-organizes as a stack of bilayers, composed mainly of GL and pigments (30–40% wt.). The main pigments are chlorophyll, the key element of photosynthesis, and carotenoids, which display an AO action, protecting the chlorophyll and the chloroplast membrane against oxidation (Hassan et al. 2017). Diverse

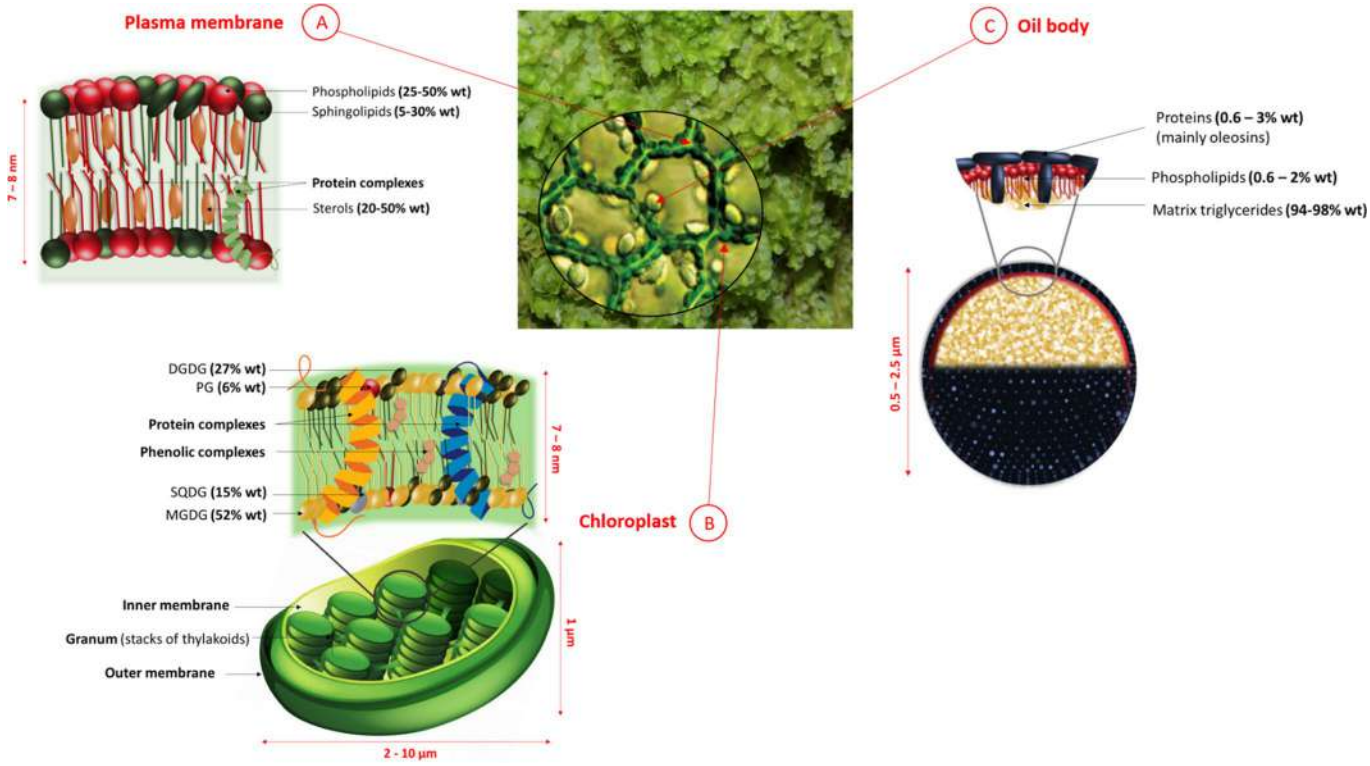

Figure 1. Vegetal assemblies' description: (A) Chloroplast, (B) Oil Body, (C) Plasma membrane – Micrograph adapted from He, Sun, and Zhu (2013).

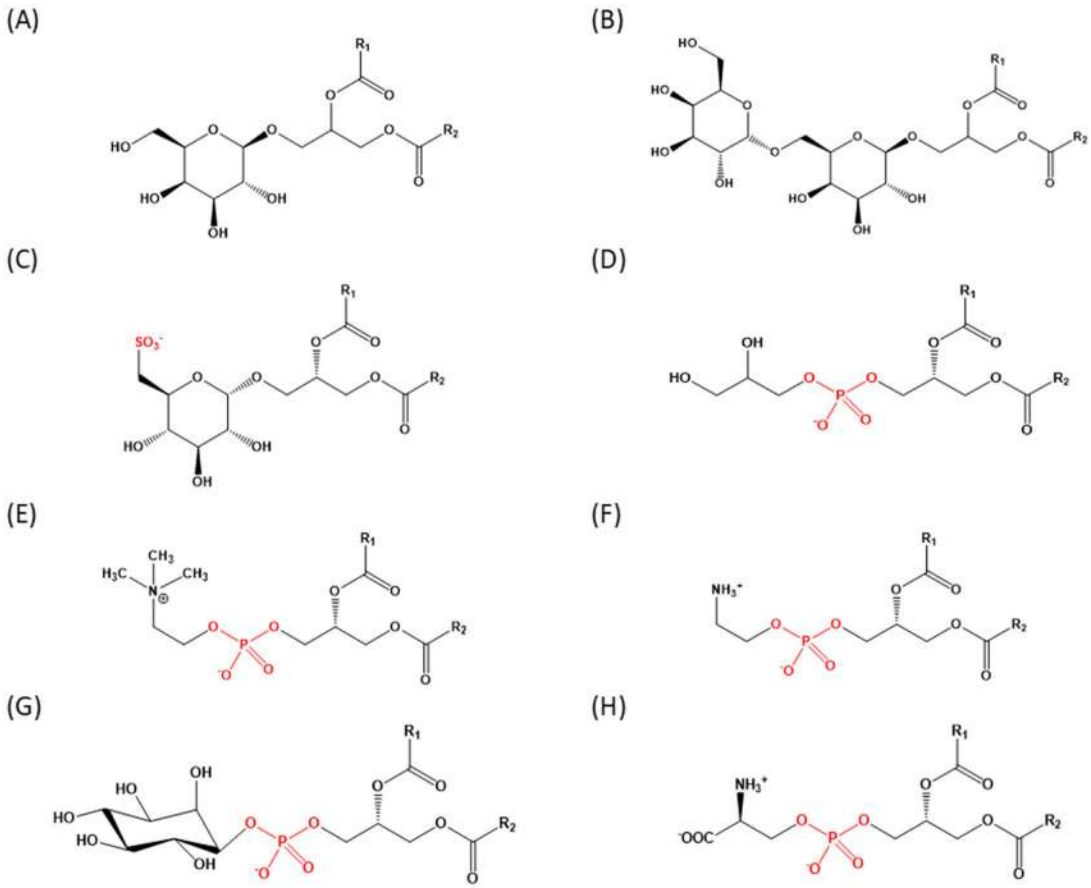

Figure 2. Structure of the main plant membrane lipids: (A) Monogalactosyldiacylglycerol (MGDG), (B) digalactosyldiacylglycerol (DGDG), (C) sulfoquinovosyldiacylglycerol (SQDG), (D) Phosphatidylglycerol (PG), (E) Phosphatidylcholine (PC), (F) Phosphatidylethanolamine (PE), (G) Phosphatidylinositol (PI), and (H) Phosphatidylserine (PS).

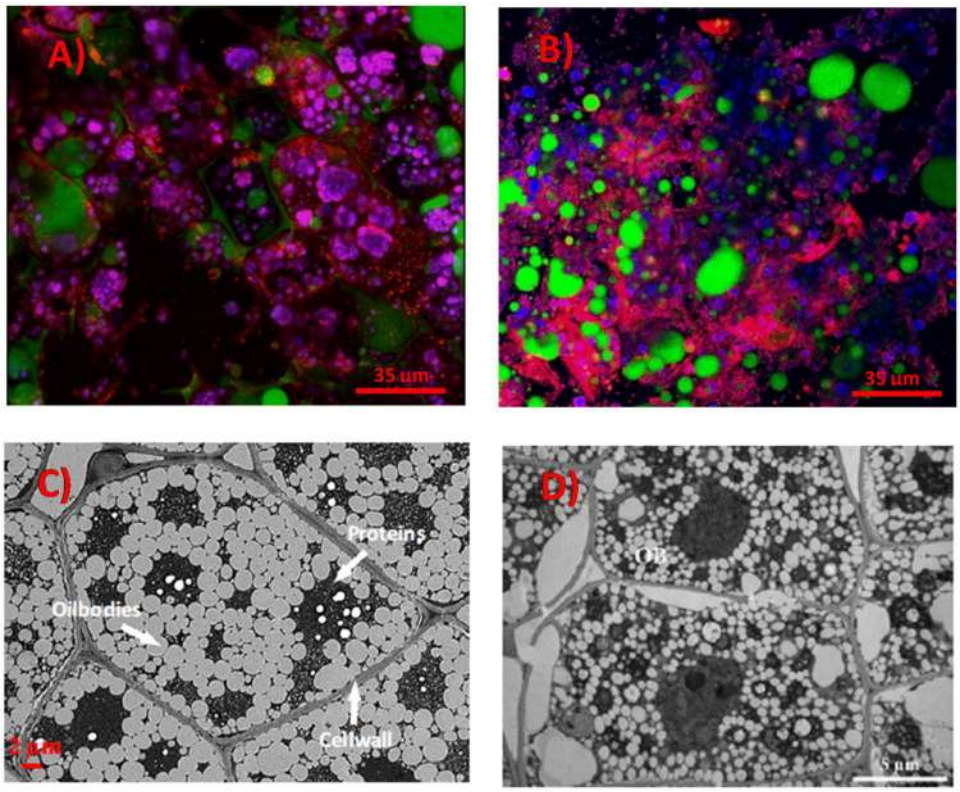

Figure 3. Micrographs of vegetal tissues with embedded OB: (A) Walnut OB (CLSM, red: PL, blue: proteins and green: TAG), unpublished results; (B) Cashew Nut OB (CLSM, red: PL, blue: proteins and green: TAG), unpublished results; (C) Almond OB (TEM), reproduced with authorization from Grundy, Lapsley, and Ellis (2016); (D) Rice OB (TEM), reproduced with authorization from Nantiyakul et al. (2012). Abbreviations. CLSM, confocal laser scanning microscopy; TEM, transmission electron microscopy.

phenolic compounds are also present in chloroplast and plant membranes, and contribute to the plant defence against external stresses. Thylakoids specificity is their unique lipid composition that is very well preserved in higher plants and cyanobacteria. Thylakoids are made up of neutral GL in the form of monogalactosyldiacylglycerols (MGDG) (53% wt.) and digalactosyldiacylglycerols (DGDG) (27% wt.), which differentiates them from most other biological membranes. These GL corresponds to 80% of the total non-pigmented lipids of these membranes in higher plants and algae (Gurevich et al. 1997). In addition to these two glycolipids, thylakoids contain the less abundant anionic glycerolipids sulfoquinovosyldiacylglycerol (SQDG) and PG, whose proportions vary according to the species.

This quartet of lipids shown in Figure 2 exhibits different phase behaviors, which govern the overall membrane behavior and thus the thylakoids architecture. Indeed, DGDG, PG and SQDG form lamellar phases (Lα), regardless of the membrane hydration rate and allow the formation of a bilayer; whereas the most abundant MGDG tends to form an inverse hexagonal structure (HII) in aqueous solution. The MGDG/DGDG ratio, hydration and lipid profile therefore modulate the bilayers self-organization, including the coexistence and transition between Lα phase and HII phase. In particular, the critical role of DGDG has been highlighted as one of the main factors in the membranes stacking by establishing hydrogen bonds between the polar heads of adjacent bilayers, leading to the dense packing of GL bilayers in thylakoids membrane. Additionally, the regularity between the stack induced by DGDG and the repulsive electrostatic forces triggered by the charged lipids PG and SQDG (Demé et al. 2014) allow a greater repulsion of water molecules. The lipids (SQDG being anionic) but also the proteins entangled in the membrane can strongly modulate the isoelectric point of thylakoids.

A distinction regarding the FA composition of GL exists between the so-called "eukaryotic" or "prokaryotic" biosynthetic pathway. Indeed, the distribution of C18 and C16 FA on the glycerol backbone depends on the site of synthesis (chloroplast or endoplasmic reticulum) of the diacyl precursors of GL. MGDG and DGDG resulting from the prokaryotic pathway (chloroplast) are mainly C18:3/C16:3 and C18:3/C16:0 respectively (as abundantly found in spinach for instance); while MGDG and DGDG from the "eukaryotic" pathway (endoplasmic reticulum) are mainly found with a composition C18:3/C18:3 (Browse and Somerville 1991; Frentzen et al. 1983). The pathways of synthesis of GL, especially DGDG and MGDG, are described in detail in the recent review of Sahaka et al. (2020).

In comparison, the outer membrane of chloroplast is depleted in MGDG and contains other glycerophospholipids (PC, PE, PS, PI…), in addition to PG. In this sense, it is much more similar in functional and compositional terms to plasma membranes or non-photosynthetic organelles.

Table 1. Size (μm) and mass percentage composition of OB isolated from various seeds.

Seed	Rapeseed	Flaxseed	Mustard	Cotton	Corn	Peanut	Sesame	Soybean	Sunflower
Diameter (μm)	0.6[a]	1.3[a]	0.7[a]	1.0[a]	1.4[a]	2.0[a]	2.0[a]	0.4[b]	1.0–2.0[d]
Neutral Lipids [% wt.]	94.2[a]	97.6[a]	94.6[a]	97.0[a]	97.6[a]	98.2[a]	97.4[a]	85.9[c]	96.0[d]
Proteins [% wt.]	3.5[a]	1.3[a]	3.2[a]	1.7[a]	1.4[a]	0.9[a]	0.6[a]	8.2[c]	(/)
PL [% wt.]	2.0[a]	0.9[a]	1.6[a]	1.2[a]	0.9[a]	0.8[a]	0.6[a]	5.8[c]	2.5[d]
FFA [% wt.]	0.4[a]	0.1[a]	0.2[a]	0.1[a]	0.1[a]	0.1[a]	0.1[a]	(/)	(/)

[a]Tzen et al. (1993).
[b]Chen and Ono (2010).
[c]Chen et al. (2014).
[d]Millichip et al. (1996).

Table 2. Mass percentage composition of PL of OB isolated from various seeds.

PL	Rapeseed	Flaxseed	Mustard	Cotton	Corn	Peanut	Sesame	Sunflower	Soybean
PC	59.9[a]	57.2[a]	53.1[a]	58.9[a]	64.1[a]	61.6[a] 60.8[b]	41.2[a]	81.0[c]	58.0[d]
PE	5.9[a]	2.8[a]	15.5[a]	4.6[a]	8.1[a]	5.0[a] 5.1[b]	15.8[a]	13.0[c]	15.0[d]
PI	14.0[a]	6.9[a]	13.1[a]	18.1[a]	7.6[a]	8.4[a] 8.6[b]	20.9[a]	5.0[c]	14.0[d]
PG	(/)	(/)	(/)	(/)	(/)	(/)	(/)	(/)	(/)
PS	20.2[a]	33.1[a]	18.3[a]	18.7[a]	20.2[a]	25.0[a] 25.5[b]	22.1[a]	(/)	(/)

[a]Tzen et al. (1993).
[b]Zhou et al. (2019).
[c]Millichip et al. (1996).
[d]Simpson and Nakamura (1989).

2.3. Oil body assemblies and oil body membranes

In seeds, nuts, and some other plant tissues, lipids can be found in the form of lipoprotein assemblies - called oleosomes or oil bodies (OB) -, ranging in size from 500 nm to 2.5 μm (Frandsen, Mundy, and Tzen 2001), depending on growing conditions and environmental factors (Figure 3). These OB are very promising functional food ingredients as recently underlined by Abdullah and Zhang (2020). The main physiological function of these entities is the storage of energy in the form of TAG, but they also play a role in many cellular processes, including the lipid transport, the membrane synthesis, and the protein storage and degradation (Khor, Shen, and Kraemer 2013; Walther and Farese 2012).

Representing up to 75% of the seed volumes, particularly in oilseeds and protein crops, OB are composed by a TAG core (94–98% wt.), covered by a monolayer of proteins (0.6–3% wt.) embedded in a PL monolayer (0.6–2% wt.) (Nikiforidis, Matsakidou, and Kiosseoglou 2014) (Figure 1C). This membrane protects the OB from chemical or mechanical stress. The membrane of OB is composed by strong amphiphilic proteins (mainly oleosins), that confers natural emulsifying properties to OB and allows them to be located at the water/oil interface (Huang 1992).

Oleosins are alkaline proteins ranging in size from 15 to 26 kDa depending on the seeds and isoforms (Tzen et al. 1990). Oleosins exhibit N- and C-terminal hydrophilic domains, presumably oriented horizontally or extended at the surface of the OB, that frame a highly hydrophobic core domain. It is assumed that this domain of 72 uncharged and uninterrupted residues fold into an hydrophobic hairpin with two branches of about 30 residues penetrating into the TAG core of OB (Huang 1992). The secondary and tertiary structures of this central domain remain however unknown, probably due to the fact that purified oleosins or oleosins present in artificial OB may not adopt their native conformation (Huang and Huang 2017; Li et al. 2002; Vindigni et al. 2013). The presumed hairpin structure would extend over a length of 5 to 6 nm. Analyses performed on 1000 oleosins from various plants and green algae revealed no exceptions to this corresponding sequence $X_{30}PX_5SPX_3PX_{30}$ (with X representing a large non-polar residue in X_5 and X_3 and a hydrophobic residue in X_{30}) (Huang and Huang 2015). A transcribed gene coding for an oleosin-like protein has been observed in two species of primitive modern green algae, *Chlamydomonas* and *Volvox*. This protein could be the precursor of oleosin, which is believed to have evolved in green algae to give rise to universal oleosins, whose genes are present in all evolved plant species. Despite these evolutionary diversifications, these specialized oleosins conserve the central hydrophobic hairpin domain.

The isoelectric point of OB oleosins determined on seven species by isoelectric focusing indicated a range of 5.7–6.6 (rapeseed 6.5, mustard 5.7, cotton 6.3, flax 6.0, maize 6.3, peanuts 6.6, sesame 6.4) (Tzen et al. 1993). This acid pI contributes to the stability of OB by bringing negative charges at physiological pH to the membrane, which lead to electrostatic repulsion and steric hindrance between objects, thus avoiding aggregation and coalescence phenomena. Depending on the content of protein and PL, which vary according to the type of seed, there is an increase in the overall size of the OB when these percentages decrease. The size and mass composition of OB isolated from different seeds are listed in Table 1.

Many studies have analyzed the lipid composition of different oilseeds but there is less chemical characterization data on OB from these seeds, as their compositions are

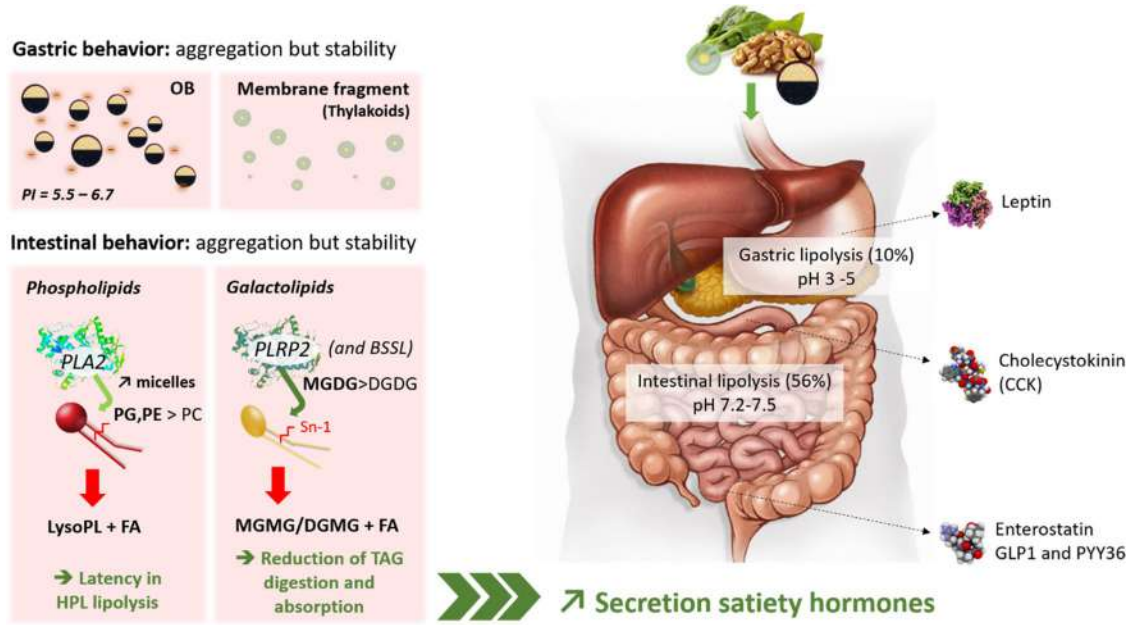

Figure 4. Schematic overview of the gastrointestinal behavior of plant membrane molecules, fragments and assemblies, and their modulating digestion effects.

not exactly similar. The FA profile of polar lipids in OB is generally enriched in unsaturated FA compared to the TAG profile but keeps the same pattern in terms of predominant PUFA. The PL classes present in OB include five types: PC, PE, PI, PG and PS. PC is consistently in the largest proportion, representing between 40 and 65% wt. of PL. PE and PI are then present at 5–15% wt. of PL. PE is functionally very important due to its small polar head, that favors membrane curvatures (Millichip et al. 1996). PL distribution in different oilseed species is shown in Table 2.

OB extraction from plant seed by aqueous extraction results in a naturally emulsified product with a higher stability than emulsions prepared using surfactants such as Tween 20, or proteins such as caseinates or whey protein isolate (WPI) (Ding et al. 2020). The natural stability of OB (Kergomard et al. 2021) has raised interest for their application in many areas, from cosmetic and pharmaceutical to food industry (Deckers et al. 2002; Maurice, Joseph, and Gijs 2000), which explains why their use is quite widespread in the preparation of food emulsions such as creams, salad dressings, mayonnaise or liquors (Nikiforidis 2019).

Plant polar lipids take part into the human diet, either under concentrated form (lecithin) or as naturally-assemblies (nut consumption, green vegetable consumption…), but are differently digested than TAG and can modulate TAG digestion.

3. Digestibility and digestion modulation properties of plant membrane lipids

The digestion of lipids depends on their chemical nature, but also on their dispersion state and on the stability of this dispersion during digestion. Indeed, the hydrolases (lipases, phospholipases and galactolipases) that are involved in the digestion, act at lipid-water interfaces.

The molecular characteristics of these lipid molecules have an impact on their hydrolysis and adsorption kinetics but also on their metabolic fate. Lipids represent an extremely wide range of molecules with diverse structures and functions, whose behavior, due to their different physico-chemical properties, is not the same in the digestive system (Berry and Sanders 2005). The gastrointestinal behavior of molecules, membrane fragments and assemblies, as well as their effect on digestion are presented in the schematic overview Figure 4.

3.1. Digestibility of plant polar lipids: enzymes at work, influence of chemical and physical properties

3.1.1. Enzymes involved in plant polar lipid hydrolysis in humans

In humans, no lipolytic enzyme acting on polar lipids is produced in the upper part of the gastrointestinal tract (oral cavity, esophagus and stomach). Hence, the lipolysis of these polar lipids starts in the small intestine. Several lipolytic enzymes are secreted by the exocrine pancreas into the duodenum, and work together to digest dietary lipids: colipase-dependent pancreatic lipase (HPL), pancreatic phospholipase A2 (PLA2), pancreatic carboxyl ester hydrolase (CEH) also called bile-salt simulated lipase (BSSL), and pancreatic lipase related protein 2 (PLRP2) (N'Goma et al. 2012). Lipolytic enzymes exhibit a more or less extensive specificity for their substrate. Human PLA2 (14,000 Da, 125 AA) is responsible for the intestinal hydrolysis of glycerophospholipids, including the conversion of PC into 1-lysophosphatidylcholine (1-lysoPC). In adults, PLA2 represents only a small portion of the lipolytic enzymes, with HPL and CEH accounting for the largest part (Sternby

et al. 1991). HPL is the main enzyme responsible for the efficient intestinal digestion of dietary TAG in humans. Its enzymatic activity is dependent on its specific cofactor colipase. It has been estimated that HPL is responsible for the release of 56% of TAG acyl chains in the lumen, whereas human gastric lipase (HGL) only achieves 10 to 25% in the stomach, depending on the type of ingested meal.

Galactolipase activity has also been found in human pancreatic juice and in duodenal content (Andersson et al. 1995; De Caro et al. 2004; Wattanakul et al. 2019). In contrast to HPL, PLRP2 (50 kDa) has been shown to efficiently hydrolyze GL in the human pancreatic juice, to a similar level to PLRP2 of rats in vivo where little or no tritium-labeled GL were found intact in the chyle (Ohlsson 2000). De Caro et al. (2004) characterized the specificity of human PLRP2 (HPLRP2), and demonstrated that HPLRP2 activity toward TAG and PL was very low, but was high on MGDG monomolecular films. PLRP2 with similar structure has also been found in the intestines of other species, with higher galactolipase activities in particular in monogastric herbivores, such as guinea pig (GPLRP2), whose diets contain a significant amount of GL due to their herbivore dietary habits. The structural features of enzymes with galactolipase activity in humans, monogastric herbivorous species but also in some fish, foliovorous insects and microorganisms have been reviewed in detail by Sahaka et al. (2020).

CEH (72 kDa, 753 AA) has also been shown to possess galactolipase activity (Amara et al. 2009), but to a lesser extent than PLRP2. Like HPLRP2, this nonspecific enzyme is able to hydrolyze various lipid substrates including TAG, PL, cholesterol and vitamin esters, in addition to GL. CEH is present in higher concentration than HPLRP2 in human pancreatic juice and duodenal content, which suggests a significant contribution to the digestion of GL (N'Goma et al. 2012; Salhi et al. 2020). Like PLRP2, CEH is more active on its substrates in the presence of bile salts. CEH is also able to hydrolyze the three TAG positions without distinction, but has a strong preference for MAG, thus contributing to the total hydrolysis of TAG in synergy with other lipases. This specificity distinguishes CEH from other digestive esterases and allows it to hydrolyze partial acylglycerols into final reaction products (free fatty acids (FFA) and glycerol) in newborns (Bourlieu et al. 2014).

3.1.2. Digestibility of plant polar lipids: the influence of (i) the structural organization of the substrate and (ii) the enzyme specificity within the same substrate group

Lipolysis is a complex interfacial process, where the bioaccessibility of lipids depends on several parameters, including the structure and the composition of the food matrix, the lipid physical states and the enzyme specificities. The lipase action in the duodenum depends on the structure of its substrate but also on the structural changes that the substrate undergoes during digestion.

In the diet, lipids are mostly found in the emulsified form, which is constitutively closest to their native structure. Recent studies in the field of nutrition have shown that the organization of lipids in an emulsified form would modulate the digestion and bioavailability of fatty acids (Michalski et al. 2013); these studies have highlighted the importance of the interfacial activation of enzymes involved in the digestion of emulsified lipid droplets (Golding and Wooster 2010; Sintra, Ventura, and Coutinho 2014). Indeed, some lipases are inactive in the bulk phase, the lid covering the active site being in a close conformation. When the lipolytic enzyme encounters an interface, the lid undergoes conformational changes, allowing the substrate access to the hydrophobic cavity surrounding the active site of the enzyme. One has to be cautious however with the assignment of interfacial activation to the opening of a lid controlling the access to the enzyme active site. PLA2 for instance shows interfacial activation on PL micelles although it has no lid. A more general definition of the interfacial activation of lipolytic enzymes is a much higher activity on their lipid substrates when forming a supramolecular assembly, *i.e.*, emulsion for lipases and micelles or liposomes for phospholipases. PLA2 for instance is weakly active on monomeric medium-chain PL but its activity is drastically increased when the substrate concentration exceeds the Critical Micelle Concentration (CMC), above which micelles are formed (N'Goma et al. 2012). In addition, the hydrolytic activity of pancreatic PLA2 requires the presence of a calcium ion that interacts with the substrate and will activate the catalytic effect of the active site of the enzyme. This interfacial activation process is different for human pancreatic lipase (HPL), which does not require calcium and is active at the oil-water interface. The presence of a lid in lipases and its conformational changes are certainly associated with this drastic environmental change for a water-soluble protein. Changes in the lid conformation result in the exposure of a large hydrophobic surface that allows lipase adsorption at the oil-water interface. While HPL can bind to the lipid droplets and hydrolyze TAG on its own *in vitro*, it requires the presence of a colipase to access its substrate in the presence of bile salts. Indeed, it has been established that the action of HPL on TAG emulsions *in vitro* is inhibited by bile salts, which hinders the adsorption of lipase at the lipid-water interface. The presence of a colipase, a 10 kDa protein produced by the pancreas, allows the specific anchoring of the lipase through the formation of a 1:1 complex in the presence of bile. However, some gastrointestinal lipases do not need interfacial activation, such as HPLRP2, which, on the contrary to HPL, acts preferentially on substrates forming monomers or small aggregates dispersed in solution, such as MAG, PL, and GL (Eydoux et al. 2008).

The physical state of the emulsified lipids is also of importance for the hydrolytic activity of the enzymes. It seems indeed quite intuitive that solid state lipids will not get hydrolyzed due to the reduced molecular motions and diffusion rate in solid substrates. More importantly, a study on the action of pancreatic lipase on various water-soluble and water-insoluble substrates revealed that the hydrolysis activity only occurred when lipid saturation was exceeded, the rate of reaction depending on the surface concentration of the substrate per unit volume (N'Goma et al. 2012). Additionally, it is now well-established that the specific

surface area of the emulsion is often correlated with lipolytic activity. Nevertheless, the presence of surfactants - bile salts, PL, proteins - can modulate this correlation by promoting the reversibility of interfacial adsorption of lipase by forming a barrier or simply by competitive effects.

The enzymes specificity toward their substrates is also important and may not be equivalent within the same lipid group. Overall, several PLA2 have been shown to have a PL head group specificity and a preference for anionic substrates such as PG and PE, more than for zwitterionic PL such as PC (Han, Lee, and Cho 1997). The substrate specificity is slightly different in the case of pancreatic PLA2, whose physiological substrates in the small intestine are the dispersions of long-chain PC in bile salts. A study by Borgström (1993) has investigated the aqueous long-chain PC/sodium cholate system as a substrate for PLA2. The results showed that PC was a good substrate for PLA2 in the form of large mixed micelles of PC and bile salts, with a PC/cholate molar ratio of approximately 0.8. Similar results were obtained by Nalbone et al. (1980), who showed an optimum activity of pancreatic PLA2 on mixed micelles of bile salts and PC at a PC/bile salt ratio of 0.5.

Amara et al. (2010) studied the *in vitro* HPLRP2 hydrolysis of natural long-chain MGDG and DGDG extracted from spinach leaves, compared to the hydrolysis of synthetic medium acyl chain MGDG and DGDG. A continuous pH-stat assay was established, based on the titration of FFA released from the hydrolysis of mixed micelles of GL and bile salts. The galactolipase activity of PLRP2 was found to be weakly affected by the acyl chain length, in contrast to the bile salt/substrate ratio, which governs the micellar solubilization of DGDG and MGDG. This ratio is therefore an important parameter in determining the optimum conditions for measuring the activity of PLRP2. Overall, both the acyl chain length and size of the polar head have no major impact on the active site of PLRP2 compared to classical HPL (Eydoux et al. 2008). The analysis of lipolysis product of MGDG and DGDG including the FA profile analysis also confirmed the specificity of HPLRP2 for the hydrolysis of the ester bond at the *sn*-1 position of acylglycerolipids (Amara et al. 2010). Since ALA is the main FA (>60%) found at this position in MGDG and DGDG isolated from chloroplast, it is the main FA released upon the hydrolysis of GL by PLRP2.

3.2. Digestibility of natural assemblies

3.2.1. Chloroplasts

The enzymatic hydrolysis of galactolipids from thylakoid membranes and their effects on the digestive system have been the subject of several studies. As previously mentioned, GL, including chloroplast rich fraction (CRF) and thus thylakoid membranes, are digested by enzymes in the pancreatic juice, including PLRP2 and CEH to a lesser extent (N'Goma et al. 2012). Indeed, Wattanakul et al. (2019) have studied the *in vitro* digestion of CRF from pea vine field residue and spinach leaves by the human pancreatic juice, where MGDG and DGDG were rapidly hydrolyzed in monogalactosylmonoacylglycerol (MGMG) and digalactosylmonoacylglycerol (DGMG). The impact of thylakoid supplementation upon digestion have been summarized in a recent review by Pourteymour Fard Tabrizi and Abbasalizad Farhangi (2020). Overall, the reviewed studies indicate that the thylakoid membranes have been found to reduce the digestion and absorption of TAG. Indeed, the thylakoid supplementation in humans induces an increase in the secretion of the satiety hormones cholecystokinin (CCK) and glucagon-like peptide 1 (GLP-1) as well as the suppression of the hunger hormone ghrelin, allowing the blood glucose regulation through the increase of insulin secretion and the decrease of appetite. The reduced appetite due to the secretion of satiety hormones suggests a delayed absorption of the nutrients in the intestine, which causes the prolongation of lipid digestion, as demonstrated by in vivo studies on animal (Köhnke, Lindqvist, et al. 2009) but also on human cohorts (Köhnke, Lindbo, et al. 2009). The observed effects on the hepatic metabolism led to a decrease in circulating LDL and total cholesterol, as well as in the plasma lipid and glucose levels. Also, a decrease in the secretion of leptin was observed, which regulates the storage of fat and glucose in the body, raising the interest of the probable anti-diabetes effect of thylakoids. A decrease in serum TAG levels as a consequence of thylakoid supplementation in mice was observed by Stenkula et al. (2017). The effects of spinach thylakoids on the distribution of fat content in the body, the feces and the liver were studied. The results showed in mice an increase in fecal fat content (23 mg/day compared with 10 mg/day in the control), a decrease in body fat deposition and a reduction of liver fat accumulation; this led to an overall weight loss in mice supplemented with thylakoids compared to the control. Reduced distribution of fat cells in these mice was also observed, ranging from 30 to 100 µm compared to 50–150 µm in the control mice, suggesting that a thylakoid supplementation would stimulate lipid storage in smaller cells through precursor recruitment, thus avoiding inflammation of over-extended cells and alteration of metabolic homeostasis. A similar phenomenon was also reported by Vors et al. (2020), who observed a decrease in the cholesterol absorption in the human subjects supplemented with milk PL and sphingomyelin (SM), but also a decrease in the degree of reabsorption of endogenous cholesterol from the intestinal mucosa. Indeed, 20 to 25% of the ingested SM had been found intact in the ileum, suggesting that their interactions by the formation of a complex with cholesterol could explain the significant cholesterol reflux in the ileum after meals (1510–1750 mg).

The hypothesis of the absence of polar lipid digestion must be excluded to explain the overall decrease in intestinal absorption of TAG induced by thylakoid membrane supplementation. Indeed, thylakoid membranes have been shown to have an inhibitory effect on the HPL complex *in vitro*, even in the presence of bile salts, which reduced the fat digestion by 80% (Albertsson et al. 2007). The analyses performed on thylakoids treated with trypsin showed that the inhibitory effects on HPL were provided by intrinsic transmembrane protein complexes, and especially by the

presence of several hydrophobic groups. One of the possible mechanisms put forward by Albertsson et al. (2007) to explain the regulation of appetite was based on a competitive phenomenon at the lipid-water interface. The hypothesis was that thylakoid membranes can adsorb directly to the surface of the lipid substrate because of their tendency to be at a liquid-liquid interface, preventing access of the lipase-colipase complex by steric hindrance. Nevertheless, the hypothesis of the inhibition of intestinal lipolysis by GL was based on *in vitro* digestion studies performed with classical pancreatic lipase only by and the possible hydrolysis of GL of the thylakoid membrane by PLRP2 and CEH was not considered. The observed satiety effects observed by Albertsson et al. (2007) could thus have been generated by other thylakoids components (proteins and liposoluble compounds).

The intestinal absorption and the metabolic fate of GL in rats were studied by Ohlsson (2000). In these experiments, rats were fed with [^{3}H]FA-labeled DGDG and [^{14}C]-labeled DGDG mixed with soybean oil enriched or not in PC to determine whether the GL were completely hydrolyzed and re-esterified to TAG and PL in the chylomicrons, or whether some could be absorbed as such. After the recovery of total lipid extracts and aqueous phases from blood and gastrointestinal organs, the individual lipid classes were separated by thin layer chromatography (TLC) and the radioactivity was measured in the different extracts. In most tissues the presence of [^{3}H] radioactivity was associated with TAG and PL, indicating that DGDG given orally to rats were hydrolyzed and their FA further re-esterified in TAG and PL synthesized in the enterocytes and subsequently found in the chyle and the plasma. These studies excluded a direct absorption of lyso-GL in the intestine nor their use for the resynthesis of GL in enterocytes.

Most of the answers concerning the digestion of GL were obtained on MGDG, DGDG, and SQDG purified from leaf lipid extracts such as spinach. However, further studies on the mechanisms of GL digestion by direct action of pancreatic enzymes are still required on more varied and complex sources, such as not purified whole plant material, in order to elucidate complex mechanisms regarding the inhibition and synergistic effects. Studies performed with CRF represent one step forward in this direction.

3.2.2. Oil bodies

OB are not highly concentrated in plant polar lipids, but they form quasi-natural or at least minimally processed emulsions when OB have been extracted from their natural matrix and redispersed in a water phase. For this reason, their digestion has attracted a lot of attention over the last decade.

Several data have been collected on the stability and the behavior of OB during digestion (Nikiforidis 2019). Gallier et al. (Gallier and Singh 2012; Gallier, Tate, and Singh 2013) studied the behavior of almond OB during their *in vitro* gastric and intestinal digestion. Acid aggregation was the most important phenomena observed under gastric conditions, reflecting that gastric pH brought OB close to their pI. A partial proteolysis of at least a part of the oleosins composing the membrane was also postulated. During the transit through the intestinal compartment, the transition to a neutral pH and the addition of bile salts led to the rupture of the aggregates formed in the gastric phase of digestion. The results indicated a lag phase before the onset of lipolysis, due to a delayed adsorption of HPL, suggesting that the preserved membrane structure of the OB could hinder the pancreatic lipase access to the oil/water (o/w) interface. Similar results had been obtained by Beisson et al. (2001), who studied almond OB as substrates for several purified lipases, including HPL and GPRLP2. These two lipases were found to be active on OB, but with a lower activity (18 to 38%) than that observed on artificial almond oil emulsions. The protein/PL layer covering the OB was found to slow down the hydrolysis by decreasing the specific activity of the enzyme, and a more or less long lag phase before the onset of hydrolysis was observed. This lag phase was quite characteristic of high packing lipid systems, such as chylomicrons, which have a relatively close structure to OB, as well as milk fat globules. GPLRP2 and the HPL/colipase complex had also been found to have phospholipase activity on PL of the PL/oleosin layer, despite the presence of the proteins. The phospholipase activity, even low, could be one of the mechanisms that could explain the action of lipases on OB TAG. Indeed, the introduction of defects in the PL layer would allow the lipase to penetrate the membrane and hydrolyze the TAG core. This hypothesis had been put forward by Noll, May, and Kindl (2000), who showed that the action of a phospholipase was required before the action of the plant lipase to access the core of TAG during the growth of cucumber seeds. Another possible mechanism would be related to the TAG partitioning at the OB o/w interface, which would be hydrolyzed by lipases bound to the interface without penetrating the membrane.

Makkhun et al. (2015) studied the impact of exogenous proteins on the fate of OB from sunflower seeds in the gastrointestinal (GI) tract during their *in vitro* digestion. SDS-PAGE analyses of crude OB (COB) and washed OB (WOB) emulsions indicated a more or less extensive degradation of oleosins after the gastric digestion step in the presence of pepsin, followed by the intestinal digestion in the presence of bile salts and porcine pancreatic lipase. A qualitative analysis of the SDS-PAGE results concluded to a quasi-complete degradation of WOB proteins after two hours of digestion under gastric conditions, suggesting hydrolysis and/or removal of all oleosins by pepsin cleavage. In the case of WOB nevertheless, the SDS-PAGE results indicated the presence of a 6.7 kDa protein fragment after the gastric digestion phase, which may represent the central hydrophobic domain (as well as residual fragments of terminal hydrophilic domain) of oleosins, which remained anchored to the oil phase despite the pepsin action on the groups exposed to the aqueous phase. Additionally, data indicate the presence of oleosins that remained "intact" despite gastric digestion. The exogenous proteins present in sunflower seed could explain this only partial hydrolysis of oleosins on the surface of COB. Since sunflower OB are

able to associate with exogenous proteins, the latter could have formed a protective layer covering the OB, thus affecting their surface potential as confirmed by ζ-potential measurements, and partially shielding the oleosin domains exposed to digestion. This "apparent protection" from enzymatic digestion was not found at such level in the case of WOB enriched in WPI or caseinates, which raises the interest of using OB in their native non-isolated form. The different behavior of OB during the gastric phase induced significant changes in the droplet morphology at the beginning of the duodenal phase. Although bile salts were dominant at the interface of all droplets, COB exhibited significantly smaller droplet sizes than WOB emulsions, whether or not enriched with WPI or caseinates; this may have impacted the rate of digestion of OB. Finally, a net reduction of the protein band was observed in all types of emulsions (COB, WOB, WOB-WPI, WOB-caseinates) after the intestinal digestion phase *in vitro*, indicating the removal of the oleosins remaining on the surface of OB by the bile salts.

The formation of an exogenous protein layer on the surface of unwashed OB droplets may explain the similar protection by oleosins observed in the case of *in vitro* GI digestion of almond OB (Gallier and Singh 2012). Indeed, SDS-PAGE analyses indicated the presence of almond peptides, resistant to pepsin hydrolysis on OB surface even after 15 minutes under gastric conditions. Confocal laser scanning microscopy (CLSM) images supported this observation, showing that the surface of the almond OB was completely covered with proteins, with the almond proteins and their digestion peptides remaining attached to the surface of OB under gastric conditions. During the duodenal phase, despite the hydrolysis of some surface proteins into smaller fragments, a 2-minutes lag phase was observed before the release of the FFA, suggesting a slower penetration of pancreatic lipase at the droplet interface, probably hindered by the membrane assembly of the almond OB and the protective layer formed by exogenous proteins.

3.3. Effect of the addition of isolated constituents from plant assembly on TAG digestion

3.3.1. Effect of GL addition on TAG emulsion digestion

The digestion behavior of lecithin-stabilized olive oil emulsion droplets coated with various amounts of spinach GL was studied by Chu et al. (2009), the objective of this work being to quantify the effects of MGDG and DGDG on the *in vitro* activity of porcine pancreatic lipase under duodenal conditions. The results indicated that DGDG adsorbed at the droplet interface interfere with the adsorption and penetration of the lipase-colipase complex, preventing close contact with the substrate, and thus may have an inhibitory effect on the intestinal lipolysis. Interface measurements indicated significant molecular interactions between the heads of the DGDG, resulting in a tighter molecular arrangement, slowing down the interfacial penetration of pancreatic lipase. The inhibitory effect persists under physiological conditions, since DGDG are highly surfactant molecules, they are not entirely displaced by bile salts. As a result, it slows down the enzymatic hydrolysis of TAG by pancreatic lipase and may be used to trigger the secretion of satiety hormones by the delivery of undigested fat in the distal ileum, subsequently leading to a loss of appetite. Because of their ability to delay and slow down the lipolysis of lipid droplets, DGDG appear to be effective tools in the development of novel food emulsions to regulate the fat intake and in the treatment of metabolic disorders such as obesity. Such inhibition effects of GL on the pancreatic lipase activity are interesting but they should be tested under conditions involving all pancreatic lipolytic enzymes, including PLRP2 and CEH, to validate this approach. Indeed, Chu et al. (2009) only tested these effects of GL on the HPL-colipase complex without taking into account the possible lipolysis of GL under normal physiological conditions.

3.3.2. Effect of the addition of glycero-PL as plant lecithin on TAG emulsion digestion

Plant lecithins are also believed to modulate the lipid digestion, thus influencing the lipid metabolism, as oil emulsification with lecithin has been shown to increase the bioavailability of FA during intestinal absorption (Robert, Couëdelo, Vaysse, et al. 2020). Indeed, as previously mentioned, the amphiphilic nature of PL brings them natural emulsifiers properties, which results in the spatial arrangement of PL at the surface of lipid droplets, either in the course of the emulsion preparation or in the GI tract upon mixing of dietary lipids with that contains endogenous PC (95% wt.). By promoting the emulsification of dietary fat, PL allow increasing the specific area available for the lipase adsorption thereby increasing the rate of lipolysis and the subsequent intestinal adsorption. The direct dose-dependent impact of rapeseed lecithin just blended in bulk oil to increase the lymphatic lipids and the ALA bioavailability was also very recently reported in rat by Robert, Couëdelo, Knibbe, et al. (2020).

Regarding the impact of various interfaces on lipid digestion, Couëdelo et al. (2015) showed that the *in vitro* gastric lipolysis of a linseed oil emulsion was increased by 30% when the lipid droplets were coated with soy lecithins instead of caseinate or Tween 80. These results were confirmed in vivo, with the faster intestinal absorption and bioavailability of ALA observed with soy lecithin, compared to other emulsifiers. Plant lecithins have also been shown to exhibit a potential beneficial impact on lipid absorption and a subsequent enhancement of lipid profile in plasma, liver and adipose tissues (Robert, Couëdelo, Vaysse, et al. 2020). Lee et al. (2014) have shown that the long-term supplementation of soy-derived PC in hyperlipidaemic mice prevented lipid accumulation by lowering the plasma TAG, cholesterol and leptin levels, thereby lowering the LDL/HDL ratio and alleviating obesity-related complications. These results suggest the potential of soy lecithins in the delivery of certain specific FA to certain tissues and in the prevention of obesity-related cardiometabolic disorders. However, further research is needed to determine whether these effects are found under normal human lipidemic conditions and

to investigate the effects of lecithins from other sources with different lipid composition. To balance these potential beneficial effects, it is however worth nothing that the use of lecithin as emulsifier may bypass the satiety mechanisms triggered in the distal part of the small intestine due to a faster gastrointestinal lipolysis and a subsequent fat absorption (Couëdelo et al. 2015). Liquid test meals containing a lecithin stabilized emulsion are digested at a much higher rate than normal solid-liquid meals with non-pre-emulsified fat (N'Goma et al. 2012). Overall the lipolysis measured at the Angle of Treitz (end of duodenum) can thus reach around 60% with this type of liquid meal while it is only around 30% with a normal meal. Other studies in healthy volunteers and obese patients (Vors et al. 2013; Vors et al. 2017) have shown a faster absorption of emulsified dairy fat compared to the same amount of non-emulsified fat. Altogether, these findings may lead to lower levels of undigested fat and FFA in the lower part of the small intestine and thus impair the release of satiety hormones like GLP-1 and peptide YY (PYY). Thus, a risk/benefit assessment should be performed before developing food product with additional plant lecithins. Improving the fat digestion and absorption could be interesting to avoid malnutrition in premature infants and elderly for instance, while it could be an aggravating factor of obesity in other subjects.

3.3.3. Effect of oleosin addition on TAG emulsions digestion

To our knowledge, the effect of the addition of purified oleosins on the digestion of lipid emulsion droplets has not been documented to date. Nevertheless, Beisson et al. (2001) have investigated the susceptibility of almond OB to the *in vitro* lipolysis by various purified lipases. From the known behavior of these lipases on PL-stabilized emulsions like Intralipid (soybean oil emulsified with egg lecithins), it is possible to deduce some effects of oleosins on lipolysis. Depending on the lipase, the specific activity measured on OB was found to range from 18 to 38% of the specific activity measured on almond oil emulsified by Arabic gum, indicating that oleosins combined with PL have an overall negative effect on lipolysis. For instance, human gastric lipase (HGL) shows a specific activity of 71 ± 3 U/mg on almond OB versus 202 ± 21 U/mg on Arabic gum-emulsified almond oil, and around 600 U/mg on Intralipid (Soybean-oil inwater emulsion) (Gargouri et al. 1986). While PL favor the activity of HGL on soybean oil (Intralipid), their combination with oleosins in OB results in an 8-fold lower activity. These effects on HGL can be compared to those of casein that also reduces the activity of gastric lipase on rapeseed (Vors et al. 2012) and flaxseed (Couëdelo et al. 2015) oils compared to lecithin alone. With human pancreatic lipase (HPL), colipase is required to measure the activity on almond OB in the absence of bile salts, while HPL alone is active on almond oil emulsified by Arabic gum. As seen with HGL, PL activity on OB (1079 ± 98 U/mg) is reduced compared to its activity on Arabic gum-emulsified almond oil (2865 ± 269 U/mg), but only 23-fold. This activity is characterized by a lag-time before steady state kinetics are observed. It is worth nothing that, on the contrary to HGL, HPL is not readily active on Intralipid and other emulsions presenting PL at their surface like milk fat globule (Gargouri et al. 1986). HPL activity on these substrates usually needs to be triggered by the addition of FFA or the combined action of other enzymes like HGL or PLA2. FFA favor the adsorption of HPL at the oil-water interface. Similarly, the combination of PL and oleosins in OB allows the binding and action of HPL associated with colipase. Therefore, oleosins may also have positive effects on lipolysis.

Oleosins are known to have a stabilizing role in OB, and this interfacial part very likely modulates their digestion. Indeed, as natural surfactant components of OB, they provide an electrostatic and steric stabilization of OB assembly at a physiological pH. Their degradation has been observed to decrease the OB emulsions stability by Maurer et al. (2013), which was illustrated by an increase in the polydispersity of the OB size, a decrease in the interfacial layers elasticity and alterations of interactions between droplets.

The behavior at the air-water interface of purified oleosins extracted from maize germ OB was studied by Nikiforidis et al. (2013). It appeared that the behavior of maize oleosins at the air-water interface was comparable to that of milk proteins and egg yolk alipoproteins, which are used to stabilize many food preparations. The high surface activity of these proteins is of interest to their use as emulsifiers to stabilize foods. Nevertheless, a review by Barre et al. (2018) reported the allergenicity of peanut, hazelnut and sesame oleosins, identified and characterized as major lipophilic allergens in susceptible individuals. This explains why the use of oleosins as emulsifiers or encapsulants for protein or lipidic drug substances raises certain health issues, particularly for cosmetic, pharmaceutical or food applications. For example, James (2002) proposed that increasing the oleosin content in cocoa beans would promote a mechanism to enhance cocoa flavor by generating more hydrophilic peptides and hydrophobic amino acids, the precursors of key components of cocoa flavor. Depending on the application, the patents submitted raise the importance of removing contaminants such as other proteins from the OB during purification, with the aim of reducing allergenicity, color and odor and specially to increase the stability.

3.4. Potential of plant membranes to vectorize compounds of interest in food applications

3.4.1. GL composition and ability to vectorize essential ω3 PUFAs

Due to their abundant presence in nature, thylakoid lipid membranes represent an important source of essential fatty acids, especially thanks to the unique composition of GL, which are rich in PUFA and in particular ALA. Among the numerous botanical sources offered by vegetal biodiversity, spinach thylakoids have been the subject of many scientific studies (Anderson, McCarty, and Zimmer 1974; Krumova et al. 2008; Douce, Holtz, and Benson 1973). The thylakoid lipids of spinach are composed of the quartet MGDG, DGDG, SQDG, and PG, in proportions presented in Table

Table 3. Lipid composition (in percent by weight) of spinach leaves chloroplasts membrane and wheat flour.

		MGDG	DGDG	SQDG	PG	Others
Chloroplast	Thylakoids[a]	53.0	27.0	7.0	7.0	6.0
	Inner membrane[b]	49.0	30.0	5.0	8.0	8.0
	Outer membrane[b]	17.0	29.0	6.0	10.0	38.0
Amyloplasts	Wheat flour[c]	0.4	1.0	–	–	0.4

Source: Kobayashi (2016).
[a]Isolated from spinach leaves [%wt.] (Dorne et al. 1990).
[b]Isolated from spinach leaves [%wt.] (Block et al. 1983).
[c]Spring wheat flour [%w.] (Konopka, Czaplicki, and Rotkiewicz 2006).

3, according to a review by Kobayashi (2016). In comparison, non-photosynthetic sources, such as seeds, possess a different lipid profile, with still GL, but in a lower proportion and different distribution and FA composition. For example, in wheat flour, DGDG and MGDG account for 77% wt. of total GL, but DGDG are present in higher amounts than MGDG, contrary to what is found in the leaves. GL are mainly found in amyloplasts, whose number and size thus influence the concentration of GL found in wheat flour. As a comparison, the GL composition of wheat flour in spring is provided in Table 3, according to Konopka, Czaplicki, and Rotkiewicz (2006).

3.4.2. Ability of plant lecithins to encapsulate molecules of interest

In a recent study, Vergara et al. (2020) have evidenced the ability of liposomes made from rapeseed PL and stigmasterol (ST) at low concentration to protect lactoferrin during gastrointestinal digestion *in vitro*. The stability, size and organization of the liposomal vesicles were studied. The good balance in the membrane composition of the formulated liposomes made it possible to delay their hydrolysis during the gastric and intestinal digestion phases, thus making it possible to obtain a significant quantity of intact lactoferrin in the intestine after 120 minutes of digestion. Overall, liposomes made with rapeseed PL, properly combined with other lipids, have shown their potential to be used as an oral delivery system for the molecules sensitive to the digestive enzymes, such as lactoferrin, thanks to their protective capacity throughout the digestive process.

4. Oxidation of membrane compounds and modulating effects on the different compartments of the digestive system

4.1. Susceptibility to oxidation of plant polar lipids

4.1.1. Lipid oxidation

To increase the PUFA intake and especially dietary ω3, it is of the upmost importance that the plant membranes lipids are stable to oxidation. Reactive oxygen species (ROS) are generated in cell membranes and are responsible for the degradation of many cellular compounds, including lipids, proteins and prooxidant (PO) or antioxidant species such as chlorophyll, carotenoids and phenolic compounds. Treatments such as heating or exposure to light, or the presence of trace metals in raw materials also play a catalytic role in triggering the oxidation of lipids in food matrix during their storage (Waraho, McClements, and Decker 2011).

Lipid oxidation is a phenomenon whose main mechanisms, kinetics, and factors of variation are well known today. This radical chain reaction affects the unsaturated fatty acids present in oil, fat or structural lipids and is generally schematized according to three main steps. (i) The first step of initiation leads to the formation of a first alkyl radical by the abstraction of a hydrogen atom on methylene group either between two double bonds (at a bis-allylic position) or adjacent to a double bond (allylic hydrogen atom) by the ROS. This removal thus constitutes the limiting step of the reaction since it requires the availability of a hydrogen, which is only the case in lipids having one or more unsaturated chains. This explains the susceptibility of PUFA to oxidation, whose stability is inversely proportional to the number of unsaturation they contain. (ii) During the second step of propagation, the alkyl radicals formed during the initiation step react with molecular oxygen, leading to the formation of a peroxyl radical; which in turn react with other unsaturated FA to form hydroperoxides. The latter primary oxidation products are highly unstable and can be converted into secondary oxidation products. (iii) The final termination step then closes the reaction chain when two radical products react with each other to form a non-radical product.

The oxidation of lipids is a phenomenon that one seeks to avoid since it is responsible for (1) irreversible loss of essential PUFA, (2) early reactions that favor the faster propagation of oxidation, and (3) the organoleptic degradation of food products, through the formation of secondary oxidation products, sometimes toxic, that can enter the blood circulation through the diet and be further absorbed in body tissues, inducing the development of cancer, atherosclerosis and inflammatory diseases (Shahidi and Zhong 2010).

Delaying the onset of lipid oxidation is thus crucial, since it can cause the deterioration of food products and reduce their shelf life (Berton-Carabin, Ropers, and Genot 2014; Decker et al. 2017).

4.1.2. The structural factors within the plant polar lipids that conditions their sensitivity to oxidation

The sensitivity of lipids to oxidation increases with their level of unsaturation whatever their form: homogeneous lipid medium (oil), biphasic system (o/w emulsion), dispersion (liposomes in aqueous phase). Nevertheless, many

exceptions to this simple rule can be observed depending on the chemical structure of the lipid containing the unsaturation (FA, TAG, or PL esters), its physical state and its environment (presence of PO metal ions, initial oxidation state, initial degree of hydrolysis, presence of other AO, partition coefficient in oil/water emulsion and proximity with interface, etc.) (Berton-Carabin, Ropers, and Genot 2014; Decker et al. 2017). At a given unsaturation level and in a given environment, the susceptibility of the lipid molecule to oxidation will mainly depend on the Dissociating Bond Energy (DBE) necessary to break the carbon-hydrogen (C-H) bond of allylic or bi-allylic hydrogen atom. The lower this DBE, the faster the oxidation of the molecule. However, the access to this data for GL in comparison with phospholipids or TAG is not straightforward but can be inferred from bibliographic data obtained on molecules having similar acyl chains. Within PL, PE, which is often the most unsaturated and plasmalogen-rich, is the most rapidly degraded. Conversely, PC is more resistant. The oxidative stability of GL has been less documented although their PUFA content makes them potentially very sensitive to oxidation (Hazahari, Hosokawa, and Miyashita 2018; Yamauchi et al. 1983). The comparisons of GL, PL, and TAG reactivity have been conducted using sources with different unsaturation levels and they tend to indicate a higher stability of GL over PL, which are also more stable than TAG. In these experiments, the impact of natural PO or AO is limited by the fact that the extracts have been purified, but differences in the physical state of molecule can also modulate the oxidative reactivity. The physical state (solid/liquid) of TAG, PL, or GL (either in hexagonal packing in micelles or in bilayers under condensed liquid, expended liquid, or gel) will determine the phase distributions and the local concentrations of substrates. PO or AO agents can also influence the oxidation kinetics, as well as the quality of the local environment around the molecule. For instance, hydrolysis reactions generating FFA promote oxidation via interaction phenomena with metal ions that boosts the initiation and propagation of the oxidation reaction. The control of all these factors is difficult and may explain some opposition in studies seeking to link the molecular form and the sensitivity to oxidation.

4.2. Reactivity of polar lipids in natural plant membrane assembly

In the plant kingdom, membrane defence systems are set up to control the ROS concentration and thus protect the cells. The plants possess several types of AO but also innate enzymes that are able of neutralizing ROS or regenerating the active forms of AO species. This explains why a relative chemical stability to oxidation is observed in the different native forms of plant membrane assemblies.

4.2.1. Chloroplasts

Thylakoid GL are continuously exposed to oxidative stress due to their very high levels of PUFA as well as their light exposure during photosynthesis (Yamaguchi et al. 2012). GL may have a different response to oxidative stress than other classes of lipids such as PL or TAG.

The composition of various AO molecules in different spinach extracts was recently investigated by St-Pierre et al. (2019), who studied the AO properties of thylakoids and their possible application in the cells protection against ultraviolet (UV) radiation. The examined thylakoid extracts contained phenolic compounds (*i.e.*, flavonoids, tannins) as well as pigments (*i.e.*, chlorophyll and carotenoids). All thylakoid extracts tested by the ORAC assay in this study demonstrated AO capacities that were maintained during storage at 4 °C for 1 to 79 months, although these decreased over time. In addition to various AO molecules, the presence of AO enzymes was reported in spinach thylakoids, including superoxide dismutase, which regulates the level of damaging radicals by scavenging superoxide anions, and whose activity does not appear to have been affected by storage. The enzymatic activity and structural constituents of thylakoids are believed to be responsible for the potential antioxidant activity of chloroplast in their native form in situ.

4.2.2. Oil bodies

In addition to their significant physical stability, OB exhibit relatively high chemical stability to oxidation during storage, despite the presence of a significant amount of unsaturated fatty acids in the majority of oilseeds (Kapchie et al. 2013; Chen et al. 2012; Nikiforidis, Kiosseoglou, and Scholten 2013; Gray et al. 2010). The presence of endogenous proteins in the mixed PL/protein membrane surrounding the TAG core, but also of exogenous storage proteins in the continuous phase in nut-derived juice for instance; partly explains the oxidative stability of unsaturated FA (Nikiforidis, Matsakidou, and Kiosseoglou 2014). In addition to proteins and lipids, OB also constitute a rich source of AO bioactive compounds, including tocopherols and phytosterols, which have been shown to be associated with the surface of objects. In particular (Fisk et al. 2006), reported the presence of a high amount of tocopherol in sunflower OB (0.57 mg/g lipid) extracted by a single wash cycle with sodium phosphate buffer. Further extraction of the organelles with a 9 M urea solution removed the OB exogenous proteins as well as some phenolic compounds less hydrophobic than tocopherols, resulting in a significant increase in the OB tocopherols concentration, supporting the hypothesis that the tocopherols are intrinsically bound to the structure of oilseed OB.

The presence of a high amounts of tocopherols and phenolic AO compounds has been found in several types of oilseeds, allowing the protection of OB PUFA from oxidation and thus contributing to their oxidative stability in vivo in seed grain.

4.2.3. Lecithins

In addition to their multiple above-mentioned biological and biochemical properties, plant lecithins have shown AO properties regardless of the source, which is partly attributable to their high concentration of PL. Indeed, PL possess

various AO properties, the mechanisms of which were clearly detailed in a recent review by Cui and Decker (2016) and also elucidated in terms of chemical mechanisms by Reis and Spickett (2012). In particular, PL exhibit an AO role by chelating the PO metal species and are able to displacing or regenerating the primary AO species. In addition, scientific studies have shown that the presence of phenols in plant lecithins, in synergy with PL, increased the AO capacity of lecithins (Li and Guo 2016). For instance, the reactive polar head of PL (amine for PE and PC, reducing sugar for PI) have been shown to develop synergy with tocopherols, enhancing the capacity of free radical termination of this latter (Judde et al. 2003). To explain such synergy, it was hypothesized that PL could facilitate the hydrogen or electron transfer to tocopherols and its regeneration. However, as for OB, these AO capacities are highly dependent on the quality and the structure of food matrix, and can thus be altered by processing.

4.3. Uses of plant polar lipids protection against oxidation reported in literature

In emulsions, the molecules are distributed according to their polarity and surface activity within the different phases, which are the oil phase, the water phase and the interfacial region. In these systems, lipid oxidation is a phenomenon that occurs at the droplet interface, where the presence of a large surface area facilitates interactions between lipids and water-soluble PO species. Many factors influence the rate of lipid oxidation in these emulsified systems, including the physico-chemical properties of the interface (thickness, charge, composition, rheology, permeability) and those of the continuous phase (oxygen concentration, AO and PO composition, pH, etc.). The current trend toward PUFA-rich, but also minimally-processed products limits the use of traditional oxidation control methods such as synthetic AO; therefore, the natural stable systems where lipid oxidation can be controlled, such as plant membrane, have raised interest over the last few years.

4.3.1. Chloroplasts membrane

The emulsions stabilized by chloroplast thylakoid membrane have been proposed as functional food to promote satiety and were characterized in terms of stability, interfacial tension and droplet size but not in terms of stability to oxidation (Rayner et al. 2011). The stability to oxidation of chloroplast membrane polar lipids with different levels of unsaturation has been studied. Yamaguchi et al. (2012) compared the oxidative stability of GL (MGDG, DGDG and SQDG) from spinach and algae to PC from salmon oil and to TAG from soybean and sardine oil. Data were obtained after purification of all lipids to avoid the influence of potentials AO and PO which are naturally present in these products, such as chlorophyll, carotenoids or tocopherols. The results of the analyses indicated that MGDG and DGDG of spinach and algae had an overall higher oxidation stability than that of TAG or PC from marine animal sources. MGDG and DGDG from spinach and algae showed the same oxidative stability as TAG from soybean oil, whereas the latter had a lower number of unsaturation numbers. SQDG from spinach and algae showed even a greater oxidative stability than MGDG and DGDG but presented on average a lower number of unsaturation than GL fraction of the same sources. Altogether, these results suggested that the galactosyl and sulfoquinovosyl residues of GL could protect the PUFA unsaturation by enhancing the DBE of allylic hydrogen and/or through different intermolecular interactions which could modify the molecules packing and reactivity.

More recently, Hazahari, Hosokawa, and Miyashita (2018) have evaluated the oxidative stability of three types of lipids: MGDG and DGDG of spinach and algae, as well as TAG from linseed oil, previously purified from AO and PO impurities. The greater oxidative stability of DGDG and MGDG compared to TAG from linseed oil was evidenced, regardless of the source and despite higher unsaturation levels than in the TAG fraction. Within GL classes, a greater oxidative stability of DGDG from spinach and algae compared to MGDG from the same sources was evidenced. In addition to the modulation of allylic hydrogen BDE, differences in self-assembly structure and physical state between MGDG and DGDG cannot be excluded. Indeed, Bottier et al. (2007) established that MGDG form at the interface a less compact structure than DGDG, with galactosyl headgroup extended at the interface. On the other hand, DGDG could pack their galactosyl moieties at the interface, adopting a lamellar phase Lα with parallel orientation of the headgroups with respect to the plane of the bilayer. This organization of DGDG enhanced their compacity and steric hindrance at the interface in comparison with MGDG, possibly limiting the interaction with ROS.

4.3.2. Oil bodies

Scientific studies have raised the interest of natural OB emulsions for the preparation of stable emulsions, since they have a remarkable chemical stability compared to synthetic OB emulsions prepared with other surfactants. In particular, the stability of OB extracted from *Echium Plantagineum* has been studied ex vivo by Gray et al. (2010). The interest of this plant is that its consumption has a potentially beneficial effect on health since *E. Plantagineum* contains a high concentration of PUFA, half of which is part of ω3 and includes a significant amount of stearidonic acid (SDA, C18:4, ω3) (14% wt.), which is converted to up to 30% in EPA in the human body. Despite the natural oxidative stability of oilseeds in vivo during storage, a high concentration of PUFA results in a susceptibility to oxidation after oil extraction from the seed. The oxidative stability of emulsions of *E. Plantagineum* washed OB dispersed in an aqueous phase was compared to that of synthetic emulsions of *E. Plantagineum* oil stabilized by emulsifiers: SDS and Tween 20; as well as to that of bulk oil. After 7 days of incubation at 40 °C, a significantly less marked oxidation was evidenced in the case of the natural *E. Plantagineum* OB emulsion. Different hypotheses have been proposed to explain this conservation of the oxidative stability of natural OB

Table 4. Main data and hypothesis of structural level that determine plant PL susceptibility to oxidation.

Compounds/assembly	Molecular stability to oxidation	Partition in O/W system	Chelating effect	Physical assembly	References
Galactolipids	Galactolipids > PC > TAG;SQGD > galactolipids				Yamaguchi et al. (2012)
Galactolipids	DGDG > MGDG			Potential effect of Lα packing of DGDG	Hazahari, Hosokawa, and Miyashita (2018)
Phospholipids	PL > TAG		Chelating pro-oxidant metals	Segregate PC in membrane	Cui and Decker (2016)
Phospholipids		Synergy with tocopherol: facilitate its regeneration through H transfer from amine functions of the PC, PS or PE, and the sugar residue of the PI			Judde et al. (2003); Hildebrand, Terao, and Kito (1984)
OB	OB > reconstituted artificial emulsion with same TAG core	Potential AO effect of oleosin at interface			Gray et al. (2010); Fisk et al. (2008)

emulsions ex vivo: (i) the potential AO role of oleosins on the surface of OB by metal chelation or through sacrificial oxidation; (ii) the formation of a thin and compact layer by protein (oleosin) arrangement on the surface of OB, which stabilizes the droplet interface and provides a barrier to oxygen and reactive species; (iii) the differences in surface area/volume ratio between the natural OB emulsion and the stabilized synthetic emulsions, which would reduce the effective surface concentration of tocopherols in the processed emulsions and explain the observed oxidation differences.

Similar results had been previously obtained by Fisk et al. (2008), who compared the oxidative stability of natural suspensions of washed sunflower OB with that of formulated sunflower oil emulsions stabilized with SDS and Tween 20. The results indicated higher concentrations of primary and secondary oxidation products in the formulated emulsions. The presence of a stable lipid-water interface was suggested as an argument for the oxidative stability of the natural sunflower OB emulsion, in addition to the presence of seed protein residues in the continuous phase, which are preferentially oxidized or chelated by free metal ions. However, it should be pointed out that the method of OB extraction may affect their physical integrity, and therefore their recovery method is crucial in maintaining the emulsion chemical stability (Karkani et al. 2013).

OB therefore appear as a natural form of oil encapsulation, providing significant protection against oxidative stress. As developed in paragraph 4.2.2, the presence of tocopherols and phenolic compounds closely associated with OB in significant concentrations also raises the interest in the application of OB as a deliver agent for AO such as vitamin E.

4.3.3. Lecithins

Lecithins have been shown to be suitable for use as emulsifiers but also because of their AO activity, especially in bulk vegetal oils. Indeed, some PL present in plant lecithins showed the ability to act in synergy with tocopherols, thus improving AO activity (Shanbhag 2018). This property would be related to the ability of PL to give a hydrogen atom of their amine function, allowing the regeneration of the oxidized tocopherol quinone in its initial form. The amine functions of PC, PS or PE, and the sugar residue of PI have also been shown to exhibit metal chelation properties.

Judde et al. (2003) studied the AO effects of soybean lecithins on the oxidative stability of several vegetal bulk oils, as well as their synergistic effect with different forms of tocopherols. The best protective effects against oxidation were observed after incorporation of 5% wt. of lecithin containing high proportions of PC and PE, especially in oils rich in LA, such as rapeseed, walnut or soybean. Also, the combination of these lecithins with the γ- and δ-tocopherol forms was shown to be more effective than with the α-tocopherol or the compounds in their individual forms. This study showed in particular the potential use of lecithins in the protection of refined vegetal oils against oxidation. Nevertheless, PC was also shown to have no synergistic effect with tocopherols, and even in some cases to exhibit PO properties. Indeed, the study by Kashima et al. (1991) on the AO activity of PL on perilla oil had shown the AO efficacy of PE and PS in synergy with a mixture of tocopherols, whereas PC had shown little effect. Also, PE had been shown to increase the activity of α-tocopherol, but not PC (Takenaka, Hosokawa, and Miyashita 2007). Due to its intermediate hydrophilic-lipophilic balance (HLB), PC exhibits the ability to form reverse micelles when its concentration is above the CMC, which themselves have been reported to have PO activity (Cui and Decker 2016).

In emulsified fish oil systems, lecithins appear to promote the dispersion of other active AO, thereby limiting the free-radical propagation in the medium (Yi, Han, and Shin 1991). Nevertheless, studies are needed on the synergistic effects of lecithins with phenolic compounds in emulsified vegetal oil systems, as data are, to our knowledge, still lacking.

4.4. Plant polar lipids oxidation through digestive system

Oxidation of plant lipids can occur prior the ingestion, but can also takes place during the digestion (Márquez-Ruiz, García-Martínez, and Holgado 2008). During the oral phase, oxidation phenomenon is quite limited in time and the enzyme activity is supposed to be low. Conversely, the gastric digestion phase takes place at low pH in the presence of oxygen and catalysts found in food, and the oxidation phenomenon can thus be quite high and leads to vegetal oil peroxidation and oxidation of vitamin E, C and beta-carotene. Some AO of food such as polyphenols and glutathione peroxidases can help to reduce the hydroperoxides production in gastric phase. Gastrointestinal glutathione peroxidases are also important actors limiting gastric hydroperoxides. TAG monohydroxyperoxydes can be hydrolyzed by HPL almost similarly to non-oxidized TAG but non-absorbable oxidized lipids can also reach the distal part of the intestine and may favor oxidation and inflammation. The peculiar oxidative behavior and AO effect of PL from plant membrane in the gastrointestinal part is still unknown and should be further investigated. Main data and hypothesis of structural level that determine plant polar lipids susceptibility to oxidation are summarize in Table 4.

5. Conclusions

The plant membrane gathers a diversity of GL and phospholipids, selectively acylated with PUFA and are already organized as lamellar structure, embedded with proteins and phenolic compounds.

Among these polar lipids, GL concentrating ALA and phospholipids can be used as specific vector of PUFA. They are hydrolyzed by specific intestinal enzymes (PLRP2, PLA2, and CEH) and allow the reduction of the TAG digestion and absorption. GL specifically can activate the ileal break. Concerning the potential inhibition activity on pancreatic lipase, *in vitro* studies involving all pancreatic enzymes are needed to determine the exact involved mechanisms.

These plant polar lipids also intrinsically present AO activity (higher stability to oxidation than TAG) and metal chelating activity. In addition, their natural association with the phenolic compounds in membrane assemblies and their physical state (Lα state of DGDG) can enhance their stability to oxidation.

Minimally-processed plant assemblies such as OB or chloroplasts which have acidic isoelectric point and are not hydrolyzed by gastric enzyme can thus be preserved during this phase and be conveyed with minimal transformation to duodenum. Their stability to oxidation in gastric phase remains to be elucidated.

Altogether, all these elements make these plant membrane molecules and assemblies very promising components with a wide range of application to vectorize ω3 PUFA and equilibrate human diet.

Abbreviations

1-lysoPC	1-lysophosphatidylcholine
ALA	α-linolenic acid
ANSES	French National Agency for Food, Environmental and Work Health Safety
AO	Antioxidant
ARA	Arachidonic acid
BSSL	Bile-salt simulated lipase
CCK	Cholecystokinin
CEH	Carboxyl ester hydrolase (pancreatic)
CLSM	Confocal laser scanning microscopy
CMC	Critical Micelle Concentration
COB	Crude OB
CRF	Chloroplast rich fraction
DBE	Dissociating Bond Energy
DGDG	Digalactosyldiacylglycerol
DGMG	Digalactosylmonoacylglycerol
DHA	Docosahexaenoic acid
EPA	Eicosapentaenoic acid
FA	Fatty acid
FFA	Free Fatty acid
GI	Gastrointestinal
GL	Galactolipid
GLP-1	Glucagon-like peptide 1
GPLRP2	Guinea pig pancreatic lipase related protein 2
HGL	Human gastric lipase
HII	Inverse hexagonal phase
HPL	Human pancreatic lipase
HPLRP2	Human pancreatic lipase related protein 2
LA	Linoleic acid
Lα	Lamellar phase
LC-PUFA	Long chain polyunsaturated fatty acid
MGDG	Monogalactosyldiacylglycerol
MGMG	Monogalactosylmonoacylglycerol
OB	Oil body
PA	Phosphatidic acid
PC	Phosphatidylcholine
PE	Phosphatidylethanolamine
PG	Phosphatidylglycerol
PI	Phosphatidylinositol
PL	Phospholipid
PLA2	Phospholipase A2 (pancreatic)
PLRP2	Pancreatic lipase related protein 2
PO	Prooxidant
PS	Phosphatidylserine
PUFA	Polyunsaturated fatty acid
PYY	Peptide YY
ROS	Reactive oxygen specie
SDA	Stearidonic acid
SM	Sphingomyelin
SQDG	Sulfoquinovosyldiacylglycerol
TAG	Triacylglyceride
TLC	Thin layer chromatography
UV	Ultraviolet
WOB	Washed OB
WPI	Whey protein isolate

Author contributions

C. Bourlieu, V. Vié and J. Kergomard determined the outline and content of the review, designed the tables and figures, J. Kergomard wrote the review, all authors corrected and implemented the review.

Disclosure statement

No potential conflict of interest was reported by the authors.

Funding

The author(s) reported there is no funding associated with the work featured in this article.

References

Abdullah, J. W., and H. Zhang. 2020. Recent advances in the composition, extraction and food applications of plant-derived oleosomes. *Trends in Food Science & Technology* 106:322–32.

Albertsson, P.-A., R. Köhnke, S. C. Emek, J. Mei, J. F. Rehfeld, H.-E. Akerlund, and C. Erlanson-Albertsson. 2007. Chloroplast membranes retard fat digestion and induce satiety: Effect of biological membranes on pancreatic lipase/co-lipase. *The Biochemical Journal* 401 (3):727–33. doi: 10.1042/BJ20061463.

Amara, S., N. Barouh, J. Lecomte, D. Lafont, S. Robert, P. Villeneuve, A. De Caro, and F. Carrière. 2010. Lipolysis of natural long chain and synthetic medium chain galactolipids by pancreatic lipase-related protein 2. *Biochimica et Biophysica Acta* 1801 (4):508–16. doi: 10.1016/j.bbalip.2010.01.003.

Amara, S., D. Lafont, B. Fiorentino, P. Boullanger, F. Carrière, and A. De Caro. 2009. Continuous measurement of galactolipid hydrolysis by pancreatic lipolytic enzymes using the pH-stat technique and a medium chain monogalactosyl diglyceride as substrate. *Biochimica et Biophysica Acta* 1791 (10):983–90. doi: 10.1016/j.bbalip.2009.05.002.

Anderson, M. M., R. E. McCarty, and E. A. Zimmer. 1974. The role of galactolipids in spinach chloroplast lamellar membranes: I. Partial purification of a bean leaf galactolipid lipase and its action on subchloroplast particles. *Plant Physiology* 53 (5):699–704. doi: 10.1104/pp.53.5.699.

Andersson, L., C. Bratt, K. C. Arnoldsson, B. Herslöf, N. U. Olsson, B. Sternby, and A. Nilsson. 1995. Hydrolysis of galactolipids by human pancreatic lipolytic enzymes and duodenal contents. *Journal of Lipid Research* 36 (6):1392–400. doi: 10.1016/S0022-2275(20)41146-0.

Anomynous. 2011. *Saisine n° 2006-SA-0359, ANC AG, ANSES, Editor, Avis de l'Agence française de sécurité sanitaire des aliments relatif à l'actualisation des apports nutritionnels conseillés pour les acides gras.* https://www.anses.fr/fr/system/files/NUT2006sa0359.pdf

Barre, A., M. Simplicien, G. Cassan, H. Benoist, and P. Rougé. 2018. Oil bodies (oleosomes): Occurrence, structure, allergenicity. *Revue Française D'Allergologie* 58 (8):574–80. doi: 10.1016/j.reval.2018.10.005.

Beisson, F., N. Ferté, S. Bruley, R. Voultoury, R. Verger, and V. Arondel. 2001. Oil-bodies as substrates for lipolytic enzymes. *Biochimica et Biophysica Acta (BBA) - Molecular and Cell Biology of Lipids* 1531 (1-2):47–58. doi: 10.1016/S1388-1981(01)00086-5.

Berry, S. E. E., and T. A. B. Sanders. 2005. Influence of triacylglycerol structure of stearic acid-rich fats on postprandial lipaemia. *The Proceedings of the Nutrition Society* 64 (2):205–12. doi: 10.1079/pns2005422.

Berton-Carabin, C. C., M.-H. Ropers, and C. Genot. 2014. Lipid oxidation in oil-in-water emulsions: Involvement of the interfacial layer. *Comprehensive Reviews in Food Science and Food Safety* 13 (5):945–77. doi: 10.1111/1541-4337.12097.

Block, M. A., A. J. Dorne, J. Joyard, and R. Douce. 1983. Preparation and characterization of membrane fractions enriched in outer and inner envelope membranes from spinach chloroplasts. II. Biochemical characterization. *Journal of Biological Chemistry* 258 (21):13281–6. doi: 10.1016/S0021-9258(17)44113-5.

Borgström, B. 1993. Phosphatidylcholine as substrate for human pancreatic phospholipase A2. Importance of the physical state of the substrate. *Lipids* 28 (5):371–5. doi: 10.1007/BF02535932.

Bottier, C., J. Géan, F. Artzner, B. Desbat, M. Pézolet, A. Renault, D. Marion, and V. Vié. 2007. Galactosyl headgroup interactions control the molecular packing of wheat lipids in Langmuir films and in hydrated liquid-crystalline mesophases. *Biochimica et Biophysica Acta* 1768 (6):1526–40. doi: 10.1016/j.bbamem.2007.02.021.

Bourlieu, C., O. Ménard, K. Bouzerzour, G. Mandalari, A. Macierzanka, A. R. Mackie, and D. Dupont. 2014. Specificity of infant digestive conditions: Some clues for developing relevant *in vitro* models. *Critical Reviews in Food Science and Nutrition* 54 (11):1427–57. doi: 10.1080/10408398.2011.640757.

Browse, J., and C. Somerville. 1991. Glycerolipid synthesis: Biochemistry and regulation. *Annual Review of Plant Physiology and Plant Molecular Biology* 42 (1):467–506. doi: 10.1146/annurev.pp.42.060191.002343.

Chen, B., D. J. McClements, D. A. Gray, and E. A. Decker. 2012. Physical and oxidative stability of pre-emulsified oil bodies extracted from soybeans. *Food Chemistry* 132 (3):1514–20. doi: 10.1016/j.foodchem.2011.11.144.

Chen, Y., Y. Cao, L. Zhao, X. Kong, and Y. Hua. 2014. Macronutrients and micronutrients of soybean oil bodies extracted at different pH. *Journal of Food Science* 79 (7):C1285–C1291. doi: 10.1111/1750-3841.12516.

Chen, Y., and T. Ono. 2010. Simple extraction method of non-allergenic intact soybean oil bodies that are thermally stable in an aqueous medium. *Journal of Agricultural and Food Chemistry* 58 (12):7402–7. doi: 10.1021/jf1006159.

Chu, B.-S., G. T. Rich, M. J. Ridout, R. M. Faulks, M. S. J. Wickham, and P. J. Wilde. 2009. Modulating pancreatic lipase activity with galactolipids: Effects of emulsion interfacial composition. *Langmuir: The ACS Journal of Surfaces and Colloids* 25 (16):9352–60. doi: 10.1021/la9008174.

Couëdelo, L., S. Amara, M. Lecomte, E. Meugnier, J. Monteil, L. Fonseca, G. Pineau, M. Cansell, F. Carrière, M. C. Michalski, et al. 2015. Impact of various emulsifiers on ALA bioavailability and chylomicron synthesis through changes in gastrointestinal lipolysis. *Food & Function* 6 (5):1726–35. doi: 10.1039/C5FO00070J.

Cui, L., and E. A. Decker. 2016. Phospholipids in foods: Prooxidants or antioxidants? *Journal of the Science of Food and Agriculture* 96 (1):18–31. doi: 10.1002/jsfa.7320.

De Caro, J., C. Eydoux, S. Chérif, R. Lebrun, Y. Gargouri, F. Carrière, and A. De Caro. 2008. Occurrence of pancreatic lipase-related protein-2 in various species and its relationship with herbivore diet. *Comparative Biochemistry and Physiology. Part B, Biochemistry & Molecular Biology* 150 (1):1–9. doi: 10.1016/j.cbpb.2008.01.007.

De Caro, J., B. Sias, P. Grandval, F. Ferrato, H. Halimi, F. Carrière, and A. De Caro. 2004. Characterization of pancreatic lipase-related protein 2 isolated from human pancreatic juice. *Biochimica et Biophysica Acta* 1701 (1-2):89–99. doi: 10.1016/j.bbapap.2004.06.005.

Decker, E. A., D. J. McClements, C. Bourlieu-Lacanal, E. Durand, M. C. Figueroa-Espinoza, J. Lecomte, and P. Villeneuve. 2017. Hurdles in predicting antioxidant efficacy in oil-in-water emulsions. *Trends in Food Science & Technology* 67:183–94. doi: 10.1016/j.tifs.2017.07.001.

Deckers, H.M., G. Van Rooijen, J. Boothe, J. Goll, M. M. Moloney. 2002. Products for topical applications comprising oil bodies. United States Patent Application 20020106337.

Demé, B., C. Cataye, M. A. Block, E. Maréchal, and J. Jouhet. 2014. Contribution of galactoglycerolipids to the 3-dimensional architecture of thylakoids. *FASEB Journal: Official Publication of the Federation of American Societies for Experimental Biology* 28 (8):3373–83. doi: 10.1096/fj.13-247395.

Ding, J., Z. Xu, B. Qi, Z. Liu, L. Yu, Z. Yan, L. Jiang, and X. Sui. 2020. Thermally treated soya bean oleosomes: The changes in their stability and associated proteins. *International Journal of Food Science & Technology* 55 (1):229–38. doi: 10.1111/ijfs.14266.

Dorne, A. J., J. Joyard, and R. Douce. 1990. Do thylakoids really contain phosphatidylcholine? *Proceedings of the National Academy of Sciences of the United States of America* 87 (1):71–4. doi: 10.1073/pnas.87.1.71.

Douce, R., R. B. Holtz, and A. A. Benson. 1973. Isolation and properties of the envelope of spinach chloroplasts. *Journal of Biological Chemistry* 248 (20):7215–22. doi: 10.1016/S0021-9258(19)43381-4.

El Hadi, H., A. Di Vincenzo, R. Vettor, and M. Rossato. 2019. Cardio-metabolic disorders in non-alcoholic fatty liver disease. *International Journal of Molecular Sciences* 20 (9):2215. doi: 10.3390/ijms20092215.

Enos, R. T., K. T. Velázquez, J. L. McClellan, T. L. Cranford, M. D. Walla, and E. A. Murphy. 2014. Reducing the dietary omega-6:omega-3 utilizing α-linolenic acid; not a sufficient therapy for attenuating high-fat-diet-induced obesity development nor related detrimental metabolic and adipose tissue inflammatory outcomes. *PLoS One* 9 (4):e94897. doi: 10.1371/journal.pone.0094897.

Eydoux, C., S. Spinelli, T. L. Davis, J. R. Walker, A. Seitova, S. Dhe-Paganon, A. De Caro, C. Cambillau, and F. Carrière. 2008. Structure of human pancreatic lipase-related protein 2 with the lid in an open conformation. *Biochemistry* 47 (36):9553–64. doi: 10.1021/bi8005576.

Fisk, I. D., D. A. White, A. Carvalho, and D. A. Gray. 2006. Tocopherol—An intrinsic component of sunflower seed oil bodies. *Journal of the American Oil Chemists' Society* 83 (4):341–4. doi: 10.1007/s11746-006-1210-2.

Fisk, I. D., D. A. White, M. Lad, and D. A. Gray. 2008. Oxidative stability of sunflower oil bodies. *European Journal of Lipid Science and Technology* 110 (10):962–8. doi: 10.1002/ejlt.200800051.

Frandsen, G. I., J. Mundy, and J. T. C. Tzen. 2001. Oil bodies and their associated proteins, oleosin and caleosin. *Physiologia Plantarum* 112 (3):301–7. doi: 10.1034/j.1399-3054.2001.1120301.x.

Frentzen, M., E. Heinz, T. A. McKeon, and P. K. Stumpf. 1983. Specificities and selectivities of glycerol-3-phosphate acyltransferase and monoacylglycerol-3-phosphate acyltransferase from pea and spinach chloroplasts. *European Journal of Biochemistry* 129 (3):629–36. doi: 10.1111/j.1432-1033.1983.tb07096.x.

Furt, F., F. Simon-Plas, and S. Mongrand. 2011. Lipids of the plant plasma membrane. In *The plant plasma membrane*, ed. A. S. Murphy, B. Schulz, and W. Peer, 3–30. Berlin: Springer.

Gallier, S., and H. Singh. 2012. Behavior of almond oil bodies during *in vitro* gastric and intestinal digestion. *Food & Function* 3 (5):547–55. doi: 10.1039/c2fo10259e.

Gallier, S., H. Tate, and H. Singh. 2013. *In vitro* gastric and intestinal digestion of a walnut oil body dispersion. *Journal of Agricultural and Food Chemistry* 61 (2):410–7. doi: 10.1021/jf303456a.

Gargouri, Y., G. Pieroni, C. Riviere, J.-F. Sauniere, P. A. Lowe, L. Sarda, and R. Verger. 1986. Kinetics assay of human gastric lipase on short and long chain triacylglycerol emulsions. *Gastroenterology* 91 (4):919–25. doi: 10.1016/0016-5085(86)90695-5.

Golding, M., and T. J. Wooster. 2010. The influence of emulsion structure and stability on lipid digestion. *Current Opinion in Colloid & Interface Science* 15 (1-2):90–101. doi: 10.1016/j.cocis.2009.11.006.

Gounaris, K., and J. Barber. 1983. Monogalactosyldiacylglycerol: The most abundant polar lipid in nature. *Trends in Biochemical Sciences* 8 (10):378–81. doi: 10.1016/0968-0004(83)90366-3.

Gray, D. A., G. Payne, D. J. McClements, E. A. Decker, and M. Lad. 2010. Oxidative stability of Echium plantagineum seed oil bodies. *European Journal of Lipid Science and Technology* 112 (7):741–9. doi: 10.1002/ejlt.200900280.

Grundy, M. M.-L., K. Lapsley, and P. R. Ellis. 2016. A review of the impact of processing on nutrient bioaccessibility and digestion of almonds. *International Journal of Food Science & Technology* 51 (9):1937–46. doi: 10.1111/ijfs.13192.

Gurevich, V., B. B. Bondarenko, K. J. Gundermann, R. Schumacher, T. Astashkina, V. Ivanov, Y. Popov, L. Shatilina, and N. Kazennova. 1997. Polyunsaturated phospholipids increase the hypolipidemic effect of Lovastatin. *European Journal of Internal Medicine* 8:13–8.

Han, S. K., B. I. Lee, and W. Cho. 1997. Bacterial expression and characterization of human pancreatic phospholipase A2. *Biochimica et Biophysica Acta* 1346 (2):185–92. doi: 10.1016/S0005-2760(97)00034-9.

Hassan, Z., S. Ali, R. Ahmad, M. Rizwan, F. Abbas, T. Yasmeen, and M. Iqbal. 2017. Biochemical and molecular responses of oilseed crops to heavy metal stress. In *Oilseed crops*, ed. P. Ahmad, 236–48. John Wiley & Sons, Ltd.doi: 10.1002/9781119048800

Hazahari, N. Y. B., M. Hosokawa, and K. Miyashita. 2018. Comparison of oxidative stability of monogalactosyl diacylglycerol, digalactosyl diacylglycerol, and triacylglycerol containing polyunsaturated fatty acids. *Food and Nutrition Sciences* 9: 221–234. doi: 10.4236/fns.2018.93017.

He, X., Y. Sun, and R.-L. Zhu. 2013. The oil bodies of liverworts: Unique and important organelles in land plants. *Critical Reviews in Plant Sciences* 32 (5):293–302. doi: 10.1080/07352689.2013.765765.

Hildebrand, D. H., J. Terao, and M. Kito. 1984. Phospholipids plus tocopherols increase soybean oil stability. *Journal of the American Oil Chemists' Society* 61 (3):552–5. doi: 10.1007/BF02677029.

Huang, A. H. C. 1992. Oil bodies and oleosins in seeds. *Annual Review of Plant Physiology and Plant Molecular Biology* 43 (1):177–200. doi: 10.1146/annurev.pp.43.060192.001141.

Huang, C.-Y., and A. H. C. Huang. 2017. Unique motifs and length of hairpin in oleosin target the cytosolic side of endoplasmic reticulum and budding lipid droplet. *Plant Physiology* 174 (4):2248–60. doi: 10.1104/pp.17.00366.

Huang, M.-D., and A. H. C. Huang. 2015. Bioinformatics reveal five lineages of oleosins and the mechanism of lineage evolution related to structure/function from green algae to seed plants. *Plant Physiology* 169 (1):453–70. doi: 10.1104/pp.15.00634.

James, M. 2002. *Recombinant oleosins from cacao and their use as flavoring or emulsifying agents*. Nestec SA. EP1235919B1.

Judde, A., P. Villeneuve, A. Rossignol-Castera, and A. Le Guillou. 2003. Antioxidant effect of soy lecithins on vegetable oil stability and their synergism with tocopherols. *Journal of the American Oil Chemists' Society* 80 (12):1209–15. doi: 10.1007/s11746-003-0844-4.

Kapchie, V. N., L. Yao, C. C. Hauck, T. Wang, and P. A. Murphy. 2013. Oxidative stability of soybean oil in oleosomes as affected by pH and iron. *Food Chemistry* 141 (3):2286–93. doi: 10.1016/j.foodchem.2013.05.018.

Karkani, O. A., N. Nenadis, C. V. Nikiforidis, and V. Kiosseoglou. 2013. Effect of recovery methods on the oxidative and physical stability of oil body emulsions. *Food Chemistry* 139 (1-4):640–8. doi: 10.1016/j.foodchem.2012.12.055.

Kashima, M., G.-S. Cha, Y. Isoda, J. Hirano, and T. Miyazawa. 1991. The antioxidant effects of phospholipids on perilla oil. *Journal of the American Oil Chemists' Society* 68 (2):119–22. doi: 10.1007/BF02662331.

Kergomard, J., G. Paboeuf, N. Barouh, P. Villeneuve, O. Schafer, T. J. Wooster, C. Bourlieu, and V. Vié. 2021. Stability to oxidation and interfacial behavior at the air/water interface of minimally-processed versus processed walnut oil-bodies. *Food Chemistry* 360:129880. doi: 10.1016/j.foodchem.2021.129880.

Khor, V. K., W.-J. Shen, and F. B. Kraemer. 2013. Lipid droplet metabolism. *Current Opinion in Clinical Nutrition and Metabolic Care* 16 (6):632–7.

Kobayashi, K. 2016. Role of membrane glycerolipids in photosynthesis, thylakoid biogenesis and chloroplast development. *Journal of Plant Research* 129 (4):565–80. doi: 10.1007/s10265-016-0827-y.

Köhnke, R., A. Lindbo, T. Larsson, A. Lindqvist, M. Rayner, S. C. Emek, P.-A. Albertsson, J. F. Rehfeld, M. Landin-Olsson, and C. Erlanson-Albertsson. 2009. Thylakoids promote release of the satiety hormone cholecystokinin while reducing insulin in healthy humans. *Scandinavian Journal of Gastroenterology* 44 (6):712–9. doi: 10.1080/00365520902803499.

Köhnke, R., A. Lindqvist, N. Göransson, S. C. Emek, P.-A. Albertsson, J. F. Rehfeld, A. Hultgårdh-Nilsson, and C. Erlanson-Albertsson. 2009. Thylakoids suppress appetite by increasing cholecystokinin resulting in lower food intake and body weight in high-fat fed mice. *Phytotherapy Research: PTR* 23 (12):1778–83. doi: 10.1002/ptr.2855.

Konopka, I., S. Czaplicki, and D. Rotkiewicz. 2006. Differences in content and composition of free lipids and carotenoids in flour of spring and winter wheat cultivated in Poland. *Food Chemistry* 95 (2):290–300. doi: 10.1016/j.foodchem.2005.01.011.

Krumova, S. B., C. Dijkema, P. de Waard, H. Van As, G. Garab, and H. van Amerongen. 2008. Phase behavior of phosphatidylglycerol in spinach thylakoid membranes as revealed by 31P-NMR. *Biochimica et Biophysica Acta* 1778 (4):997–1003. doi: 10.1016/j.bbamem.2008.01.004.

Lane, K., E. Derbyshire, W. Li, and C. Brennan. 2014. Bioavailability and potential uses of vegetarian sources of omega-3 fatty acids: A

review of the literature. *Critical Reviews in Food Science and Nutrition* 54 (5):572–9. doi: 10.1080/10408398.2011.596292.
Lee, H. S., Y. Nam, Y. H. Chung, H. R. Kim, E. S. Park, S. J. Chung, J. H. Kim, U. D. Sohn, H.-C. Kim, K. W. Oh, et al. 2014. Beneficial effects of phosphatidylcholine on high-fat diet-induced obesity, hyperlipidemia and fatty liver in mice. *Life Sciences* 118 (1):7–14. doi: 10.1016/j.lfs.2014.09.027.
Li, J., and Z. Guo. 2016. Identification and quantification of phenolic compounds in rapeseed originated lecithin and antioxidant activity evaluation. *LWT* 73:397–405. doi: 10.1016/j.lwt.2016.06.039.
Li, M., D. J. Murphy, K.-H. K. Lee, R. Wilson, L. J. Smith, D. C. Clark, and J.-Y. Sung. 2002. Purification and structural characterization of the central hydrophobic domain of oleosin. *The Journal of Biological Chemistry* 277 (40):37888–95. doi: 10.1074/jbc.M202721200.
Makkhun, S., A. Khosla, T. Foster, D. J. McClements, M. M. L. Grundy, and D. A. Gray. 2015. Impact of extraneous proteins on the gastrointestinal fate of sunflower seed (Helianthus annuus) oil bodies: A simulated gastrointestinal tract study. *Food & Function* 6 (1):125–34. doi: 10.1039/c4fo00422a.
Márquez-Ruiz, G., M. C. García-Martínez, and F. Holgado. 2008. Changes and effects of dietary oxidized lipids in the gastrointestinal tract. *Lipid Insights* 2:LPI.S904. doi: 10.4137/LPI.S904.
Maurer, S., G. Waschatko, D. Schach, B. I. Zielbauer, J. Dahl, T. Weidner, M. Bonn, and T. A. Vilgis. 2013. The role of intact oleosin for stabilization and function of oleosomes. *The Journal of Physical Chemistry. B* 117 (44):13872–83. doi: 10.1021/jp403893n.
Maurice, M., B. Joseph, and V. R. Gijs. 2000. *Oil bodies and associated proteins as affinity matrices*. Sembiosys Genetics Inc. US5856452A. https://patents.google.com/patent/US5856452A/en
Michalski, M. C., C. Genot, C. Gayet, C. Lopez, F. Fine, F. Joffre, J. L. Vendeuvre, J. Bouvier, J. M. Chardigny, and K. Raynal-Ljutovac. 2013. Multiscale structures of lipids in foods as parameters affecting fatty acid bioavailability and lipid metabolism. *Progress in Lipid Research* 52 (4):354–73. doi: 10.1016/j.plipres.2013.04.004.
Millichip, M., A. S. Tatham, F. Jackson, G. Griffiths, P. R. Shewry, and A. K. Stobart. 1996. Purification and characterization of oil-bodies (oleosomes) and oil-body boundary proteins (oleosins) from the developing cotyledons of sunflower (*Helianthus annuus* L.). *Biochemical Journal* 314 (1):333–7. doi: 10.1042/bj3140333.
N'Goma, J.-C. B., S. Amara, K. Dridi, V. Jannin, and F. Carrière. 2012. Understanding the lipid-digestion processes in the GI tract before designing lipid-based drug-delivery systems. *Therapeutic Delivery* 3 (1):105–24. doi: 10.4155/tde.11.138.
Nalbone, G., D. Lairon, M. Charbonnier-Augeire, J.-L. Vigne, J. Leonardi, C. Chabert, J. C. Hauton, and R. Verger. 1980. Pancreatic phospholipase A2 hydrolysis of phosphatidylcholines in various physicochemical states. *Biochimica et Biophysica Acta (BBA) - Lipids and Lipid Metabolism* 620 (3):612–25. doi: 10.1016/0005-v2760(80)90153-8.
Nantiyakul, N., S. Furse, I. Fisk, T. J. Foster, G. Tucker, and D. A. Gray. 2012. Phytochemical composition of *Oryza sativa* (Rice) bran oil bodies in crude and purified isolates. *Journal of the American Oil Chemists' Society* 89 (10):1867–72. doi: 10.1007/s11746-012-2078-y.
Nikiforidis, C. V. 2019. Structure and functions of oleosomes (oil bodies). *Advances in Colloid and Interface Science* 274:102039.
Nikiforidis, C. V., C. Ampatzidis, S. Lalou, E. Scholten, T. D. Karapantsios, and V. Kiosseoglou. 2013. Purified oleosins at air–water interfaces. *Soft Matter* 9 (4):1354–63. doi: 10.1039/C2SM27118D.
Nikiforidis, C. V., V. Kiosseoglou, and E. Scholten. 2013. Oil bodies: An insight on their microstructure — maize germ vs sunflower seed. *Food Research International* 52 (1):136–41. doi: 10.1016/j.foodres.2013.02.052.
Nikiforidis, C. V., A. Matsakidou, and V. Kiosseoglou. 2014. Composition, properties and potential food applications of natural emulsions and cream materials based on oil bodies. *RSC Advances.* 4 (48):25067–78. doi: 10.1039/C4RA00903G.
Noll, F., C. May, and H. Kindl. 2000. Phospholipid monolayer of plant lipid bodies attacked by phospholipase A2 shows 80 nm holes analyzed by atomic force microscopy. *Biophysical Chemistry* 86 (1):29–35. doi: 10.1016/S0301-4622(00)00156-3.
Ohlsson, L. 2000. *Digestion and absorption of galactolipids*. Lund: Institute of Medicine, University Hospital of Lund.
Piironen, V., D. G. Lindsay, T. A. Miettinen, J. Toivo, and A.-M. Lampi. 2000. Plant sterols: Biosynthesis, biological function and their importance to human nutrition. *Journal of the Science of Food and Agriculture* 80 (7):939–66. doi: 10.1002/(SICI)1097-0010(20000515)80:7<939::AID-JSFA644>3.0.CO;2-C.
Pourteymour Fard Tabrizi, F., and M. Abbasalizad Farhangi. 2020. A systematic review of the potential effects of thylakoids in the management of obesity and its related issues. *Food Reviews International* 37 (5):469–90.
Pribil, M., M. Labs, and D. Leister. 2014. Structure and dynamics of thylakoids in land plants. *Journal of Experimental Botany* 65 (8):1955–72. doi: 10.1093/jxb/eru090.
Rayner, M., H. Ljusberg, S. C. Emek, E. Sellman, C. Erlanson-Albertsson, and P.-Å. Albertsson. 2011. Chloroplast thylakoid membrane-stabilised emulsions. *Journal of the Science of Food and Agriculture* 91 (2):315–21. doi: 10.1002/jsfa.4187.
Reis, A., and C. M. Spickett. 2012. Chemistry of phospholipid oxidation. *Biochimica et Biophysica Acta* 1818 (10):2374–87. doi: 10.1016/j.bbamem.2012.02.002.
Robert, C., C. Buisson, F. Laugerette, H. Abrous, D. Rainteau, L. Humbert, J. Vande Weghe, E. Meugnier, E. Loizon, F. Caillet, et al. 2021. Impact of rapeseed and soy lecithin on postprandial lipid metabolism, bile acid profile, and gut bacteria in mice. *Molecular Nutrition & Food Research* 65 (9):2001068. doi: 10.1002/mnfr.202001068.
Robert, C., L. Couëdelo, C. Knibbe, L. Fonseca, C. Buisson, E. Errazuriz-Cerda, E. Meugnier, E. Loizon, C. Vaysse, and M.-C. Michalski. 2020. Rapeseed lecithin increases lymphatic lipid output and α-linolenic acid bioavailability in rats. *The Journal of Nutrition* 150 (11):2900–11. doi: 10.1093/jn/nxaa244.
Robert, C., L. Couëdelo, C. Vaysse, and M.-C. Michalski. 2020. Vegetable lecithins: A review of their compositional diversity, impact on lipid metabolism and potential in cardiometabolic disease prevention. *Biochimie* 169:121–32. doi: 10.1016/j.biochi.2019.11.017.
Sahaka, M., S. Amara, J. Wattanakul, M. A. Gedi, N. Aldai, G. Parsiegla, J. Lecomte, J. T. Christeller, D. Gray, B. Gontero, et al. 2020. The digestion of galactolipids and its ubiquitous function in Nature for the uptake of the essential α-linolenic acid. *Food & Function* 11 (8):6710–44. doi: 10.1039/D0FO01040E.
Saini, R. K., and Y.-S. Keum. 2018. Omega-3 and omega-6 polyunsaturated fatty acids: Dietary sources, metabolism, and significance - A review. *Life Sciences* 203:255–67. doi: 10.1016/j.lfs.2018.04.049.
Salhi, A., S. Amara, P. Mansuelle, R. Puppo, R. Lebrun, B. Gontero, A. Aloulou, and F. Carrière. 2020. Characterization of all the lipolytic activities in pancreatin and comparison with porcine and human pancreatic juices. *Biochimie* 169:106–20. doi: 10.1016/j.biochi.2019.07.004.
Shahidi, F., and Y. Zhong. 2010. Lipid oxidation and improving the oxidative stability. *Chemical Society Reviews* 39 (11):4067–79. doi: 10.1039/b922183m.
Shanbhag, A. 2018. Utilization of modified lecithin to control lipid oxidation in bulk oils. Masters theses. University of Massachusetts. https://scholarworks.umass.edu/cgi/viewcontent.cgi?article=1648&context=masters_theses_2
Simpson, T. D., and L. K. Nakamura. 1989. Phospholipid degradation in membranes of isolated soybean lipid bodies. *Journal of the American Oil Chemists' Society* 66 (8):1093–6. doi: 10.1007/BF02670091.
Sintra, T. E., S. P. M. Ventura, and J. A. P. Coutinho. 2014. Superactivity induced by micellar systems as the key for boosting the yield of enzymatic reactions. *Journal of Molecular Catalysis B: Enzymatic* 107:140–51. doi: 10.1016/j.molcatb.2014.06.001.
Stenkula, K. G., E.-L. Stenblom, C. Montelius, E. Egecioglu, and C. Erlanson-Albertsson. 2017. Thylakoids reduce body fat and fat cell size by binding to dietary fat making it less available for absorption in high-fat fed mice. *Nutrition & Metabolism* 14:4. doi: 10.1186/s12986-016-0160-4.
Sternby, B., A. Nilsson, T. Melin, and B. Borgström. 1991. Pancreatic lipolytic enzymes in human duodenal contents radioimmunoassay compared with enzyme activity. *Scandinavian Journal of Gastroenterology* 26 (8):859–66. doi: 10.3109/00365529109037023.

St-Pierre, A., D. Blondeau, M. Boivin, V. Beaupré, N. Boucher, and I. Desgagné-Penix. 2019. Study of antioxidant properties of thylakoids and application in UV protection and repair of UV-induced damage. *Journal of Cosmetic Dermatology* 18 (6):1980–91. doi: 10.1111/jocd.12936.

Takenaka, A., M. Hosokawa, and K. Miyashita. 2007. Unsaturated Phosphatidylethanolamine as effective synergist in combination with alpha-tocopherol. *Journal of Oleo Science* 56 (10):511–6. doi: 10.5650/jos.56.511.

Tzen, J. T. C., Y. Cao, P. Laurent, C. Ratnayake, and A. H. C. Huang. 1993. Lipids, proteins, and structure of seed oil bodies from diverse species. *Plant Physiology* 101 (1):267–76. doi: 10.1104/pp.101.1.267.

Tzen, J. T., Y. K. Lai, K. L. Chan, and A. H. Huang. 1990. Oleosin isoforms of high and low molecular weights are present in the oil bodies of diverse seed species. *Plant Physiology* 94 (3):1282–9. doi: 10.1104/pp.94.3.1282.

Vergara, D., O. López, M. Bustamante, and C. Shene. 2020. An *in vitro* digestion study of encapsulated lactoferrin in rapeseed phospholipid–based liposomes. *Food Chemistry* 321:126717. doi: 10.1016/j.foodchem.2020.126717.

Vindigni, J.-D., F. Wien, A. Giuliani, Z. Erpapazoglou, R. Tache, F. Jagic, T. Chardot, Y. Gohon, and M. Froissard. 2013. Fold of an oleosin targeted to cellular oil bodies. *Biochimica et Biophysica Acta* 1828 (8):1881–8. doi: 10.1016/j.bbamem.2013.04.009.

Vors, C., P. Capolino, C. Guérin, E. Meugnier, S. Pesenti, M.-A. Chauvin, J. Monteil, N. Peretti, M. Cansell, F. Carrière, et al. 2012. Coupling *in vitro* gastrointestinal lipolysis and Caco-2 cell cultures for testing the absorption of different food emulsion. *Food & Function* 3 (5):537–46. doi: 10.1039/c2fo10248j.

Vors, C., J. Drai, G. Pineau, M. Laville, H. Vidal, F. Laugerette, and M.-C. Michalski. 2017. Emulsifying dietary fat modulates postprandial endotoxemia associated with chylomicronemia in obese men: A pilot randomized crossover study. *Lipids in Health and Disease* 16 (1):97. doi: 10.1186/s12944-017-0486-6.

Vors, C., L. Joumard-Cubizolles, M. Lecomte, E. Combe, L. Ouchchane, J. Drai, K. Raynal, F. Joffre, L. Meiller, M. Le Barz, et al. 2020. Milk polar lipids reduce lipid cardiovascular risk factors in overweight postmenopausal women: Towards a gut sphingomyelin-cholesterol interplay. *Gut* 69 (3):487–501. doi: 10.1136/gutjnl-2018-318155.

Vors, C., G. Pineau, L. Gabert, J. Drai, C. Louche-Pélissier, C. Defoort, D. Lairon, M. Désage, S. Danthine, S. Lambert-Porcheron, et al. 2013. Modulating absorption and postprandial handling of dietary fatty acids by structuring fat in the meal: A randomized crossover clinical trial. *The American Journal of Clinical Nutrition* 97 (1):23–36. doi: 10.3945/ajcn.112.043976.

Walther, T. C., and R. V. Farese. 2012. Lipid droplets and cellular lipid metabolism. *Annual Review of Biochemistry* 81 (1):687–714. doi: 10.1146/annurev-biochem-061009-102430.

Waraho, T., D. J. McClements, and E. A. Decker. 2011. Mechanisms of lipid oxidation in food dispersions. *Trends in Food Science & Technology* 22 (1):3–13. doi: 10.1016/j.tifs.2010.11.003.

Wattanakul, J., M. Sahaka, S. Amara, S. Mansor, B. Gontero, F. Carrière, and D. Gray. 2019. *In vitro* digestion of galactolipids from chloroplast-rich fraction (CRF) of postharvest, pea vine field residue (haulm) and spinach leaves. *Food & Function* 10 (12):7806–17. doi: 10.1039/c9fo01867k.

Yamaguchi, T., R. Sugimura, J. Shimajiri, M. Suda, M. Abe, M. Hosokawa, and K. Miyashita. 2012. Oxidative stability of glycero-glycolipids containing polyunsaturated fatty acids. *Journal of Oleo Science* 61 (9):505–13. doi: 10.5650/jos.61.505.

Yamauchi, R., M. Kojima, K. Kato, and Y. Ueno. 1983. Autoxidation products of polyunsaturated galactolipids. *Agricultural and Biological Chemistry* 47 (11):2625–30. doi: 10.1080/00021369.1983.10866000.

Yi, O.-S., D. Han, and H.-K. Shin. 1991. Synergistic antioxidative effects of tocopherol and ascorbic acid in fish oil/lecithin/water system. *Journal of the American Oil Chemists' Society* 68 (11):881–3. doi: 10.1007/BF02660606.

Zhou, L.-z., F.-s. Chen, L.-h. Hao, Y. Du, and C. Liu. 2019. Peanut oil body composition and stability. *Journal of Food Science* 84 (10):2812–9. doi: 10.1111/1750-3841.14801.

Colloids and Surfaces B: Biointerfaces 217 (2022) 112646

Contents lists available at ScienceDirect

Colloids and Surfaces B: Biointerfaces

journal homepage: www.elsevier.com/locate/colsurfb

Interfacial organization and phase behavior of mixed galactolipid-DPPC-phytosterol assemblies at the air-water interface and in hydrated mesophases

Jeanne Kergomard [a,b], Frédéric Carrière [c], Gilles Paboeuf [a], Franck Artzner [a], Nathalie Barouh [d,e], Claire Bourlieu [b], Véronique Vié [a,f,*,1]

[a] IPR Institute of Physics, UMR UR1 CNRS 6251, Rennes 1 University, France
[b] INRAE/CIRAD/UM/Institut Agro Montpellier UMR 1208 IATE, France
[c] Aix-Marseille Université, CNRS, UMR7281 Bioénergétique et Ingénierie des Protéines, Marseille, France
[d] CIRAD, UMR QUALISUD, F34398 Montpellier, France
[e] Qualisud, Univ Montpellier, Avignon Université, CIRAD, Institut Agro, Université de La Réunion, Montpellier, France
[f] Univ Rennes 1, CNRS, ScanMAT - UMS 2001, F-35042 Renne, France

ARTICLE INFO

Keywords:
Galactolipid
Phytosterol
Natural surfactant
Vegetal photosynthetic assemblies

ABSTRACT

The structural behavior of model assemblies composed of monogalactosyldiacylglycerol (MGDG) and digalactosyldiacylglycerol (DGDG), the two main galactolipids found in plants, was investigated at the air/water interface and in aqueous dispersion. To approach the composition of the natural photosynthetic membranes, tunable Langmuir model membrane of galactolipids (GL) were used, and were complexified to form either heterogenous binary or ternary assemblies of GL, phospholipids (PL), and phytosterols (pS).

The impact of pS, 1,2-dipalmitoyl-sn-glycero-3-phosphocholine (DPPC) or both on the structural properties of GL membrane was studied. The nature of the interactions between the different molecules was investigated using biophysical characterizations (ellipsometry, tensiometry, atomic force microscopy). In addition, the phase behavior was determined by SAXS analysis on the model assemblies in aqueous dispersions.

Results revealed the good interfacial stability of these specific plant membrane lipids. The morphology of the GL film was characteristic of a fluid phase, with an interfacial roughness induced by the intercalation of monogalactosyl and digalactosyl polar heads of MGDG and DGDG, respectively. A phase heterogeneity in the monolayer was induced by the addition of DPPC and/or pS, which resulted in the modification of galactolipid organization and headgroup interactions. These structural changes were confirmed by SAXS analysis, showing more favorable interactions between MGDG and DPPC than between DGDG and DPPC in aqueous dispersion. This phenomenon was exacerbated in the presence of pS.

1. Introduction

Galactolipids are the most abundant polar lipids found in higher plants. These glycolipids are actively involved in the structuration of the plant membranes and are particularly concentrated in the photosynthetic chloroplast membranes (80 % wt. of total non-pigmented lipids), which contain large amounts of monogalactosyldiacylglycerol (MGDG, 53% wt.) and digalactosyldiacylglycerol (DGDG, 27 % wt.) [1]. MGDG possess a small 1-β-galactose polar head bound to a diacylglycerol, giving it a conical shape, which can induce curvatures in lamellar phases [2]. On the other hand, DGDG has a larger polar head with an additional α-galactose, linked to β-galactose [3] and adopts a cylindrical shape in solution. Both GL possess two esterified acyl chains at the *sn*-1 and *sn*-2 position of the glycerol backbone, whose molecular motion depends on the number of unsaturation.

Due to their different structure, MGDG and DGDG exhibit distinct

Abbreviations: AFM, atomic force microscopy; DGDG, digalactosyldiacylglycerol; DPPC, 1,2-dipalmitoyl-sn-glycero-3-phosphocholine; GL, galactolipid; MGDG, monogalactosyldiacylglycerol; PL, phospholipid; pS, phytosterol; PUFA, polyunsaturated fatty acids; SAXS, X-ray scattering.

* Correspondence to: Institut de Physique de Rennes, Campus de Beaulieu, UMR UR1 CNRS 6251, Université de Rennes 1, 35042 Rennes cedex, France.
E-mail address: veronique.vie@univ-rennes1.fr (V. Vié).
[1] **Present/permanent address:** Institut de Physique de Rennes, campus de Beaulieu, 35042 Rennes cedex, France

https://doi.org/10.1016/j.colsurfb.2022.112646
Received 12 April 2022; Received in revised form 19 May 2022; Accepted 14 June 2022
Available online 22 June 2022

phase behaviors, which govern the overall membrane architecture (Fig. 1). Indeed, studies on the phase behavior of GL have shown that DGDG forms lamellar phases (L_α) and induces bilayer formation, whereas unsaturated MGDG tends to form inverted hexagonal structures (H_{II}) in aqueous solution [4]. In addition to their biological functions in photosynthetic membranes, GL are of nutritional interest since they are rich in polyunsaturated fatty acids (PUFA), and their consumption provides essential ω3 fatty acids [5].

Phytosterols (pS) are also among the major compounds of photosynthetic plant membranes where they play crucial roles in regulating the physical properties of membranes [6,7]. More than 250 species of phytosterols have been reported, the most abundant being β-sitosterol (70 % wt.), stigmasterol (20 % wt.) and campesterol (5 % wt.) [6]. These pS in their free form participate in the structuration of membranes by stabilizing polar lipid bilayers, although to a lesser extent than their cholesterol counterpart in animal cell membranes [8]. Beyond their structural properties, phytosterols are also compounds of nutritional and medical importance. Their consumption from fruits and vegetables has been shown to lower the total cholesterol and LDL levels in plasma in humans [9]. The interesting structural and nutritional properties of GL and pS have raised interest in their use in various applications, which requires a deep understanding of the organization and interactions of these plant polar lipids.

The monolayer behavior of saturated GL has already been extensively studied at the air/water interface [10,11]. Nevertheless, it should be noted that GL acyl chains in higher plants are mostly polyunsaturated, and thus less stable since they are more susceptible to oxidation [12]. Monolayer studies have also been performed on GL mixtures with unsaturation indices greater than 1, highlighting the differences in interfacial behavior between saturated and unsaturated GL. Using Langmuir films, Bottier et al. [13] studied the interfacial behavior of GL from different wheat tissues and highlighted the miscibility of MGDG and DGDG in water but also their tendency to phase separation in mixture. Overall, interface organization and packing were governed by interactions between the sugar polar heads of GL [14], but also depended on their fatty acid composition and the number of unsaturations.

The impact of plant sterols in polar lipid bilayers has already been studied extensively, showing that they alter phase transitions and membrane fluidity [15,16], depending on their chemical structure and concentration [17]. The interactions between pS and dipalmitoylphosphatidylcholine (DPPC) have also been studied in model Langmuir films at the air/water interface, and the incorporation of β-sitosterol and stigmasterol into PL monolayers has been shown to increase their packing [18]. Nevertheless, to the best of our knowledge, few results are available today concerning the impact of pS and phospholipids on GL interactions and packing in monolayers.

The interfacial properties of MGDG and DGDG, as well as their modulation by DPPC and/or pS in mixed Langmuir monolayers at the air/water interface were studied by ellipsometry, tensiometry and atomic force microscopy (AFM). The phase behavior and physical properties of these mixtures in hydrated mesophases were also studied by small angle X-ray scattering (SAXS).

2. Experimental section

2.1. Lipids

1,2-dipalmitoylphosphatidylcholine (DPPC), monogalactosyldiacylglycerol (MGDG) and digalactosyldiacylglycerol (DGDG) were purchased from Avanti Polar Lipids (see Table S1 in the supplementary material for the fatty acid repartition). Canola phytosterols were a gift from Cognis France (Estarac, France) obtained from desodorization distillates of canola oil. Typical molar composition (calculated from usual normalized GC procedures) was: β-sitosterol (50 mol%), campesterol (40 mol%) and brassicasterol (10 mol%).

2.2. Preparation of multicomponent lipid blends

Simple binary mixture of MGDG and DGDG (60:40, mol/mol) was prepared, namely GL. Ternary and quaternary mixtures of glycerophospholipids, galactolipids and phytosterols (see Table 1 for relative molar composition) were prepared to add some phase heterogeneity and to mimic the composition of natural plant photosynthetic membranes.

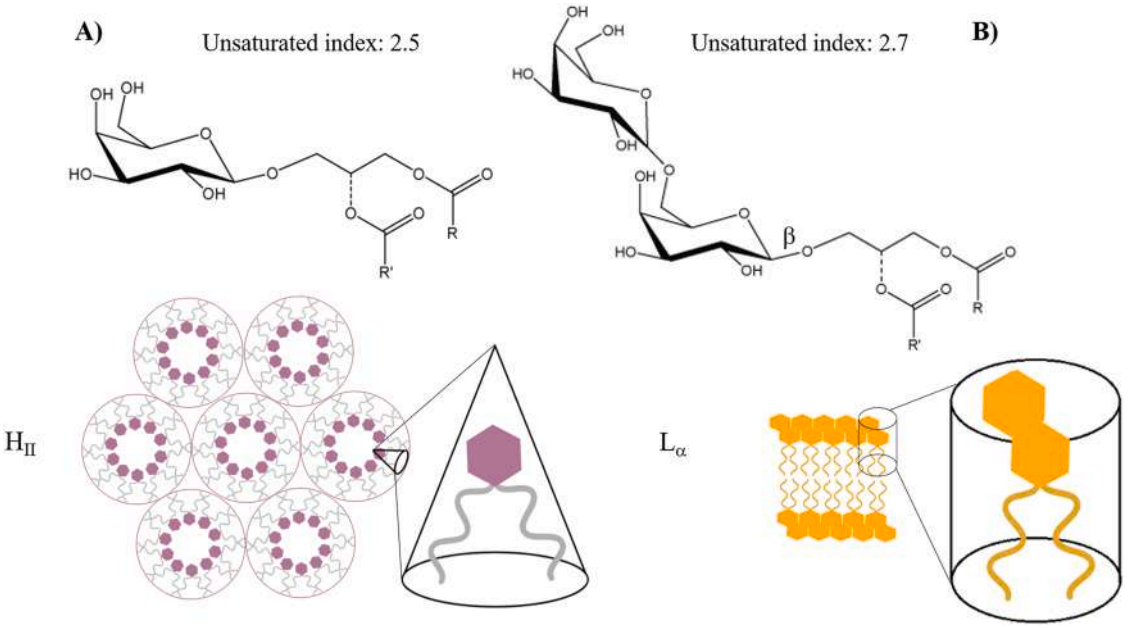

Fig. 1. Molecular structure and phase behaviour of A) monogalactodiacylglycerol (MGDG) and B) digalactosyldiacylglycerol (DGDG). Lα standing for lamellar phase and HII standing for hexagonal inverted phase.

Table 1
Molar composition of mixed Langmuir monolayers used as model membranes.

	Monolayer composition
GL	MGDG/DGDG 60:40 mol/mol
$GL_{50}/DPPC_{50}$	MGDG/DGDG/DPPC 30:20:50 mol/mol/mol
$GL_{45}/DPPC_{45}/pS_{10}$	MGDG/DGDG/DPPC/pS 27:18:45:10 mol/mol/mol/mol

pS: β-sitosterol, campesterol, brassicasterol 50:40:10 mol/mol/mol

2.3. Ellipsometry and surface pressure measurements at the air/water interface

All reported experiments were performed at least in duplicate, using a computer controlled and user-programmable LB Teflon Langmuir trough (KSV Nima, Helsinki, Finland) of 77 cm^2, equipped with two mobile barriers, allowing to vary the surface. Before each experiment, the trough was carefully cleaned with ultrapure water and ethanol to get rid of the surface-active residual impurities. The surface pressure was measured using a Wilhelmy balance connected to a microelectronic feedback system (Nima Technology, Cambridge, UK). The values of surface pressure (π) were recorded every 15 s with a precision of 0.2 mN/m. A home-made automated ellipsometer in a "null ellipsometer" configuration was used to carry out the ellipsometric angle (Δ) measurement [19]. The laser beam probed a surface of 1 mm^2 and a depth of 1 μm and allowed the qualitative monitoring of the thickness of the lipid monolayer formed at the air/water interface. Values of Δ were recorded every 15 s with a precision of ± 0.5°.

2.3.1. Formation of the lipid monolayers and Langmuir Blodgett transfer

For all the characterizations, the aqueous phase was composed of a 10 mM Tris HCl buffer solution (100 mM NaCl, 5 mM CaCl2, 10 mM Tris) at pH 7. The monolayers were formed by spreading a few microliters of 1 mM solution of lipids in $CHCl_3$/MeOH (2:1, v/v) at the air/water interface using a Hamilton microliter syringe. The surface area of the Langmuir trough was set at 35 cm^2 and the lipids were deposited up to a surface pressure of 20 mN/m. The film was then equilibrated for 10 min before each measurement, allowing the evaporation of solvent and lipid organization at the air/water interface. After 10 min equilibrium, the interfacial film was transferred onto a freshly cleaved mica plate, using the Langmuir Blodgett method (lipid-transfer ratio ~ 1.0). All lipid layers were sampled at a very low speed (0.5 $mm.min^{-1}$) by raising vertically the mica plate through the air/water interface. The surface pressure was kept constant during the sampling to maintain the lateral organization of lipids and thus avoid desorption phenomena and interfacial disorganization.

2.3.2. Compression isotherms and compressibility modulus C^{-1}

The surface area of the Langmuir trough was set at 77 cm^2 before compression. Few microliters of 1 mM solution of lipids in $CHCl_3$/MeOH (2:1, v/v) were spread at the interface until the pressure reaches 0.1 mN/m. The surface pressure as a function the surface area of the trough (π-A isotherm) was then recorded upon a symmetrical compression of the lipid monolayer using the two barriers, from 77 cm^2 to 21 cm^2, until the collapse of the film. The barrier speed was set at 5 mm^2/min.

Compression isotherms allow to obtain several parameters on the behavior of monolayers under compression. The minimum molecular area corresponds to the mean molecular area occupied by the molecules at the collapse of the film and was calculated as the intercept value between the pressure plateau at collapse and the tangent at the end of the π-A isotherm. The lift-off area was determined as the mean molecular area occupied by the molecules when the pressure begins to increase under compression. Finally, the monolayer compressibility was obtained from the first derivate of π-A isotherm and the mean molecular area of lipids deposited at the interface [20,21]. The Eq. (1) was used to determine the compressibility coefficient (Cs) of the monolayer.

$$Cs = -\frac{1}{A} \times \frac{dA}{d\pi} \quad (1)$$

where π is the surface pressure and A is the mean molecular area of the lipids forming the monolayer, estimated from the surface of the trough and the amounts of lipids deposited. The reciprocal of compressibility coefficient, the compressibility modulus, i.e., C_s^{-1} was represented as a function of the mean molecular area ($Å^2$/molecules). C_s^{-1} values were obtained at equally spaced surface pressures (0.2 mN/m intervals).

2.4. Topographic visualization of the monolayer interface using atomic force microscopy

Imaging of the films transferred to mica plates was carried out using an AFM (Multimode Nanoscope 5, Bruker, France). The PeakForce Quantitative Nanomechanical Mapping (QNM in air, 20 °C) was used in all the experiments. This mode provides high-resolution AFM images of the sample nanoscale surface topography, as well as the modulus and adhesion, at an acquisition speed comparable to the tapping mode. A standard silicon cantilever was used (0.06 N/m, SNL-10, Bruker, France), and the scan rate was set at 1 Hz. The force was minimized during all scans and the scanner size was 100 × 100 $μm^2$. The processed images analyzed by the open-source platform Gwyddion are representative of at least duplicated experiments. The differences of height of the LC and LE domains were assessed by the plot of height profile based on three cross-sections of the image using the software Gwyddion (2.55). For all AFM images, the color scale covers a height range of 15 nm, with the darkest color corresponding to the lowest domains and the lightest color to the highest domains, the fluid background corresponding to zero. A color scale is provided in to facilitate interpretation of the images.

2.5. Determination of the phase behavior of the model lipid mixture in aqueous dispersions by SAXS

The phase behavior of the model lipid mixture was investigated in aqueous dispersions using X-ray scattering with a homemade set-up at the Rennes Physique Institute. The X-ray scattering results were collected with a Pilatus 300 K (Dectris, Switzerland), mounted on a microsource X-ray generator GeniX 3D (Xenocs, France) operating at 30 W. The monochromatic CuKa radiation was of l = 1.541 Å. The X-ray diffraction patterns were recorded in a reciprocal space q = (4π. sinθ)/λ from repetitive distances q= 0.012–1.742 $Å^{-1}$. Small Angle X-ray Scattering (SAXS) and Wide-Angle X-ray Scattering (WAXS) regions were used to determine the supramolecular organization (long range order) of the lipid/water systems and the packing of acyl chains (short range order), respectively. The samples were prepared by evaporation of the solvent containing the solubilized lipids and then hydration at 5 % wt of the lipid films in a Tris buffer solution pH 7 (0.5 mg of lipids hydrated in 10 μL of Tris buffer). The samples were then introduced in thin calibrated quartz capillaries (Ø 1.5 mm, GLAS W. Muller, Berlin, Germany) before being centrifuged and sealed with candle wax. For the analysis, they have been introduced in a capillary holder accommodating 19 capillaries at controlled temperature. The homogeneity of the sample was checked at two y-positions. The analyses were carried out following a heating and cooling temperature ramp from 12 °C to 42 °C and 42–12 °C, respectively, every 8 °C with an exposure time per point of 10 min. The results were collected by a homemade program and the positions of Bragg reflections were determined by the Igor Pro 7.0 software (Wavemetrics, US).

3. Results and discussion

3.1. Study of the compression isotherms π-A of the GL_x/pS_y systems – influence of the pS concentration

The absence of shoulder and/or inflection point on the compression isotherm of the GL mixture (Fig. 2. A) was characteristic of a homogeneous liquid-expanded (LE) single phase, which could be explained by the high unsaturation content of the mixture. Indeed, the unsaturations decreased the intensity of van der Walls interactions between the acyl chains, and could hinder the establishment of a tight packing between GL molecules in the monolayer. The isotherm of the GL film indicated a lift-off area at around 230.8 ± 1.8 Å^2/molecule (2.3 nm^2/molecule) and showed a regular increase of the surface pressure until the collapse of the film at π = 39.9 ± 0.2 mN/m and at a limiting area of 81.0 ± 0.6 Å^2/molecule (0.8 nm^2/molecule). The evolution of the π-A isotherm of the GL film was consistent with the study of Bottier et al. [13] on purified wheat MGDG and DGDG monolayers, pure or in mixture. Nevertheless, a higher collapse pressure of 47 mN/m had been obtained for the less unsaturated wheat MGDG/DGDG equimolar mixture, at a lower mean molecular area of 70 Å^2/molecule (0.7 nm^2/molecule). This result was not surprising, as unsaturated acyl chains cannot adopt a very tight packing, which explains a larger average molecular area and a lower surface pressure at collapse as the number of unsaturation increases. The presence of unsaturations in the alkyl chains could also explains the significantly lower Cs^{-1}_{max} which was obtain for the GL monolayer in our study (Fig. 2. B) compared to the Cs^{-1}_{max} reported by Hoyo et al. [10] on the 2:1 mixture of saturated GL (48 versus 247 mN/m respectively). These values were determined for pressure values of interest, between 30 and 40 mN/m, π = 35 mN/m having been proposed as the equivalence surface pressure between lipid monolayers and cellular bilayers [22,23]. This decrease in Cs^{-1}_{max} with increasing unsaturation number had also been reported by Gzyl-Malcher, Filek, Makyła, et al. [24], reflecting the higher lateral elasticity of unsaturated monolayers compared to the saturated ones.

The addition of pS in the GL mixture did not significantly impact the surface pressure at the collapse of the film (Fig. 2. A). The addition of 5 and 10 mol% pS to the GL mixture did not significantly impact the limiting area. In contrast, the limiting area was affected by the addition of 30 mol% of pS and shifted from 81.0 ± 0.6–66.1 ± 0.5 Å^2/molecule (0.8–0.7 nm^2/molecule). The inclusion of pS has also significantly altered the Cs^{-1}_{max} of the monolayers (Fig. 2.B., logarithmic scale), and this effect was particularly marked in the presence of 30 mol% of pS in the GL mixture. Indeed, a Cs^{-1}_{max} of 85.7 mN/m was reached for the GL_{70}/pS_{30} blend, compared to 72.8 mN/m for the GL_{90}/pS_{10} and GL_{95}/pS_5 blends and 48.0 mN/m for the pure GL system. The greater impact of phytosterols for a content of 0.3 mol% on the compressibility of the monolayer was consistent with the results presented in Fig. 2.D. Indeed, the phase diagram showed a non-ideal behavior of the GL and pS blends, and this effect was even more noticeable for a molar concentration of pS of 30 % in the system. The reduction of the mean molecular area at collapse and the increase of Cs^{-1}_{max} with the increase of pS concentration could be attributed either to the condensation of the unsaturated acyl chains or to the reorientation of the sugar polar heads, induced by the presence of the pS molecule, thus decreasing the lateral elasticity of the monolayers [25]. Indeed, the presence of a largely hydrophobic small

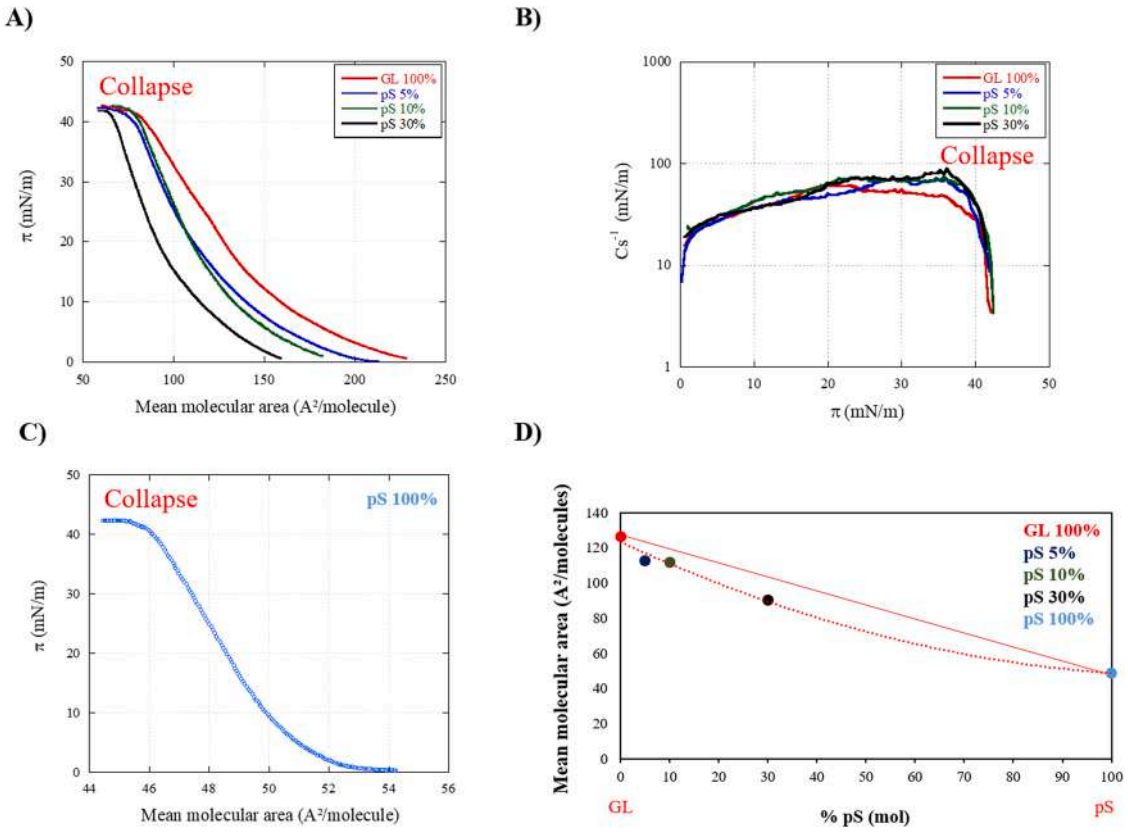

Fig. 2. Compression isotherms of 1) GL (red), 2) GL_{95}/pS_5 (deep blue), 3) GL_{90}/pS_{10} (green), 4) GL_{70}/pS_{30} (black) monolayers at the air/water interface. A) The graph corresponds to the evolution of π (mN/m) as a function of the mean molecular area (Å^2/molecules). B) The graph corresponds to the evolution of the surface compressibility moduli (C_s^{-1}, calculated following the Eq. (1)), as a function of π (mN/m) of 1), 2), 3) and 4). C) The graph corresponds to the evolution of π (mN/m) as a function of the mean molecular area (Å^2/molecules) of the pure pS system. D) The graph corresponds to the mean molecular area (Å^2/molecules) at 20 mN/m of each monolayer as a function of the percentage of pS in the systems (pure pS monolayer in light blue). The experiments were performed using Tris HCl buffer at pH 7 and were done in duplicate. Values of π were given with a standard deviation on duplicate measurements of ± 0.2 mN/m.

molecule such as pS will also impact the tilt of the polar heads, which will increase the possibility of packing of the molecules, explaining the non-ideal behavior observed in the case of unsaturated GL monolayers. Nevertheless, the animal counterpart of pS, the cholesterol, was shown to establish weaker interactions with unsaturated lipids, in comparison with saturated lipids [26], so the addition of DPPC in the mixtures could drastically alter the phenomena observed in GL-pS monolayers [27].

3.2. Influence of GL, DPPC, and pS interfacial composition on collapse pressure and ellipsometric angle values

Ellipsometry combined with tensiometry were used on Langmuir trough to determine the values of surface pressure (π, mN/m), ellipsometric angle (Δ, °) and limiting molecular area (Å^2/molecule) at the collapse of mixed heterogenous films with various compositions in GL, DPPC and pS. The values of π and Δ at the collapse of the films are presented in Table 2.

The addition of 10 mol% of pS in the GL mixture has induced a clear increase in the film thickness at collapse (8.2 versus 7.3 ± 0.5° for the GL_{90}/pS_{10} versus GL mixture, respectively), while there was no significant change in collapse pressure, neither in the limiting area. These results tend to indicate that the inclusion of the pS only impacted the orientation of the GL sugar polar heads, and not the acyl chain organization.

The addition of 50 mol% DPPC in the GL mixture led to an increase of the collapse surface pressure to π = 44.1 ± 0.2 mN/m (versus 39.9 ± 0.2 mN/m for the GL monolayer) as well as a shift in the mean molecular area at collapse to 60.4 ± 1.0 Å^2/molecules (0.6 nm^2/molecule), versus 81.0 ± 0.6 Å^2/molecule (0.8 nm^2/molecule) for the GL monolayer. These results indicated a strong condensing effect of DPPC, which could be explained by the presence of saturated acyl chains and smaller polar head of DPPC, which decreased the steric hindrance. An increase in the film thickness at collapse induced by the presence of DPPC was also observed (Δ = 8.9° vs 7.30° for the GL film), suggesting a reorientation of the sugar polar heads of GL, as well as the formation of condensed domains upon compression [28].

The addition of phytosterols at 10 mol% in the GL/DPPC film did not induce a significative variation of the collapse pressure (44.4 ± 0.2 mN/m versus 44.1 mN/m for the GL/DPPC) but triggered a shift of the limiting molecular area from 60.4 ± 1.0–55.0 ± 1.7 Å^2/molecule (0.6–0.5 nm^2/molecule), indicating an increase of the packing in the mixture in presence of pS. This decrease in the limiting area was not expected, given that pS probably interacts preferentially with DPPC than with PUFA-containing GL. Indeed, Botet-Carreras et al. [29] have studied the impact of cholesterol on homo- and hetero-acids phospholipid monolayers by AFM and AFM-FS, confirming that the effect of cholesterol on unsaturated PL was weaker than the one exerted on saturated PL. Additionally, a variety of biophysical measurements have revealed that sterols have an aversion to PUFA [30–33], explaining the lower impact of pS in the presence of GL in the GL_{90}/pS_{10} mixture, which contain a significant amount of PUFA. One possible explanation for such aversion of sterols for PUFA is the high disorder of PUFA acyl chains, which is incompatible with the usual orientation of cholesterol vertically with respect to interface plane. Thus, one can expect a change in the orientation of the sterol backbone [34]. Additionally, cholesterol has already been shown to induce order in lipids in fluid phase, whereas it has the opposite effect on lipids present in gel phase [35]. Given these general effects of sterols and their aversion to PUFA, we were expected a more pronounced disorganization of DPPC molecules than a condensation effect of GL polyunsaturated lipid chains, and thus a larger limiting area for the $GL_{45}/DPPC_{45}/pS_{10}$ mixture compared to the $GL_{50}/DPPC_{50}$ mixture. Nevertheless, given the decrease in the limiting area of the mixture in the presence of pS, it is likely that the addition of pS induced GL organization in the presence of DPPC, raising the question of a potential miscibility between DPPC and MGDG and/or DGDG in the presence of pS, reflecting a more complex mixture.

Table 2
Values of π (mN/m), Δ (°) and limiting molecular area (Å^2/molecule) at the collapse of mixed GL, DPPC and pS monolayers.

Monolayer composition	π (mN/m)	Δ (°)	Limiting area (Å^2/molecule)
(1) GL	39.9 ± 0.2	7.3 ± 0.5	81.0 ± 0.6
(2) DPPC	55.3 ± 0.2	10.8 ± 0.5	44.1 ± 0.7
(3) $GL_{50}/DPPC_{50}$	44.1 ± 0.2	8.9 ± 0.5	60.4 ± 1.0
(4) GL_{90}/pS_{10}	41.1 ± 0.1	8.2 ± 0.5	79.5 ± 0.9
(5) $GL_{45}/DPPC_{45}/pS_{10}$	44.4 ± 0.2	8.6 ± 0.5	55.0 ± 1.7

± stands for calculated standard deviation on duplicated measurement; for Δ, since the system/instrumentation error is ± 0.5°, calculated SD ≤ 0.5 were minored by this instrumentation error.

3.3. Characterization by ellipsometry of interfacial films at 20 mN/m

The thickness of the three model systems was determined by ellipsometry at a surface pressure of 20 mN/m. The detailed molar compositions are given in Table 1. The values of ellipsometric angles obtained at 20 mN/m are presented in Table 3. Eight sub-model systems were also prepared to give a better understanding of the organization and interactions between polar lipids at the air/water interface (see supplementary data S1 for the detailed molar compositions and S2 for the ellipsometric angle values at 20 mN/m).

An ellipsometric angle of 7.5° was obtained for the mixed GL monolayer at 20 mN/m., which was identical to the value obtained with DGDG alone and higher than the value for MGDG (7.5 and 6.3 ± 0.5° respectively). This result was expected as the DGDG lipid film has already been shown to be thicker than the MGDG monolayer [36].

The addition of DPPC to GL at a molar fraction of 0.5 did not induce a significant variation in the thickness at 20 mN/m. This result was consistent with the data obtained with the sub-model systems $MGDG_{50}/DPPC_{50}$ and $DGDG_{50}/DPPC_{50}$ (6.3 and 7.4 ± 0.5°, respectively), in which the addition of DPPC did not induce a significant variation of the ellipsometric angle at 20 mN/m.

The addition of pS to the mixed model system of GL and DPPC, at a molar content of 10 %, led to a slight decrease of the ellipsometric angle at 20 mN/m, but it was not significant. By comparison, pS induced a clear decrease in the thickness of the $MGDG_{45}/DPPC_{45}/pS_{10}$ and $DGDG_{45}/DPPC_{45}/pS_{10}$ sub-model systems (5.5 and 6.0 ± 0.5°, respectively), compared to the $MGDG_{50}/DPPC_{50}$ and $DGDG_{50}/DPPC_{50}$ systems (6.3 and 7.4 ± 0.5°, respectively). However, no significant variation in thickness was obtained for the sub-models $MGDG_{90}/pS_{10}$ and $DGDG_{90}/pS_{10}$, in comparison with the pure MGDG and DGDG systems. These results tend to indicate different interactions of pS with GL-DPPC mixed films and pure MGDG and DGDG.

In order to better understand the differences in the organization of

Table 3
Ellipsometric angle values of the lipid films at a surface pressure of 20 mN/m at the air/water interface.

Monolayer composition	Δ (°)
MGDG	6.3 ± 0.5
DGDG	7.5 ± 0.5
(1) GL	7.5 ± 0.5
(2) $GL_{50}/DPPC_{50}$	**7.1** ± 0.5
(3) $GL_{45}/DPPC_{45}/pS_{10}$	**7.0** ± 0.5

± stands for calculated standard deviation on duplicated measurement; the system/instrumentation error is ± 0.5°. Calculated SD ≤ 0.5 were minored by this instrumentation error.

the different models and sub-models, atomic force microscopy was used to visualize the interface of the films obtained by Langmuir Blodgett sampling.

3.4. Nanoscale topographic visualization of interfacial films at 20 mN/m using atomic force microscopy

Fig. 3 shows AFM images of the interfacial organization of the three main model monolayers GL, $GL_{50}/DPPC_{50}$, and $GL_{45}/DPPC_{45}/pS_{10}$ after their transfer by the Langmuir-Blodgett technique onto a mica plate and at a surface pressure of 20 ± 0.5 mN/m. The scale used was composed of different shades of brown, related to the differences in height in the monolayers. These color variations were correlated with the different tilt values of the lipid molecules and thus provide information on the orientation of the molecules and their physical state.

The 5 × 5 μm^2 AFM image of the GL system (Fig. 3. A), was characteristic of a homogeneous liquid-expanded (LE) phase without phase separation, consistent with the presence of unsaturated acyl chains in the fluid phase. However, the 1 × 1 μm^2 image highlights the presence of surface roughness, with height differences between 2 and 8 Å (0.2–0.8 nm) with respect to the baseline. A similar segregation was previously observed by AFM on mixed films of MGDG:DGDG (68:32 mol/mol) by Sarkis et al. [37]. Additionally, Bottier et al. [13] had observed the presence of irregular protrusions of 7 Å (0.7 nm) and 4 Å (0.4 nm) at surface pressures above 25 mN/m on monolayers of pure MGDG or in equimolar mixture with DGDG, respectively. The presence of these protrusions had been attributed to a specific organization of the MGDG polar heads between them or with those of DGDG, this roughness being absent on the AFM images of the DGDG monolayer. Indeed, a particular orientation of DGDG polar heads induced by the interactions between GL had been highlighted by PM-IRRAS data. The assumption was that the monogalactosyl polar head of MGDG could be responsible for the orientation of the digalactosyl group of DGDG parallel to the interface, with the formation of a network of hydrogen bridges between the polar heads and the water molecules at the interface [38].

The addition of DPPC to the system (2) (Fig. 3. B) resulted in the appearance of 1 nm high condensed domains of varying shapes and sizes at the interface (5 ×5 μm^2 image), likely to be enriched in DPPC, given their degree of saturation. Additionally, a loss of the granularity on 1 × 1 μm^2 images suggests changes in the orientation of the galactosyl polar heads of GL, that could result from a modification by DPPC of the interactions between MGDG and DGDG. This would fit with the previous results obtained on the compressibility of the film.

The addition of pS to the $GL_{50}/DPPC_{50}$ mixture (Fig. 3. C) resulted in a subsequent dilution of the domains in the LC condensed phase, as well as a significant increase in the thickness of the domains (h=1.6 nm versus h=1.0 nm, with and without pS, respectively), in contrast to the unchanged value of the ellipsometric angle. The irregular domain boundaries also indicated a change in line tension induced upon addition of pS in the GL/DPPC system, and suggests a change in interactions

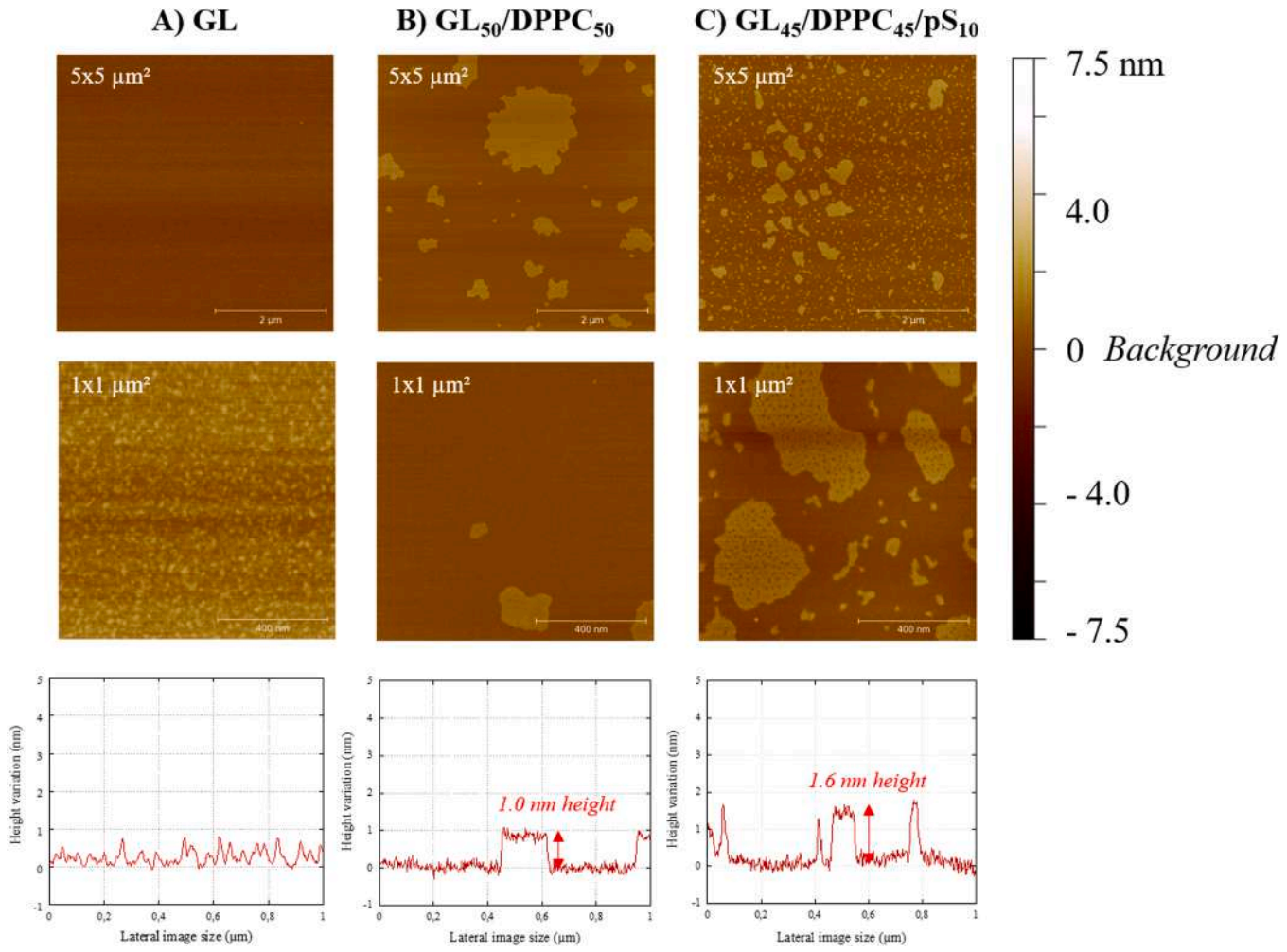

Fig. 3. 5 × 5 μm^2 and 1 × 1 μm^2 AFM topographic images of A) GL, B) $GL_{50}/DPPC_{50}$, and C) $GL_{45}/DPPC_{45}/pS_{10}$ model monolayers. The height profiles were performed on a cross-section of the 1 × 1 μm^2 image. The Langmuir films were transfer at a surface pressure of 20 ± 0.5 mN/m on a mica plate using the Langmuir Blodgett method. Experiments were performed in a Tris HCl buffer at pH 7 and done in duplicate.

between the different classes of lipids, with miscibility regions between the different components. Defects were also visible at the condensed phase domains, probably induced by the inclusion of pS and the local subsequent disorganization of the saturated acyl chains of DPPC.

In order to investigate the composition of the condensed phase domains and to better understand the interactions involved between the different classes of lipids, four sub-model systems were prepared, namely $MGDG_{50}/DPPC_{50}$, $DGDG_{50}/DPPC_{50}$, $MGDG_{30}/DPPC_{60}/pS_{10}$ and $DGDG_{30}/DPPC_{60}/pS_{10}$ (mol%) mixtures. AFM images and height profiles of these sub-models are presented Fig. 4.

In the absence of pS, the 5 × 5 μm^2 AFM image of the $MGDG_{50}/DPPC_{50}$ mixture (Fig. 4. A) showed the presence of LC phase domains (average domain area=0.1 μm^2), of irregular shape and 1.7 nm height, as well as a background characteristic of a homogeneous fluid phase. The $DGDG_{50}/DPPC_{50}$ film (Fig. 4. B) presented a similar fluid background. However, the LC phase domains are more abundant but smaller (average domain area=0.0002 μm^2), and present a greater height of 1.9 nm, in accordance with the higher ellipsometric angle for this mixture (6.3° versus 7.4° for the $MGDG_{50}/DPPC_{50}$ and $DGDG_{50}/DPPC_{50}$ mixtures, respectively). These observations confirm the different nature of MGDG and DGDG interactions with DPPC and question a possible segregation of MGDG-DGDG interactions in the presence of DPPC.

The addition of pS up to 10 mol% in these two previous sub-model systems changed the appearance of the interfacial films. First, the addition of pS in the MGDG/DPPC system (Fig. 4. C) induced a change in the line tension of the condensed phase domains, which showed irregular edges as well as the presence of defects at the larger domains, probably induced by the presence of pS, similar to the previous observations on the model systems. Nevertheless, a significant decrease of 18 % in the height of these domains (1.7 nm vs. 1.4 nm in height, without and with pS, respectively) was observed, consistent with the evolution of the ellipsometric angle (6.3° vs. 5.5°, without and with pS, respectively). The addition of pS in the DGDG/DPPC mixture induced a similar evolution of the interface (Fig. 4. D): the line tension and the thickness of the condensed domains were also modified according to the same trend (16 % decrease in thickness), and the presence of defects at the larger domains with irregular edges was still visible. This change in thickness did not showed the same trend as that observed in the $GL_{45}/DPPC_{45}/pS_{10}$ model, for which a 45 % increase in domain thickness was observed.

Overall, the results confirm the hypotheses of a different miscibility between DPPC and MGDG and between DPPC and DGDG. Moreover, it seems that the inclusion of pS in the systems induced, on the one hand, a transition from the DPPC-enriched gel phase to a less ordered phase, with the apparition of defects, and on the other hand, a transition from a fluid phase to a less ordered zone, with reduced height mismatch and a decrease of the line tension in the ternary systems. To validate these hypotheses and determine the miscibility of DPPC in mixture with MGDG or DGDG, as well as the impact of pS in GL/DPPC lipid systems, SAXS experiments were performed, in the presence of water in excess.

3.5. Phase behavior of mixed galactolipid mixtures in hydrated mesophase (SAXS)

The three-dimensional structures of unsaturated MGDG and DGDG, alone or in their equimolar mixture, have already been studied by analysis of the X-ray diffraction patterns and electron density profile at 20 °C in excess of water [10,13]. On one hand, the lamellar structure L_α of DGDG was evidenced by the presence of single peaks regularly spaced, with a lamellar periodicity of 54.9 Å. On the other hand, the X-ray diffraction profile obtained for MGDG showed six Bragg diffraction pics, with a hexagonal periodicity of 67.2 Å, that were attributed to an inverse hexagonal phase (H_{II}) distribution, which has been observed in other studies over a wide temperature range (−15 to 80 °C) [39]. The ability of unsaturated MGDG to form non-lamellar structures can be neutralized by mixing it with at least 50 % of lipids forming lamellar phases. However, unsaturated MGDG can induce defects in the lamellar structure of MGDG/lipid mixtures forming bilayers when its proportion is between 20 % and 50 % [40]. Nevertheless, for the equimolar mixture of MGDG and DGDG in excess of water, the SAXS diffraction pattern obtained by Bottier et al. was the signature of a bicontinuous cubic phase (*Im3m* space group) with a cubic lattice parameter of 202 Å, showing the

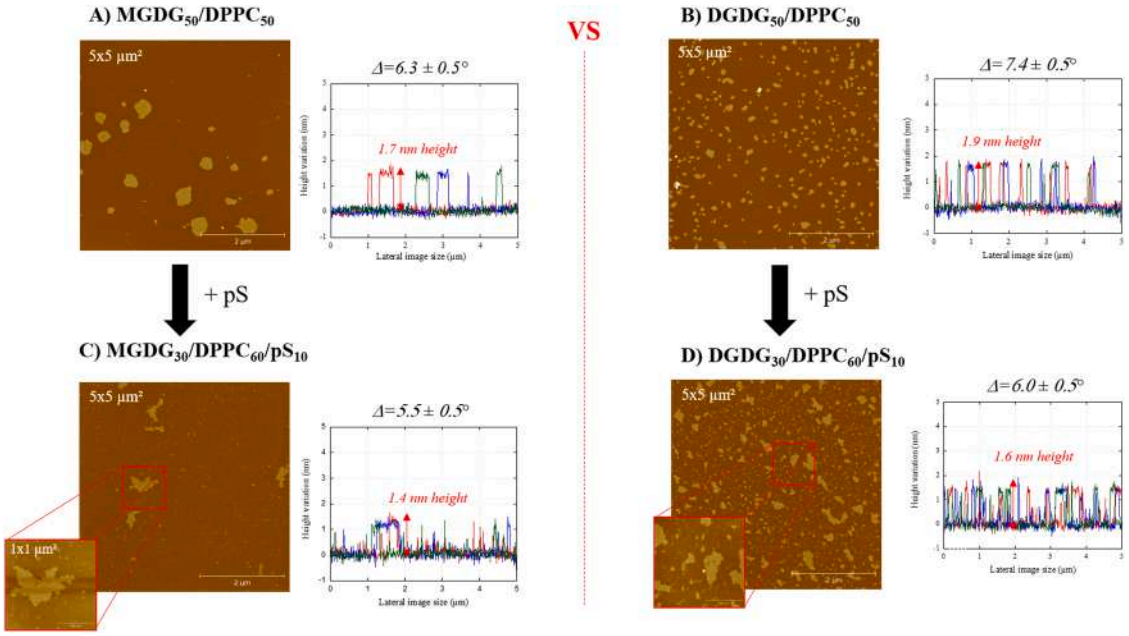

Fig. 4. 5 × 5 μm^2 AFM topographic images of A) $MGDG_{50}/DPPC_{50}$, B) $DGDG_{50}/DPPC_{50}$, C) $MGDG_{30}/DPPC_{60}/pS_{10}$, and D) $DGDG_{30}/DPPC_{60}/pS_{10}$ monolayers. Zooms to 1 × 1 μm^2 were performed on samples C) and D) to allow visualization of defects in condensed areas. The height profiles were performed on three different cross-sections of the 5 × 5 μm^2 image. The Langmuir films were transfer at a surface pressure of 20 ± 0.5 mN/m on a mica plate using the Langmuir Blodgett method. The ellipsometric angle value at 20 mN/m was reported to compare the thickness between the four monolayers. Experiments were performed in a Tris HCl buffer at pH 7 and done in duplicate.

specific behavior of MGDG and DGDG in the equimolar mixture compared to the pure lipids. Indeed, the formation of an *Im3m* space group could result from specific interactions between the polar sugar heads of the MGDG and DGDG.

The three-dimensional organization of DPPC has also already been extensively studied by SAXS, showing a well-ordered multilayer structure in excess of water due to the so-called L_β gel phase at 20 °C [41,42]. Nevertheless, the miscibility of the mixture of GL with DPPC forming lamellar phases has never been studied by SAXS.

First of all, the present study investigated the three-dimensional organization of heterogenous $GL_x/DPPC_y$ mixtures in excess of water, and as a function of DPPC proportion. Fig. 5. A presented the X-Ray diffraction patterns of three mixtures of $GL_x/DPPC_y$ in water, with DPPC at 66 (black curve), 50 (blue curve), and 33 mol% (green curve), respectively. The results showed that DPPC in large amount of 66 mol% induced a segregation between the components in water. Indeed, on the diffraction pattern (black line), the large diffraction peaks visible at 0.09 and 0.18 $Å^{-1}$ were identified as the ones related to the L_β phase formed by pure DPPC at 20 °C. Additionally, a peak and a shoulder were visible on the diffraction pattern at 0.06 and 0.11 $Å^{-1}$, respectively, that could correspond to the diffraction pattern of the cubic phase of the MGDG-DGDG mixture in water, consistent with the results of Bottier et al. [13]. These results tend to indicate a segregation between DPPC and the MGDG-DGDG mixture in water, leading to the existence of two non-miscible phases. Nevertheless, DPPC may also have disrupted the cubic phase by diluting the MGDG-DGDG interactions, coinciding with the distorted pattern of the MGDG-DGDG cubic phase. When DPPC was added at 50 mol% in the GL mixture, the diffraction pattern (blue line) showed a better miscibility between the three components of the system. Indeed, the intensity of the peaks presumably related to the cubic phase of the GL mixture was decreased and the pic 0.06 $Å^{-1}$ was no longer visible, tending to show the existence of two miscible phases. These results were consistent with AFM images of the $GL_{50}DPPC_{50}$ mixture, where a fluid phase was visible, probably composed of a mixture of MGDG, DGDG and DPPC, as well as condensed domains, likely enriched in DPPC. At a ratio of 33 mol% DPPC, the diffraction pattern (green line) indicates that the concentration of DPPC was not sufficient enough to segregate the three components of the system, and the slightly weaker MGDG-DGDG interactions have probably prevailed, leading to the existence of a single organized phase composed by MGDG, DGDG and DPPC. Overall, the SAXS data confirm the presence of significant segregation in the systems, depending on the DPPC proportion and implying the existence of very selective interactions between the different types of lipids.

To our knowledge, this study is the first on the impact of pS on heterogenous model plant membranes, while the impact of cholesterol on model of animal membranes made of phospholipid bilayers has been extensively studied. To better understand the impact of pS and the interactions between DPPC and MGDG/DGDG, the SAXS diffraction patterns of three other model systems were studied, i.e. $MGDG_{45}DPPC_{45}pS_{10}$, $GL_{45}/DPPC_{45}/pS_{10}$ and $DGDG_{45}/DPPC_{45}/pS_{10}$ (Fig. 5. B).

On one hand, results tend to show that MGDG and DGDG did not interact equivalently with the DPPC-pS mixture. First of all, the mixture of DGDG with DPPC-pS did not promote the presence of a single organized phase in water (see green line). Indeed, the diffraction pattern of the pure DPPC was clearly visible, with the L_β lamellar phase peaks at 0.09, 0.18, and 0.27 $Å^{-1}$. The diffraction pattern of the pure DGDG was also clearly evidenced, with the diffraction peaks reflecting the L_α phase at 0.11 and 0.22 $Å^{-1}$. These results are consistent with those obtained by Bottier et al. [13] on the wheat DGDG/water system and they highlight the poor miscibility of DGDG with DPPC-pS system. On the contrary, in the case of the $MGDG_{45}/DPPC_{45}/pS_{10}$ mixture (blue pattern), only one phase was clearly visible, with two peaks reflecting a lamellar phase at 0.09 and 0.18 $Å^{-1}$, but slightly shifted compared to pure DPPC in water. In the case of the $GL_{45}/DPPC_{45}/pS_{10}$ mixture in water (black pattern), a shoulder was also visible at 0.11 $Å^{-1}$, compared to the diffraction pattern of the $MGDG_{45}/DPPC_{45}/pS_{10}$ mixture, highlighting the formation of two phases: one phase enriched in MGDG-DPPC-pS and one phase containing a mixture of MGDG-DGDG. These results showed drastically different interactions between MGDG and DGDG, respectively, and the DPPC-pS mixture, and highlight the preferential miscibility of MGDG with the DPPC-pS mixture.

On the other hand, the comparison between the $GL_{50}/DPPC_{50}$ (fig. 5. A, blue pattern) and the $GL_{45}/DPPC_{45}/pS_{10}$ (Fig. 5. B, black pattern) mixtures in water allowed us to highlight the impact of 10 mol% of pS in the system. As expected, pS did not formed a phase on its own but triggered a modification of the organization of the existing phases. Indeed, the inclusion of pS in the GL/DPPC system did not induce the appearance of new diffraction peaks, but has led to a contraction of the L_β diffraction peaks at 0.09 and 0.18 $Å^{-1}$, indication a homogenization in the miscibility of the two phases.

Overall, the results were consistent with the AFM images obtained on the $GL_{45}/DPPC_{45}/pS_{10}$ monolayer, with the visualization of a fluid

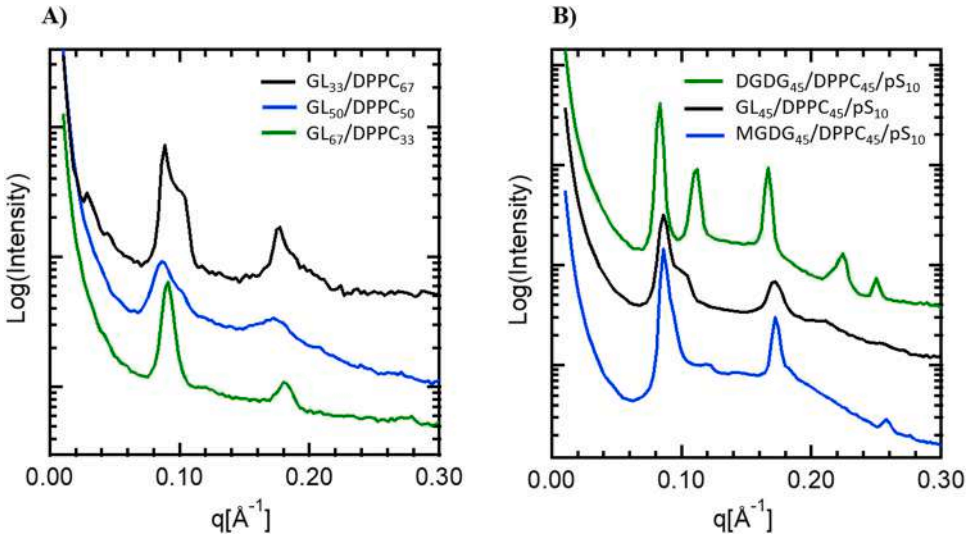

Fig. 5. SAXS patterns of the model systems recorded at 20 ± 0.5 °C. A) GL/DPPC systems at different ratios: 33:67 mol/mol (black curve), 50:50 mol/mol (blue curve) and 67:33 mol/mol (green curve). B) DGDG/DPPC/pS (45:45:10 mol/mol/mol, green curve), GL/DPPC/pS (45:45:10 mol/mol/mol, black curve), MGDG/DPPC/pS (45:45:10 mol/mol/mol, blue curve).

phase composing the background, probably enriched in MGDG-DGDG, and the presence of a gel phase enriched in MGDG-DPPC, in which the inclusion of pS has induced the formation of defects, leading to a thickening of the gel phase by decreasing the packing. Additionally, the observation of smaller domains in presence of pS on the AFM images was consistent with a lowering of the line tension at the edges of the gel domains, resulting from a better miscibility between the two phases and thus a reduced height mismatch.

4. Conclusion

In this study, tunable Langmuir model membrane of heterogenous assemblies of GL, DPPC and pS were used to study the structural behavior of the main polar lipids of vegetal photosynthetic membrane (MGDG and DGDG) at the air/water interface. The impact of pS and 1,2-dipalmitoyl-sn-glycero-3-phosphocholine (DPPC) or both on the structural properties of GL membrane was studied.

The biophysical results obtained confirmed the good surfactant properties of these polar lipids. The addition of pS in the mixed GL systems up to 30 mol% induced a reorientation of the sugar polar heads, leading to a more important packing and thus to a reduction of the lateral elasticity of the monolayer. The study of the compressibility isotherms of the different films also allowed to highlight the complex miscibility of the heterogeneous ternary mixtures, and their singular behavior compared to the pure systems. Indeed, the results obtained on the $GL_{45}/DPPC_{45}/pS_{10}$ mixture indicated preferential DPPC-pS interactions but a decrease in lateral elasticity despite the disorganization effect of pS on saturated lipids.

The inclusion of pS into the gel phase regions was visible on the AFM images, leading to a thickening of the domains and a local decrease of packing by the appearance of defects. This result highlighted phase miscibility between DPPC and GL, and in particular with MGDG, which was confirmed by AFM images and SAXS diffraction patterns. The favorable interaction between DPPC and pS may have caused the appearance of segregated zones, on one side, devoid of pS and enriched in MGDG-DGDG in the fluid phase, and on the other, enriched in pS and DPPC.

The pS-DPPC-rich areas could also have included the presence of MGDG, due to more favorable DPPC-MGDG interactions than DPPC-DGDG, raising the hypothesis of a heterogeneous MGDG-DPPC-pS composition of the gel phase domains. The characterization of these kinds of plant lipid mixtures is useful for the understanding of mechanisms such as their digestion by specific digestive enzymes.

CRediT authorship contribution statement

C. Bourlieu, V. Vié and J. Kergomard determined the outline and the content of the manuscript. J. Kergomard wrote the manuscript and all the co-authors participated in the experimental design, the collection, the interpretation of data and the correction and implementation of the manuscript. All co-authors have approved the final article.

Declaration of Competing Interest

The authors declare that they have no known competing financial interests or personal relationships that could have appeared to influence the work reported in this paper.

Acknowledgments

The authors would like to acknowledge the BIOMIF platform ('Biological Molecules at fluid interfaces', IPR, Rennes, France) for allowing the biophysical characterization of samples presented in this article.

C. Bourlieu, V. Vié and J. Kergomard determined the outline and the content of the manuscript. J. Kergomard wrote the manuscript and all the co-authors participated in the experimental design, the collection, the interpretation of data and the correction and implementation of the manuscript. All co-authors have approved the final article.

Appendix A. Supporting information

Supplementary data associated with this article can be found in the online version at doi:10.1016/j.colsurfb.2022.112646.

References

[1] V. Gurevich, B. Bondarenko, K.J. Gundermann, R. Schumacher, T. Astashkina, V. Ivanov, Y. Popov, L. Shatilina, N. Kazennova, Poly-unsaturated phospholipids increase the hypolipidemic effect of Lovastatin, Eur. J. Intern. Med. 8 (1) (1997) 15–20.
[2] A.G. Lee, Membrane lipids: it's only a phase, Curr. Biol. 10 (10) (2000) R377–R380, https://doi.org/10.1016/S0960-9822(00)00477-2.
[3] N. Mizusawa, H. Wada, The role of lipids in photosystem II, Biochim. Et. Biophys. Acta (BBA) - Bioenerg. 1817 (1) (2012) 194–208, https://doi.org/10.1016/j.bbabio.2011.04.008.
[4] I. Brentel, E. Selstam, G. Lindblom, Phase equilibria of mixtures of plant galactolipids. The formation of a bicontinuous cubic phase, Biochim. Et. Biophys. Acta (BBA) - Biomembr. 812 (3) (1985) 816–826, https://doi.org/10.1016/0005-2736(85)90277-9.
[5] M. Sahaka, S. Amara, J. Wattanakul, M.A. Gedi, N. Aldai, G. Parsiegla, J. Lecomte, J.T. Christeller, D. Gray, B. Gontero, P. Villeneuve, F. Carrière, The digestion of galactolipids and its ubiquitous function in Nature for the uptake of the essential α-linolenic acid, Food Funct. (2020), https://doi.org/10.1039/D0FO01040E.
[6] Evans, C.S., 1991. J. B. Harborne (ED.) Methods in plant biochemistry: 1. plant phenolics. Academic Press, New York and London, 1990. Phytochemical Analysis, 2(1), 48–48. https://doi.org/10.1002/pca.2800020110.
[7] R.E. Ostlund, Phytosterols in human nutrition, Annu. Rev. Nutr. 22 (2002), https://doi.org/10.1146/annurev.nutr.22.020702.075220.
[8] R.A. Moreau, B.D. Whitaker, K.B. Hicks, Phytosterols, phytostanols, and their conjugates in foods: structural diversity, quantitative analysis, and health-promoting uses, Prog. Lipid Res. 41 (6) (2002) 457–500, https://doi.org/10.1016/s0163-7827(02)00006-1.
[9] M.-P. St-Onge, P.J.H. Jones, Phytosterols and human lipid metabolism: efficacy, safety, and novel foods, Lipids 38 (4) (2003) 367–375, https://doi.org/10.1007/s11745-003-1071-3.
[10] J. Hoyo, E. Guaus, J. Torrent-Burgués, Monogalactosyldiacylglycerol and digalactosyldiacylglycerol role, physical states, applications and biomimetic monolayer films, Eur. Phys. J. E 39 (3) (2016) 39, https://doi.org/10.1140/epje/i2016-16039-0.
[11] M. Tomoaia-Cotişel, J. Zsako, E. Chifu, P.J. Quinn, Hysteresis in compression-expansion cycles of distearoylmonogalactosylglycerol monolayers, Chem. Phys. Lipids 50 (2) (1989) 127–133, https://doi.org/10.1016/0009-3084(89)90036-4.
[12] M. Tomoala-Cotişel, J. Zsakó, E. Chifu, P.J. Quinn, Influence of electrolytes on the monolayer properties of saturated galactolipids at the air-water interface, Chem. Phys. Lipids 34 (1983) 55–64, https://doi.org/10.1016/0009-3084(83)90059-2.
[13] C. Bottier, J. Géan, F. Artzner, B. Desbat, M. Pézolet, A. Renault, D. Marion, V. Vié, Galactosyl headgroup interactions control the molecular packing of wheat lipids in Langmuir films and in hydrated liquid-crystalline mesophases, Biochim. Et. Biophys. Acta 1768 (6) (2007) 1526–1540, https://doi.org/10.1016/j.bbamem.2007.02.021.
[14] D.G. Bishop, J.R. Kenrick, J.H. Bayston, A.S. Macpherson, S.R. Johns, Monolayer properties of chloroplast lipids, Biochim. Et. Biophys. Acta (BBA) - Biomembr. 602 (2) (1980) 248–259, https://doi.org/10.1016/0005-2736(80)90308-9.
[15] H. Itzhaki, A. Borochov, S. Mayak, Age-related changes in petal membranes from attached and detached rose flowers, Plant Physiol. 94 (3) (1990) 1233–1236.
[16] B.D. McKersie, J.E. Thompson, Influence of plant sterols on the phase properties of phospholipid bilayers 1, Plant Physiol. 63 (5) (1979) 802–805.
[17] Md Arif Kamal, V.A. Raghunathan, Phase behavior of phospholipid–phytosterol membranes, Soft Matter 8 (2021) 8952–8958, https://doi.org/10.1039/C2SM25912E.
[18] Y. Su, Q. Li, L. Chen, Z. Yu, Condensation effect of cholesterol, stigmasterol, and sitosterol on dipalmitoylphosphatidylcholine in molecular monolayers, Colloids Surf. A: Physicochem. Eng. Asp. 293 (1) (2007) 123–129, https://doi.org/10.1016/j.colsurfa.2006.07.016.
[19] B. Berge, A. Renault, Ellipsometry study of 2D crystallization of 1-alcohol monolayers at the water surface, Europhys. Lett. (EPL) 21 (7) (1993) 773–777, https://doi.org/10.1209/0295-5075/21/7/010.
[20] Gaines, G.L., Prigogine, I.P. ,1966. Insoluble monolayers at liquid-gas interfaces.
[21] J.M. Smaby, M.M. Momsen, H.L. Brockman, R.E. Brown, Phosphatidylcholine acyl unsaturation modulates the decrease in interfacial elasticity induced by cholesterol, Biophys. J. 73 (3) (1997) 1492–1505, https://doi.org/10.1016/S0006-3495(97)78181-5.
[22] Di Marsh, Lateral pressure in membranes, Biochim. Et. Biophys. Acta (BBA) - Rev. Biomembr. 1286 (3) (1996) 183–223, https://doi.org/10.1016/S0304-4157(96)00009-3.
[23] D. Marsh, Lateral pressure profile, spontaneous curvature frustration, and the incorporation and conformation of proteins in membranes, Biophys. J. 93 (11) (2007) 3884–3899, https://doi.org/10.1529/biophysj.107.107938.

[24] B. Gzyl-Malcher, M. Filek, K. Makyła, M. Paluch, Differences in surface behaviour of galactolipoids originating from different kind of wheat tissue cultivated in vitro, Chem. Phys. Lipids 155 (1) (2008) 24–30, https://doi.org/10.1016/j.chemphyslip.2008.06.004.
[25] X.-M. Li, M.M. Momsen, J.M. Smaby, H.L. Brockman, R.E. Brown, Cholesterol decreases the interfacial elasticity and detergent solubility of sphingomyelins, Biochemistry 40 (20) (2001) 5954–5963, https://doi.org/10.1021/bi002791n.
[26] J.R. Silvius, Role of cholesterol in lipid raft formation: lessons from lipid model systems, Biochim. Et. Biophys. Acta 1610 (2) (2003) 174–183, https://doi.org/10.1016/s0005-2736(03)00016-6.
[27] M. Jurak, Thermodynamic aspects of cholesterol effect on properties of phospholipid monolayers: langmuir and langmuir–blodgett monolayer study, J. Phys. Chem. B 117 (13) (2013) 3496–3502, https://doi.org/10.1021/jp401182c.
[28] V. Vié, N. Van Mau, E. Lesniewska, J.P. Goudonnet, F. Heitz, C. Le Grimellec, Distribution of Ganglioside GM1 between Two-Component, Two-Phase Phosphatidylcholine Monolayers, Langmuir 14 (1998) 4574–4583, https://doi.org/10.1021/la980203p.
[29] A. Botet-Carreras, M.T. Montero, Ò. Domènech, J.H. Borrell, Effect of cholesterol on monolayer structure of different acyl chained phospholipids, Colloids Surf. B: Biointerfaces 174 (2019) 374–383, https://doi.org/10.1016/j.colsurfb.2018.11.040.
[30] D. Huster, K. Arnold, K. Gawrisch, Influence of Docosahexaenoic Acid and Cholesterol on Lateral Lipid Organization in Phospholipid Mixtures, Biochemistry 37 (1998) 17299–17308, https://doi.org/10.1021/bi980078g.
[31] S.-L. Niu, B.J. Litman, Determination of membrane cholesterol partition coefficient using a lipid vesicle-cyclodextrin binary system: effect of phospholipid acyl chain unsaturation and headgroup composition, Biophys. J. 83 (2002) 3408–3415, https://doi.org/10.1016/S0006-3495(02)75340-X.
[32] M.C. Pitman, F. Suits, A.D. Mackerell, S.E. Feller, Molecular-level organization of saturated and polyunsaturated fatty acids in a phosphatidylcholine bilayer containing cholesterol, Biochemistry 43 (2004) 15318–15328, https://doi.org/10.1021/bi048231w.
[33] S.R. Wassall, M.R. Brzustowicz, S.R. Shaikh, V. Cherezov, M. Caffrey, W. Stillwell, Order from disorder, corralling cholesterol with chaotic lipids. The role of polyunsaturated lipids in membrane raft formation, Chem. Phys. Lipids 132 (2004) 79–88, https://doi.org/10.1016/j.chemphyslip.2004.09.007.
[34] T.A. Harroun, J. Katsaras, S.R. Wassall, Cholesterol Hydroxyl Group Is Found To Reside in the Center of a Polyunsaturated Lipid Membrane, Biochemistry 45 (2006) 1227–1233, https://doi.org/10.1021/bi0520840.
[35] S. Garcia-Manyes, L. Redondo-Morata, G. Oncins, F. Sanz, Nanomechanics of lipid bilayers: heads or tails? J. Am. Chem. Soc. 132 (37) (2010) 12874–12886, https://doi.org/10.1021/ja1002185.
[36] Bottier, C. , 2006. Caractérisation des puroindolines, des galactolipides du blé et de leurs interactions: Mesures physiques aux interfaces [Phdthesis, Université Rennes 1]. https://tel.archives-ouvertes.fr/tel-00148405.
[37] J. Sarkis, J. Rocha, O. Maniti, J. Jouhet, V. Vié, M.A. Block, C. Breton, E. Maréchal, A. Girard-Egrot, The influence of lipids on MGD1 membrane binding highlights novel mechanisms for galactolipid biosynthesis regulation in chloroplasts, FASEB J. 28 (7) (2014) 3114–3123, https://doi.org/10.1096/fj.14-250415.
[38] M. Kanduc, A. Schlaich, A.H. de Vries, J. Jouhet, E. Marechal, B. Deme, R.R. Netz, E. Schneck, Tight cohesion between glycolipid membranes results from balanced water-headgroup interactions, Nat. Commun. 8 (2017) 14899, https://doi.org/10.1038/ncomms14899.
[39] A.V. Popova, D.K. Hincha, Thermotropic phase behavior and headgroup interactions of the nonbilayer lipids phosphatidylethanolamine and monogalactosyldiacylglycerol in the dry state, BMC Biophys. 4 (1) (2011) 11, https://doi.org/10.1186/2046-1682-4-11.
[40] V. Castro, S.V. Dvinskikh, G. Widmalm, D. Sandström, A. Maliniak, NMR studies of membranes composed of glycolipids and phospholipids, Biochim. Et. Biophys. Acta (BBA) - Biomembr. 1768 (10) (2007) 2432–2437, https://doi.org/10.1016/j.bbamem.2007.05.010.
[41] O. Et-Thakafy, N. Delorme, C. Gaillard, C. Mériadec, F. Artzner, C. Lopez, F. Guyomarc'h, Mechanical properties of membranes composed of gel-phase or fluid-phase phospholipids probed on liposomes by atomic force spectroscopy, Langmuir 33 (21) (2017) 5117–5126, https://doi.org/10.1021/acs.langmuir.7b00363.
[42] Z. Varga, A. Bóta, G. Goerigk, Localization of dihalogenated phenols in vesicle systems determined by contrast variation X-ray scattering, J. Appl. Crystallogr. 40 (s1) (2007) s205–s22208, https://doi.org/10.1107/S0021889807001987.

Colloids and Surfaces B: Biointerfaces 220 (2022) 112933

Contents lists available at ScienceDirect

Colloids and Surfaces B: Biointerfaces

journal homepage: www.elsevier.com/locate/colsurfb

Modulation of gastric lipase adsorption onto mixed galactolipid-phospholipid films by addition of phytosterols

Jeanne Kergomard [a,b], Frédéric Carrière [c], Gilles Paboeuf [a], Nathalie Barouh [d,e], Claire Bourlieu-Lacanal [b,*,1], Véronique Vié [a,f,**,1]

[a] IPR Institute of Physics, UMR UR1 CNRS 6251, Rennes 1 University, France
[b] INRAE/UM/Institut Agro Montpellier UMR 1208 IATE, France
[c] Aix-Marseille Université, CNRS, UMR7281 Bioénergétique et Ingénierie des Protéines, Marseille, France
[d] CIRAD, UMR QUALISUD, F34398 Montpellier, France
[e] Qualisud, Univ Montpellier, Avignon Université, CIRAD, Institut Agro, Université de La Réunion, Montpellier, France
[f] Univ Rennes 1, CNRS, ScanMAT - UMS 2001, F-35042 Rennes, France

ARTICLE INFO

Keywords:
Adsorption
Gastric lipase
Galactolipids
Heterogeneous biomimetic membranes
Plant lipids
Ellipsometry/tensiometry
Atomic force microscopy

ABSTRACT

The rapid and preferential adsorption of a gastric lipase recombinant dog gastric lipase (rDGL) in heterogeneous films of phospholipids and triacylglycerols has previously been unveiled using Langmuir films analyzed by tensiometry, ellipsometry and Langmuir-Blodgett transfer coupled to atomic force microscopy. Here we invest the adsorption behavior of rDGL in heterogeneous galactolipid and mixed galactolipid-phospholipid or galactolipid-phospholipid-phytosterol films representative of plant membrane. Again rDGL, preferentially got adsorbed at the expanded lipid phases of the films underlining the genericity of such adsorption behavior. The addition of phytosterols to these mixtures resulted in the creation of defects, favoring the adsorption of rDGL at the fluid phases, but also improving the adsorption capacities of the lipase at the phase boundaries and towards the defects in the condensed phase. rDGL, like all gastric lipases, does not show any activity on galactolipids and phospholipids but its adsorption impacts their lateral organization and may change the adsorption and activity of other lipolytic enzymes in the course of digestion.

1. Introduction

Lipases (EC 3.1.1.3, triacylglycerol hydrolase) play an important role in lipid metabolism, and have been found in most living organisms, from the plant kingdom to microorganisms and animals [1,2]. Lipases are water-soluble enzymes that catalyze the hydrolysis of the ester bonds of insoluble triacylglycerols (TAG). Prior to the hydrolysis of their substrates, lipases must therefore get adsorbed onto the lipid-water interface [3]. The digestion of lipids is a complex phenomenon, which depends on their chemical structure, their organization in water (monolayers, bilayers, micelles, oil/water emulsions…) and the ability of lipolytic enzymes to interact with these lipid assemblies. Indeed, the mechanisms involved in enzymatic lipolysis depends on the interfacial organization of the lipid substrates.

In humans, lipid digestion starts in the stomach where gastric lipase is responsible for 10–25 % of the TAG total digestion [4,5] and is very central during neonatal period as it is mature at birth [6]. It is worth nothing that gastric lipase is a true lipase, acting on TAG digestion but not on polar lipids, such as phospholipids or galactolipids. Human gastric lipase (HGL) is a globular enzyme of 50 kDa, belonging to the α/β hydrolase family, and possessing a classical Ser-His-Asp catalytic triad [7,8]. The active site is covered by a lid, which has to be displaced to permit the TAG substrates to have access to the enzyme active site. Changes in the conformation (opening) of the lid have been observed in

Abbreviations: AFM, atomic force microscopy; BMM, bovine milk membranes; DGDG, digalactosyldiacylglycerol; DPPC, dipalmitoylphosphatidylcholine; GL, galactolipids; HGL, human gastric lipase; HMM, human milk membranes; IRS, Interfacial recognition site; LC, liquid condensed phase; LE, liquid expanded phase; MGDG, monogalactosyldiacylglycerol; MPL, milk polar lipids; PTL, pancreatic triacylglycerol lipase; rDGL, recombinant dog gastric lipase.

* Correspondence to: UMR 1208 IATE, 2 Place Pierre Viala, Bât. 31, INRAE/UM/Institut Agro Montpellier, F34060 Montpellier Cedex 1, France.
** Correspondence to: Institut de Physique de Rennes, Campus de Beaulieu, UMR UR1 CNRS 6251, Université de Rennes 1, 35042 Rennes Cedex, France.
E-mail addresses: claire.bourlieu-lacanal@inrae.fr (C. Bourlieu-Lacanal), veronique.vie@univ-rennes1.fr (V. Vié).
[1] Present/permanent address: Institut de Physique de Rennes, campus de Beaulieu, 35042 Rennes cedex – France

https://doi.org/10.1016/j.colsurfb.2022.112933
Received 21 June 2022; Received in revised form 20 September 2022; Accepted 13 October 2022
Available online 19 October 2022

the homologous dog gastric lipase, co-crystallized in the presence of substrate analogs [9]. The lid opening generates a large hydrophobic ring, that is part of the interfacial recognition site (IRS) located around the active site entrance (Fig. 1).

Gastric lipase has been found to be highly active in the acidic environment of the stomach with an optimum at pH 4–5.4, thanks to a remarkable stability and adsorption capacity at the lipid/water interface at low pH, in contrast to other lipases [12,13]. This pH-dependent interfacial adsorption is driven by hydrophobic interactions between the substrates and the large hydrophobic ring, part of the IRS (Fig. 1. B) [13] and electrostatic interactions, rDGL surface potential being mostly positive at low pH (Fig. 1. C). This combination of interactions probably explains why rDGL is a highly tensioactive lipase with a high penetration capacity into phospholipid layers [12].

Prior to hydrolyzing TAG, lipases frequently have to get adsorbed onto interfacial films composed of polar lipids and/or amphiphilic proteins [14], in which a small fraction of TAG playing various metabolic part can also be found [15]. This is typically the case of milk fat globules and phospholipid-stabilized emulsions. Polar lipids are not hydrolyzed in the upper gastrointestinal tract by gastric lipase, but this enzyme has a strong ability to get inserted into phospholipid (PL) monolayers thanks to its high surfactant capacity [12,16] and thus, has access to the TAG substrate. In addition, gastric lipolysis favors the activity of pancreatic lipase [17] and has been recently reported to significantly affect the production and the degradation of intermediate TAG digestion products during the intestinal phase [18]. Given the synergy between the gastric and intestinal digestion phases, it is crucial to obtain knowledge on the protein-lipid interactions occurring during the gastric phase, including the impact of gastric lipase adsorption onto the interfacial organization of membrane lipids, even though gastric lipase is not active on phospholipids [19] nor on galactolipids [20].

Polar lipid films are useful tools to study the interfacial properties of lipases, irrespective of their lipolytic activity. Langmuir films used as model interfaces allows determining the impact of various physico-chemical parameters, including the lipid packing and composition at the air/water interface, on the adsorption and insertion capacity of a lipase. The variations of surface pressure are related to interactions between molecules, which are directly connected to the variations of molecular areas. The coupling of surface pressure measurements and ellipsometry provides insights on the thickness and refractive index of the surface layer formed, and thus on the phenomena occurring in one micrometer range below the interface.

Previous studies have been done on the adsorption behavior of gastric lipase onto model heterogenous films mimicking the outer layer of the membrane of human and bovine milk fat globule [21,22]. These studies have shown that the coexistence of expanded and condensed phases influenced sternly lipase adsorption: lipase got rapidly inserted onto the fluid phase and at the phase boundaries. In addition, different levels of insertion were observed suggesting a molecular cooperation and besides hydrophobic interactions local negative charges reinforced adsorption.

However, to the best of our knowledge, no study has yet tackled the question of adsorption and penetration mechanisms of gastric lipase onto plant cell membranes, especially the nature widespread photosynthetic membranes. On the contrary to animal cell membranes, plant photosynthetic membranes to save up phosphorus do not contain phospholipids but galactoglycerophospholipids (or galactolipids), which accounts for more than 70% of polar lipids [23]. In addition to their biological and structural functions in membranes, galactolipids are of nutritional importance since they are rich in polyunsaturated fatty acids (PUFA), essentials to cell functions in the human body, and especially in the α-linolenic acid (C18:3 n-3, ALA) [24]. Phytosterols and carotenes are also major constituents of plant cell membranes [25,26]. They play a key role in maintaining biologic properties of membranes by controlling their structural properties such as their permeability, fluidity and rigidity [27,28]. The chemical structures of phytosterols are similar

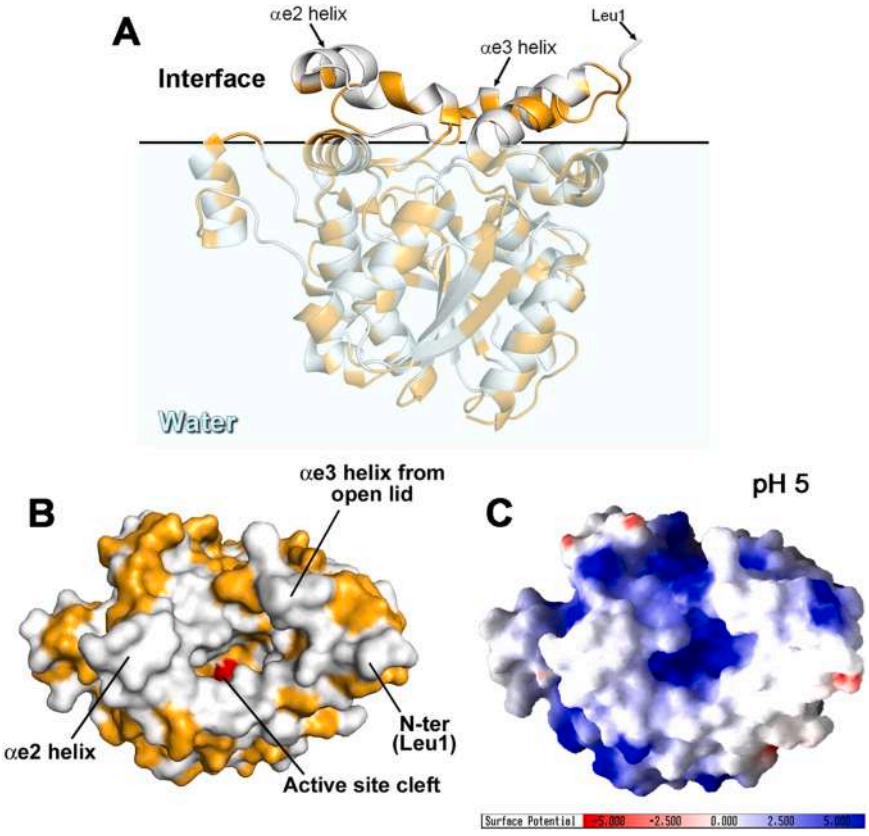

Fig. 1. 3D structure of recombinant dog gastric lipase showing the interfacial recognition site (IRS). Panel A: ribbon model showing the secondary structure elements of rDGL with the lid in the open conformation and putative orientation at lipid-water interface based on the localization of the IRS. Panel B: Top view and molecular surface representation (white=hydrophobic; yellow=polar) of rDGL showing the hydrophobic ring surrounding the active site entrance. Panel C: Top view and molecular surface representation showing its surface potential at pH 5 Surface potential scale is given below the rDGL structure, with red and blue colors corresponding to negative and positive potential, respectively. Views were prepared using PyMol software (Schrodinger, L. (2010) The PyMOL Molecular Graphics System, Version 1.3r1.) and the crystal structure of rDGL (PDB: 1K8Q). Surface potential was estimated using the TITRA software program [10] and the protein surfaces were generated using GRASP [11].

to those of animal cholesterol, nevertheless the absorption of the majority of phytosterols in the intestinal tract of mammals is up to ten times lower than that of cholesterol [29]. In humans, phytosterol consumption has been shown to induce a lowering of plasma cholesterol levels, thus preventing cardiovascular diseases and atherosclerosis [30]. Sterol molecules are known to promote hydrophobic interactions between membrane lipid acyl chains, which introduce a higher order and a subsequent rigidification of membranes [31]. At the air/water interface, the incorporation of phytosterols molecules in a phospholipid film has been shown to reorganize the monolayer, by modifying the packing and orientation of the polar heads of phospholipids [32].

In this context, the present work aimed at determining the interaction of gastric lipase with mixed films of galactolipids, galactolipids/phospholipids, and galactolipids/phospholipids/phytosterols, mimicking plant photosynthetic membranes. Biophysical tools such as the combination of ellipsometry and tensiometry were used to monitored the lipid-protein interactions at the air/water interface. Atomic force microscopy was further used to study the distribution of the enzyme into the heterogeneous lipid systems. Recombinant dog gastric lipase (Fig. 1) was used as a representative gastric lipase available in a purified and well characterized form [8] and with close homology with human gastric lipase. Vegetal membrane composition was approached using mixed monolayers of purified phospholipids (PL), galactolipids (GL) and phytosterols (pS) presenting liquid expended/liquid condensed (LE/LC) phase coexistence at 20 mN/m and 20 °C.

2. Experimental section

Chloroform and methanol were purchased from Sigma Aldrich Ltd. (St. Quentin Fallavier, France). If not stated otherwise, all biophysical characterizations were conducted at least in triplicate.

2.1. Preparation of lipid mixtures

Glycerophospholipids (dipalmitoylphosphatidylcholine, DPPC) and galactolipids (monogalactosyldiacylglycerol, MGDG, and digalactosyldiacylglycerol, DGDG) were purchased from Avanti Polar Lipids (see supplementary data for their fatty acid composition). Canola phytosterols (pS) from the deodorization distillates of canola oil were obtained as a gift from Cognis France (Estarac, France). The typical molar composition (estimated from usual normalized GC procedures) was: β-sitosterol (50.3 mol%), campesterol (38.9 mol%) and brassicasterol (10.5 mol%). β-sitosterol and campesterol are the most commonly found in the human diet due to their high composition in nuts and oilseed species [33,34]. Brassicasterol is a phytosterol found in some unicellular algae and terrestrial plants such as rapeseed [35,36].

Simple binary mixture of MGDG and DGDG (60:40, mol/mol) was prepared, namely GL. Ternary and quaternary mixtures of GL, DPPC and pS, namely GL/DPPC (50:50, mol/mol) and GL/DPPC/pS (45:45:10 mol/mol/mol), respectively, were also prepared to mimic the composition of natural vegetal membrane (see Table 1 for relative molar composition). Lipid-lipid interactions and molecular organization at the air/water interface of the three monolayers studied are reported in [37].

2.2. Enzyme purifications and preparation of aliquots

Recombinant dog gastric lipase (rDGL) (86 % amino acid sequence identity with HGL) was produced in transgenic maize by Meristem Therapeutics (Clermont-Ferrand, France) and purified as described previously [8]. rDGL stock solution was prepared at a concentration of 1.8 mg/mL in 10 mM sodium acetate buffer, 100 mM NaCl, 20 mM $CaCl_2$, pH 5, and stored at − 20 °C. Diluted aliquots at a final concentration of 1.92 mg/mL (40 nM) were prepared in the same buffer before being used in monolayer experiments.

Table 1 -
Model system compositions.

	Monolayer composition
(1) GL	MGDG/DGDG 60:40 mol/mol
(2) GL/DPPC	GL/DPPC 50:50 mol/mol
(3) GL/DPPC/pS	GL/DPPC/pS* 45:45:10 mol/mol/mol

* β-sitosterol, campesterol, brassicasterol 50:40:10 mol/mol/mol

2.3. Ellipsometry and surface pressure measurements at the air/water interface

Kinetic measurements over 5 h were performed using circular Teflon trough of 8 mL (surface area of 27 cm^2). Kinetic measurements over 2 h before Langmuir Blodgett transfer of the interfacial film were performed using Langmuir trough of 50 mL and a surface area of 35 cm^2.

Before each experiment, the Teflon trough have been carefully cleaned with UP water and ethanol to get rid of surface-active residual impurities. Control ellipsometric and tensiometric measurements were performed during half an hour on 10 mM acetate buffer, 100 mM NaCl, 20 mM $CaCl_2$, pH 5 before experiments to check the cleaned surface before experiments. The surface pressure (π) and the ellipsometric angle (Δ) were recorded at the same time. π was measured according to the Wilhelmy-plate method using a filter paper connected to a microelectronic feedback system to measure the surface pressure (Nima Technology, UK). Values of π were recorded every 4 s with a precision of ± 0.2 mN/m. Ellipsometric measurements were carried out using a home-made automated ellipsometer in a "null ellipsometer" configuration [22,38]. The laser beam probed a surface of 1 mm^2 and a depth in the order of 1 μm and provided insight on the thickness of the interfacial film formed at the interface. Values of the ellipsometric angle (Δ, °) were recorded every 4 s with a precision of ± 0.5°.

2.4. Adsorption of rDGL onto multicomponent lipid monolayers and at the air/water interface

A homogenous monolayer was formed by spreading a few microliters of 1 mM solution of lipids in $CHCl_3$/MeOH (2:1, v/v) over the surface of the buffer solution until an initial pressure of 20 ± 1 mN/m was reached [12]. After stabilization of the film over 5 min, rDGL was further injected in the sub-phase at a final concentration of 40 nM. The increase of the surface pressure and ellipsometric angle due to protein adsorption onto the lipid monolayer was continuously monitored until reaching the equilibrium.

2.5. Visualization of phase separations and lipase distribution in heterogeneous film by atomic force microscopy

For AFM imaging, interfacial films were transferred onto a freshly-cleaved mica plate using the Langmuir-Blodgett method. The transfer was processed after 2 h kinetics at a constant surface pressure and at a very low speed (0.5 $mm.min^{-1}$). Imaging was carried out with an AFM (Multimode Nanoscope 5, Bruker, France) in contact mode QNM in air (20 °C), using a standard silicon cantilever (0.06 N/m, SNL-10, Bruker, France), and at a scan rate of 1 Hz. The force was minimized during all scans and the scanner size was 100 × 100 $μm^2$. The processed images analyzed by the open-source platform Gwyddion are representative of at least duplicated experiments. ImageJ software was used to perform the analysis of AFM images. The functions *Plot Profile*, *Threshold*, *Particle Analysis*, *Make Binary* and *Dilate* were applied to study the different height levels as well as the shape of the protein networks. ImageJ software was used to perform different height analyses (based on the analyses of five plot profiles taken randomly in the AFM image) and thresholds on the raw AFM images (see supplementary data), in line with the study of [21].

3. Results

3.1. Ellipsometric and tensiometric adsorption kinetics of rDGL onto galactolipids (homogenous phase) and mixed galactolipid-phospholipids (heterogenous phase) monolayers

The adsorption kinetics of rDGL onto the GL monolayer was studied by tensiometry and ellipsometry, at 20 mN/m. Under these conditions, the GL monolayer forms a liquid expanded (LE) phase. The results obtained on this homogenous system were then compared with the rDGL adsorption kinetics onto heterogenous film based on mixture of galactolipids and phospholipids (GL/DPPC monolayer). Under these conditions, some phase separation occurs with the coexistence of liquid condensed (LC) and LE phases at 20 mN/m.

The gastric lipase was injected into the subphase after 5 min equilibrium of the GL and GL/DPPC lipid films, respectively. The adsorption kinetics were monitored over five hours. The variations with time in the ellipsometric angle and surface pressure are shown Fig. 2.

In Fig. 2. A, the surface pressure increased quickly after the injection of the enzyme in the subphase below the GL monolayer, while the ellipsometric angle remained stable over the first few minutes of kinetics, reflecting the accumulation of the gastric lipase below the air/water interface. After one hour kinetic, the surface pressure started to slowly decrease, together with a drastic increase in the ellipsometric angle from 6.9° to a maximum value of 12.9°, reflecting a reorganization at the interface and the subsequent adsorption of the enzyme onto the lipid monolayer. The evolution of the surface pressure and ellipsometric angle after injection of gastric lipase in the subphase of the GL/DPPC system (Fig. 2. B) followed a similar evolution. The maximum increase in the surface pressure ($\Delta\pi_{max}$) was similar for both systems ($\Delta\pi_{max}$=1.2 mN/m vs 1.4 mN/m, for GL and GL/DPPC films, respectively). Nevertheless, for the $GL_{50}/DPPC_{50}$ monolayer, the ellipsometric angle started to increase right after the injection of the lipase into the subphase, reflecting a faster adsorption of the rDGL onto the heterogeneous film, probably due to the different orientation of the GL polar heads in the presence of DPPC. Indeed, the lag phase before the start of rDGL adsorption observed in the case of the GL monolayer could be due to the packing and orientation of the GL polar heads, which could hinder the access of the enzyme active site to the interface. In addition, it is important to point that addition of DPPC triggers phase separation which has been demonstrated as a structural feature favoring rDGL adsorption. For both systems, an equilibrium plateau was reached from 3 h and until the end of the kinetics, with similar values for both GL and GL/DPPC systems ($\delta\Delta$=10.5 ± 0.5°).

The $\Delta\pi_{max}$ values obtained upon rDGL adsorption on GL and GL/DPPC films are lower than those previously recorded upon rDGL adsorption onto pure phospholipid (PC) films [14] or films mimicking bovine milk fat membranes and presenting phases coexistence [21]. This may result from weaker electrostatic interactions of rDGL with the neutral GL (compared to milk polar lipids (MPL)) which in general have charged polar heads. In addition to weaker electrostatic interactions, the galactose residues of GL polar heads may also generate some steric hindrance for lipase penetration into the film. Difference in fatty acyl moieties (chain length and unsaturation degree) may also influence lipid packing and rDGL adsorption.

3.2. Visualization of lipase organization into galactolipid monolayers by atomic force microscopy

AFM images of monomolecular films in the presence of rDGL were made after sampling the interface using the Langmuir Blodgett method after 2 h of kinetics. The use of AFM allowed the topographic visualization of the interface at the nanoscopic scale. The AFM images of the interface were compared before and after the rDGL injection to highlight the distribution of the enzyme in the GL films and to determine the reorganization of the monolayers induced by the lipid-protein interactions. Details on AFM study on GL mixed films in the absence of rDGL are reported in [37].

The injection of rDGL in the subphase (40 nM) clearly modified the morphology of the GL film (Fig. 3) and triggered the formation of homogeneous patches onto the fluid phase after 2 h of kinetics. These patches, assumed to reflect protein adsorption, had a mean width of 300 nm, which could correspond to 60 rDGL molecules, taking a width of about 5 nm for a rDGL molecule [12]. The roughness of the GL film before the enzyme injection was no longer visible on the AFM images in the presence of rDGL, suggesting a modification of the galactolipid-galactolipid interactions as well as a reorganization of the galactolipid polar heads induced by the adsorption of the rDGL onto the lipid film. Based on the analysis of five sections of the AFM image, the height variations of the fluid lipid background ranged from 0 to 0.5 nm (average height=0.24 ± 0.12 nm), representing about 57 % of the interfacial film. After rDGL adsorption, the cross-section profiles of the AFM images displayed several peaks of varying heights and were divided into two categories depending on their height levels and

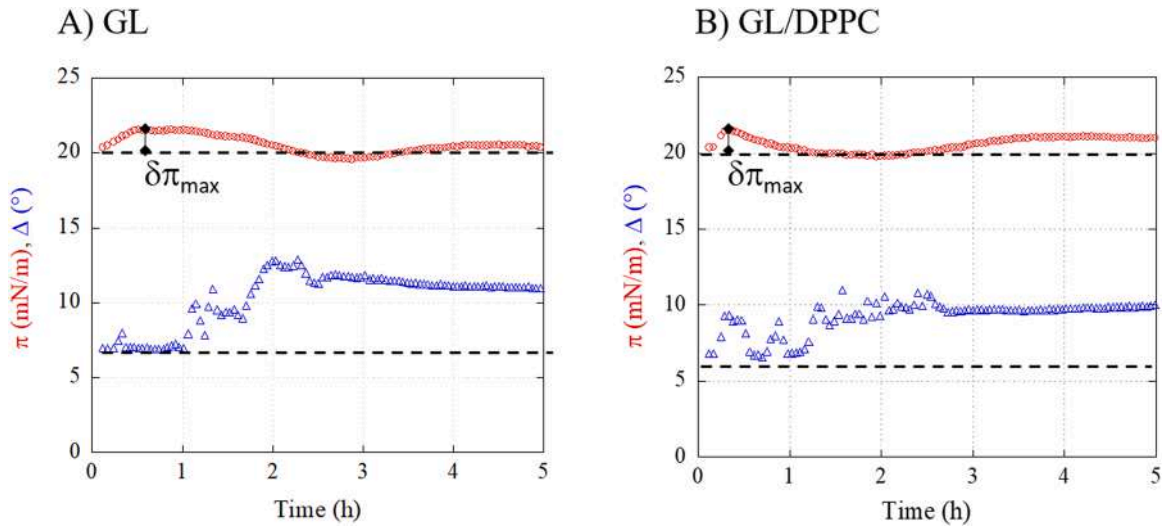

Fig. 2. (A) Kinetic evolution of the surface pressure (circle, red) and ellipsometric angle (triangle, blue) upon rDGL adsorption at the air/water interface onto GL lipid film and, (B) Kinetic evolution of the surface pressure (circle, red) and ellipsometric angle (triangle, blue) upon rDGL adsorption onto $GL_{50}/DPPC_{50}$ monolayers performed at an initial surface pressure of 20 mN/m. The rDGL was injected in the subphase after 5 min stabilization of the monolayers at the air/water interface.

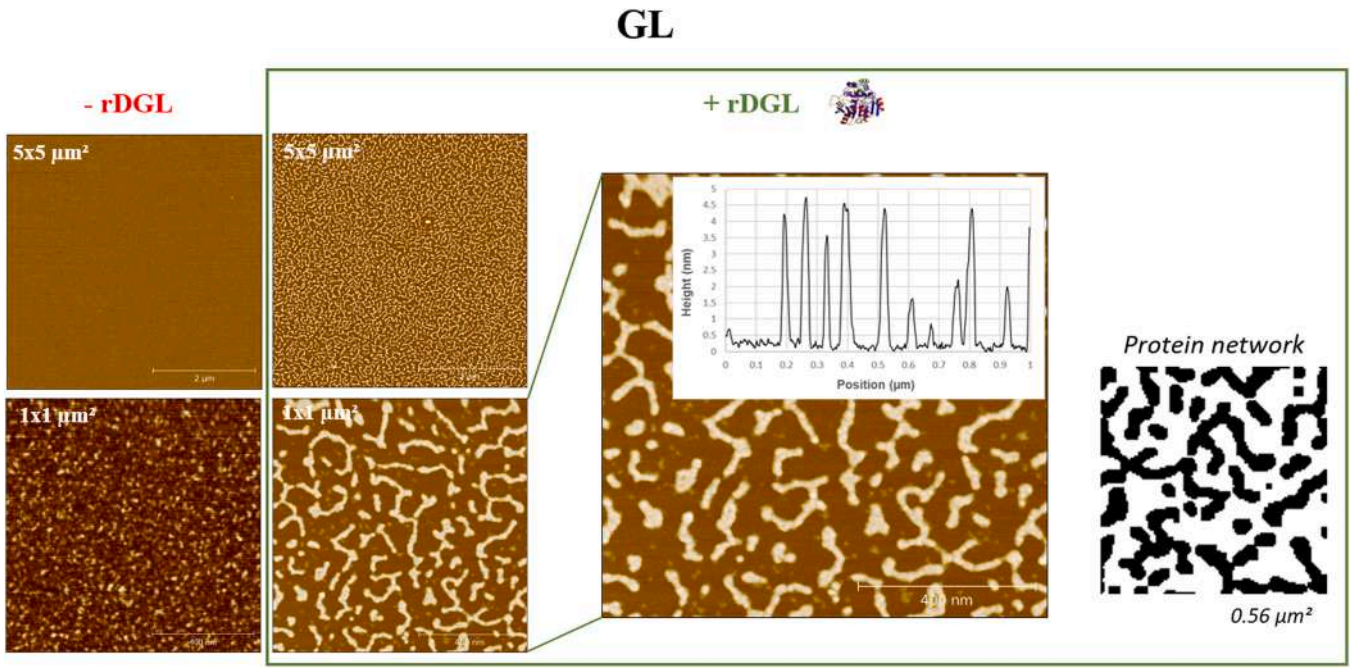

Fig. 3. AFM images (5 ×5 µm^2 and 1 ×1 µm^2) of GL monolayers at an initial surface pressure of 20 mN/m before (-rDGL, red) and after (+rDGL, green) rDGL injection (40 nM final concentration, 5 h kinetics). A cross-section of height profile is representative for 1 × 1 µm^2 image after rDGL injection. ImageJ analysis was performed on a 0.56 µm^2 crop to determine the shape of the protein network (see material and methods). The vertical color scale from dark brown to white corresponds to an overall height of 15 nm.

occurrences. A first height level was identified, with peaks ranging from 0.5 to 2.0 nm (average height=0.98 ± 0.4 nm), accounting for 17 % of the interfacial film. A second level was also detected, with heights ranging from 2.0 nm to 5.5 nm (average height=4.0 ± 0.8 nm), representing about 26 % of the interface on the AFM image. On this second height population, 55 % of the heights were included between 3.9 and

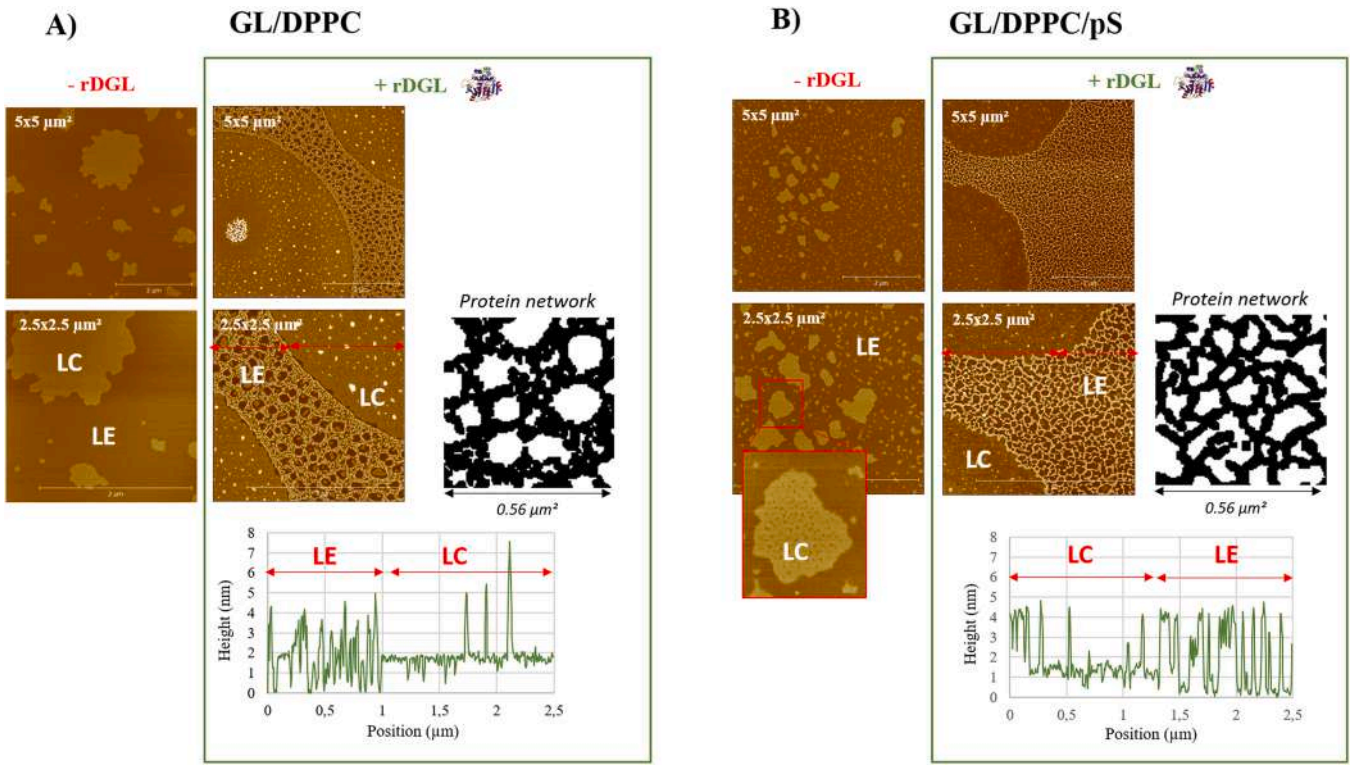

Fig. 4. AFM images (5 ×5 µm^2 and 2.5 ×2.5 µm^2) at an initial surface pressure of 20 mN/m before (-rDGL, red) and after (+rDGL, green) rDGL injection (40 nM final concentration, 5 h kinetics) of A) GL/DPPC monolayer (50:50 mol/mol) and B) GL/DPPC/pS monolayer (45:45:10 mol/mol/mol). Cross-sections of height profiles are representative for 2.5 × 2.5 µm^2 image after rDGL injection. (LE – Liquid Expended, fluid phase; LC – Liquid Condensed, gel phase). The vertical color scale from dark brown to white corresponds to an overall height of 15 nm.

4.5 nm, which could correspond to the entire cross-section of rDGL molecules [9] and thus of protein patches covering an average area of 336 nm^2 (15 pixels per AFM image), which would correspond to a consistent value of 47 rDGL molecules, taking a cross-sectional area of 7.2 nm^2 at 20 mN/m, as reported by [12].

3.3. Visualization of lipase organization into galactolipid-phospholipids monolayers by atomic force microscopy

A saturated phospholipid (DPPC) was added at a molar ratio of 50% in the GL mixture, in order to induce phase heterogeneity and determine the impact of such heterogeneity on the rDGL adsorption by introduction of a liquid condensed phase (LC) in the monolayer. The AFM images (5 ×5 μm^2 and 2.5 ×2.5 μm^2) of the interfacial film before and after the injection of the rDGL in the subphase of the GL/DPPC monolayer are presented Fig. 4A.

After injection of the enzyme, the LC domains have merged, adopting a more circular shape, with heights of 1.7–2.3 nm (average height=1.8 ± 0.1 nm), covering an average surface of 36 % of the interfacial film. At the very center and on the sides of the LC domains, bright peaks of 2.0–8.0 nm in height were also visible, circularly distributed, pointing the heterogeneity of the gel phase domains. Onto the fluid phase (LE), an irregular protein network was formed, much denser than the one observed in the case of the GL film (Fig. 3), and made of small grains forming interconnected units of 50.0 ± 20.0 nm width. A sharp demarcation was also visible between the protein network in the fluid phase and the condensed domains, indicating rDGL exclusion from the LC-LE phase boundary and LC domains.

Size analyses and thresholds on AFM images led to the identification of height levels induced by the interactions of rDGL with the heterogeneous membrane, which are summarized Table 2. As for the GL monolayer, two different height profiles were identified at the fluid phase level, with similar profiles, indicating the preferential adsorption of the enzyme at the level of the fluid phase. A new higher height profile was identified at the level of the condensed domains, where the lipase probably has more difficulty to adsorb due to the high packing.

3.4. Impact of phytosterol addition in galactolipid-phospholipids mixture on the adsorption behavior of the gastric lipase

The inclusion of phytosterols in the GL/DPPC mixture has been shown to generate defects at the level of the condensed phase, due to the preferential interactions between the phytosterols and the saturated fatty acids [37]. The AFM images Fig. 4. B revealed that 2 h after the injection of rDGL into the subphase, a regular protein network has formed onto the fluid phase. This network is composed of interconnected units of the same width as the protein network formed at the interface of the GL film (30.0 ± 0.0 nm), suggesting a similar organization of the proteins. Additionally, the delineation between the fluid phase protein network and the condensed phase domains was no longer visible on the AFM images, in contrast to the $GL_{50}/DPPC_{50}$ film, indicating a modification of the protein-lipid interactions and probably a better miscibility of the components at the interface when pS were added in the system. As for the two previous samples, image and size analyses have revealed different levels of rDGL adsorption on the lipid film, which are reported Table 2.

Table 2 -
Summary of height levels identified in AFM images and related to rDGL interactions with model membranes. Height values are given in nm. The percentages given are the percentage of pixels covered by the indicated height range (-). Values obtained were based on the analysis of five plot profiles taken randomly in the AFM image.

Monolayer	Protein adsorption (nm)		
GL	h1 = 0.98 ± 0.4 (0.5 – 2) 17 %	h2 = 2.0 ± 5.5 (2.0 – 5.5) 26 %	–
$GL_{50}/DPPC_{50}$	h1 = 0.4 ± 0.1 (0.2 – 1.7) 32 %	h2 = 2.6 ± 0.2 (2.3 – 4.8) 26 %	h3 = 5.5 ± 0.7 (>5.5) 2 %
$GL_{45}/DPPC_{45}/pS_{10}$	h1 = 1.2 ± 0.2 0.6 – 1.5 34 %	h2 = 3.6 ± 0.6 (2.3 – 5.0) 24 %	–

4. Discussion

rDGL has been shown to exhibit a high affinity for the air/water or lipid/water interface covered by polar lipids and to form monolayers, which distinguishes it from other globular proteins that tend to form multilayers [21,39]. The formation of a monolayer was also deduced from rDGL adsorption onto a siliconized hydrophobic surface, monitored using a quartz crystal microbalance [13]. This is probably due to its structural adaptation that avoids interfacial denaturation and involves a localized conformation change (lid opening) with the formation of an IRS on one side of the molecule (Fig. 1) [40]. The binding capacity of the rDGL at the air/water interface was monitored as the increase in the surface pressure π_{max}, correlated to the variations of the lipid packing and the adsorption of enzyme molecules onto the monolayer. Here, the combination of data obtained with ellipsometry, tensiometry, and atomic force microscopy analyses provided insights on the physicochemical behavior and the distribution of rDGL in mixed GL films at the air/water interface.

4.1. The particular orientation of the galactolipid polar heads could limit the enzyme adsorption at the interface of the monolayer despite the high surface activity of rDGL

The adsorption of rDGL onto mixed GL film (initial $\pi = 20$ mN/m) triggered a slight increase in the surface pressure ($\Delta\pi_{max}$=1.2 mN/m). Although this result reflects lipid-protein interactions at the air-water interface, this increase in the surface pressure was more discrete than those reported by [41] upon the adsorption of pin-a isoform of puroindoline, a small globular protein (13 kDa), onto homogenous monolayers of pure MGDG or DGDG isolated from wheat. Indeed, a pressure increase of 4.4 and 2.5 mN/m at 20 mN/m was obtained upon adsorption of pin-a onto pure MGDG and DGDG films, respectively. The insertion of pin-a onto the GL films could be explained by the fluidity of GL as well as by the establishment of hydrophobic and Van der Walls interactions between the galactosyl head groups and the numerous tryptophan moieties of puroindolines, favoring their penetration into GL films. Furthermore, the overlap of the MGDG heads from 20 mN/m could have induced the formation of local instabilities, favoring the insertion of the protein in the film, explaining the greater increase of pressure. Conversely, the larger polar heads of DGDG could have limited the insertion of pin-a, thus explaining the lower pressure increase. Indeed, despite the larger polar head of DGDG than MGDG, digalactosyl residues possess the ability to adopt a tilted orientation, at 40° to the interface normal, in contrast to the polar head of pure MGDG, which was oriented parallel to the interface [41]. The particular orientation of the digalactosyl residue of DGDG is consistent with the results obtained by [42] on the digestibility of an olive oil stabilized by either DPPC or DGDG, showing that the air/water interface occupied by DGDG was more resistant to the adsorption of bile salts, pancreatic lipase and colipase compared to the interface occupied by DPPC.

The small increase in surface pressure and the latency phase observed before the increase of the ellipsometric angle in the case of rDGL is therefore more consistent with a discrete adsorption behavior onto the mixed GL monolayers at 20 mN/m. The more limited insertion of rDGL could have been due to the larger size of the protein (50 kDa versus 13 kDa for pin-a puroindoline), but also to the fact that the monolayer was composed of a mixture of GL, and not of pure MGDG or

DGDG. Indeed, in the equimolar mixture, a reorientation of the DGDG polar heads was observed, with the digalactosyl moiety orienting parallel to the interface, suggesting strong interactions between MGDG and DGDG and allowing tighter packing of mixed galactolipid molecules at the interface that could inhibit the lipase adsorption [41]. Moreover, the adsorption kinetics properties of gastric lipase could also result from the interactions between the substrates and the active site of the enzyme. The IRS of rDGL being composed of several basic residues (Fig. 1. C), it is less likely to develop electrostatic interactions with an uncharged galactolipid monolayer than with a charged phospholipid monolayer. This feature probably explains the lower adsorption capacity of rDGL to GL monolayer. The absence of charge at an interface decreases the establishment of electrostatic interactions with the enzyme, which could slow down or even hinder its adsorption.

Overall, the extend of rDGL adsorption onto the lipid monolayer seems to be highly dependent on the lipid packing and acyl chain composition. Indeed, a higher increase of π ($\Delta\pi_{max}$=8 mN/m) was reported for the rDGL adsorption onto 1,2-dilauroyl-sn-glycero-3-phosphocholine (DLPC) monolayer in the same conditions [12]. Moreover, rDGL shows a higher penetration capacity into medium chain DLPC than into long chain egg PC monolayers, with critical surface pressures of insertion (π_c) of 30.3 mN/m and 21.5 mN/m, respectively. The surface pressure chosen here with GL film (π = 20 mN/m) therefore represents harsh conditions for rDGL adsorption and penetration. An higher increase of the surface pressure was also reported by [21] on milk polar lipids with or without residual triacylglycerols MPL and MPL_{TC} ($\Delta\pi_{max}$=2.4 mN/m and $\Delta\pi_{max}$=6.1 mN/m, respectively).

In our study, the ellipsometric data suggested that a significant amount of rDGL was adsorbed onto the GL monolayer after 1 h latency phase, with a high ellipsometric angle variation of δΔ= 4.2° obtained after 2 h of kinetics. This value was higher than that obtained on MPL (δΔ=3.1°) but much lower (δΔ=18.3°) than that obtained on MPL_{TC} after 5 h of kinetics. Overall, the results of tensiometry and ellipsometry analysis confirmed the adsorption of rDGL onto the GL monolayer, although to a lesser extent than for bovine milk membranes (MPL and MPL_{TC}) due to the particular orientation of the polar head of galactolipids and the uncharged surface of the monolayer.

4.2. rDGL undergoes conformational changes upon adsorption, explaining the different level of adsorption/insertion onto the GL films

The AFM images of the GL film evidenced the formation of protein patches at two different height levels in the fluid phase 2 h after the injection of rDGL in the subphase. Different levels of rDGL adsorption have already been reported [12,14,21,22] as being dependent on the monolayer composition but also on the conformation of the adsorbed enzyme, which reflect its level of interaction and activity with the substrate. This may result from structural changes occurring upon protein adsorption at the air/water (or lipid/water) interface. The unfolding and denaturation of proteins at the interfaces are well-known behaviors, especially when interfacial tension is high. For example, lipases are rapidly inactivated at the oil-water interface when using pure triacylglycerols [3]. Nevertheless, denaturation can be avoided using surfactants decreasing the interfacial tension or by the enzyme itself. Lipases like gastric lipase are also known to undergo a localized conformational change with a lid opening that controls the interfacial recognition site and activity [40]. Coagulation/aggregation are additional phenomena that may also occur with proteins at interfaces [43]. All these phenomena were likely to explain the different levels of insertion of the rDGL in the mixed GL film. Indeed, the lowest height level could correspond to some denatured rDGL, unfolded upon adsorption and resulting in an increase in the surface pressure, more favorable to the adsorption of the enzyme in its active conformation. The second height level corresponding to homogeneous peak sizes between 2.0 and 5.5 nm is likely to correspond to the adsorption of rDGL in its active conformation, at a depth of 1–2 nm in the GL monolayer onto the GL monolayer at the air/water interface. This level of rDGL would fit with the adsorption model previously proposed for rDGL [12]. A model for the rDGL distribution in the GL monolayer under gastric conditions is proposed Fig. 5.

4.3. rDGL is excluded from condensed phase domains in mixed heterogeneous GL-DPPC systems and exhibits similar adsorption behavior to other small globular proteins

Numerous studies have been conducted in AFM to investigate the adsorption of various lipases and phospholipases onto heterogenous supported monolayers and bilayers at the air/water interface [44,45]. Overall, results have indicated the preferential adsorption of these enzymes at the edges of low molecular packing domains, where the increase of the curvature favor the amphiphile adsorption [46,47].

The lateral distribution of the gastric lipase in monolayers of milk fat globules with phase heterogeneity has been studied in both human and bovine systems [21,22]. The coexistence of liquid condensed/liquid expanded (LC/LE) phases in milk fat globule monolayers has been shown to impact the adsorption of gastric lipase. Indeed, the rDGL gets really rapidly adsorbed in the LE phase or at the phase boundaries in the bovine milk membrane (BMM) and human milk membrane (HMM) extracts, showing that the coexistence of LC/LE phase was an important driver of the rDGL adsorption.

Here, we introduced some phase heterogeneity in the GL monolayer by adding DPPC. As expected, the AFM images (Fig. 4. A) revealed that the rDGL was excluded from the LC phase, and preferentially adsorb onto the LE phase of GL-DPPC monolayer, which present a lower molecular packing, probably due to the high composition in PUFA of GL. Indeed, the condensed domains were likely to include DPPC, with tight packing of its saturated acyl chains preventing lipase penetration. Nevertheless, the bright peaks visible in the center of the condensed domains seemed to indicate an adsorption of rDGL at this level, probably due to some compositional heterogeneity between the center and the edge of the LC domains, favoring a less dense packing or the appearance of defects at the central level. On the other hand, the adsorption of the rDGL onto the LE phase triggered the formation of a dense protein network, composed by small interconnected nanodomains of irregular shape and width, in contrast to the discontinuous homogeneous network previously formed in the GL film. Several levels of rDGL insertions were identified, in line with the results of [21] on bovine milk fat model membranes (MPL and MPL_{TC}), with slightly different height values in those different heterogenous systems, which could be explain by the differences of composition and lipid packing between the monolayers.

Additionally, the condensed domains composing the LC phase merged and their circularity was increased, indicating the existence of a line tension at the interface of the LC/LE phases. Indeed, [48] have shown that the size and the shape of LC domains composed by sphingomyelin and cholesterol depend on the balance between the line tension, which tends to increase the size of the domains in order to reduce the total length of the boundaries, and the entropic and electrostatic repulsions, which prevent the fusion of the LC domains. Thus, the increase of the LC domain size in our study is consistent with a higher line tension at their edges. This change in line tension could be triggered by the greater height difference between the two phases LC and LE, induced by the adsorption of rDGL onto the fluid phase. Indeed, this height difference has an unfavorable energy cut per unit length, and as a result, the domain boundary deforms to counteract this phenomenon, inducing line tension, which may be unfavorable for rDGL adsorption. Indeed, the sharp domain delineation visible on the AFM image between the fluid-phase protein network and the LC domains seems to indicate that the rDGL poorly adsorbs at the phase boundaries.

The adsorption behavior of rDGL on heterogeneous lipid films from animal or plant sources can be compared to other globular proteins. [49] studied the adsorption behavior of several lipid membrane proteins, including N-Ras, a small globular protein (21 kDa), onto heterogeneous

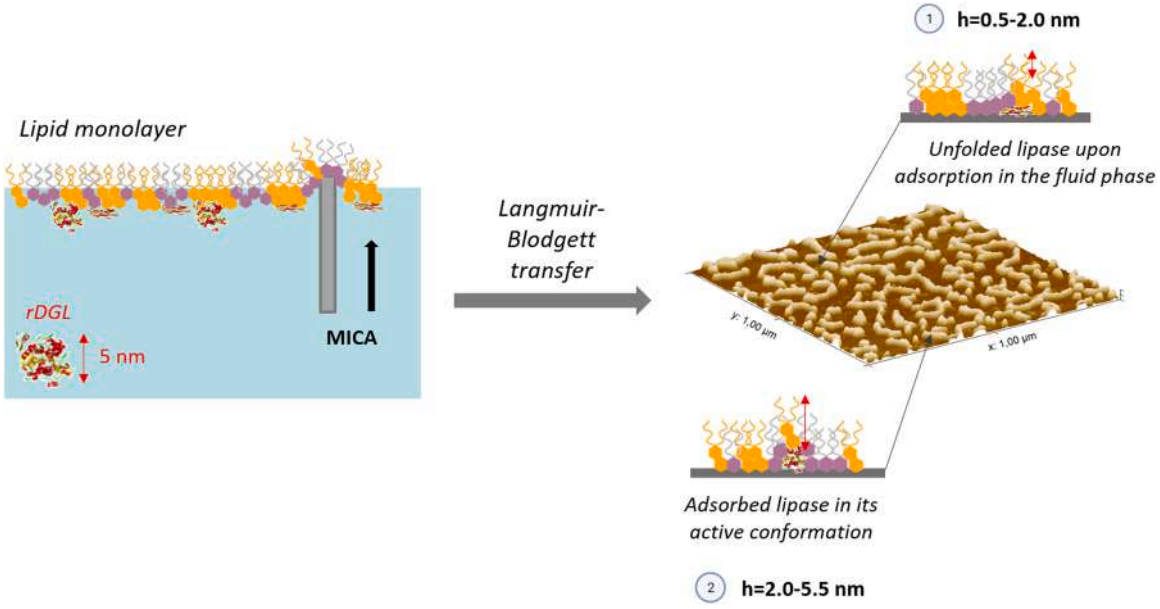

Fig. 5. Proposed model of rDGL distribution in homogenous galactolipid monolayer under gastric conditions.

model membranes with coexisting fluid/gel phases. The results of this study provided direct evidence of the preferential distribution of the N-Ras protein in the fluid phase, but also at the edges of the LC phase domains, leading to a favorable decrease of the energy between the phases. This adsorption of proteins at boundary phases was characteristic of proteins inserted into multiphase lipid systems but which do not show specific preferences for a given phase, so that they are expelled toward the boundaries. This localization and accumulation of proteins at the phase interface to decrease the line tension could explain the adsorption behavior of rDGL in the presence of pS.

4.4. The addition of pS modulated the rDGL adsorption onto mixed GL-DPPC monolayers at the air/water interface

In our previous study, the inclusion of phytosterols (pS) in the GL/DPPC film induced a drastic modification of the interfacial organization, with a dilution of the domains as well as an increase in the thickness of the condensed phases. This was attributed to interactions between GL and PL and a condensation effect of pS [50,51]. Moreover, the addition of pS to mixed DPPC and GL monolayers was found to trigger the appearance of defects into the condensed phase domains. Previous studies on various other lipases found that defects in lipid packing could constituted preferential sites for the enzyme anchoring [52,44,53,54]. The presence of local defects in the LC phase GL/DPPC/pS film reflects a less dense molecular packing, which could favor rDGL adsorption. Indeed, AFM images recorded after rDGL injection in the subphase of the films revealed significant differences in the organization at the interface between GL/DPPC and GL/DPPC/pS films. In the presence of pS, a regular protein network was visible on the AFM images, not only at the fluid phase but also at the phase domain boundaries and at the defects present on the condensed phase domains. The absence of a marked delineation of the protein network level between the LE and LC phases contrasts with the system without pS. It points to an enhancement of the rDGL adsorption onto the LC domains and at the boundary phase, leading to a decrease of the height difference between the LC/LE phases and thus to a decrease of the line tension (Fig. 4. B), favoring a more homogenous adsorption of rDGL at the interface. This modulation of rDGL adsorption in the presence of pS could also be explained by a modification of the lipid-lipid and protein-lipid interactions. Indeed, hydrogen bridges could be established with the hydroxyl groups of pS, as well as stacking between rDGL aromatic residues and the sterol backbone, leading to a different interfacial organization and favoring the rDGL adsorption.

Moreover, the two different levels of rDGL insertion with homogeneous peak sizes onto the GL-DPPC-pS film (h2, h3) were comparable to those identified in the case of rDGL adsorption onto models of HMM by [22]. In contrast, rDGL insertion onto BMM was less homogeneous, with 3 levels of heights described, similar to the ones evidenced for the GL-DPPC film. It was speculated by the authors that the particular composition of HMM (high PUFA content, presence of DHA, presence of anionic PL, coexistence of LC/LE phase) was more favorable to the action of rDGL than the composition of BMM. Indeed, HMM contained more anionic phospholipids, which have been shown to enhance the adsorption of rDGL at pH 5 thanks to a better reorientation of the charged active site.

4.5. Interest of the study for the adsorption of gastric lipase onto natural plant cell membranes

Plant cell membranes are complex systems containing a large variety of lipid and protein molecules. The high proportion of DPPC in our model systems (50%) was explained by the need to create a heterogeneous system, presenting a coexistence of LC/LE phase observable in AFM, but was actually far from the palmitic acid compositions (C16:0) found in natural plant membrane systems (plasma membrane, chloroplast thylakoids, oleosomes) [55]. Indeed, the proportion of palmitoyl chains in natural plant systems is on average between 5% and 20% wt. of total lipids [56,57]. Nevertheless, the raft theory in plant membrane systems predicts the existence of lipid assemblies locally enriched in phytosterol and sphingolipid molecules [58], which are known to contain liquid-ordered domains in a fluid environment [59]. These plant membrane rafts are biochemical homologues of mammalian cell membrane rafts rich in sphingomyelin and cholesterol, known for their transient dynamic structure in the nanometer range and involved in signaling and protein transport processes and other cellular processes [60-62].

Thus, although our biomimetic membranes constituted a simplified model somewhat far from the natural plant membrane composition, the general physicochemical trends and adsorption behavior of gastric lipase at these heterogeneous model membrane systems remain extendable to the protein-lipid interactions occurring at the so-called raft zones in plant cells. In particular, it appeared that the presence of

phytosterols in condensed domains and, by extension, in plant rafts, may enhance the rDGL adsorption at Lo or gel phase (LC) domains.

5. Conclusion

We have shown that Langmuir films and their analysis by tensiometry, ellipsometry and Langmuir-Blodgett transfer coupled to atomic force microscopy provide a suitable tool for studying the adsorption and interactions of gastric lipase with biomimetic vegetal membranes. Gastric lipase binds to these heterogenous membranes with a preference for phase boundaries and defects. It induces changes in the interfacial organization of lipids although it does not display any activity on polar acylglycerols from plant membranes [20]. Since gastric lipase is known to promote the action of pancreatic lipase through the release of fatty acids and changes in interfacial properties [17], the changes observed with plant polar lipids, without lipolysis, may also trigger the adsorption and activity of other pancreatic enzymes. This will be the objective of further studies, but the present one is a step forward in the comprehension of gastrointestinal lipase interactions with plant membranes, an overlooked aspect of lipid digestion [24].

CRediT authorship contribution statement

C. Bourlieu, V. Vié and J. Kergomard determined the outline and the content of the manuscript. J. Kergomard wrote the manuscript and all the co-authors participated in the experimental design, the collection, the interpretation of data and the correction and implementation of the manuscript. All co-authors have approved the final article.

Declaration of Competing Interest

The authors declare that they have no known competing financial interests or personal relationships that could have appeared to influence the work reported in this paper.

Data Availability

Data will be made available on request.

Acknowledgments

The authors would like to acknowledge the BIOMIF platform ('Biological Molecules at fluid interfaces', IPR, Rennes, France) for allowing the biophysical characterization of samples presented in this article. C. Bourlieu, V. Vié and J. Kergomard determined the outline and the content of the manuscript. J. Kergomard wrote the manuscript and all the co-authors participated in the experimental design, the collection, the interpretation of data and the correction and implementation of the manuscript. All co-authors have approved the final article.

Appendix A. Supporting information

Supplementary data associated with this article can be found in the online version at doi:10.1016/j.colsurfb.2022.112933.

References

[1] A.H.C. Huang, 4—lipases, in: P.K. Stumpf (Ed.), Lipids: Structure and Function, Vol. 9, Academic Press, 1987, pp. 91–119, https://doi.org/10.1016/B978-0-12-675409-4.50010-1.
[2] K.E. Jaeger, S. Ransac, B.W. Dijkstra, C. Colson, M. van Heuvel, O. Misset, Bacterial lipases, FEMS Microbiol. Rev. 15 (1) (1994) 29–63, https://doi.org/10.1111/j.1574-6976.1994.tb00121.x.
[3] A. Aloulou, J.A. Rodriguez, S. Fernandez, D. van Oosterhout, D. Puccinelli, F. Carrière, Exploring the specific features of interfacial enzymology based on lipase studies, Biochim. Et Biophys. Acta (BBA) - Mol. Cell Biol. Lipids 1761 (9) (2006) 995–1013, https://doi.org/10.1016/j.bbalip.2006.06.009.
[4] F. Carrière, C. Renou, S. Ransac, V. Lopez, J. De Caro, F. Ferrato, A. De Caro, A. Fleury, P. Sanwald-Ducray, H. Lengsfeld, C. Beglinger, P. Hadvary, R. Verger, R. Laugier, Inhibition of gastrointestinal lipolysis by Orlistat during digestion of test meals in healthy volunteers, Am. J. Physiol. -Gastrointest. Liver Physiol. 281 (1) (2001) G16–G28, https://doi.org/10.1152/ajpgi.2001.281.1.G16.
[5] Lengsfeld, H., Beaumier-Gallon, G., Chahinian, H., De Caro, A., Verger, R., Laugier, R., & Carrière, F. (2004). Physiology of Gastrointestinal Lipolysis and Therapeutical Use of Lipases and Digestive Lipase Inhibitors. In *Lipases and Phospholipases in Drug Development* (p. 195–229). John Wiley & Sons, Ltd. https://doi.org/10.1002/3527601910.ch10.
[6] C. Bourlieu, O. Ménard, A. De La Chevasnerie, L. Sams, F. Rousseau, M.-N. Madec, B. Robert, A. Deglaire, S. Pezennec, S. Bouhallab, F. Carrière, D. Dupont, The structure of infant formulas impacts their lipolysis, proteolysis and disintegration during in vitro gastric digestion, Food Chem. 182 (2015) 224–235, https://doi.org/10.1016/j.foodchem.2015.03.001.
[7] S. Canaan, A. Roussel, R. Verger, C. Cambillau, Gastric lipase: crystal structure and activity, Biochim. Et Biophys. Acta (BBA) - Mol. Cell Biol. Lipids 1441 (2) (1999) 197–204, https://doi.org/10.1016/S1388-1981(99)00160-2.
[8] A. Roussel, S. Canaan, M.-P. Egloff, M. Rivière, L. Dupuis, R. Verger, C. Cambillau, Crystal structure of human gastric lipase and model of lysosomal acid lipase, two lipolytic enzymes of medical interest, J. Biol. Chem. 274 (24) (1999) 16995–17002, https://doi.org/10.1074/jbc.274.24.16995.
[9] A. Roussel, N. Miled, L. Berti-Dupuis, M. Rivière, S. Spinelli, P. Berna, V. Gruber, R. Verger, C. Cambillau, Crystal structure of the open form of dog gastric lipase in complex with a phosphonate inhibitor, J. Biol. Chem. 277 (3) (2002) 2266–2274, https://doi.org/10.1074/jbc.M109484200.
[10] S.B. Petersen, P. Fojan, E.I. Petersen, M.T.N. Petersen, The thermal stability of the Fusarium solani pisi cutinase as a function of pH, J. Biomed. Biotechnol. 1 (2) (2001) 62–69, https://doi.org/10.1155/S1110724301000249.
[11] A.J. Nicholls, GRASP Manual, Columbia University, 1993.
[12] A. Bénarouche, V. Point, G. Parsiegla, F. Carrière, J.-F. Cavalier, New insights into the pH-dependent interfacial adsorption of dog gastric lipase using the monolayer technique, Colloids Surf. B: Biointerfaces 111 (2013) 306–312, https://doi.org/10.1016/j.colsurfb.2013.06.025.
[13] H. Chahinian, T. Snabe, C. Attias, P. Fojan, S.B. Petersen, F. Carrière, How gastric lipase, an interfacial enzyme with a ser-his-asp catalytic triad, acts optimally at acidic pH, Biochemistry 45 (3) (2006) 993–1001, https://doi.org/10.1021/bi0518803.
[14] A. Bénarouche, L. Sams, C. Bourlieu, V. Vié, V. Point, J.F. Cavalier, F. Carrière, Chapter eleven—studying gastric lipase adsorption onto phospholipid monolayers by surface tensiometry, ellipsometry, and atomic force microscopy, in: M.H. Gelb (Ed.), Methods in Enzymology, Vol. 583, Academic Press, 2017, pp. 255–278, https://doi.org/10.1016/bs.mie.2016.09.039.
[15] B. Lerique, J. Lepetit-Thévenin, A. Vérine, C. Delpéro, J. Boyer, Triacylglycerol in biomembranes, Life Sci. 54 (13) (1994) 831–840, https://doi.org/10.1016/0024-3205(94)00619-9.
[16] L. de La Fournière, M.G. Ivanova, J.-P. Blond, F. Carrière, R. Verger, Surface behaviour of human pancreatic and gastric lipases, Colloids Surf. B: Biointerfaces 2 (6) (1994) 585–593, https://doi.org/10.1016/0927-7765(94)80069-3.
[17] Y. Gargouri, G. Pieroni, C. Rivière, P.A. Lowe, J.F. Saunière, L. Sarda, R. Verger, Importance of human gastric lipase for intestinal lipolysis: an in vitro study, Biochim. Et Biophys. Acta 879 (3) (1986) 419–423, https://doi.org/10.1016/0005-2760(86)90234-1.
[18] M.R. Infantes-Garcia, S.H.E. Verkempinck, M.E. Hendrickx, T. Grauwet, Kinetic modeling of in vitro small intestinal lipid digestion as affected by the emulsion interfacial composition and gastric prelipolysis, J. Agric. Food Chem. 69 (16) (2021) 4708–4719, https://doi.org/10.1021/acs.jafc.1c00432.
[19] F. Carrière, H. Moreau, V. Raphel, R. Laugier, C. Benicourt, J.L. Junien, R. Verger, Purification and biochemical characterization of dog gastric lipase, Eur. J. Biochem. 202 (1) (1991) 75–83, https://doi.org/10.1111/j.1432-1033.1991.tb16346.x.
[20] J. Wattanakul, M. Sahaka, S. Amara, S. Mansor, B. Gontero, F. Carrière, D. Gray, In vitro digestion of galactolipids from chloroplast-rich fraction (CRF) of postharvest, pea vine field residue (haulm) and spinach leaves, Food Funct. 10 (12) (2019) 7806–7817, https://doi.org/10.1039/C9FO01867K.
[21] C. Bourlieu, G. Paboeuf, S. Chever, S. Pezennec, J.-F. Cavalier, F. Guyomarc'h, A. Deglaire, S. Bouhallab, D. Dupont, F. Carrière, V. Vié, Adsorption of gastric lipase onto multicomponent model lipid monolayers with phase separation, Colloids Surf. B: Biointerfaces 143 (2016) 97–106, https://doi.org/10.1016/j.colsurfb.2016.03.032.
[22] C. Bourlieu, W. Mahdoueni, G. Paboeuf, E. Gicquel, O. Ménard, S. Pezennec, S. Bouhallab, A. Deglaire, D. Dupont, F. Carrière, V. Vié, Physico-chemical behaviors of human and bovine milk membrane extracts and their influence on gastric lipase adsorption, Biochimie 169 (2020) 95–105, https://doi.org/10.1016/j.biochi.2019.12.003.
[23] P. Dörmann, C. Benning, Galactolipids rule in seed plants, Trends Plant Sci. 7 (3) (2002) 112–118, https://doi.org/10.1016/S1360-1385(01)02216-6.
[24] M. Sahaka, S. Amara, J. Wattanakul, M.A. Gedi, N. Aldai, G. Parsiegla, J. Lecomte, J.T. Christeller, D. Gray, B. Gontero, P. Villeneuve, F. Carrière, The digestion of galactolipids and its ubiquitous function in nature for the uptake of the essential α-linolenic acid, Food Funct. (2020), https://doi.org/10.1039/D0FO01040E.
[25] K. Grosjean, S. Mongrand, L. Beney, F. Simon-Plas, P. Gerbeau-Pissot, Differential effect of plant lipids on membrane organization: specificities of phytosphingolipids and phytosterols, J. Biol. Chem. 290 (9) (2015) 5810–5825, https://doi.org/10.1074/jbc.M114.598805.

[26] J.R. Silvius, Partitioning of membrane molecules between raft and non-raft domains: insights from model-membrane studies, Biochim. Et Biophys. Acta (BBA) - Mol. Cell Res. 1746 (3) (2005) 193–202, https://doi.org/10.1016/j.bbamcr.2005.09.003.
[27] E.J. Dufourc, The role of phytosterols in plant adaptation to temperature, Plant Signal. Behav. 3 (2) (2008) 133–134, https://doi.org/10.4161/psb.3.2.5051.
[28] C. Silva, F.J. Aranda, A. Ortiz, M. Carvajal, V. Martínez, J.A. Teruel, Root plasma membrane lipid changes in relation to water transport in pepper: a response to NaCl and CaCl2 treatment, J. Plant Biol. 50 (6) (2007) 650–657, https://doi.org/10.1007/BF03030609.
[29] K. von Bergmann, T. Sudhop, D. Lütjohann, Cholesterol and plant sterol absorption: recent insights, *Am. J. Cardiol.* (2005) 10–14, https://doi.org/10.1016/j.amjcard.2005.03.014.
[30] M.H. Moghadasian, J.J. Frohlich, Effects of dietary phytosterols on cholesterol metabolism and atherosclerosis: Clinical and experimental evidence, Am. J. Med. 107 (6) (1999) 588–594, https://doi.org/10.1016/S0002-9343(99)00285-5.
[31] C. Silva, F.J. Aranda, A. Ortiz, V. Martínez, M. Carvajal, J.A. Teruel, Molecular aspects of the interaction between plants sterols and DPPC bilayers: an experimental and theoretical approach, J. Colloid Interface Sci. 358 (1) (2011) 192–201, https://doi.org/10.1016/j.jcis.2011.02.048.
[32] K. Hąc-Wydro, P. Wydro, A. Jagoda, J. Kapusta, The study on the interaction between phytosterols and phospholipids in model membranes, Chem. Phys. Lipids 150 (1) (2007) 22–34, https://doi.org/10.1016/j.chemphyslip.2007.06.211.
[33] B. Cañabate-Díaz, A. Segura Carretero, A. Fernández-Gutiérrez, A. Belmonte Vega, A. Garrido Frenich, J.L. Martínez Vidal, J. Duran Martos, Separation and determination of sterols in olive oil by HPLC-MS, Food Chem. 102 (3) (2007) 593–598, https://doi.org/10.1016/j.foodchem.2006.05.038.
[34] K.M. Phillips, D.M. Ruggio, M. Ashraf-Khorassani, Phytosterol composition of nuts and seeds commonly consumed in the United States, J. Agric. Food Chem. 53 (24) (2005) 9436–9445, https://doi.org/10.1021/jf051505h.
[35] N. Ikekawa, N. Morisaki, K. Tsuda, T. Yoshida, Sterol compositions in some green algae and brown algae, Steroids 12 (1) (1968) 41–48, https://doi.org/10.1016/S0039-128X(68)80078-9.
[36] Itoh, T., Tamura, T., Matsumoto, T., & Surugadai, K. (1973). Sterol composition of 19 vegetable oils. 4.
[37] J. Kergomard, F. Carrière, G. Paboeuf, F. Artzner, N. Barouh, C. Bourlieu, V. Vié, Interfacial organization and phase behavior of mixed galactolipid-DPPC-phytosterol assemblies at the air-water interface and in hydrated mesophases, Colloids Surf. B: Biointerfaces (2022), 112646, https://doi.org/10.1016/j.colsurfb.2022.112646.
[38] B. Berge, A. Renault, Ellipsometry study of 2D crystallization of 1-alcohol monolayers at the water surface, Europhys. Lett. 21 (7) (1993) 773–777, https://doi.org/10.1209/0295-5075/21/7/010.
[39] V.M. Bolanos-Garcia, A. Renault, S. Beaufils, Surface rheology and adsorption kinetics reveal the relative amphiphilicity, interfacial activity, and stability of human exchangeable apolipoproteins, Biophys. J. 94 (5) (2008) 1735–1745, https://doi.org/10.1529/biophysj.107.115220.
[40] E. Mateos-Diaz, S. Amara, A. Roussel, S. Longhi, C. Cambillau, F. Carrière, Probing conformational changes and interfacial recognition site of lipases with surfactants and inhibitors, Methods Enzymol. 583 (2017) 279–307, https://doi.org/10.1016/bs.mie.2016.09.040.
[41] Bottier, C. (2006). Caractérisation des puroindolines, des galactolipides du blé et de leurs interactions: Mesures physiques aux interfaces [Phdthesis, Université Rennes 1]. ⟨https://tel.archives-ouvertes.fr/tel-00148405⟩.
[42] B.-S. Chu, A.P. Gunning, G.T. Rich, M.J. Ridout, R.M. Faulks, M.S.J. Wickham, V. J. Morris, P.J. Wilde, Adsorption of bile salts and pancreatic colipase and lipase onto digalactosyldiacylglycerol and dipalmitoylphosphatidylcholine monolayers, Langmuir 26 (12) (2010) 9782–9793, https://doi.org/10.1021/la1000446.
[43] L.K. James, L.G. Augenstein, Adsorption of enzymes at interfaces: film formation and the effect on activity, Adv. Enzymol. Relat. Areas Mol. Biol. 28 (1966) 1–40, https://doi.org/10.1002/9780470122730.ch1.
[44] K. Balashev, N. John DiNardo, T.H. Callisen, A. Svendsen, T. Bjørnholm, Atomic force microscope visualization of lipid bilayer degradation due to action of phospholipase A2 and Humicola lanuginosa lipase, Biochim. Et Biophys. Acta (BBA) - Biomembr. 1768 (1) (2007) 90–99, https://doi.org/10.1016/j.bbamem.2006.09.028.
[45] M. Rangl, L. Rima, J. Klement, A. Miyagi, S. Keller, S. Scheuring, Real-time visualization of phospholipid degradation by outer membrane phospholipase a using high-speed atomic force microscopy, J. Mol. Biol. 429 (7) (2017) 977–986, https://doi.org/10.1016/j.jmb.2017.03.004.
[46] L.K. Nielsen, J. Risbo, T.H. Callisen, T. Bjørnholm, Lag-burst kinetics in phospholipase A2 hydrolysis of DPPC bilayers visualized by atomic force microscopy, Biochim. Et Biophys. Acta (BBA) - Biomembr. 1420 (1) (1999) 266–271, https://doi.org/10.1016/S0005-2736(99)00103-0.
[47] N. Prim, L. Iversen, P. Diaz, T. Bjørnholm, Atomic force microscope studies on the interactions of Candida rugosa lipase and supported lipidic bilayers, Colloids Surf. B: Biointerfaces 52 (2) (2006) 138–142, https://doi.org/10.1016/j.colsurfb.2006.05.018.
[48] A.J. García-Sáez, S. Chiantia, P. Schwille, Effect of line tension on the lateral organization of lipid membranes, J. Biol. Chem. 282 (46) (2007) 33537–33544, https://doi.org/10.1074/jbc.M706162200.
[49] K. Weise, G. Triola, S. Janosch, H. Waldmann, R. Winter, Visualizing association of lipidated signaling proteins in heterogeneous membranes−Partitioning into subdomains, lipid sorting, interfacial adsorption, and protein association, Biochim. Et Biophys. Acta (BBA) - Biomembr. 1798 (7) (2010) 1409–1417, https://doi.org/10.1016/j.bbamem.2009.12.006.
[50] X.-M. Li, M.M. Momsen, H.L. Brockman, R.E. Brown, Sterol structure and sphingomyelin acyl chain length modulate lateral packing elasticity and detergent solubility in model membranes, Biophys. J. 85 (6) (2003) 3788–3801.
[51] Y. Su, Q. Li, L. Chen, Z. Yu, Condensation effect of cholesterol, stigmasterol, and sitosterol on dipalmitoylphosphatidylcholine in molecular monolayers, Colloids Surf. A: Physicochem. Eng. Asp. 293 (1) (2007) 123–129, https://doi.org/10.1016/j.colsurfa.2006.07.016.
[52] K. Balashev, T.R. Jensen, K. Kjaer, T. Bjørnholm, Novel methods for studying lipids and lipases and their mutual interaction at interfaces. Part I. Atomic force microscopy, Biochimie 83 (5) (2001) 387–397, https://doi.org/10.1016/S0300-9084(01)01264-0.
[53] G. Brezesinski, H. Möhwald, Langmuir monolayers to study interactions at model membrane surfaces, Adv. Colloid Interface Sci. 100–102 (2003) 563–584, https://doi.org/10.1016/S0001-8686(02)00071-4.
[54] L.K. Nielsen, K. Balashev, T.H. Callisen, T. Bjørnholm, Influence of product phase separation on phospholipase A(2) hydrolysis of supported phospholipid bilayers studied by force microscopy, Biophys. J. 83 (5) (2002) 2617–2624.
[55] J. Kergomard, F. Carrière, N. Barouh, P. Villeneuve, V. Vié, C. Bourlieu, Digestibility and oxidative stability of plant lipid assemblies: an underexplored source of potentially bioactive surfactants? Crit. Rev. Food Sci. Nutr. (2021) 1–20, https://doi.org/10.1080/10408398.2021.2005532.
[56] D.-S. Lee, B.-S. Noh, S.-Y. Bae, K. Kim, Characterization of fatty acids composition in vegetable oils by gas chromatography and chemometrics, Anal. Chim. Acta 358 (2) (1998) 163–175, https://doi.org/10.1016/S0003-2670(97)00574-6.
[57] M. Venkatachalam, S.K. Sathe, Chemical composition of selected edible nut seeds, J. Agric. Food Chem. 54 (13) (2006) 4705–4714, https://doi.org/10.1021/jf0606959.
[58] S. Mongrand, T. Stanislas, E.M.F. Bayer, J. Lherminier, F. Simon-Plas, Membrane rafts in plant cells, Trends Plant Sci. 15 (12) (2010) 656–663, https://doi.org/10.1016/j.tplants.2010.09.003.
[59] R.A. Bhat, R. Panstruga, Lipid rafts in plants, Planta 223 (1) (2005) 5, https://doi.org/10.1007/s00425-005-0096-9.
[60] J.F. Hancock, Lipid rafts: contentious only from simplistic standpoints, Nat. Rev. Mol. Cell Biol. 7 (6) (2006) 456–462, https://doi.org/10.1038/nrm1925.
[61] K. Jacobson, O.G. Mouritsen, R.G.W. Anderson, Lipid rafts: at a crossroad between cell biology and physics, Nat. Cell Biol. 9 (1) (2007) 7–14, https://doi.org/10.1038/ncb0107-7.
[62] S. Munro, Lipid rafts: elusive or illusive? Cell 115 (4) (2003) 377–388, https://doi.org/10.1016/S0092-8674(03)00882-1.

Interfacial adsorption and activity of pancreatic lipase-related protein 2 onto heterogeneous plant lipid model membrane

Jeanne Kergomard, Frédéric Carrière, Gilles Paboeuf, Lauriane Chonchon, Nathalie Barouh, Véronique Vié, Claire Bourlieu

PII: S0300-9084(23)00078-0

DOI: https://doi.org/10.1016/j.biochi.2023.04.001

Reference: BIOCHI 6496

To appear in: *Biochimie*

Received Date: 20 December 2022

Revised Date: 24 March 2023

Accepted Date: 4 April 2023

Please cite this article as: J. Kergomard, Fréé. Carrière, G. Paboeuf, L. Chonchon, N. Barouh, Vé. Vié, C. Bourlieu, Interfacial adsorption and activity of pancreatic lipase-related protein 2 onto heterogeneous plant lipid model membrane, *Biochimie* (2023), doi: https://doi.org/10.1016/j.biochi.2023.04.001.

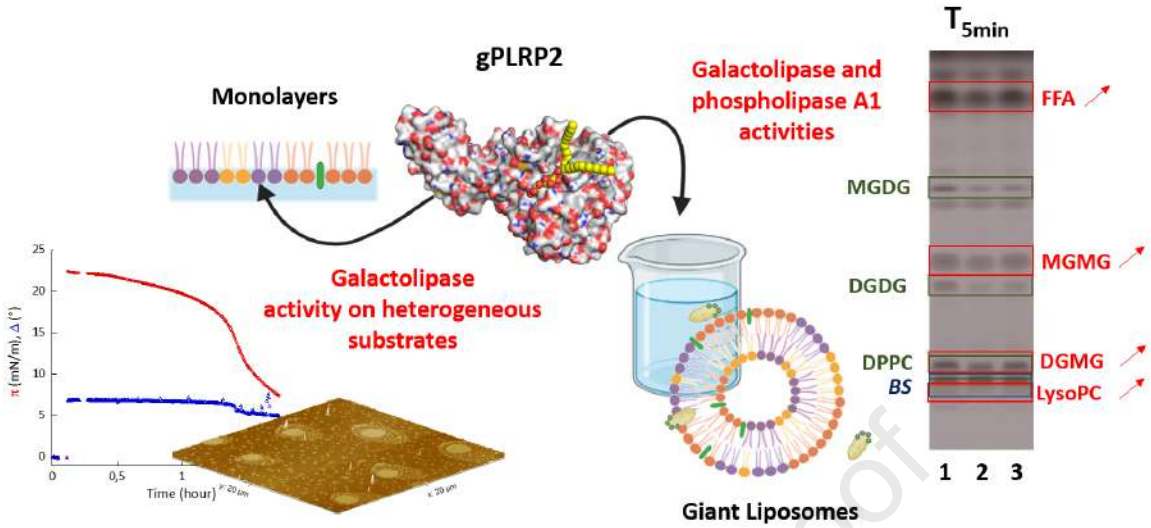

Title: Interfacial adsorption and activity of pancreatic lipase-related protein 2 onto heterogeneous plant lipid model membrane

Name(s) of Author(s) Jeanne Kergomard[1,2], Frédéric Carrière[3], Gilles Paboeuf[1], Lauriane Chonchon[1], Nathalie Barouh[4,5], Véronique Vié[1*] & Claire Bourlieu[2**]

Author Affiliation(s) [1]IPR Institute of Physics, Rennes 1 University, France; [2]INRAE/UM/Institut Agro Montpellier UMR 1208 IATE, France; [3]Aix-Marseille Université, CNRS, UMR7281 Bioénergétique et Ingénierie des Protéines, Marseille, France ; [4]CIRAD, UMR QUALISUD, F34398 Montpellier-France, [5]Qualisud, Univ Montpellier, Avignon Université, CIRAD, Institut Agro, Université de La Réunion, Montpellier, France.

C**orresponding authors:**

***Dr. Véronique Vié, Institut de Physique de Rennes, Campus de Beaulieu, UMR UR1 CNRS 6251, Université de Rennes 1, 35042 Rennes cedex,** phone number: 33 (0)2 23 23 56 45 and E-mail address : veronique.vie@univ-rennes1.fr;

****Dr. C. Bourlieu-Lacanal, UMR 1208 IATE, 2 Place Pierre Viala, Bât. 31, INRAE/UM/Institut Agro Montpellier, F34060 MONTPELLIER CEDEX 1**, France, phone number: 33 (0)4 99 61 22 03 and E-mail address : claire.bourlieu-lacanal@inrae.fr

Word count: 7018

Total number of tables/figures: 9

Abbreviations

DGDG: digalactosyldiacylglycerol

DGG: digalactosylglycerol

DGMG: digalactosylmonoacylglycerol

DLS: dynamic light scattering

FFA: free fatty acids

GL: galactolipids (model system)

gPLRP2: guinea pig protein lipase related-protein 2

hPLRP2: human protein lipase related-protein 2

MGDG: monogalactosyldiacylglycerol

MGG: monogalactosylglycerol

MGMG: monogalactosylmonoacylglycerol

PL: phospholipids

PLRP2: protein lipase related-protein 2

PUFA: polyunsaturated fatty acids

pS: phytosterols

ABSTRACT

Pancreatic lipase related-protein 2 (PLRP2) exhibits remarkable galactolipase and phospholipase A1 activities, which depend greatly on the supramolecular organization of the substrates and the presence of surfactant molecules such as bile salts. The objective of the study was to understand the modulation of the adsorption mechanisms and enzymatic activity of Guinea pig PLRP2 (gPLRP2), by the physical environment of the enzyme and the physical state of its substrate. Langmuir monolayers were used to reproduce homogeneous and heterogeneous photosynthetic model membranes containing galactolipids (GL), and/or phospholipids (PL), and/or phytosterols (pS), presenting uncharged or charged interfaces. The same lipid mixtures were also used to form micrometric liposomes, and their gPLRP2 catalyzed digestion kinetics were investigated in presence or in absence of bile salts (NaTDC) during static *in vitro*, so called "bulk", digestion.

The enzymatic activity of gPLRP2 onto the galactolipid-based monolayers was characterized with an optimum activity at 15 mN/m, in the absence of bile salts. gPLRP2 showed enhanced adsorption onto biomimetic model monolayer containing negatively charged lipids. However, the compositional complexity in the heterogeneous uncharged model systems induced a lag phase before the initiation of lipolysis. In bulk, no enzymatic activity could be demonstrated on GL-based liposomes in the absence of bile salts, probably due to the high lateral pressure of the lipid bilayers. In the presence of NaTDC (4 mM), however, gPLRP2 showed both high galactolipase and moderate phospholipase A1 activities on liposomes, probably due to a decrease in packing and lateral pressure upon NaTDC adsorption, and subsequent disruption of liposomes.

KEYWORDS: pancreatic lipase related-protein 2, heterogeneous monolayers, galactolipids, monolayer, liposomes

1 INTRODUCTION

Galactolipids (GL) are the main lipids found in the photosynthetic membrane of plants and algae, accounting for more than 70% wt. of the total membrane lipids [1–3]. Due to the natural abundance of plants and algae on Earth, GL represent the most important class of lipids, and therefore, the most important reservoir of fatty acids (80% versus 20% wt. for plant phospholipids (PL) and TAG), including some essential polyunsaturated fatty acids (PUFA) (Gounaris & Barber, 1983). The two main GL composing the photosynthetic membranes of plants are the neutral monogalactosyldiacylglycerol (MGDG, 53% wt.) and digalactosyldiacylglycerol (DGDG, 27% wt.). MGDG possess a unique small 1-β-galactose polar head bound at the *sn-3* position to a diacylglycerol [4], whereas DGDG has a larger polar head with an additional α-galactose, linked to β-galactose [5]. Both galactolipids possess two esterified acyl chains of fatty acids at the *sn*-1 and *sn*-2 position of the glycerol backbone, whose nature depends mainly on the synthesis pathway of GL [6,7]. In addition to these two glycolipids, photosynthetic plant membranes contain smaller amounts of charges lipids, sulfoquinovosyldiacylglycerol (SQDG) and phosphatidylglycerol (PG), the proportions of which vary between photosynthetic plant species. GL are naturally rich in the essential α-linolenic acid (ALA, C18:3 ω3), which is the precursor of longer chain ω3 fatty acids, the eicosapentaenoic acid (EPA, C20:5, ω3), and the docosahexaenoic acid (DHA, C22:6 ω3), resulting from elongation and desaturation reactions [8]. In particular, these two long-chain PUFA play a crucial role in the homeostatic regulation of the human body by being the precursors of signaling oxygenated lipids involved in inflammation resolution processes in our body [9]. GL also contain a significant amount of hexadecatrienoic acid (HTA, C16:3 ω3), an unusual fatty acid found mainly in green plants and algae. The nutritional benefits of HTA have been scarcely studied, although it represents a unique biomarker of the digestion, absorption, and accretion of GL

FA. Indeed, it has been found in tissues of zebrafish fed with chloroplast-rich fractions [10], as well as in the meat of horses [11], and has been identified as a potential precursor of ALA in rodents [12]. The interesting nutritional profile of GL makes them compounds of interest for the development of food products rich in ω3 PUFA. Nevertheless, in order to exploit the nutritional properties of GL in potential food applications, it is necessary to determine their digestibility by humans.

Regarding this digestibility, human pancreatic juice and duodenal contents have been shown to exhibit galactolipase activity [13]. This activity was associated to PLRP2 [14], as well as, to a lesser extent, to the bile salt-simulated lipase/carboxyl ester hydrolase (BSSL/CEH) [15,16]. PLRP2 shows enzymatic activity on polar lipid substrates with larger heads in comparison with other classical pancreatic lipases such as HPL. Indeed, in addition to limited lipase activity (1250 *versus* 8500 U/mg for HPL on tributyrin), PLRP2 exhibits limited phospholipase A1 (74 U/mg on purified L-α-PC) and high galactolipase (~2800 U/mg on MGDG for instance) activities [7,17–19]. This enzymatic activity on a wider range of substrates than HPL is explained by the unusual conformation of the lid controlling the access to the active site of hPLRP2 [20]. PLRP2 is also present in the digestive system of other species, and in particular in monogastric herbivores such as the guinea pig (gPLRP2), whose diet contains significant amounts of GL. Although the galactolipase activity of PLRP2 has been the subject of numerous studies, they were mainly focused on the identification and quantification of enzyme activity on synthetic (medium chain acyl GL) or natural substrates most of the time presented in the form of micelles with bile salts. In these studies, little attention was given to the local physical state, whether regarding the level of condensation, nor the presence of charged molecules. PLRP2 was also found to be active on monolayers of pure PL and GL, with an optimum activity at surface pressures below the lateral

surface pressure of membranes, *i.e.* 10-15 mN/m [21–23]. These findings, together with the absence of interaction and activity of PLRP2 on PL liposomes [24], suggest that PLRP2 may not be able to act directly on plant membranes. In the present study, gPLRP2, whose biochemical properties are close to those of hPLRP2, was used as a model PLRP2. We proposed to investigate the adsorption mechanisms of PLRP2 on plant model and natural monolayers presenting homogeneous or heterogeneous physical states at the air/water interface, as well as on GL liposomes in static dispersed condition, hereafter called "bulk", in the absence and presence of bile salts (NaTDC, 4 mM). Indeed, bile salts are biosurfactants that are secreted by the liver, and which play key contrasting roles in lipid digestion: they adsorb onto interfaces where they can compete with lipases and inhibit lipolysis [25,26], but they also remove lipolysis products from the interface, solubilizing them into micelles [27]. More importantly, they form mixed micelles with polar lipids, *i.e.* PL and GL, that are the preferred substrates for pancreatic phospholipase A2 [28] and PLRP2 [24,29], respectively.

We studied the organizational properties and enzymatic activity of gPLRP2 on different GL substrates, controlling finely their physical state, *i.e.* on systems with or without phase heterogeneities. The adsorption and enzymatic hydrolysis capacity of gPLRP2 were first tested on homogeneous and heterogeneous monolayers of GL, PL, and pS (GL and GL/DPPC/pS monolayers), as well as on more biomimetic system (MGDG/DGDG/SQDG/PG monolayer), in order to gain a mechanistic understanding of the digestion mechanisms at the lipid interface molecular level (nm). These three lipid mixtures were then formulated into liposomes and incubated in the presence of gPLRP2 to determine if galactolipase and/or phospholipase A1 activities were displayed on these dispersed micronic objects (µm) either in the absence or presence of bile salts (NaTDC).

2 EXPERIMENTAL SECTION

Chloroform, methanol, SQDG, and PG were purchased from Sigma Aldrich Ltd. (St. Louis, MO). *1,2*-dipalmitoylphosphatidylcholine (DPPC), MGDG and DGDG were purchased from Avanti Polar Lipids. Canola pS, composed of a mixture of β-sitosterol (50 mol%), campesterol (40 mol%) and brassicasterol (10 mol%), were kindly donated by Cognis France (Estarac, France). pS were collected from desodorization distillates of canola oil. If not stated otherwise, all biophysical characterizations were conducted at least in triplicate.

2.1 Preparation of lipid mixtures

Binary mixture of natural long chains MGDG and DGDG (60:40, mol/mol) was prepared, namely (1) GL. Heterogeneous mixture of GL, DPPC and pS, namely (2) GL/DPPC/pS (45:45:10, mol/mol/mol), respectively was also prepared both to simplify the composition of natural plant membrane, and to provide a pronounced phase coexistence. A biomimetic model system was also prepared, reproducing more accurately the composition of plant photosynthetic membranes, by the addition of charged polar lipids, SQDG (predominant species C18:3/C16:0) and PG, and hereafter called (3) MGDG/DGDG/SQDG/PG (56:24:10:10, mol/mol/mol/mol). Relative compositions of the model systems and fatty acid repartitions of MGDG and DGDG used in this study are given in Table S1 and Figure S2, respectively.

2.2 Enzyme purification and preparation of aliquots

Recombinant guinea pig pancreatic lipase-related protein 2 (gPLRP2) and its inactive variant gPLRP2 S125G were produced in *Aspergillus orizae* and *Pichia pastoris*, respectively, and purified as described in Hjorth et al. (1993) and Mateos-Diaz et al. (2018). For the interfacial measurements, a gPLRP2 stock solution (0.15 mg/mL) was prepared in a Tris HCl buffer (10 mM Tris, 100 mM

NaCl, 5 mM $CaCl_2$, pH 7) and aliquots were prepared in the same buffer at a final concentration of 0.128 mg/L (2.7 nM). This value is closed to the physiological concentrations divided by 100 and corresponds to the usual value used in interfacial studies to avoid saturating the interface with digestive proteins. The inactive gPLRP2 S125G variant was used as a control of the protein effect on lipids in the absence of any enzyme activity as previously shown with phospholipids (Mateos-Diaz et al., 2018). For digestion experiments in static conditions, 100 µL aliquots were prepared at a final concentration of 3.3 mg/L.

2.3 Ellipsometry and surface pressure measurements at the air/water interface

Kinetic measurements were performed over 2 hours using a computer controlled and user-programmable LB Teflon Langmuir trough (KSV Nima, Helsinki, Finland) with a surface area of 35 cm^2 controlled by two mobile barriers. The Teflon trough has been carefully cleaned with UP water and ethanol before each experiment, and ellipsometric and tensiometric measurements were performed during half an hour on pH 7 buffer to check the cleaned surface.

The surface pressure (π) was measured every 4s with a precision of ± 0.2 mN/m using a filter paper connected to a microelectronic feedback system (Nima Technology, UK), according to the Wilhelmy-plate method. The ellipsometric angle (Δ) was recorded simultaneously every 4 s with a precision of ± 0.5°, using a home-made automated ellipsometer in a "null ellipsometer" configuration [30,31]. The laser beam probed a surface of 1 mm^2 and a depth in the order of 1 µm and provided insight on the thickness of the interfacial film formed at the interface.

2.4 Monitoring of the gPLRP2 adsorption onto mixed galactolipid monolayers at the air/water interface

The three monolayers studied were formed by spreading a few microliters of 1 mM solution of lipids in $CHCl_3$/MeOH (2:1, v/v) over the surface of the buffer solution until an initial pressure of 20 ± 1 mN/m [32].

After stabilization of the film over 5 minutes, 14.6 µL of gPLRP2 solution (0.15 mg/mL) was diluted with 30 µL Tris buffer and injected in the sub-phase to achieve a final gPLRP2 concentration of 2.7 nM. The evolution of the surface pressure and ellipsometric angle due to the enzyme adsorption and lipolytic activity onto the lipid monolayer was continuously monitored over 45 minutes to 2 hours depending on the system studied, until a final surface pressure of 6 mN/m was reached, this value being the one of the gel-fluid phase transition of DPPC [33].

2.5 Analysis of the digestion products present at the interface and in the sub-phase

The interface of the GL monolayer was collected after 1h digestion kinetic, using a home-made vacuum extraction pump system. Lipids were extracted by Folch method before being analyzed by thin layer chromatography (TLC) to determine the concentrations of lipolysis products. The organic phase resulting from the extraction was separated and eluted on TLC plates using a mixture of chloroform/methanol/water (95:20:2.5, v/v/v). The TLC plate revelation was made by dipping the plate in a 50:50 v/v mixture of saturated copper acetate solution in water and 85.5% phosphoric acid solution and subsequent oven drying (180°C, 10min). Revealed bands were then scanned by densitometry (500 nm, TLC Scanner 4, CAMAG) and quantified using VisionCat software.

2.6 Visualization of lipase distribution in heterogeneous film by atomic force microscopy

For AFM imaging, interfacial films were transferred onto a freshly-cleaved mica plate using the Langmuir-Blodgett method at the end of the kinetics, at a constant surface pressure and at a very low speed (0.5 mm/min). For each monolayer, two sampling were performed at different times, in

order to observe the organization of the interface at different stages of lipase adsorption and lipolysis. For the GL monolayer, sampling was performed at 35 minutes and 1 hour, respectively. For the GL/DPPC monolayer, sampling was carried out at 45 minutes and 1 hour and 15 minutes, respectively. For the GL/DPPC/pS monolayer, sampling was done at 45 minutes and 1 hour 45 minutes, respectively. Finally, for the MGDG/DGDG/SQDG/PG, sampling was carried out after 1 hour kinetic. AFM (Multimode Nanoscope 8, Bruker, France) was used for imaging in contact mode QNM in air (20°C), using a standard silicon cantilevers (0.06 N/m, SNL-10, Bruker, France), and at a scan rate of 1 Hz. The force was minimized during all scans and the scanner size was 100×100 µm². The processed images analyzed by the open-source platform Gwyddion were representative of at least duplicated experiments.

2.7 Static digestion of liposomes made from mixed GL, GL/DPPS/pS, and MGDG/DGDG/SQDG/pS systems by gPLRP2

1 µm extruded liposomes of i) GL, ii) GL/DPPC/pS, and iii) MGDG/DGDG/SQDG/PG model solutions, respectively, were prepared at a final concentration of 0.4% wt. in Tris HCl buffer (10 mM Tris, 100 mM NaCl, 5 mM $CaCl_2$, pH 7).

2.6.1 Size distribution of liposomes by dynamic light scattering

The size (diameter, nm) distribution of liposomes was assessed by dynamic light scattering (DLS) with a Malvern Panalytical Zetasizer PRO (Malvern, Worcestershire, United Kingdom) fitted with a 633-nm He-Ne laser at 25 °C. ZS Explorer Software version 3.1.0. (Malvern) was used to collect and analyze the data. Measurement were conducted on 1 mL of liposomes dispersion (after 10 times dilution in mQ water) with equilibration time of 120 s, 10 runs of 120 s measurements were performed with a refractive index of 1.45 for liposomes, respectively. The

intensity, diameter distribution, the hydrodynamic diameter as Z-average, and the polydispersity index (PdI) were deduced from the autocorrelation fit of the data.

2.6.2 Static bulk digestion of liposomes by gPLRP2 in absence and in presence of 4 mM NaTDC

Liposomes were incubated under constant agitation in Tris HCl buffer (10 mM Tris, 100 mM NaCl, 5 mM $CaCl_2$, pH 7) containing gPLRP2 at 3.3 mg/L in absence or in presence of 4 mM NaTDC (above CMC value). 100 µL aliquots were sampled at T_0 (control) and after 5 min of gPLRP2 digestion (T_{5min}), and lipids were extracted by Folch method before being analyzed by thin layer chromatography (TLC) to determine the concentrations of residual substrates and lipolysis products. The organic phase resulting from the extraction was separated and eluted on TLC plates as detailed in section 2.5 above. It was thus possible to monitor the enzymatic activity of gPLRP2 on liposomes of both galactolipid mixtures in absence or presence of bile salt-related detergent (NaTDC, 4 mM).

3 RESULTS AND DISCUSSION

3.1. Interfacial behavior of model lipid monolayers

Lipid-lipid interactions and molecular organization at the air/water interface were investigated at 20 mN/m and pH 7 and are presented in Figure 1. We were able to form stable GL based-monolayers at the air/water interface. The GL interface was characterized by a fluid phase, presenting some roughness due to the intercalation of the polar heads of MGDG and DGDG (Figure 1.A). The GL/DPPC/pS system showed a coexistence of condensed liquid/expanded liquid phases, with the presence of condensed phase domains visible on the AFM images, enriched in DPPC-MGDG and pS (Figure 1.B). Additionally, the presence of pS in condensed domains have induced the appearance of defects, that could modulate the subsequent adsorption of lipolytic enzymes [34,35]. For the MGDG/DGDG/SQDG/PG biomimetic monolayer (Figure 1.C), small flower-shaped nanodomains of 1.6 ± 0.1 nm height were evidenced at the air/water interface, coexisting with a fluid phase.

3.2. Interfacial adsorption and enzymatic activity of gPLRP2 onto homogeneous galactolipid monolayer (GL)

The interfacial adsorption and enzymatic activity of gPLRP2 onto homogeneous GL monolayer GL was monitored using tensiometry coupled with ellipsometric measurements. Figure 2.A shows the evolution of surface pressure and ellipsometric angle over one hour after the injection of gPLRP2 at 0.128 mg/L in the subphase. Right after the injection of the enzyme below the GL monolayer, the surface pressure started to decrease drastically, reporting the modifications of the interactions between molecules at the interface and the probable lipolysis of the acyl chains of galactolipids by gPLRP2. When considering the maximal slope of this decreasing curve, it

coincided with a range of surface pressure from 15 to 10 mN/m, *i.e.* a surface pressure where the enzymatic activity of gPLRP2 was the highest. This assumption was consistent with the evolution of the ellipsometric angle, as a sharp drop of $\delta\Delta$=0.8 was obtained at π=15 mN/m (Figure 2.A). Since the activity of gPLRP2 on medium chain MGDG and DGDG monolayer was previously reported to be maximum between 10 to 15 mN/m [18,21], it is hypothesized that the changes occurring at the interface (π and Δ) results from gPLRP2 activity on the GL monolayer. Given the fact that the surface pressure did not show a significant increase after gPLRP2 injection, contrary to what had been previously observed with other lipases onto heterogeneous monolayers [34], it is hypothesized that most gPLRP2 molecules are found right below the surface and do not penetrate into the monolayer. This assumption was consistent with the ellipsometric angle data: no evolution was observed during the first 0.6 hour of kinetic after the lipase injection in the subphase. These data suggest that gPLRP2 adsorption below the surface is quite discrete and limited in comparison to gastric lipase for instance [34].

In order to understand the partitioning of the enzyme and the disorganization of the interface induced by the enzymatic activity, two Langmuir-Blodgett sampling of the interface were realized; before and after the drop of the ellipsometric angle. The 5×5 µm² AFM images of the two samples, after 35 min and 1 hour kinetic, respectively, are presented in Figure 2.B. After 35 min of enzymatic kinetic, small flower-like condensed phase domains of 1.9 ± 0.1 nm height appeared at the air/water interface, presumably attributed to the generation of digestion products by the degradation of MGDG and DGDG by gPLRP2, in agreement with the subsequent decrease of the surface pressure. Protuberances of 3.6 ± 0.3 nm height were also visible, very likely being attributed to some lipase molecules adsorbed at the interface. Indeed, such height differences had previously been shown in the literature to be associated with the presence of self-organized proteins at the interface of a lipid

monolayer [36,37]. After 1 hour kinetic, the resulting interface had evolved further. Surprisingly, gPLRP2 seems to have formed a protein network of 3.4 ± 0.1 nm in height, in addition to the protuberances observed on the 35 min images, despite the absence of increase in the surface pressure. Additionally, condensed phase domains have grown, reinforcing the hypothesis of their attribution to the generation of lipolysis products.

Indeed, gPLRP2 is known to hydrolyze the *sn*-1 position of GL, according to the reaction scheme proposed in Figure 3, generating monogalactosylmonoacylglycerol (MGMG) and digalactosylmonoacylglycerol (DGMG) in the case of MGDG and DGDG, respectively, as well as free fatty acids (FFA) [29,38]. Due to their polyunsaturated content, it is likely that MGMG and DGMG molecules remained in the fluid phase at the air/water interface, and that the condensed phase domains were probably enriched in saturated fatty acids released by PLRP2. Further hydrolysis of MGMG and DGMG by gPLRP2 can also lead to the production of water-soluble galactosylated products: monogalactosylglycerol (MGG) and digalactosylglycerol (DGG) (Figure 3) [39]. The generation of MGG and DGG could explain the decrease in surface pressure after gPLRP2 injection, as well as the drop in the ellipsometric angle corresponding to a loss of matter at the air/water interface. Additionally, the reorganization of these lipolysis products at the interface and in the aqueous subphase may have resulted in the formation of structural defects, thereby promoting lipolysis. To support the hypothesis of a galactolipid degradation by gPLRP2, leading to the generation of digestion products, the interface and subphase were collected after 1h of kinetics, and the lipid products were analyzed by TLC. The results (supplementary data, Figure S3) indicated the presence of digestion products (FFA) at the interface and in the subphase, confirming the galactolipase activity of gPLRP2 on the GL model monolayer.

To check which part of the evolution of the surface pressure and the ellipsometric angle was resulting either from the galactolipase activity of gPLRP2, or from the interactions of the protein with the lipid monolayer, the experiment was reproduced using an inactive variant (S125G) of gPLRP2. In this variant, the catalytic serine S152 was replaced by a glycine, resulting in the loss of the enzymatic activity. The S125G variant of gPLRP2 has been previously characterized using Fourier transform infrared spectroscopy (FTIR) in the study of Mateos-Diaz et al. (2018), showing that the inactive variant retained his correct folding compared to active gPLRP2, and that its interfacial behavior should not be affected.

Figure 4.A. presents the kinetic evolution of the surface pressure and ellipsometric angle over 1 hour after the injection of the inactive variant of gPLRP2 into the subphase of the GL monolayer. After the S125G gPLRP2 injection in the subphase, there was no evolution in the surface pressure, nor in the ellipsometric angle, confirming that the variations previously observed with gPLRP2 (Figure 2.A) were due to enzymatic activity. Additionally, AFM image Figure 4.B showed the presence of the same protuberances observed with the active enzyme, with similar height of 3.8 ± 0.2 nm. Thus, it seems that, despite the lack of surface pressure increase, the enzyme gets adsorbed at the interface.

3.3. Modulation of the gPLRP2 adsorption and kinetic activity onto heterogeneous model monolayer of galactolipids, phospholipids and phytosterols (GL/DPPC/pS)

Figure 5.A shows the kinetic evolution of the surface pressure and ellipsometric angle after the injection of gPLRP2 below the GL/DPPC/pS monolayer. A decrease with time in the surface pressure similar to what was observed with the GL monolayer (Figure 2.A), was observed right after the injection of the enzyme in the subphase. However, the decrease in surface pressure was slower than with the GL monolayer. A drop in the ellipsometric angle ($\delta\Delta$=0.9°) was also observed

when the surface pressure reached 15 mN/m, but it occurred at 1.4 h instead of 0.6 h (35 min) with the GL monolayer, reflecting the slowing down of the lipolysis rate. As previously, we assumed that these variations correspond to a loss of matter at the interface, upon lipolysis of the monolayer by gPLRP2 and to the generation of water-soluble MGG and DGG. The lag phase of about 50 min observed with the GL/DPPC/pS monolayer before the initiation of lipolysis could be explained by the higher packing of the heterogeneous monolayer induced by DPPC and pS, and a greater difficulty for gPLRP2 to reach the acyl chains of hydrolysable substrates (galactolipids and DPPC). The previous characterization study of homogeneous and heterogeneous GL monolayers has indeed shown that the addition of DPPC and pS to a GL monolayer led to the formation of condensed phase domains enriched in DPPC and MGDG, reducing the lateral distance between the acyl chains available for gPLRP2 to insert [35]. This higher packing could thus explain the lag phase observed before the gPLRP2 could reach its optimum activity, a high packing density at the air/water interface having been proposed to explain the long induction times observed for other lipases onto tightly packed short-chained phospholipids [40] and diacylglycerols [41] monolayers. The initiation of lipolysis of the GL/DPPC/pS led however to the formation of lipolysis products and to the subsequent decrease in surface pressure and lipid packing, that accelerate the activity of gPLRP2.

Two Langmuir-Blodgett transfers of the monolayer were taken after 45 minutes and 1h45 of kinetics, respectively, and AFM images of the interfacial organization were recorded (Figure 5.B). After 45 minutes of kinetics, condensed domains of 1.5 ± 0.2 nm in height were visible at the air/water interface. Given the low drop in surface pressure observed at 45 min, these domains are probably not related to the generation of digestion products. Furthermore, the interfacial organization and heights observed were similar to those obtained at T_0 before the injection of

gPLRP2 into the subphase (Figure 1.B), supporting the hypothesis that lipolysis is probably not yet initiated at this stage of the kinetics. At 1h45 minutes of kinetics, the surface pressure had reached π=6.3 mN/m, and AFM images of the film interface revealed a very different interfacial organization, consistent with the evolution of surface pressure and the drop in the ellipsometric angle. Thin and discontinuous lines of h_1=3.1 ± 0.2 nm in height were visible in the fluid phase and around the condensed domains, that could correspond to gPLRP2 molecules adsorbed at the monolayer interface. Condensed domains of three different heights were also identified. First, small flower-like shaped condensed domains were visible in the fluid phase, with a height h_2 of 2.0 ± 0.1 nm, probably attributed to the generation of lipolysis product MGMG and DGMG, as observed for the GL monolayer. Fragmented condensed phase domains were also revealed, composed of at least three different height levels (h3, h4, fluid bottom). This observed fragmentation could be due to the disorganization caused by the adsorption and enzymatic activity of gPLRP2, but also to the low-pressure value (π=6.3 mN/m), causing phase segregation within the condensed phase domains thought to be enriched in DPPC-MGDG-pS. Indeed, the lateral pressure was probably no longer sufficient to ensure the miscibility of DPPC and pS with MGDG, causing phase segregation which could explains the observed height differences.

These observations nevertheless confirm the miscibility of these three compounds and the phase heterogeneity in the condensed phase domains at 20 mN/m , as well as the condensation effect of DPPC and pS on MGDG chains observed in our previous study [35]. Given the molar composition of the GL/DPPC/pS monolayer, the central rounded domain (h_3=1.7 ± 0.2) observed at 1h45 of kinetic could be attributed to the presence of condensed DPPC. The smaller domains of h_3 and h_4 heights, coexisting with the fluid phase, could be attributed to the presence of FFA and pS, coexisting with MGDG and MGMG in the fluid phase.

In the considered range of surface pressure, it is indeed unlikely that gPLRP2 shows significant enzymatic activity on DPPC, since monolayer studies have shown that gPLRP2 was only active on this substrate at low surface pressure ($\pi < 5$ mN/m) and was totally inactive at $\pi > 10$ mN/m [22]. However, it remains difficult to attribute each type of domain to a species of molecule, given the complex interactions and differences in miscibility observed in this type of ternary mixture. Surface composition studies will be needed to answer these questions, but the small quantities used for interfacial characterizations do not facilitate such analyses.

3.4. Influence of the presence of charged lipids on the adsorption capacity and enzymatic activity of gPLRP2 in model biomimetic lipid monolayer (MGDG/DGDG/SQDG/PG)

The impact of a charged interface on the adsorption capacities and enzymatic activity of gPLRP2 was studied using MGDG/DGDG/SQDG/PG biomimetic model monolayer. The evolution of surface pressure and ellipsometric angle upon the adsorption of gPLRP2 at the air/water interface is presented Figure 6.A. A continuous decrease of the surface pressure was observed right after the injection of gPLRP2 in the sub-phase until it reached a value of π=8.5 mN/m after 1h of kinetic. In contrast to the GL/DPPC/pS complex system, no lag phase was observed before the onset of lipolysis, and the decrease was continuous, revealing a constant enzymatic activity of gPLRP2 over the 1h kinetic. This observation could be explained by the presence of negatively charged lipids at the interface (SQDG, PG), which could facilitate the adsorption of gPLRP2 underneath the monolayer, and the subsequent degradation of galactolipids. The facilitated adsorption onto a charged surface was previously observed for recombinant dog gastric lipase (rDGL) at the level of heterogeneous monolayers of polar dairy lipids, with the establishment of electrostatic interactions between the interface and the interfacial recognition site facilitating the orientation and approach of the active site onto the lipid substrates [34]. In our case however the surface potential

electrostatic distribution of charge is very different between rDGL and gPLRP2, but seems to result in favorable interactions with negatively charged lipid interface. The ellipsometric angle did not significantly evolved during the first 30 minutes of the kinetics. After this, it decreased again ($\delta\Delta$=-0.7°) at π=15 mN/m, in the range of the optimal surface pressure for the activity of gPLRP2, as previously observed on GL and GL/DPPC/pS monolayers. The ellipsometric angle then slowly decreased until it reached a value of Δ=5.2° after 1h kinetic, reflecting a decrease in the thickness of the monolayer due to the degradation of GL and the progressive release of polar lipolysis products into the subphase.

Langmuir-Blodgett transfer of the interface was performed on the MGDG/DGDG/SQDG/PG monolayer after 1 kinetic. AFM image (Figure 6.B) after 1h kinetic of incubation with gPLRP2 showed the coexistence of LC snowflake-shape domains of 2.2 ± 0.1 in height in the fluid phase. These domains shared a similar morphology with those obtained after 35 minutes of digestion of the GL monolayer by gPLRP2, and can therefore be attributed to the generation of FFA digestion products by galactolipid degradation. As previously observed, small protuberances of 3.3 ± 0.3 nm in height were also observed, attributed to the adsorbed gPLRP2 molecules in the fluid phase.

3.5. Interaction of liposomal structures (GL, GL/DPPC/pS, MGDG/DGDG/SQDG/PG) with bile salts

Since the interfacial characterization of gPLRP2 interaction with mixed galactolipid monolayer revealed some lipolytic activity, we then evaluate the ability of gPLRP2 to interact with liposomes made with the same lipid mixture, in the presence and absence of bile salts, to mimic the conditions found in the gastrointestinal tract. We first characterized the effects of bile salts on the liposomal dispersions using DLS.

In the absence of bile salts, GL liposomes showed a monomodal distribution centered at 198 nm while GL/DPPC/pS liposomes were much larger with a monomodal distribution centered at 2990 nm (Figure 7), although both objects had been extruded 10 times over filters of 1 µm pore diameter. Upon the addition of NaTDC (4 mM), bimodal distributions appeared with peaks at 894 and 117 nm for GL liposomes and at 2990 and 146 nm for GL/DPPC/pS. The presence of NaTDC had therefore a strong impact on lipid organization with changes in particle size distribution, a major shift towards larger objects but also the appearance of smaller populations. Ultimately, GL and PL mixed with micellar concentrations of bile salts are known to form mixed micelles with diameter of 10 to 40 nm [42]. In that case, DLS is not the most appropriate techniques for covering such large variations in particle size distribution with smaller particles. Nevertheless, it allowed showing lipid re-organization upon the addition of bile salts. The size increase observed with the larger objects could be partially explained by a destabilization of the liposomes during the adsorption of NaTDC at the interface, leading to their fusion. Additionally, the adsorption of NaTDC onto liposomes could have resulted in a diminished GL packing, explaining the larger diameter observed. The smallest objects observed could be related to the desorption of some lipid molecules from the bilayer stabilizing the liposomes. Indeed, previous studies had already investigated the interfacial behavior of NaTDC at the level of assembled lipid structures, and have highlighted its desorption capacities. As an example, Pabois et al. (2019) have studied the adsorption behavior of NaTDC at the air/water interface, and its interaction with a monolayer of phospholipids (DPPC), mimicking the organization of physiological compounds present at the interface of fat droplets. Firstly, the results showed a very fast adsorption of NaTDC at the air/water interface at low concentration (< 1 mM), forming stable but irregular film, which was attributed to its unusual polar planar structure and large surface area [44,45]. However, these bile salt concentrations were below the critical micellar concentration (CMC) [46]. At higher concentrations (> 5 mM; *i.e.* > CMC),

437 the addition of bile salts was shown to lead to a decrease in thickness, demonstrating that NaTDC
438 partially desorbs from the interface. The interaction of NaTDC with the DPPC was then studied.
439 Results showed the strong desorption of DPPC molecules (to approximately 40%) from the
440 interface upon the NaTDC adsorption, resulting in the formation of domains with distinct
441 organization. Additionally, increasing the amount of NaTDC have been shown to decrease the
442 DPPC monolayer packing. These results illustrate the well-known micellar solubilization effect of
443 bile salts, leading to the formation of mixed micelles in bulk [27,47,48].

444 In the case of the GL/DPPC/pS liposomes in the absence of bile salts, they showed an average
445 diameter of 2990 nm that was much larger than the average diameter measured in the case of the
446 GL system (198 nm). The fact that their diameter was larger than 1 µm despite the filter used during
447 extrusion indicates that these objects were relatively stable, as they were able to deform during
448 extrusion without breaking. The appearance of a population of smaller objects upon addition of
449 NaTDC could reflect the re-organization induced by NaTDC molecules. Nevertheless, it seems
450 that the GL/DPPC/pS system remains stable even in the presence of bile salts, as the population of
451 larger droplets remained similar in size in the absence and presence of bile salts

452 **3.6. Interaction of gPLRP2 with galactolipid-based liposomes in the absence and presence of**
453 **bile salts**

454 As the adsorption capacities and enzymatic activity of gPLRP2 is highly dependent on the substrate
455 organization [24,49], the changes observed with liposomes following the addition of bile salts
456 could most likely modify the access of the enzyme to its substrate and its lipolytic activity.

457 The impact of bile salt on the galactolipase and phospholipase A1 activities of gPLRP2 was thus
458 assayed in “bulk conditions” using GL/DPPC/pS dispersed liposomes, this system having been

459 shown to be the most stable even in presence of bile salts. No significant hydrolysis activity on
460 GL/DPPC/pS liposomes could be detected in the absence of bile salts after 5 minutes of incubation
461 with gPLRP2 (supplementary material, Table S4). This result was in line with the previous study
462 by Mateos-Diaz et al. (2018), which has shown that gPLRP2 did not possess enzymatic activity on
463 DPPC liposomes in absence of bile salts. These results were however in disagreement with the
464 results obtained with monolayers of the same lipid mixture, on which the lipolytic activity of
465 gPLRP2 was detected (see figure 2 presented in section 3.3 - monolayer results). Nevertheless, the
466 surface pressure of the lipid monolayer at the air/water interface was optimum for the adsorption
467 and enzymatic activity of gPLRP2, which may explain the observed lipolysis under these
468 conditions. The organization of lipids into monolayers is indeed different from that of the bilayers
469 surrounding liposomes, and higher lateral pressure and packing of the latter systems could prevent
470 gPLRP2 from penetrating and degrading its substrate [35].

471 However, when bile salts were added to GL/DPPC/pS liposomes, a lipolytic activity of gPLRP2
472 could be detected by TLC analysis of lipolysis products (Table 1). After 5-min incubation, around
473 74% wt. of MGDG and 55% wt. of DGDG were converted into MGMG and DGMG, respectively,
474 with the production of FFA. Given the differences in the substrate and lipolysis product
475 concentrations, it is likely that some MGMG and DGMG have been in turn converted into
476 monogalactosylglycerol (MGG) and digalactosylglycerol (DGG), respectively, by gPLRP2 but
477 these two compounds being water-soluble, they could not be extracted and revealed upon TLC
478 analysis of the organic phase [50]. It should be noted that the quantification of DGMG after 5
479 minutes digestion was hampered, given the fact that its retention factor was similar to that of DPPC
480 on the TLC plate. The galactolipase activity observed in the presence of bile salts could be due to
481 the adsorption of NaTDC at the liposome interface, decreasing the lateral pressure and interfacial

packing of polar lipids, as previously observed with DPPC domains (Pabois et al. 2019), and thus creating more favorable conditions for the adsorption and activity of gPLRP2. Nevertheless, it cannot be excluded that polar lipids from liposomes were gradually solubilized into mixed micelles prior to their hydrolysis by gPLRP2. This latter hypothesis is supported by the preference of gPLRP2 for micellar substrates [24]. Moreover, the difficulty for gPLRP2 to access it substrate in liposomes was confirmed here when GL/DPPC/pS liposomes were tested in the absence of bile salts.

In addition to the galactolipase activity of gPLRP2, the TLC analysis of lipolysis products also revealed the phospholipase activity of gPLRP2 on the DPPC present in GL/DPPC/pS liposomes, in the presence of bile salts. These results confirm the previous study by Mateos-Diaz et al. (2018) which has shown that gPLRP2 was active on mixed bile salts/DPPC micelles, but not on DPPC liposomes in the absence of bile salts. As in the case of galactolipid hydrolysis, two main hypotheses can be raised about the mode of action of gPLRP2 on PL: a decrease in the packing of the bilayer by bile salts that could promote gPLRP2 adsorption and activity, or the conversion of liposomes into micelles containing DPPC.

Given the lack of activity of gPLRP2 on GL-based liposomes in the absence of bile salts, mixed MGDG/DGDG/SQDG/PG liposomes mimicking the lipid composition of thylakoid membranes were also tested in presence of bile salts. After 5 minutes incubation with gPLRP2 in presence of 4 mM NaTDC (Table 1), about 90% wt. of MGDG and 94% wt. of DGDG were hydrolyzed, while FFA and MGDG were produced. More interestingly, gPLRP2 was also able to hydrolyze 91% of the initial SQDG substrate (Table 1), emphasizing its action on all galactolipids [14]. This result confirmed the ability of gPLRP2 to hydrolyze GL from liposomes in the presence of bile salts.

The ability of gPLRP2 to hydrolyze galactolipid membranes even in the absence of bile salts was however recently shown by FTIR on natural chloroplast membranes [51]. This result could be explained by the fact that these natural systems are more complex than the model systems considered in this study, and naturally include negatively charged lipids, shown to enhance the adsorption and extent of lipolysis on model monolayers, independently of the presence of bile salts. Thus, pursuing this study by exploring the degradation of liposomes with more complex compositions in the absence of bile salts, for example MGDG/DGDG/SQDG/PG, could provide insight into the composition at which a galactolipid liposome can become a gPLRP2 substrate.

3.7. Interfacial organization of GL and GL/DPPC/pS liposomes in presence of bile salts obtained at T_0 and after 5 min of gPLRP2 digestion

Lipids products obtained at T_0 and after 5 minutes incubation of GL or GL/DPPC/pS liposomes in the presence of gPLRP2 and bile salts were extracted by Folch method and deposited at the air/water interface at π=7.2 ± 0.1 mN/m. We chose to deposit the lipids at this surface pressure in order to approximate the organization of the substrates and digestion products of the interfacial films obtained at the end of the monolayer digestion kinetics for the GL, GL/DPPC/pS, and MGDG/DGDG/SQDG/PG systems, respectively (π between 5 to 8 mN/m). After stabilization of the respective T_0 and T_{5min} films, Langmuir-Blodgett samples were observed in AFM. For both systems, the images obtained at T_0 and T_{5min} are displayed in Figure 8. For the GL system, AFM images obtained at T_0 revealed the presence of small condensed domains of h_1=1.3 ± 0.1 nm height, that could be attributed to the presence of some NaTDC adsorbed at the air/water interface. At T_{5min}, flower-shape domains of $h_{1'}$=1.9 ± 0.1 nm in height were evidenced, similar to those obtained after 2h hour kinetic digestion of GL monolayer by gPLRP2 at the air/water interface. These

domains were attributed to the generation of the FFA by lipolysis of MGDG and DGDG, in agreement with their detection by TLC (Table 1).

For the GL/DPPC/pS system, the interface obtained at T_0 was clearly different from the one obtained for the GL/DPPC/pS monolayer at 20 mN/m during the interfacial study (section 3.1), but was similar to the one obtained two hours after injecting gPLRP2 in the subphase, when the surface pressure reached π=6.3 mN/m (Figure 2B). Thus, the low surface pressure could explain the fragmentation of the condensed phase domains, as previously observed, with two identified height levels (h1 and h2) probably enriched in DPPC and pS, coexisting with a fluid phase probably enriched in MGDG. Additionally, the inclusion of bile salts at the interface could have spaced out the neighboring DPPC molecules, thus disordering their tight packing and the interfacial organization [52]. At T_{5min}, the highest domains became more numerous, probably related to the generation of FFA, with a height h1'=1.7 ± 0.1 nm. The organization of the interface was similar to that obtained in the images at 2h kinetics after injection of gPLRP2 in the subphase of GL/DPPC/pS monolayers, highlighting the galactolipase activity of gPLRP2 at the level of heterogeneous liposomes in the presence of bile salts, but also at the level of heterogeneous monolayers.

OVERALL SUMMARY

The adsorption and enzymatic activity of gPLRP2 was studied on GL-based substrates exhibiting different supramolecular structures, and presenting or not phase heterogeneity. The galactolipase activity of gPLRP2 was evidenced at the level of both homogeneous GL and heterogenous GL/DPPC/pS monolayers, after a decrease in surface pressure that allowed reaching the optimum range for gPLRP2 activity on substrate monolayers [15,22,23,53]. The presence of charged lipids

548 (SQDG, PG) at the interface improved the adsorption capacities of the enzyme through the
549 establishment of electrostatic interactions between the substrate and the interfacial recognition site
550 of the active site, resulting in improved adsorption and enzymatic activity of gPLRP2. The optimal
551 activity of gPLRP2 was obtained at a surface pressure of 15 mN/m for homogeneous or
552 heterogeneous systems, even if the tighter packing of the heterogeneous monolayer has induced a
553 lag phase period before the on-set of the lipolysis.

554 However, no galactolipase activity could be detected on liposomes made with the same lipid
555 mixtures, confirming the previous finding that gPLRP2 does not interact with phospholipid (DPPC)
556 liposomes and does not display phospholipase A1 on this form of substrate. Therefore, galactolipid-
557 based liposomes are not equivalent to monolayers of the same lipids in terms of recognition by
558 gPLRP2. Since we have shown that gPLRP2 preferentially binds at boundaries between liquid and
559 condensed phases in monolayers, one can assume that lateral packing of lipid molecules and phase
560 heterogeneity are not the same in liposomes. gPLRP2 adsorption to heterogeneous monolayers
561 induces a decrease in surface pressure that further accelerates enzyme activity. This mechanism of
562 action seems to be impaired with liposomes in the absence of bile salts.

563 Nevertheless, both galactolipase and phospholipase A1 activities of gPLRP2 were detected when
564 heterogeneous GL/DPPC/pS liposomes were incubated in the presence of bile salts. Bile salt
565 adsorption onto the liposomes can accelerate enzyme activity by changing the interfacial properties
566 and this is probably one of the mechanisms by which gPLRP2 becomes active on liposomes.
567 However, knowing the micellar solubilization properties of bile salts on polar lipids and the
568 preference of gPLRP2 for micellar substrates, one can speculate that lipolysis of both GL and PL
569 rapidly proceeds through liposomes disruption and formation of mixed micelles onto which
570 gPLRP2 preferentially binds.

Monolayer studies with heterogeneous lipid films revealed that the presence of surfactants like bile salts is not an absolute requirement to accelerate gPLRP2 activity on GL. It is now tempting to investigate whether gPLRP2 can act directly on plant membranes.

CONCLUSION

The enzymatic activity of gPLRP2 was evidenced onto the galactolipid-based monolayers, with an optimum activity in the range of 10 to 15 mN/m, in the absence of bile salts. The adsorption capacity of gPLRP2 and the subsequent extent of lipolysis, however, was dependent on the chemical composition, but also on the physical environment of the monolayer substrates. In bulk, no enzymatic activity has been evidenced on GL-based liposomes in the absence of bile salts, probably due to the high lateral pressure of the lipid bilayers. In the presence of NaTDC (4 mM), however, gPLRP2 showed both high galactolipase and moderate phospholipase A1 activities on liposomes, probably due to a decrease in packing and lateral pressure upon NaTDC adsorption, and subsequent disruption of liposomes.

Declaration of Competing Interest

The authors declare that they have no known competing financial interests or personal relationships that could have appeared to influence the work reported in this paper.

Funding

This research work has been conducted thanks to a research grant from the French Ministry of Research.

Acknowledgments

The authors would like to thank the BIOMIF platform ('Biological Molecules at fluid interfaces', IPR, Rennes, France) for allowing the biophysical characterization of samples presented in this article.

C. Bourlieu, V. Vié, F. Carrière, and J. Kergomard determined the outline and the content of the manuscript. J. Kergomard wrote the manuscript and all the authors participated in the experimental design, the collection, the interpretation of data, and the correction and implementation of the manuscript. All authors have approved the final article.

References

[1] P. Dörmann, Galactolipids in Plant Membranes, in: ELS, John Wiley & Sons, Ltd, 2013. https://doi.org/10.1002/9780470015902.a0020100.pub2.

[2] R. Douce, R.B. Holtz, A.A. Benson, Isolation and Properties of the Envelope of Spinach Chloroplasts, J. Biol. Chem. 248 (1973) 7215–7222.

[3] V. Gurevich, B. Bondarenko, K.J. Gundermann, R. Schumacher, T. Astashkina, V. Ivanov, Y. Popov, L. Shatilina, N. Kazennova, Poly-unsaturated phospholipids increase the hypolipidemic effect of Lovastatin, European Journal of Internal Medicine. 8 (1997) 15–20.

[4] Lee, Membrane lipids: It's only a phase, Current Biology. 10 (2000) R377–R380. https://doi.org/10.1016/S0960-9822(00)00477-2.

[5] N. Mizusawa, H. Wada, The role of lipids in photosystem II, Biochimica et Biophysica Acta (BBA) - Bioenergetics. 1817 (2012) 194–208. https://doi.org/10.1016/j.bbabio.2011.04.008.

[6] C. Glöckner, The donor and acceptor side of photosystem II: structural and functional investigations, (2013). https://doi.org/10.14279/depositonce-152.

[7] M. Sahaka, S. Amara, J. Wattanakul, M.A. Gedi, N. Aldai, G. Parsiegla, J. Lecomte, J.T. Christeller, D. Gray, B. Gontero, P. Villeneuve, F. Carrière, The digestion of galactolipids and its ubiquitous function in Nature for the uptake of the essential α-linolenic acid, Food Funct. (2020). https://doi.org/10.1039/D0FO01040E.

[8] J. Kergomard, F. Carrière, N. Barouh, P. Villeneuve, V. Vié, C. Bourlieu, Digestibility and oxidative stability of plant lipid assemblies: An underexplored source of potentially bioactive surfactants?, Critical Reviews in Food Science and Nutrition. (2021) 1–20. https://doi.org/10.1080/10408398.2021.2005532.

[9] R.K. Saini, Y.-S. Keum, Omega-3 and omega-6 polyunsaturated fatty acids: Dietary sources, metabolism, and significance — A review, Life Sciences. 203 (2018) 255–267. https://doi.org/10.1016/j.lfs.2018.04.049.

[10] M.A. Gedi, K.J. Magee, R. Darwish, P. Eakpetch, I. Young, D.A. Gray, Impact of the partial replacement of fish meal with a chloroplast rich fraction on the growth and selected nutrient profile of zebrafish (Danio rerio), Food Funct. 10 (2019) 733–745. https://doi.org/10.1039/C8FO02109K.

[11] X. Belaunzaran, P. Lavín, A.R. Mantecón, J.K.G. Kramer, N. Aldai, Effect of slaughter age and feeding system on the neutral and polar lipid composition of horse meat, Animal : An International Journal of Animal Bioscience. 12 (2018). https://doi.org/10.1017/S1751731117001689.

[12] S.C. Cunnane, M.J. Hamadeh, A.C. Liede, L.U. Thompson, T.M. Wolever, D.J. Jenkins, Nutritional attributes of traditional flaxseed in healthy young adults, The American Journal of Clinical Nutrition. 61 (1995) 62–68. https://doi.org/10.1093/ajcn/61.1.62.

[13] L. Andersson, C. Bratt, K.C. Arnoldsson, B. Herslöf, N.U. Olsson, B. Sternby, A. Nilsson, Hydrolysis of galactolipids by human pancreatic lipolytic enzymes and duodenal contents., J. Lipid Res. 36 (1995) 1392–1400.

[14] L. Andersson, F. Carrière, M.E. Lowe, Å. Nilsson, R. Verger, Pancreatic lipase-related protein 2 but not classical pancreatic lipase hydrolyzes galactolipids, Biochimica et Biophysica Acta (BBA) - Lipids and Lipid Metabolism. 1302 (1996) 236–240. https://doi.org/10.1016/0005-2760(96)00068-9.

[15] S. Amara, D. Lafont, G. Parsiegla, V. Point, A. Chabannes, A. Rousset, F. Carrière, The galactolipase activity of some microbial lipases and pancreatic enzymes, European Journal of Lipid Science and Technology. 115 (2013) 442–451. https://doi.org/10.1002/ejlt.201300004.

[16] J.-C. Bakala N'Goma, S. Amara, K. Dridi, V. Jannin, F. Carrière, Understanding the lipid-digestion processes in the GI tract before designing lipid-based drug-delivery systems, Ther Deliv. 3 (2012) 105–124. https://doi.org/10.4155/tde.11.138.

[17] S. Amara, D. Lafont, B. Fiorentino, P. Boullanger, F. Carrière, A. De Caro, Continuous measurement of galactolipid hydrolysis by pancreatic lipolytic enzymes using the pH-stat technique and a medium chain monogalactosyl diglyceride as substrate, Biochimica et Biophysica Acta (BBA) - Molecular and Cell Biology of Lipids. 1791 (2009) 983–990. https://doi.org/10.1016/j.bbalip.2009.05.002.

[18] J. De Caro, B. Sias, P. Grandval, F. Ferrato, H. Halimi, F. Carrière, A. De Caro, Characterization of pancreatic lipase-related protein 2 isolated from human pancreatic juice, Biochimica et Biophysica Acta (BBA) - Proteins and Proteomics. 1701 (2004) 89–99. https://doi.org/10.1016/j.bbapap.2004.06.005.

[19] J. Wattanakul, M. Sahaka, S. Amara, S. Mansor, B. Gontero, F. Carrière, D. Gray, In vitro digestion of galactolipids from chloroplast-rich fraction (CRF) of postharvest, pea vine field residue (haulm) and spinach leaves, Food Funct. 10 (2019) 7806–7817. https://doi.org/10.1039/C9FO01867K.

[20] C. Eydoux, S. Spinelli, T.L. Davis, J.R. Walker, A. Seitova, S. Dhe-Paganon, A. De Caro, C. Cambillau, F. Carrière, Structure of Human Pancreatic Lipase-Related Protein 2 with the Lid in an Open Conformation, Biochemistry. 47 (2008) 9553–9564. https://doi.org/10.1021/bi8005576.

[21] C. Eydoux, J. De Caro, F. Ferrato, P. Boullanger, D. Lafont, R. Laugier, F. Carrière, A. De Caro, Further biochemical characterization of human pancreatic lipase-related protein 2 expressed in yeast cells, Journal of Lipid Research. 48 (2007) 1539–1549. https://doi.org/10.1194/jlr.M600486-JLR200.

[22] A. Hjorth, F. Carriere, C. Cudrey, H. Woldike, E. Boel, D.M. Lawson, F. Ferrato, C. Cambillau, G.G. Dodson, A structural domain (the lid) found in pancreatic lipases is absent in the guinea pig (phospho)lipase, Biochemistry. 32 (1993) 4702–4707. https://doi.org/10.1021/bi00069a003.

[23] B. Sias, F. Ferrato, P. Grandval, D. Lafont, P. Boullanger, A. De Caro, B. Leboeuf, R. Verger, F. Carrière, Human Pancreatic Lipase-Related Protein 2 Is a Galactolipase, Biochemistry. 43 (2004) 10138–10148. https://doi.org/10.1021/bi049818d.

[24] E. Mateos-Diaz, J.-C. Bakala N'Goma, D. Byrne, S. Robert, F. Carrière, H. Gaussier, IR spectroscopy analysis of pancreatic lipase-related protein 2 interaction with phospholipids: 1. Discriminative recognition of mixed micelles versus liposomes, Chem Phys Lipids. 211 (2018) 52–65. https://doi.org/10.1016/j.chemphyslip.2017.02.005.

[25] S. Bezzine, F. Ferrato, M.G. Ivanova, V. Lopez, R. Verger, F. Carrière, Human Pancreatic Lipase: Colipase Dependence and Interfacial Binding of Lid Domain Mutants, Biochemistry. 38 (1999) 5499–5510. https://doi.org/10.1021/bi982601x.

[26] B. Borgström, On the interactions between pancreatic lipase and colipase and the substrate, and the importance of bile salts, J Lipid Res. 16 (1975) 411–417.

[27] O. Pabois, R.M. Ziolek, C.D. Lorenz, S. Prévost, N. Mahmoudi, M.W.A. Skoda, R.J.L. Welbourn, M. Valero, R.D. Harvey, M.M.-L. Grundy, P.J. Wilde, I. Grillo, Y. Gerelli, C.A. Dreiss, Morphology of bile salts micelles and mixed micelles with lipolysis products, from scattering techniques and atomistic simulations, Journal of Colloid and Interface Science. 587 (2021) 522–537. https://doi.org/10.1016/j.jcis.2020.10.101.

[28] B. Borgström, Phosphatidylcholine as substrate for human pancreatic phospholipase A2. Importance of the physical state of the substrate, Lipids. 28 (1993) 371–375. https://doi.org/10.1007/BF02535932.

[29] S. Amara, N. Barouh, J. Lecomte, D. Lafont, S. Robert, P. Villeneuve, A. De Caro, F. Carrière, Lipolysis of natural long chain and synthetic medium chain galactolipids by pancreatic lipase-related protein 2, Biochimica et Biophysica Acta (BBA) - Molecular and Cell Biology of Lipids. 1801 (2010) 508–516. https://doi.org/10.1016/j.bbalip.2010.01.003.

[30] B. Berge, A. Renault, Ellipsometry Study of 2D Crystallization of 1-Alcohol Monolayers at the Water Surface, Europhysics Letters (EPL). 21 (1993) 773–777. https://doi.org/10.1209/0295-5075/21/7/010.

[31] C. Bourlieu, W. Mahdoueni, G. Paboeuf, E. Gicquel, O. Ménard, S. Pezennec, S. Bouhallab, A. Deglaire, D. Dupont, F. Carrière, V. Vié, Physico-chemical behaviors of human and bovine milk membrane extracts and their influence on gastric lipase adsorption, Biochimie. 169 (2020) 95–105. https://doi.org/10.1016/j.biochi.2019.12.003.

[32] A. Bénarouche, V. Point, G. Parsiegla, F. Carrière, J.-F. Cavalier, New insights into the pH-dependent interfacial adsorption of dog gastric lipase using the monolayer technique, Colloids and Surfaces B: Biointerfaces. 111 (2013) 306–312. https://doi.org/10.1016/j.colsurfb.2013.06.025.

[33] L. Xu, Y.Y. Zuo, Reversible Phase Transitions in the Phospholipid Monolayer, Langmuir. 34 (2018) 8694–8700. https://doi.org/10.1021/acs.langmuir.8b01544.

[34] C. Bourlieu, G. Paboeuf, S. Chever, S. Pezennec, J.-F. Cavalier, F. Guyomarc'h, A. Deglaire, S. Bouhallab, D. Dupont, F. Carrière, V. Vié, Adsorption of gastric lipase onto multicomponent model lipid monolayers with phase separation, Colloids and Surfaces B: Biointerfaces. 143 (2016) 97–106. https://doi.org/10.1016/j.colsurfb.2016.03.032.

[35] J. Kergomard, F. Carrière, G. Paboeuf, F. Artzner, N. Barouh, C. Bourlieu, V. Vié, Interfacial organization and phase behavior of mixed galactolipid-DPPC-phytosterol assemblies at the

air-water interface and in hydrated mesophases, Colloids and Surfaces B: Biointerfaces. (2022) 112646. https://doi.org/10.1016/j.colsurfb.2022.112646.

[36] J. Kergomard, F. Carrière, G. Paboeuf, N. Barouh, C. Bourlieu-Lacanal, V. Vié, Modulation of gastric lipase adsorption onto mixed galactolipid-phospholipid films by addition of phytosterols, Colloids and Surfaces B: Biointerfaces. 220 (2022) 112933. https://doi.org/10.1016/j.colsurfb.2022.112933.

[37] J. Sarkis, V. Vié, Biomimetic Models to Investigate Membrane Biophysics Affecting Lipid–Protein Interaction, Frontiers in Bioengineering and Biotechnology. 8 (2020). https://www.frontiersin.org/articles/10.3389/fbioe.2020.00270 (accessed July 18, 2022).

[38] C. Withers-Martinez, F. Carrière, R. Verger, D. Bourgeois, C. Cambillau, A pancreatic lipase with a phospholipase A1 activity: crystal structure of a chimeric pancreatic lipase-related protein 2 from guinea pig, Structure. 4 (1996) 1363–1374. https://doi.org/10.1016/S0969-2126(96)00143-8.

[39] M. Sahaka, S. Amara, J. Lecomte, J.-D. Rodier, D. Lafont, P. Villeneuve, B. Gontero, F. Carrière, Quantitative monitoring of galactolipid hydrolysis by pancreatic lipase-related protein 2 using thin layer chromatography and thymol-sulfuric acid derivatization, Journal of Chromatography B. 1173 (2021) 122674. https://doi.org/10.1016/j.jchromb.2021.122674.

[40] R. Verger, M.C.E. Mieras, G.H. de Haas, Action of Phospholipase A at Interfaces, J. Biol. Chem. 248 (1973) 4023–4034.

[41] T. Wieloch, B. Borgström, G. Piéroni, F. Pattus, R. Verger, Product activation of pancreatic lipase. Lipolytic enzymes as probes for lipid/water interfaces., Journal of Biological Chemistry. 257 (1982) 11523–11528. https://doi.org/10.1016/S0021-9258(18)33792-X.

[42] N.A. Mazer, G.B. Benedek, M.C. Carey, Quasielastic light-scattering studies of aqueous biliary lipid systems. Mixed micelle formation in bile salt-lecithin solutions, Biochemistry. 19 (1980) 601–615. https://doi.org/10.1021/bi00545a001.

[43] O. Pabois, C.D. Lorenz, R.D. Harvey, I. Grillo, M.M.-L. Grundy, P.J. Wilde, Y. Gerelli, C.A. Dreiss, Molecular insights into the behaviour of bile salts at interfaces: a key to their role in lipid digestion, Journal of Colloid and Interface Science. 556 (2019) 266–277. https://doi.org/10.1016/j.jcis.2019.08.010.

[44] J. Maldonado-Valderrama, P. Wilde, A. Macierzanka, A. Mackie, The role of bile salts in digestion, Advances in Colloid and Interface Science. 165 (2011) 36–46. https://doi.org/10.1016/j.cis.2010.12.002.

[45] J. Maldonado-Valderrama, J.L. Muros-Cobos, J.A. Holgado-Terriza, M.A. Cabrerizo-Vílchez, Bile salts at the air–water interface: Adsorption and desorption, Colloids and Surfaces B: Biointerfaces. 120 (2014) 176–183. https://doi.org/10.1016/j.colsurfb.2014.05.014.

[46] A. Roda, A.F. Hofmann, K.J. Mysels, The influence of bile salt structure on self-association in aqueous solutions, J Biol Chem. 258 (1983) 6362–6370.

[47] A.F. Hofmann, The function of bile salts in fat absorption. The solvent properties of dilute micellar solutions of conjugated bile salts, Biochem J. 89 (1963) 57–68.

[48] A.F. Hofmann, B. Borgström, The Intraluminal Phase of Fat Digestion in Man: The Lipid Content of the Micellar and Oil Phases of Intestinal Content Obtained during Fat Digestion and Absorption*, J Clin Invest. 43 (1964) 247–257.

[49] E. Mateos-Diaz, P. Sutto-Ortiz, M. Sahaka, D. Byrne, H. Gaussier, F. Carrière, IR spectroscopy analysis of pancreatic lipase-related protein 2 interaction with phospholipids: 2. Discriminative recognition of various micellar systems and characterization of PLRP2-

DPPC-bile salt complexes, Chemistry and Physics of Lipids. 211 (2018) 66–76. https://doi.org/10.1016/j.chemphyslip.2017.11.012.

[50] Sahaka, Etude de l'hydrolyse enzymatique des galactolipides par diverses approches chromatographique et spectroscopiques, These de doctorat, Aix-Marseille, 2020. http://www.theses.fr/2020AIXM0467 (accessed June 23, 2022).

[51] M. Sahaka, E. Mateos-Diaz, S. Amara, J. Wattanakul, D. Gray, D. Lafont, B. Gontero, H. Launay, F. Carrière, In situ monitoring of galactolipid digestion by infrared spectroscopy in both model micelles and spinach chloroplasts, Chemistry and Physics of Lipids. 252 (2023) 105291. https://doi.org/10.1016/j.chemphyslip.2023.105291.

[52] B.-S. Chu, A.P. Gunning, G.T. Rich, M.J. Ridout, R.M. Faulks, M.S.J. Wickham, V.J. Morris, P.J. Wilde, Adsorption of Bile Salts and Pancreatic Colipase and Lipase onto Digalactosyldiacylglycerol and Dipalmitoylphosphatidylcholine Monolayers, Langmuir. 26 (2010) 9782–9793. https://doi.org/10.1021/la1000446.

[53] C. Eydoux, J.D. Caro, F. Ferrato, P. Boullanger, D. Lafont, R. Laugier, F. Carrière, A.D. Caro, Further biochemical characterization of human pancreatic lipase-related protein 2 expressed in yeast cells, J. Lipid Res. 48 (2007) 1539–1549. https://doi.org/10.1194/jlr.M600486-JLR200.

FIGURES

Figure captions.

Figure 1 – 5×5 µm² AFM images of A) GL, B) GL/DPPC/pS, and C) MGDG/DGDG/SQDG/PG monolayers at 20 mN/m.

Figure 2 – A) Kinetic evolution of surface pressure (π, mN/m, red circles) and ellipsometric angle (Δ, °, blue triangle) upon the adsorption and kinetic activity of gPLRP2 (0.128 mg/L) onto GL monolayer. B) AFM images of Langmuir-Blodgett samples after 1) 35 minutes and 2) 1 hour kinetic of gPLRP2 adsorption onto GL monolayer, respectively.

Figure 3 – Schematic representation of galactolipid lipolysis by PLRP2. MGDG – monogalactosyldiacylglycerol, DGDG – digalactosyldiacylglycerol, FFA – Free fatty acid, MGMG – monogalactosylmonoacylglycerol, DGMG – digalactosylmonoacylglycerol, MGG – monogalactosylglycerol, DGG – digalactosylglycerol.

Figure 4 – Kinetic evolution of the surface pressure (π, mN/m, red circle) and the ellipsometric angle (Δ, °, blue triangle) over one hour after the injection of the inactive variant of gPLRP2 in the subphase of the GL monolayer. B) 5×5 µm² images of the Langmuir-Blodgett sample obtained after 1 hour kinetic.

Figure 5 – A) Kinetic evolution of surface pressure (π, mN/m, red circles) and ellipsometric angle (Δ, °, blue triangle) upon the adsorption and kinetic activity of gPLRP2 (0.128 mg/L) onto GL/DPPC/pS monolayer. B) AFM images of Langmuir-Blodgett samples after 1) 45 minutes and 2) 1h45 kinetic of gPLRP2 adsorption onto GL/DPPC/pS monolayer, respectively.

Figure 6 – A) Evolution of the surface pressure (π, red, mN/m) and the ellipsometric angle (Δ, blue, °) upon the adsorption of gPLRP2 onto MGDG/DGDG/SQDG/PG (1h kinetic). B) AFM images (5×5 µm²) of the interface of MGDG/DGDG/SQDG/PG (1h kinetic, π=8.5 mN/m, Δ=5.2°).

Figure 7 – Typical evolution of the particle diameter distribution of A) GL, and B) GL/DPPC/pS dispersed diluted liposomes (0.04%) in the absence and presence (4 mM NaTDC) of bile salts. Results were obtained by DLS measurements.

Figure 8 – AFM images (5×5 µm²) of substrates and lipolysis products obtained at T5min and deposited at 7.2 ± 0.1 mN/m at the air/water interface of A) GL, and B) GL/DPPC/pS monolayers. For each identified domain, the mean height level was given in the table and was obtained as an average over three sections of the image. Lipophilic substrates and products were extracted using Folch method.

Figure 1

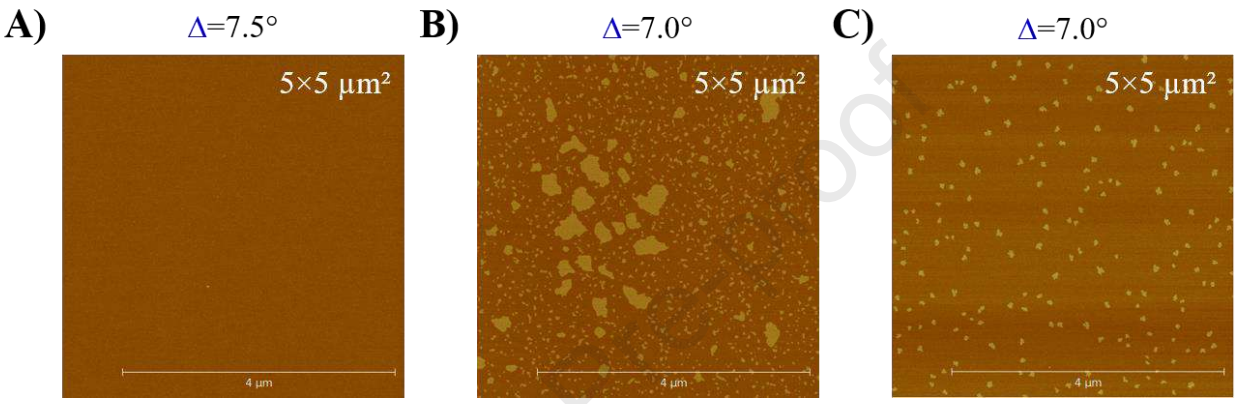

Figure 2

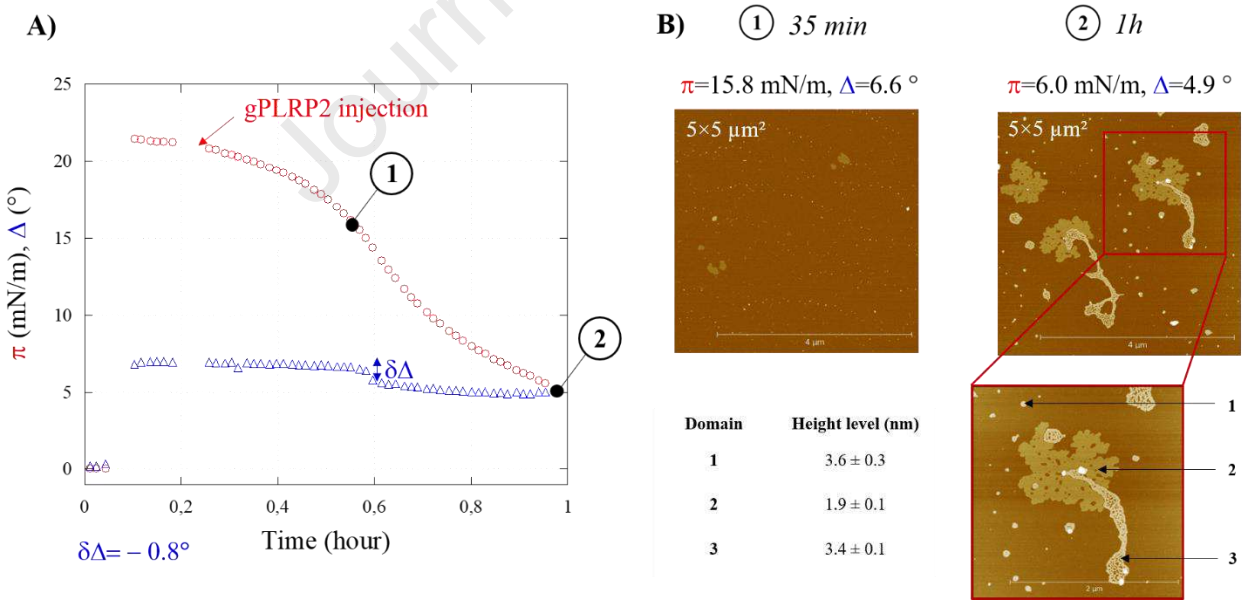

821 **Figure 3**

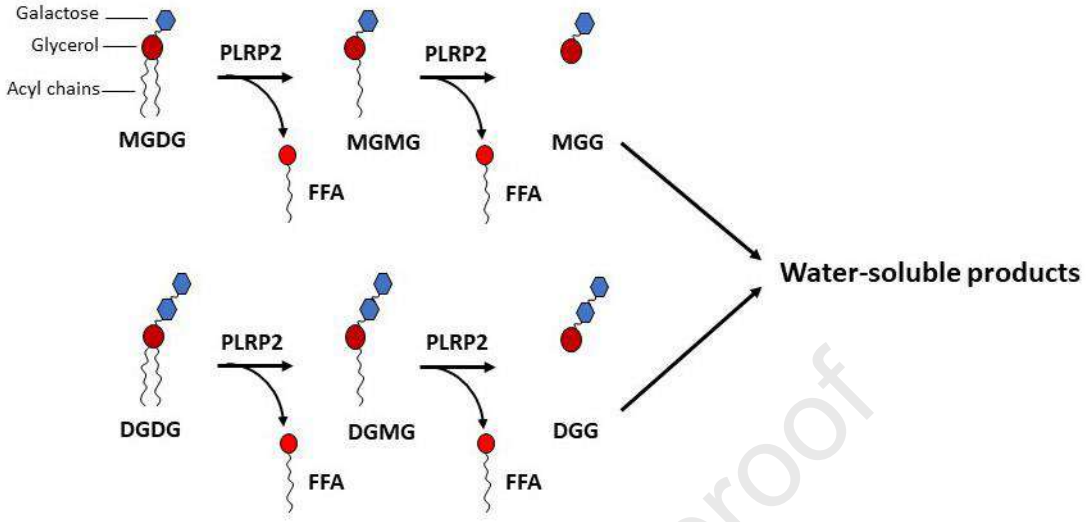

822

823 **Figure 4**

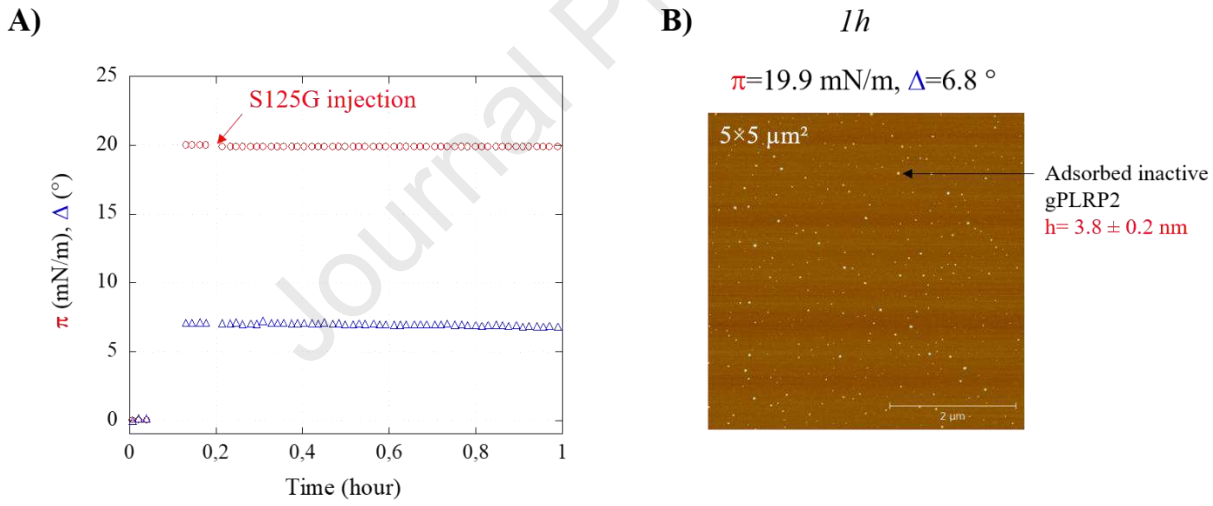

824

825

826 **Figure 5**

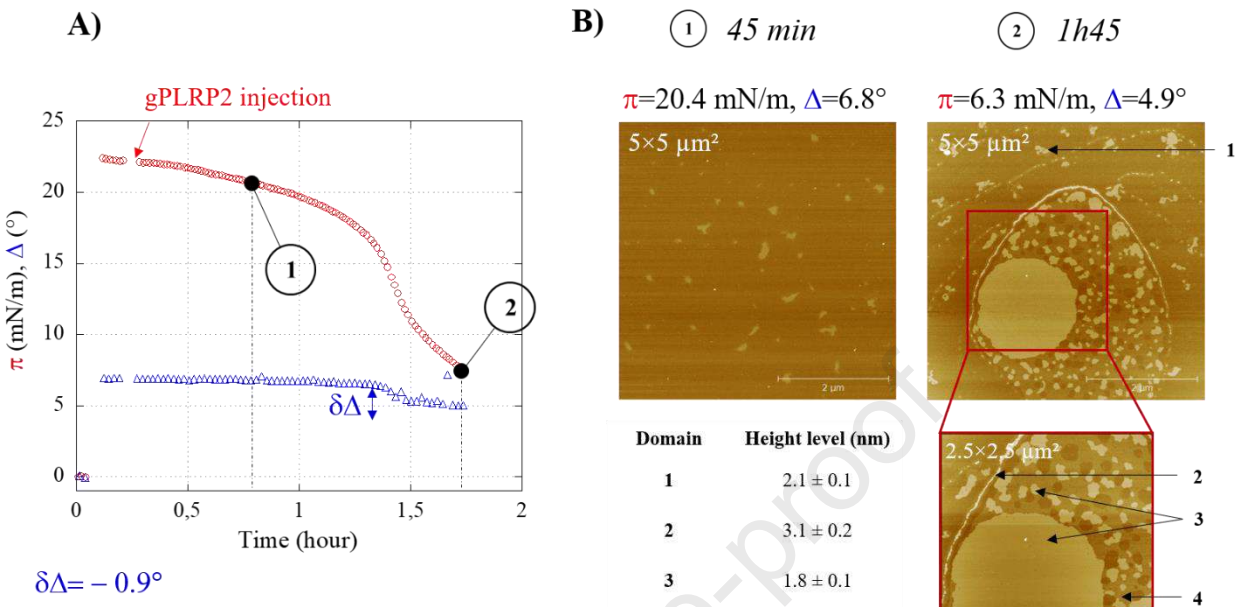

827

828 **Figure 6**

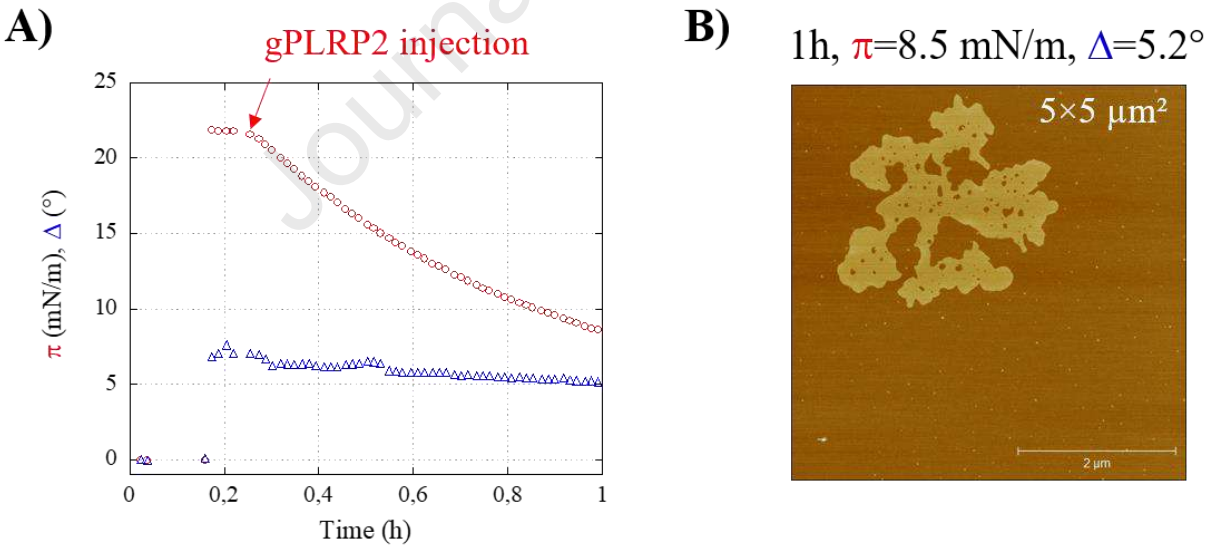

829

830

831 **Figure 7**

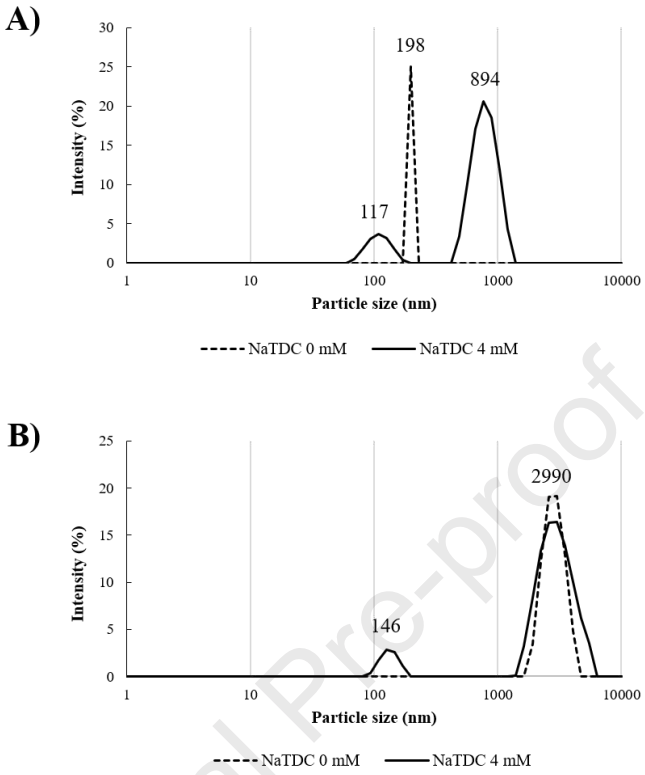

832

833 **Figure 8**

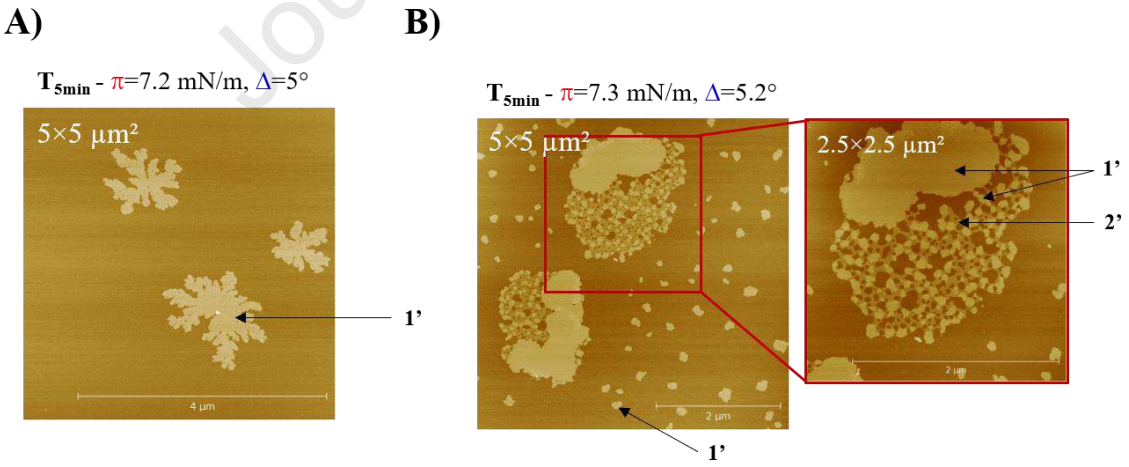

Domain	Height level (nm)
T_{5min} - 1'	1.9 ± 0.1

Domain		Height level (nm)
T_{5min}	1'	1.7 ± 0.1
	2'	1.2 ± 0.2

834

TABLES

Table 1 – Quantitative determination of lipid classes composition obtained by TLC at T_0 and after 5 minutes (T_{5min}) digestion by gPLRP2 of GL/DPPC/pS, GL, MGDG/DGDG/SQDG/PG liposomes. The reaction was performed at pH 7 in Tris HCl buffer containing 4 mM of NaTDC. Data are given in relative percentages of the total lipids.

	GL/DPPC/pS		**GL**		**MGDG/DGDG/SQDG/PG**	
Relative %	T_0	T_{5min}	T_0	T_{5min}	T_0	T_{5min}
FFA	7.2 ± 1.1	31.1 ± 4.5	-	43.8 ±7.5	-	54.3 ± 2.4
MGDG	40.3 ± 0.5	10.3 ± 3.0	48.2 ± 0.3	4.9 ± 1.5	65.4 ± 1.0	10.6 ± 0.1
MGMG	0.3 ± 0.1	20.0 ± 1.3	-	18.8 ± 2.2	-	31.3 ± 2.2
DGDG	33.9 ± 0.9	15.2 ± 0.6	51.8 ± 0.3	3.1 ± 0.8	34.6 ± 1.0	3.7 ± 0.1
DGMG	3.5 ± 2.7	3.8 ± 0.9	-	29.5 ± 3.5	*n.q.*	*n.q.*
DPPC	7.3 ± 3.7	10.1 ± 1.0	-	-	-	-
Lyso-PC	-	2.9 ± 1.6			-	-
pS	7.5 ± 0.7	6.4 ± 0.3	-	-	-	-
SQDG	-	-	-	-	24.7 ± 0.4	2.3 ± 0.3

**n.q. – non-quantifiable*

842 **Supplementary Material**

843 **Table S1 -** Molar composition of mixed Langmuir monolayers used as model membranes

	Monolayer composition
(1) GL	MGDG/DGDG 60:40 mol.mol^{-1}
(2) GL/DPPC	MGDG/DGDG/DPPC 30:20:50 mol.mol^{-1}.mol^{-1}
(3) GL/DPPC/pS	MGDG/DGDG/DPPC/pS* 27:18:45:10 mol.mol^{-1}1.mol^{-1}.mol^{-1}

β-sitosterol, campesterol, brassicasterol 50:40:10 mol.mol^{-1}.mol^{-1}

844

845 **Figure S2 –** Fatty acid distribution of MGDG and DGDG purchased from Avanti Polar Lipids

846

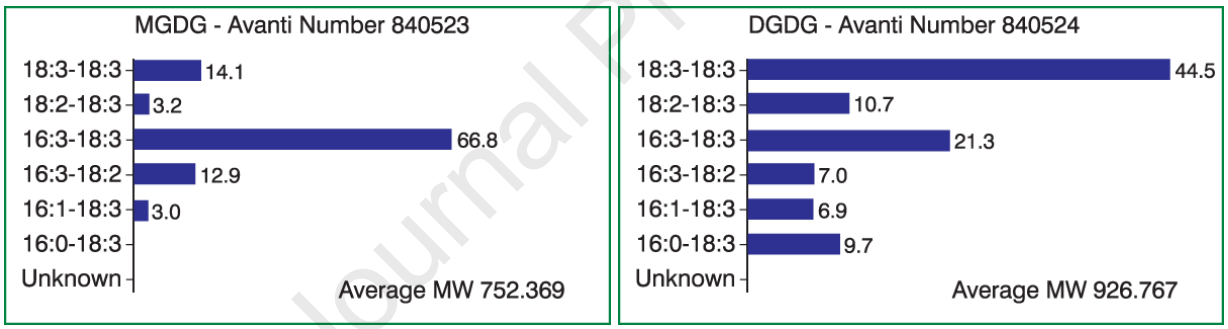

847

848

849 **Figure S3 –** Lipid classes composition obtained by TLC after 1h45 digestion by gPLRP2 of
850 GL/DPPC/pS monolayer, showing the appearance of FFA at the interface. The reaction was
851 performed at pH 7 in Tris HCl buffer in the absence of NaTDC.

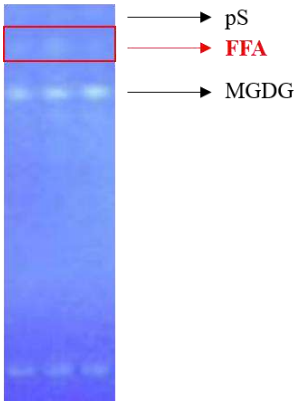

Table S4 - Quantitative determination of lipid classes composition obtained by TLC at T_0 and after 5 minutes (T_{5min}) digestion by gPLRP2 of GL/DPPC/pS liposomes **in absence of NaTDC**. The reaction was performed at pH 7 in Tris HCl buffer. Data are given in relative percentages of the total lipids.

	GL/DPPC/pS	
Relative %	T_0	T_{5min}
FFA	9.2 ± 3.1	4.9 ± 0.5
MGDG	41.2 ± 2.9	42.0 ± 1.0
MGMG	1.0 ± 1.4	0.5 ± 0.3
DGDG	35.8 ± 1.7	38.3 ± 2.3
DGMG	3.0 ± 0.5	4.9 ± 0.9
DPPC	2.0 ± 0.5	2.8 ± 0.4
LysoPC	-	-
pS	7.7 ± 0.6	6.5 ± 2.1

**n.q. – non-quantifiable*

HIGHLIGHTS

- gPLRP2 showed galactolipase activity onto heterogeneous galactolipid-based monolayers.
- Optimal enzymatic activity of gPLRP2 on monolayers was obtained at π~15 mN/m.
- No lipolytic activity of gPLRP2 was detected on liposomes in the absence of NaTDC.
- gPLRP2 showed enzymatic activities on liposomes in the presence of NaTDC.